Expansion of the Guerbet Reaction Towards Group 7 Metal Catalysts and Triglyceride Substrates

Ashley Malcolm King

July 2021

This thesis is being submitted to Cardiff University in partial fulfilment of the requirements for the degree of Doctor of Philosophy in the Faculty of Science

School of Chemistry

Abstract

This thesis aims to expand the application of the Guerbet reaction towards both new catalysts and substrates. The Guerbet reaction is used to generate longer chain alcohols from their shorter chain analogues through borrowed hydrogen chemistry; the hope being that these long-chain alcohols can find use as both renewable fuels and synthetic lubricants.

Substrate scope expansion focussed primarily on triglycerides and methyl esters, as these could be hydrogenated to the corresponding alcohol before Guerbet chemistry was employed. This represented a simple and quick route to the functionalisation of cheap, naturally occurring chemicals. The ruthenium-PNP complex, RuMACHO, showed particularly high activity for this reaction as it was able to catalyse both the hydrogenation and Guerbet step, allowing for a '2-step-1-pot' production of β-methylated alcohols. As such, a variety of different triglycerides, including the readily available coconut oil, have been investigated. Research into the direct coupling of long-chain linear alcohols has also been undertaken, these can be used as synthetic engine oils or be functionalise further to produce surfactants. For this process, a ruthenium-diphosphine bis-chelate complex was found to be most effective with high conversions and moderate yields recorded.

Expansion of catalyst scope was centred around investigating the under-utilised group 7 metals for Guerbet chemistry. Investigations focussed on the well-studied production of *iso*butanol from methanol and ethanol. Here, manganese complexes bearing diphenylphosphinomethane (dppm) ligands were found to be effective over 90 h run times. Substitution of the dppm backbone with electron donating substituents was found to increase catalytic activity. Rhenium complexes bearing both bidentate and tridentate ligands were also tested and broadly showed greater activity than their manganese analogues with shorter run times of 16 h required. Finally, ruthenium half-sandwich complexes bearing *ortho* substituted dppm ligands were examined, with the hope that this would help stabilise the catalyst under reaction conditions.

Contents

List of Figures

List of Schemes

List of Tables

Acknowledgments

Collaborator Acknowledgements

Abbreviations

General

ABE	Acetone Butanol ethanol
Ar	Aryl group
Cat	Catalyst
CP	Cloud point
CSD	Cambridge Structural Database
DCM	Dichloromethane
dcypm	1,1-bis(dicyclohexylphosphino)methane
dppa	N,N-bis(diphenylphosphino)amine
dppb	1,4-*bis*(diphenylphosphino)butane
dppe	1,2-*bis*(diphenylphosphino)ethane
dppea	2-(diphenylphosphino)ethylamine
dppm	1,1-*bis*(diphenylphosphino)methane
dppp	1,3-*bis*(diphenylphosphino)propane
dpppa	3-(diphenylphosphino)propylamine
DTF	Density functional theory
e$^-$	Electron
EPR	Electron paramagnetic resonance
fac	Facial
FAME	Fatty acid methyl ester
h/hrs	Hour/s
IPCC	Intergovernmental Panel on Climate Change
IR	Infrared
iso	Equal
KHMDS	Potassium bis(trimethylsilyl)amide
m	Meta
M	Molar
MACHO	bis(phosphino)ethylamine
mer	Meridional
o	Ortho
OPEC	Organisation of the Petroleum Exporting Countries
p	Para
PP	Pour point
PVC	Polyvinyl chloride
RON	Research octane number
RT	Room temperature
TCE	Tetrachloroethane
THF	Tetrahydrofuran
TON	Turnover number
wt%	Weight percent

Spectrochemical

br	Broad
d	Doublet
dq	Doublet or quartets
ESI	Electron spray ionisation
GC	Gas chromatography
GC-MS	Gas chromatography mass spectrometry
HR-MS	High resolution mass spectrometry
J	Coupling constant
LC-MS	Liquid chromatography mass spectrometry
m	Multiplet
m/z	Mass/charge
MS	Mass spectrometry
NMR	Nuclear magnetic resonance
ppm	Parts per million
q	Quartet
s	Singlet
t	Triplet
td	Triplet of doublets

Chapter 1: Introduction

1.1 – Global Energy Crisis

As the damaging effects of extensive fossil fuel usage on the global climate become more apparent, research into sustainable and renewable forms of energy is becoming ever more important. Global temperatures have been gradually rising since the onset of the industrial revolution, with the period from 1983-2012 likely being the warmest three decades for the last 1400 years.[1] These temperature rises are not globally uniform, and tend to be most significant over highly populated areas. Large global temperature gradients can lead to an increase in extreme weather such as El Niño events.[2] Increases in global temperature are intrinsically linked with increased fossil fuel consumption and the subsequent release of greenhouse gases, particularly carbon dioxide (CO_2). CO_2 emissions from the burning of fossil fuels were responsible for a 78% increase in total greenhouse gas emissions between 1970 and 2010, with around 32 Gt produced in 2010 alone.[3]
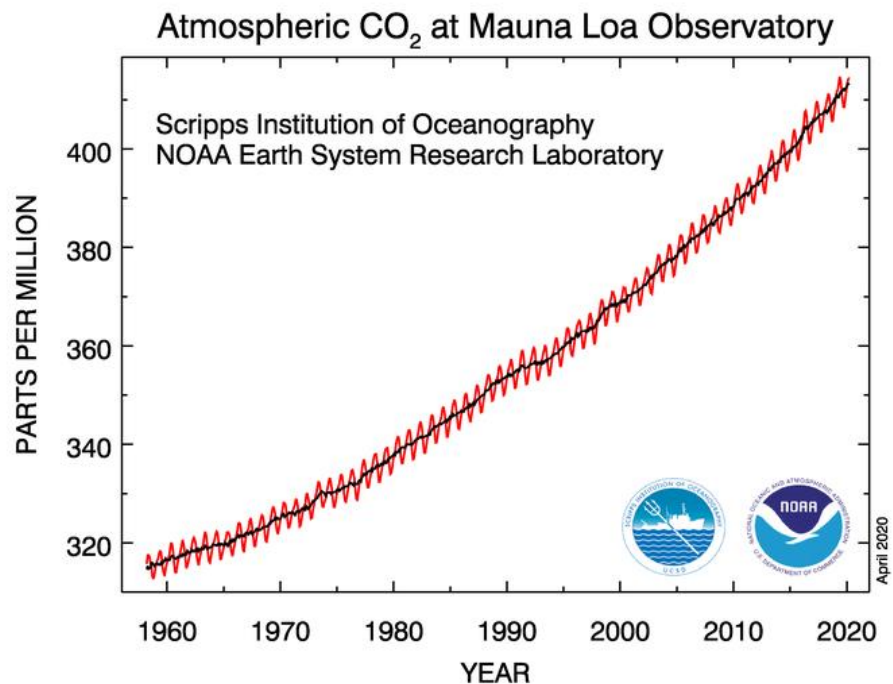
Figure 1.1: Global increases in average CO_2 levels from the Muana Loa observatory.[4]

Global atmospheric CO_2 levels recorded at the Muana Loa observatory in Hawaii have shown that CO_2 levels in 2018 were 407.4 ± 0.1 ppm and increasing by 2-2.5 ppm per year on average (Figure 1.1). This is about 100 times faster than previously recorded natural

increases.[5,4] Furthermore, an increase in average global temperature of around 1 °C since 1960 has also been recorded (Figure 1.2). Since the link between CO_2 levels and global temperature was established,[6] international focus has been directed towards reducing CO_2 emissions. Both the IPCC (Intergovernmental Panel on Climate Change) and the 2015 Paris Agreement set targets to keep global CO_2 levels below 450 ppm and temperatures below 2 °C above the pre-industrial average.[3,7]
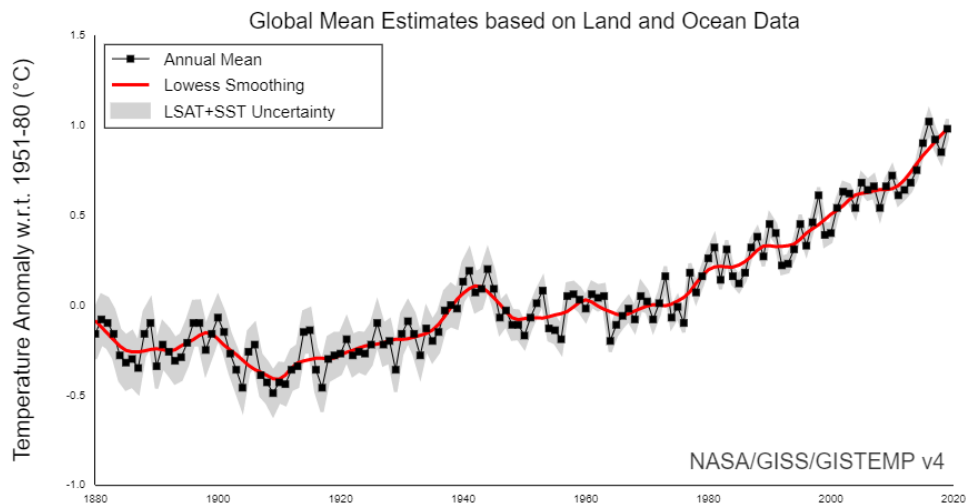
Figure 1.2: Changes in average global temperature since 1880.[8]

Despite these aims, fossil fuel usage continues to increase every year, with the daily demand for crude oil being 101 million barrels in 2019, significantly higher than the 95 million barrels required in 2015 (the year of the Paris agreement). Another key issue with the widespread usage of fossil fuels is their finite availability, as a 2019 report by BP predicted that oil reserves would only last for another 50 years, natural gas reserves for 51 years and coal reserves for 132 years.[9]

The issues with fossil fuels go beyond their damage to the environment and dwindling availability. The pursuit of fossil fuels has led to interference and exploration into dangerous, remote, and unstable areas of the globe. For example, Venezuela is home to one of the world's largest untapped oil fields, totalling around 302 billion barrels.[10] However, it is currently going through a vicious civil war, resulting in oil exploration and export being costly and dangerous. Other countries with massive oil reserves, such as Russia and Saudi Arabia,[11] are able to exert an unprecedented level of control and influence over the energy supply of the rest of the world. An example of this being in 2014 when

OPEC (Organisation of the Petroleum Exporting Countries) flooded the market with cheap crude oil in a bid to curb the newly emerging shale oil production business.[12] While emerging technologies such as hydraulic fracturing, or 'fracking', are allowing the extraction of previously inaccessible natural gas deposits, this is not without its own environmental impacts. If water used in fracking is not contained, it can release harmful organic compounds such as phenols and aromatic amines into nearby ecosystems.[13] These environmental impacts, combined with the possible threat to human life that fracking represents, has led to severe public backlash against the process, particularly in parts of the USA.[14] As such, potential fracking operations are usually hampered by court cases brought by locals and negative public opinion.

It is evident that the continued use of fossil fuels is environmentally damaging, unsustainable, and at the heart of much political unrest. As such, the issue of providing sustainable fuel and power for future generations is a critical area of research that requires a great deal of attention.

1.2 – Sustainable energy production

Renewable energy is defined as energy from a source that is not depleted when used. Use of these sources usually has a significantly lower environmental impact than the use of fossil fuels, hence the replacement of fossil fuels with renewable energy is a key focus of modern-day research. Currently the main sources of renewable energy are wind, solar, hydroelectric, geothermal and biomass.[15]

Wind power is an important and rapidly developing form of renewable energy, with numerous wind farms across much of the UK and EU (there are currently 8,588 onshore wind turbine projects in the UK alone).[16] Wind energy has great potential, being both clean and renewable, with no harmful greenhouse gasses produced after the wind turbines have been built. However, the construction of wind turbines does require a great deal of initial investment, and these up-front costs can often be enough to dissuade potential investors.[17] The noise pollution and significant visual impact caused by wind farms also make them unpopular with local residents, potentially making obtaining planning permission hard and less cost effective.[18]

Solar energy presents many of the same advantages as wind power, being from a virtually limitless source which has to date been almost completely unutilised for human needs. Furthermore, solar power is the most promising and consistent renewable resource for the production of power from heat energy.[18] However, like wind farms, solar power plants require a large initial investment. Moreover, most domestic solar panels only work at 12-16% efficiency and require rare and precious metals for manufacture.[19] They also require a great deal of land in order to operate, and only function during the daytime. Therefore, a great deal of further research is required before solar power will be able to compete with non-renewable energy sources.

Hydroelectric power, power that is generated from flowing water, is a key source of renewable energy accounting for 72.8% of all power generated from renewable sources in 2014.[15,20] Hydroelectric power also produces zero emission once the infrastructure (hydroelectric dam) has been built, furthermore, hydroelectric powerplants can quickly go from zero output to maximum power, allowing them to provide energy back-up in times of need. One of the main issues with hydropower is the effect that dams have on their immediate environment. The construction of large dams, and the subsequent creation of reservoirs, results in a large amount of damage to the ecosystem that is flooded, with a huge cost to biodiversity. This damage and the ensuing public backlash led to the 1968 Wild and Scenic Rivers Act in the United States to prevent the over damming of protected rivers.[21]

Geothermal energy is another renewable energy source with great potential. Much like solar power, it is a source of thermal energy, so can directly be used for heating as well as for energy production. Geothermal energy is also much more reliable than wind and solar power, as it can constantly be used and does not require daylight or high winds.[22] The main disadvantage of geothermal energy is that it is highly location dependant and is not readily available in many parts of the globe. It is also not a completely clean resource as gas is released from the Earth's crust during digging, and geothermal plants often use CO_2 as a heat transfer medium. Furthermore, geothermal digging can also increase the occurrence of earthquakes, posing serious risks to property and human life.[22]

Unlike the other methods of sustainable energy production previously mentioned, biomass use still produces greenhouse gasses. However, given biomass takes in CO_2 as it grows and

then releases it again upon use, it is often described as carbon neutral. Biomass is also far more versatile than other renewable energy sources, it can either be burnt directly to produce heat, or converted into other products like bioethanol, biodiesel or biogas.[23,24] Utilising energy derived from biomass has considerable limitations, mainly that vast amounts of land are needed to grow crops for biofuel production which could otherwise be used to grow food. Also, the processes used to convert biomass into usable fuels still require development. Given the large amount of energy required for biomass conversion and transportation, in reality, use of biomass cannot be regarded as truly carbon neutral.[25] Despite its drawbacks, biofuels are already being utilised for public transport in many cities around the world. One example being in London where biofuels derived from coffee beans have been blended with conventional diesel for use in buses.[26]

Another potential 'clean' energy source is nuclear power. Given the low carbon emissions of nuclear power plants it is often regarded as an environmentally friendly energy source, however, this is offset by fears over ionising radiation release and possible environmental contamination.[27] These fears were recently exemplified by the 2011 Fukushima-Daiichi nuclear incident.[28] The emergence of thorium based reactors has helped to address these concerns, as they produce significantly less long lived radioactive waste. Thorium is also significantly more abundant in nature that uranium, the previously used fuel source for nuclear reactors.[28] While nuclear power may be regarded as a clean energy source, it is not renewable as deposits of radioactive metals on earth are finite.

While many different types of clean and renewable energy are currently under investigation, none of them can currently compete with fossil fuels. In 2014 only 22.8% of global electricity came from renewable sources, with the rest being derived from nuclear and fossil fuels.[15] The transportation sector lags significantly behind this with only 3.5% of global energy demand being met by renewable resources.[15] If the effects of climate change and dwindling resources are to be delayed or avoided, significant further research and wholesale adoption of renewable resources is required.

1.2.1 – Production of sustainable fuels

While no single sustainable energy source has yet been able to compete with fossil fuels in terms of availability or energy output, there remains a great deal of on-going research into their improvement and application. The main aim of almost all renewable energy

technology is to reduce the amount of CO_2 being released into the atmosphere, and by extension, reduce the rate of global warming. The secondary focus is to find sources of energy that can be reused and replenished indefinitely. In 2016, the transportation industry was the second greatest worldwide producer of CO_2 after electricity and heating, accounting for nearly a quarter of all emissions (Figure 1.3).[29] This is largely due to the burning of petrol and diesel. Given the necessity of cars and other motorised vehicles to modern life, the transportation industry is beginning to consider the plethora of possible fuel alternatives to gasoline. Gasoline is produced from crude oil, a fossil fuel product predicted to be exhausted by 2070.[9] This underlines the urgency with which viable fuel alternatives must be found.
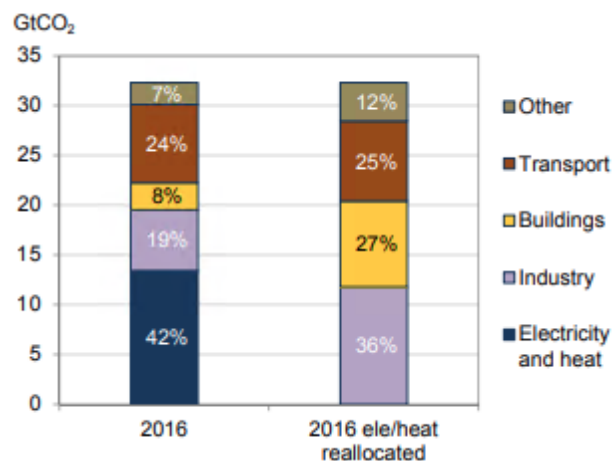
Figure 1.3: Global CO_2 emission divided across their respective industries.[29]

Currently, the most widely used gasoline alternatives are electricity, natural gas, hydrogen, propane and biofuels. While propane and natural gas have both been shown to produce lower levels of harmful emissions than gasoline, they are both still primarily derived from fossil fuels and as such do not represent a viable, long term fuel alternative. Electric cars on the other hand are an exciting and viable alternative to vehicles using standard internal combustion engines. Indeed this is one of the first alternatives to see commercial success with vehicles like the Hyundai Kona Electric, Audi e-tron and most famously the Tesla Model S all commercially available in many countries.[30] Electric cars produce zero CO_2 emissions during driving, and have the added advantage of saving money on fuel, as well as causing less noise pollution than conventional vehicles.[31] However, electric cars are not without their limitations, primarily low range and long recharge times. A great deal of the electricity

used also comes from non-renewable sources. This, coupled with the relative scarcity of recharge points compared to petrol stations, has meant that electric vehicles are yet to make a significant impact upon the automobile market. Although, their sales are increasing year on year.[32]

Hydrogen powered cars have also received a great deal a commercial attention in recent years, with the Hyundai Tucson FCEV being released in 2013. Much like electric cars, these vehicles offer a more environmentally friendly fuel alternative to gasoline with water as the only waste product generated. Hydrogen powered cars do not have the same issues with range and refill time found in electric cars. However, the production of hydrogen is energy intensive and requires the use of non-renewable feedstocks, while hydrogen transport requires low temperatures and high pressures and is potentially much more dangerous than gasoline.[33] As such, the infrastructure for fuelling hydrogen cars lags significantly behind that of electric vehicles.

To overcome some of the inherent limitations of electric and hydrogen powered vehicles, biofuels can be used and distributed with much of the current infrastructure, while still being significantly less environmentally damaging than conventional gasoline. As such, a great deal of research has been conducted into their potential use in the transportation industry.

1.3 – Biofuels

1.3.1 – Biodiesel

Biodiesel is one of three 'first generation biofuels' (alongside bioethanol and biogas). A first-generation biofuel can be blended with petroleum-based fuels for use in conventional internal combustions engines and transported using existing infrastructure.[34] It can sometimes be used as a drop in (direct replacement) for gasoline, however, this requires significant engine modification.

Biodiesels (or fatty acid methyl esters) are produced from triglycerides *via* transesterification with an alcohol, usually methanol, using a basic catalyst (Scheme 1.1). They are preferred over using triglycerides directly due to their significantly lower viscosity. While the first reported use of biodiesel came in 1837,[35] its use has seen a modern day resurgence with a renewed focus on sustainable and clean (non-polluting) fuel sources.[36]

Globally, biofuel production is becoming a major business, with 30 billion litres produced in 2014 alone,[15] and with usage increasing, standards such as the European standard EN 14214 have been introduced to govern the quality and composition of the fuel.[37] This dictates maximum levels of contaminates such as free glycerol and monoacylglycerides, and it also assigns maximum and minimum viscosities for the fuel.
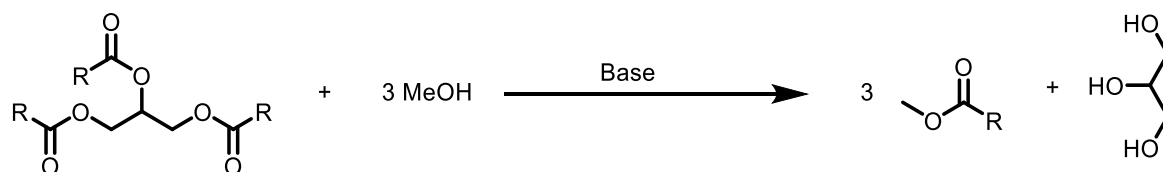
Scheme 1.1: Formation of biodiesel via transesterification of triglyceride. R represents different fatty acid chains.

Biodiesel has a flash point of 150 °C (the temperature at which vapours will ignite when exposed to a flame), which is significantly higher than the flash point of gasoline (55-66 °C),[38] meaning the fuel is safer to transport. It also has a higher cetane number (the speed of fuel combustion once injected into the engine) than regular diesel, so it can be used in conventional engines in low blends without the need for any alteration. Owing to its high oxygen content, and renewable source, biodiesel also produces 78% less CO_2 in its life cycle than regular diesel.[38] However, biodiesel is not without its drawbacks such as a high pour point (the temperature at which the fuel loses its flow characteristics), along with low oxidative stability (See Section 2.1 for more detail). The energy density of biodiesel is 12% lower than petroleum diesel, thus leading to higher fuel consumption and poor vehicle efficiency. Owing to issues like its higher viscosity and lower volatility than conventional diesel, minor engine modifications are needed to use blends over 20% (B20).[39]

1.3.2 – Bioethanol

Bioethanol as a first-generation biofuel is mainly produced by the fermentation of sugar or starch containing crops (Scheme 1.2)[34,40] in processes catalysed by yeast or bacterium, such as *Zymomonas moblis*, *via* enzymatic hydrolysis of starch. This is currently the dominant biofuel, accounting for over 73% of biofuel production in 2014.[15] One of the main issues with ethanol production by fermentation is that the ethanol produced is toxic to yeast bacteria in high quantities. However, recent genetic modification experiments have sought to increase bacterial tolerance to ethanol.[41]

Much bioethanol is produced using glucose as a feedstock which often comes from potentially edible crops. This ignites the 'food versus fuel' argument concerning whether it is ethical to use crops to make fuel instead of feeding people.[42] Furthermore there is a great deal of controversy surrounding the clearing of forests to produce farmland for bioethanol production.

As such, a great deal of research has been conducted into bioethanol production from non-edible biomass sources. This research focuses primarily on lignocellulosic feedstocks, often from agricultural residue, although grasses and forestry residues are other potential sources.[43] Bioethanol derived from this lignocellulosic biomass is regarded as a second generation biofuel, as its feedstocks is not also used for food production.[44] It can often be produced from agricultural waste which is otherwise burnt, preventing the release of CO_2 into the atmosphere in this manner. Lignocellulose is made up of cellulose, hemi-cellulose, lignin and solvent extractives, the exact chemical composition of this will dictate how efficient subsequent biofuel production will be.[44]
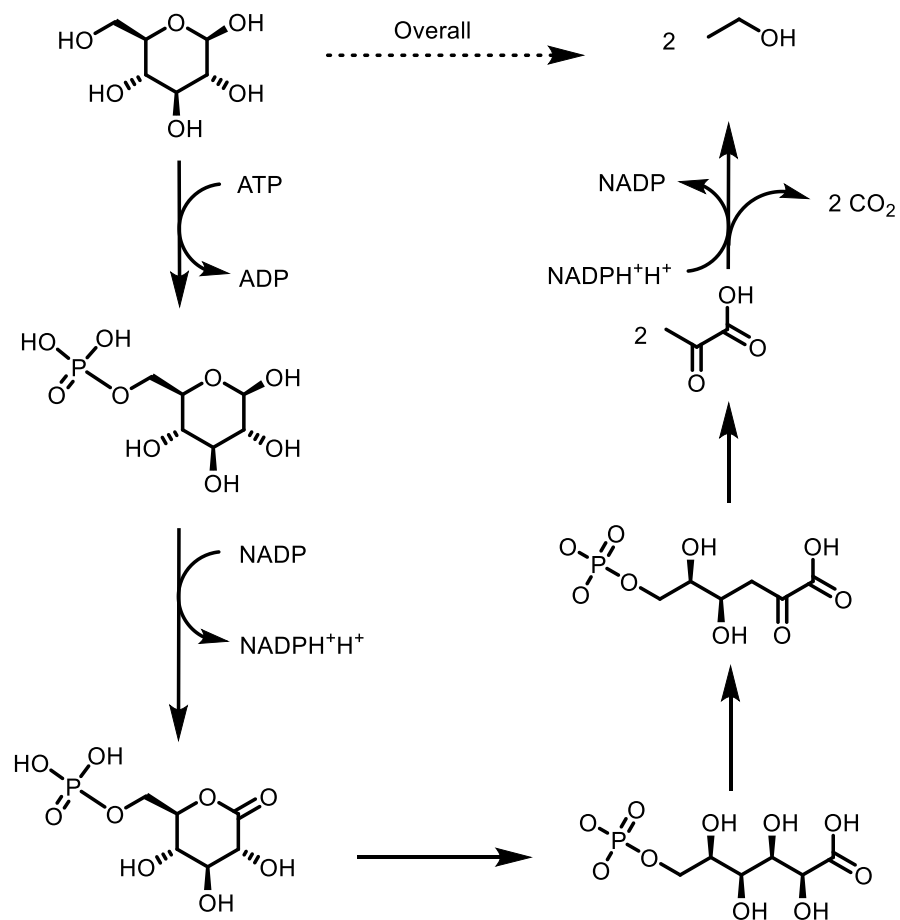
Scheme 1.2: Formation of ethanol from glucose using Zymomonas moblis (simplified).[40]

Despite its advantages, second generation bioethanol is not without some drawbacks. Several steps are required before a viable fuel is produced, including: pre-treatment (chemical, biological, mechanical or physicochemical), hydrolysis, fermentation and distillation.[45] The primary reason second generation bioethanol production is so challenging is it works from a polysaccharide based starting material, while fermentation bacteria are only able to digest simple sugars. Therefore, the long sugar chains making up cellulose and hemi-cellulose must be broken down before they can be used for fermentation. Hydrolysis breaks down these chains into glucose (in the case of cellulose) and a mixture of C5 and C6 sugars (in the case of hemi-cellulose) using either an enzymatic or acidic catalyst (Scheme 1.3). Enzymatic catalysts are currently considered too expensive for commercial use, however, they require much milder conditions than acid catalysed hydrolysis and thus are an area of current research interest.[46]
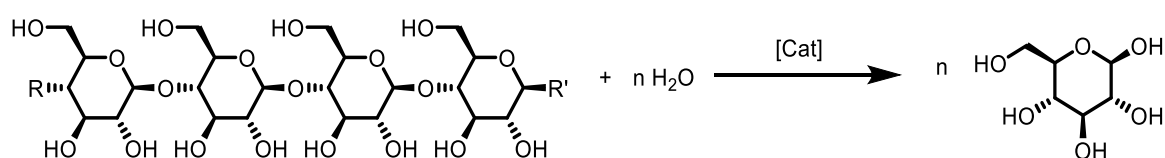
Scheme 1.3: Production of glucose from cellulose via hydrolysis using either an enzymatic or acidic catalyst.

Before hydrolysis is possible the lignocellulose also needs to be pre-treated. This fulfils many functions but is primarily to: reduce the physical size the material takes up, separate the cellulose from the hemicellulose and lignin, and to allow for easier break-up of the cellulose chains by hydrolysis. Pre-treatment reduces the level of crystallinity in the cellulose matrix, and increases the proportion of amorphous cellulose, which is more easily broken-down during hydrolysis.[45,47] Effective pre-treatment can significantly reduce the cost and energy demand of second generation bioethanol production. Given the large amount of pre-treatment required before fermentation of lignocellulosic feedstocks, it is perhaps unsurprising that this process lags behind conventional bioethanol production in terms of cost effectiveness.[47] Further work on streamlining the process of second-generation bioethanol production is required before it can compete commercially.

1.3.2.1 – Bioethanol as a fuel

Bioethanol has many properties that make it favourable for usage as a fuel. For example, it has preferable anti-knocking properties compared to gasoline (meaning it is less likely to

prematurely ignite), and it can also generate a higher product volume upon ignition, leading to greater efficiency from spark ignition engines.[48] However, ethanol is most commonly seen in fuel blends of 10%, this is known as E10 (10% ethanol, 90% gasoline). Higher blends such as E15 or E85 are in much less demand.[49] This is for a number of reasons, including ethanol's low energy density (roughly 67% that of gasoline) combined with its hygroscopic nature, meaning it readily absorbs water over time, leading to phase separation in storage tanks.[50,51] Pure ethanol also has a low vapor pressure, making starting the engine from cold challenging, and is corrosive to fuel tanks making long term storage problematic.[52] This corrosion is in part due to impurities like acetic acid in the ethanol, and in part due to the ethanol itself.[51] Ethanol-gasoline blends show a maximum volatility at around 5% ethanol, this then decreases as ethanol content increases with pure ethanol having lower volatility than pure gasoline. This increased volatility leads to greater fuel loss and increases the chance of explosion and may be a reason why 10% ethanol blends are more popular.[52]

Given the inherent properties of ethanol, it is unlikely to ever be used as a 'drop-in' replacement for gasoline. This leads to debate over its use as a renewable resource, given it requires gasoline to function. An ideal biofuel would be produced quickly and inexpensively from readily available resources (like bioethanol) but should also be able to be used as a direct replacement for gasoline, allowing it to be distributed using existing fuel infrastructure.

1.4 – Advanced biofuels

Second generation biofuels are often referred to as 'advanced' biofuels. This is due to their production from non-food-based feedstocks, along with their relative low cost and potential to provide long term solutions to the issues associated with fossil fuels. Advanced biofuels should also be able to be distributed and consumed using current infrastructure, with little to no modification required.[53] Due to the issues outlined in Section 1.3.2.1 it is arguable whether ethanol can ever be regarded as an advanced biofuel, as it is only practical to use in low percentage blends with gasoline. Ideal advanced biofuels need to be drop-in alternatives for gasoline, with little to no modification required.

1.4.1 – Butanol as an advanced biofuel

With the likelihood of ethanol being a viable long-term alternative to gasoline decreasing, attention has changed to other potential fuel sources. A major emerging option is biobutanol, given it has properties which are significantly closer to those of gasoline than ethanol (Table 1.1).

Butanol has a volumetric energy density that is 91% that of gasoline, a value significantly higher than ethanol (67%). This means that the distance a car could travel on a single tank of butanol is longer than when using the equivalent volume of ethanol, and is comparable to when gasoline is used as a fuel source. Butanol is also significantly less likely to absorb water than ethanol, possibly due to the increased influence of the hydrophobic carbon chain. Only 7.7 wt% water is soluble in butanol, whereas ethanol and water are completely miscible, which means butanol can be blended with gasoline well before distribution with no fear of degradation in fuel quality. The research octane number (RON) of ethanol is higher than both butanol and gasoline, meaning it is less likely to ignite upon compression and thus it is safer to transport and less likely to cause engine knocking. While this is advantageous as suppliers can buy low octane rated fuel and blend it with ethanol to increase its octane rating,[54] this does not give it any favourable fuel properties. This is because gasoline, with an octane number of 88-98, is already deemed safe for transportation. Butanol has also been found to be less corrosive than ethanol, meaning storage and use alongside current infrastructure is possible without fear of shortened lifespan.[55]

Table 1.1: Comparison of the properties of gasoline, ethanol, and n-butanol with relation to their use as fuel alternatives. Adapted from several sources.[56,57]

	Gasoline	Ethanol	*n*-Butanol
Energy Density (MJ L^{-1})	32	19.6	29.2
Latent heat of vaporisation (kJ kg^{-1})	352	919.6	707.9
Research Octane Number (RON)	88-98	109	98
Solubility of water in compound (wt%)	negligible	100	7.7
Air-fuel ratio	14.6	8.94	11.12
Viscosity at 20 °C (cSt)	0.37-0.44	1.5	3.6
Vapour pressure at 20 °C (kPa)	50-100	5.8	0.58
Auto ignition temperature (°C)	257	363	343
Boiling Point (°C)	27-225	78	117.7

The increase in vapour pressure seen at low ethanol-gasoline blends is due to disruption in the hydrogen bonding between the ethanol molecules (Figure 1.4). Hydrogen bonds help to reduce the vapour pressure of pure ethanol below what would be expected for its molecular size, but when these bonds are interrupted by ethanol dilution this effect is no longer seen, and thus ethanol can more readily evaporate. When considering butanol this effect is much less pronounced due to the longer carbon chain increasing solubility in gasoline. As a result, butanol blends of any proportion have a lower vapour pressure than pure gasoline,[56] which is both advantageous and detrimental when considering using butanol as a fuel. Although higher vapour pressures make starting engines in cold air easier, the lower vapour pressure displayed by butanol results in less unwanted fuel loss in hot temperatures[56] The unwanted evaporation of ethanol from gasoline-ethanol blends can lead to an increased concentration of water and other corrosive impurities in engines, reducing efficiency and lifetime. As butanol-gasoline blends have a lower vapour pressure than pure gasoline this is not an issue. Lower vapour pressures also reduce the risk of fire and explosion, and thus makes transportation safer.[55] While butanol has a lower vapour pressure than ethanol, it also has a lower autoignition temperature, which can actually make starting engines in cold weather easier.[58]
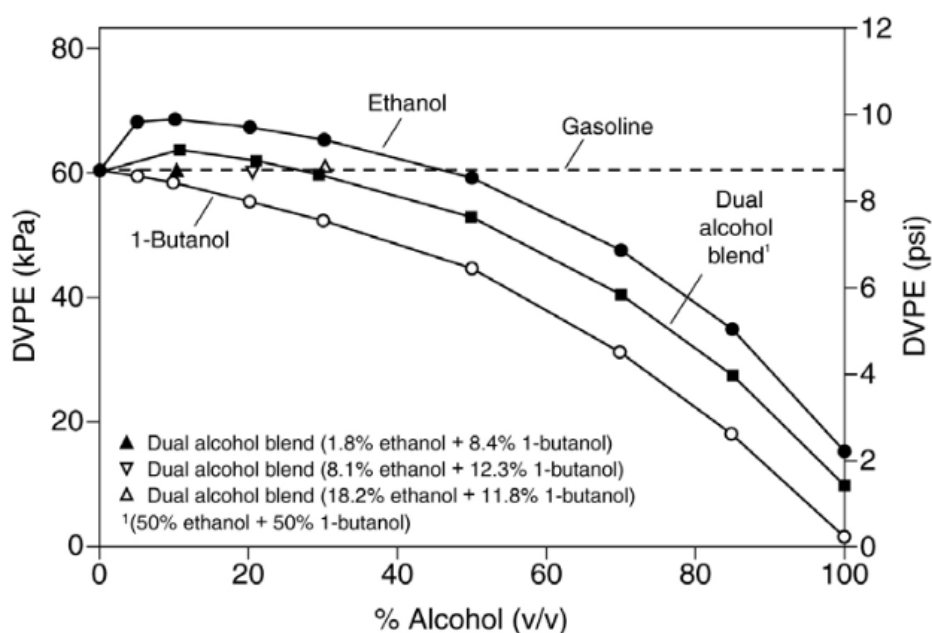
Figure 1.4: The effect on dry vapour pressure (DVPE) of different percentage blends of ethanol and butanol in gasoline.[59]

The advantageous properties of *n*-butanol over ethanol mean it can be transported and stored using current infrastructure without issue. Also, it can be used in blends of any concentration, or as a neat fuel, in modern car engines without the need for any modification. Therefore, butanol is a prime candidate for use as an advanced biofuel.

1.5 – Current Butanol Production

For butanol to be considered a possible gasoline replacement, production on a large industrial scale at low cost must be possible. Furthermore, for butanol to qualify as an advanced biofuel it will have to be produced from renewable resources and not impact any food crops or rely on currently used feedstocks.

1.5.1 – The Oxo process

Butanol, along with various other primary and secondary alcohols can be produced *via* the Oxo process (Scheme 1.4). For butanol specifically this process involves the hydroformylation of propene. This process was first discovered by Otto Roelen in 1938 and initially used cobalt or iron catalysts supported on silica,[60,61] although the process was later expanded towards homogeneous catalysts containing a variety of different metal centres supported by phosphine or arsine ligands.[62,63] Industrially, the use of rhodium catalysts is preferred as they are 100-1000 times more active than the equivalent cobalt complexes.[64]
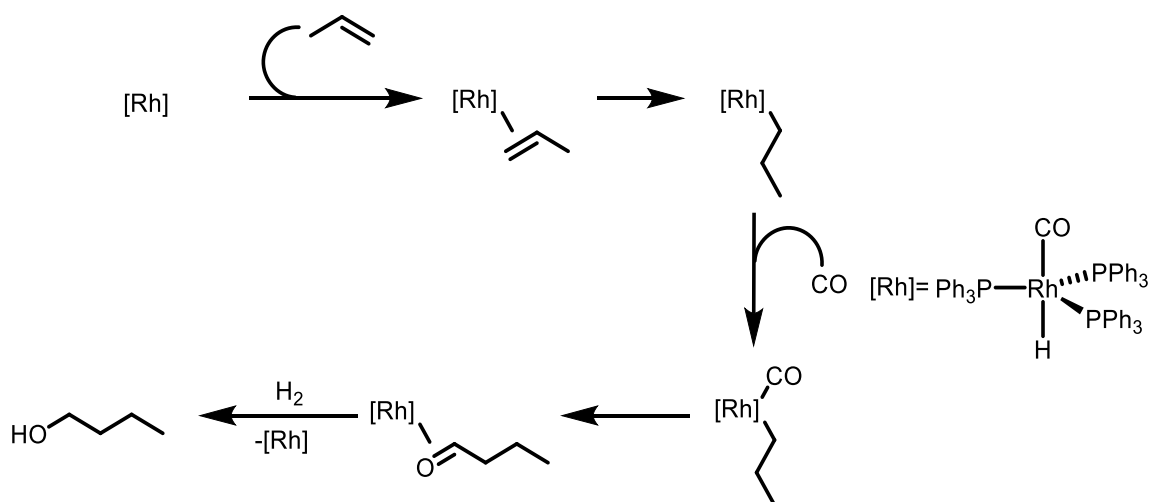
Scheme 1.4: Formation of n-butanol via hydroformylation of propene and an example of one of the most common rhodium catalysts.[65, 64]

Formation of the branched isomer *iso*butanol is also possible *via* this process (Scheme 1.5), and selectivity is highly dependent on the catalyst, loading and synthesis gas concentration. For example, rhodium carbonyl complexes give greater proportions of the branched isomer, although this selectivity can be completely suppressed by the addition of phosphines or arsines to the catalyst system.[64] Butanol formation by this method requires propene and synthesis gas, both of which are derived from fossil fuels. As such, this process is not a viable option for biofuel production.
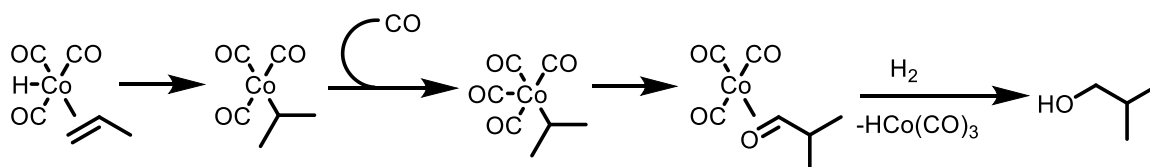
Scheme 1.5: Formation of isobutanol via hydroformylation of propylene.[65]

1.5.2 – ABE process

Sustainable production of butanol is possible from the fermentation of sugars. This is known as ABE (acetone, butanol, ethanol) fermentation and employs the bacterium *Clostridium acetobutylicum*. As its name suggests both ethanol, and acetone are produced as well as butanol, however, this is in a 3:6:1 ratio, so butanol is still the major product (Scheme 1.6). Industrialisation of the ABE fermentation process began in 1912, making it one of the oldest commercial fermentation processes,[58] but as the production of butanol *via* the Oxo process became cheaper, ABE fermentation fell out of favour. The main issue with ABE fermentation is self-inhibition due to the toxicity of *n*-butanol to the culture,

where some of the highest reported yields before culture death are just 3 wt%.[66] However, this situation can be improved by using techniques such as vacuum fermentation, where toxic products like butanol are removed by applying a vacuum to the bioreactor.[67] The possibility of improving butanol yields by genetic modification of the bacteria involved is also an area of ongoing research.[68]
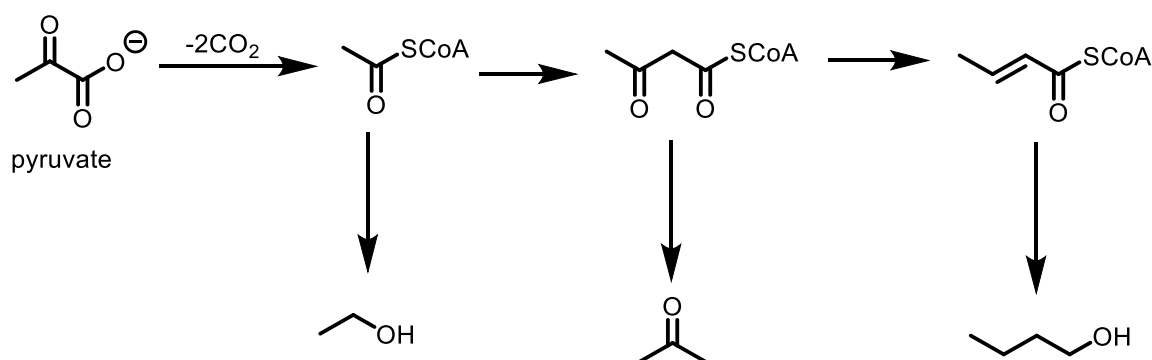
Scheme 1.6: *Abridged ABE fermentation pathway. Pyruvate produced from the fermentation of glucose[69] (SCoA = S-coenzyme A).*

Fundamentally, butanol production via ABE fermentation suffers from the same issue as first-generation bioethanol production as it requires glucose from biomass as a feedstock. This once again is subject to the 'food-versus-fuel' debate. Furthermore, production of butanol *via* this process is 10-30 times slower than pure ethanol production from fermentation by yeast, which makes bioethanol production a more attractive commercial process.[58] Butanol production from lignocellulosic biomass is currently under investigation. However, this process is still far from commercial viability.[70,71]

While production of butanol *via* ABE fermentation is sustainable, it is not practical for large scale synthesis. As such, a method of producing butanol in a high yield and selectively from cheap and abundant feedstocks needs to be developed before the possibility of it rivalling gasoline as a fuel can truly be considered. One potential method currently under investigation is the coupling of two ethanol molecules to produce one molecule of *n*-butanol, by transition metal catalysis.

1.6 – Ethanol coupling *via* the Guerbet reaction

The coupling of two primary alcohols mediated by a basic catalyst was first reported in 1899 by M. Guerbet.[72] This protocol required high temperatures (>300 $^\circ$C) and no transition

metal cocatalyst was used, however, later work found that the addition of a Raney-Ni catalyst significantly improved yields.[73,74] It was not until the late 1960s that Veibel and Nielsen proposed a general reaction mechanism (Scheme 1.7).[75] This proceeds by dehydrogenation of the alcohol, generating the analogous aldehyde (step 1) which then undergoes rapid base catalysed aldol coupling followed by dehydration to generate the longer chain α,β-unsaturated aldehyde (step 2). Finally, this is re-hydrogenated to produce the longer chain alcohol Guerbet product (step 3). The only by-product of this reaction is water, therefore the reaction is regarded as being atom economical and sustainable.
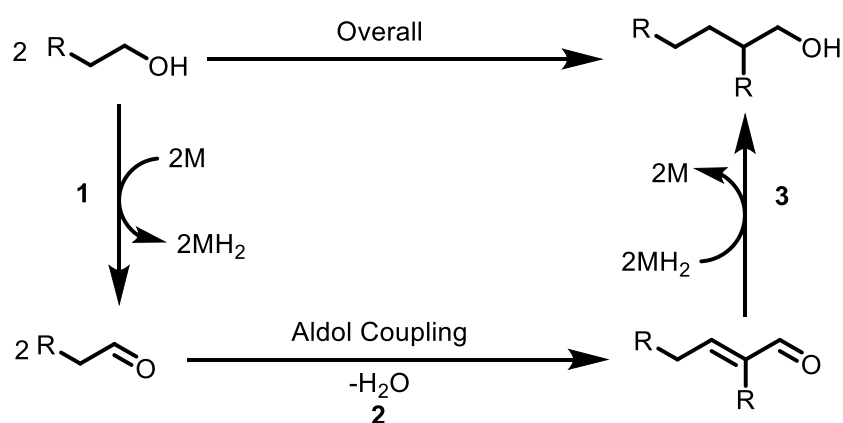
Scheme 1.7: The mechanism of the Guerbet reaction, as proposed by Veibel and Nielsen.[75]

This type of chemistry is often referred to as 'borrowed hydrogen' chemistry, as it requires no external hydrogen source for hydrogenation to occur.[76] The hydrogen removed from the substrate in step 1 is redelivered to the coupled product in step 3 (Scheme 1.7). Borrowed hydrogen chemistry has wider scope than just the Guerbet reaction and has also been applied to C-N bond formation *via* the coupling of alcohols and amines.[77] As there is no need for molecular hydrogen, borrowed hydrogen processes are often compared to transfer hydrogenation (the addition of hydrogen to a molecule from a non-H_2 source). However, in transfer hydrogenations a dehydrogenated by-product is also produced during reaction, so it can be considered less atom economical. As both processes do not involve the use of high hydrogen pressures, they are considered much safer than conventional hydrogenation reactions.[78]

One key issue with this reaction is a fundamental lack of selectivity, as the higher alcohol produced can re-enter the cycle as a reactant. This can lead to a complex mixture of higher alcohol products requiring further separation. This issue is seen particularly in the case of

ethanol coupling where minor products of C6, C8 and even C10 alcohols can be produced alongside the major C4 product. A limiting factor in the application of this chemistry towards ethanol upgrading is its extremely high energy of dehydrogenation. Dehydrogenation of alcohols becomes more facile as the chain length increases, and as such it is unsurprising that shorter chain alcohol coupling is rarely observed without a transition metal catalyst.[79]

The development of cheap and effective catalysts for the conversion of ethanol to butanol is of vital importance if butanol is to become an effective and widely available biofuel.

1.7 – The development of transition metal Guerbet catalysts

As mentioned above, most early work on catalysts for the Guerbet reaction focused on heterogeneous systems using Raney-Ni or metal oxides.[80] Homogeneous catalysts emerged in 1972 with a seminal paper by Ugo *et al.,* who reported the use of tertiary phosphine metal complexes for the coupling of *n*-butanol to form 2-ethylhexanol.[81] Unlike the previous heterogeneous systems, these reactions could be performed at relatively mild temperatures (120 °C). In 1985 this work was expanded upon by Burk *et al.* who applied a rhodium system **1.1** to the coupling of both *n*-butanol and *n*-pentanol (Figure 1.5).[82] Here it was found that the addition of a bidentate 1,1-bis(diphenylphosphino)methane (dppm) ligand, **L1**, gave better yields of the Guerbet alcohol, but it was later established that most of the observed reactivity was due to the formation of a heterogeneous catalyst. These systems were highly moisture sensitive, which is problematic considering water is the sole by-product of Guerbet coupling. This work also showed the importance of an alkoxide cocatalyst for product formation.
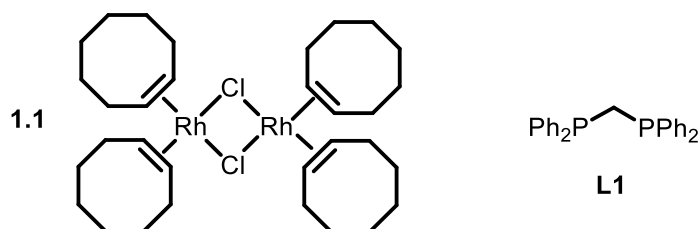
Figure 1.5: A homogeneous system for the coupling of butanol and pentanol.[82]

In 2004 Carlini *et al*. reported a variety of homo- and heterogeneous systems for *n*-butanol coupling using palladium catalysts at 200 °C. A Pd(II) metal centre supported by a bidentate 1,2-bis(diphenylphosphino)ethane (dppe) ligand was found to be just as effective as

heterogeneous Pd/C. Both this system and the Burk system discussed above are slowly deactivated over time due to hydrolysis of the alkoxide base by water produced from Guerbet coupling.[82,83]

More recently, Ishii and co-workers have reported a variety of different iridium catalyst precursors for the coupling of a plethora of long chain primary alcohols.[84] This was also one of the first examples of a branched alcohol being coupled, with the homocoupling of 3-methylbutan-1-ol giving a 50% yield of the highly branched alcohol product shown in Scheme 1.8. This system used *p*-xylene as a solvent and required the addition of 1,7-octadiene as a hydrogen acceptor. The role of the diene in this reaction is not completely clear, however, it seems likely that it is involved with catalyst activation as much lower conversions are reported without it. Furthermore, even with the addition of the hydrogen donor, a 2-hour pre-activation period was required before addition of the alcohol. It is of note that this system showed significantly higher water tolerance than any of those previously reported.
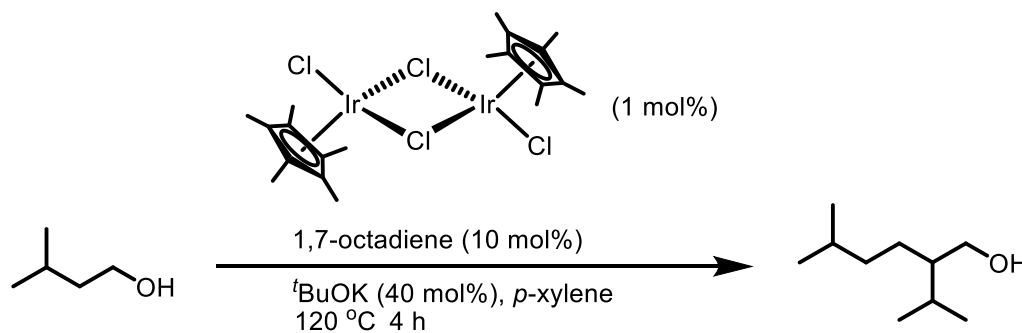
Scheme 1.8: Homocoupling of 3-methylbutan-1-ol using an iridium based catalyst, as reported by Ishii et al.[84]

1.7.1 – Homogeneous catalysts for the coupling of ethanol

In 2009, Ishii reported the first truly homogeneous system for the homocoupling of ethanol to *n-b*utanol.[85] This system used the iridium pre-catalyst **1.2**, this time bearing acetylacetonate and cyclooctadiene ligands (Scheme 1.9), that facilitated turnover numbers (TON) as high as 1220. Again, a hydrogen donor, along with an alkoxide base was required for high substrate conversion. Unlike the previous Ishii system (shown in Scheme 1.8), a variety of phosphine ligands were used in combination with the iridium pre-catalyst, with the active catalyst being formed *in situ*. Here, bidentate ligands were found to be superior to monodentate ligands and increasing the bite angle of the ligand (ie. moving

from dppe to dppp) increased activity, although increasing the ligand bite angle further and using dppb decreased activity again. It was found that using the corresponding alkoxide base to the alcohol being coupled, in this case sodium ethoxide, gave the greatest yields.
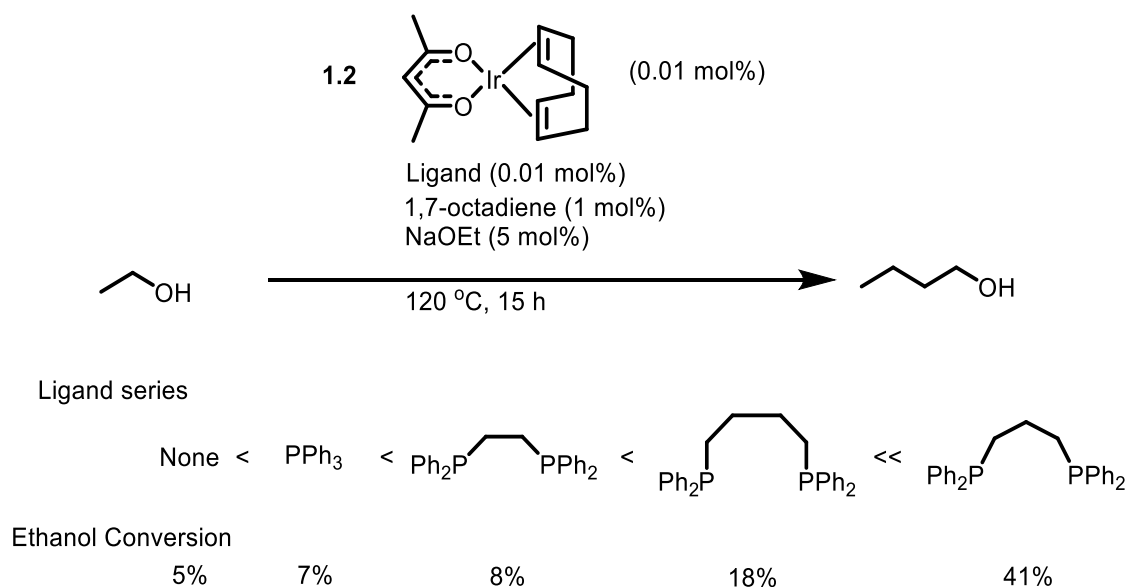
Scheme 1.9: Production of n-butanol from ethanol as reported by Ishii et al., and the effect of phosphine ligands on ethanol conversion.[85]

Despite ethanol coupling *via* homogeneous catalysis finally being realised, selectivity remains an important issue. When utilising the dppp ligand, selectivity to butanol was only 51% with large amounts of higher alcohols like *n*-hexanol, 2-ethylbutanol, *n*-octanol and 2-ethylhexanol also being produced. While it gave lower conversion, the use of dppb did increase selectivity to 67%. Once again, this system required the addition of 1,7-octadiene, and Ishii *et al.* proposed that this may act as a weakly coordinating ligand to stabilise the intermediate iridium species. As the net Guerbet reaction is hydrogen neutral, it seems likely this hydrogen acceptor is required only for catalyst initiation. If it was removing hydrogen from the system, greater quantities of non-Guerbet products such as ethyl acetate or metal acetates (formed *via* Tishchenko and Cannizzaro type chemistry) would be seen (see Sections 3.6 and 4.2.3 for further information) .[86]

Ruthenium has previously shown activity for borrowed hydrogen chemistry,[77,87] and in a 2010 patent, a variety of ruthenium precursors were used for the homocoupling of ethanol (Figure 1.6).[88] In the above patent, these precursors were combined with triphenylphosphine, generating the active catalyst *in situ*. Using 0.18 mol% **1.3**, along with 1 mol% PPh$_3$, 3.5 mol% ^{t}BuOK and 3.1 MPa H$_2$ at 180 °C for 3 hours, butanol yields of 20%

with selectivities as high as 92% were observed. Similar yields could be obtained with a lower hydrogen pressure and PPh$_3$ loading by using pre-catalyst **1.4** and *o*-xylene solvent. While acceptable yields and high selectivities were possible, the requirement for high hydrogen pressure was an issue.

1.3   **1.4**
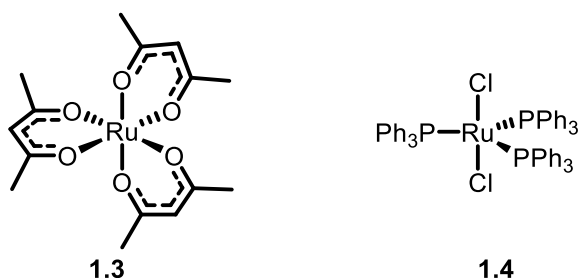
Figure 1.6: Ruthenium precursors used for the homocoupling of ethanol.[88]

1.7.2 – Previous Wass group Guerbet systems

The Wass group reported a variety of ruthenium based systems for the coupling of ethanol to *n*-butanol in 2013[89] that showed unprecedented activity for ethanol conversion and selectivity for *n*-butanol (Scheme 1.10). The active catalyst was formed *in situ*, using **1.5** as a precursor to produce a monochelate complex. While ligands **L1 – L3** were all active for *n*-butanol formation, the small bite angle diphosphine **L1** was by far the most active giving an *n*-butanol yield of 17.5% in 90% selectivity over just 4 hours. Interestingly, this is the opposite effect to that observed by Ishii *et al.*, where larger bite angle ligands performed better.[85] While these catalysts showed impressive activity over short run times, they suffered from a lack of stability with little further activity observed by extending run times to 20 h. Stability could be improved by adding an extra equivalent of ligand to the catalytic system, so that the ligand and **1.5** were in a 3:1 molar ratio. While this resulted in a slight decrease in activity, it almost completely halted catalyst decomposition. These catalysts were able to surpass the monochelate systems in terms of *n*-butanol production by increasing run time, albeit at the cost of selectivity. When 2 equivalents of the ligand were added the bis-chelate complexes (**Cat-1 – Cat-3**) were formed (Figure 1.7). If these complexes were pre-formed, they showed equivalent or superior activity to formation *in situ* (32.6% *n*-butanol, 85.1% selectivity over 20 h for **Cat-1**)*.*
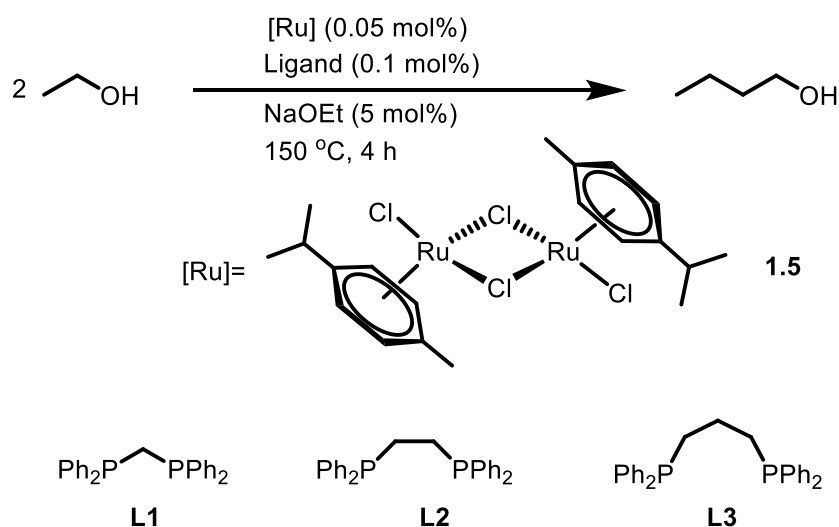
Scheme 1.10: Ruthenium pre-catalyst and ligands for the conversion of ethanol to butanol.[89]

It is of note that this system doesn't require a hydrogen acceptor, or high hydrogen pressures in order to show significant activity. The very high selectivity of this reaction (regularly above 90%) was proposed to be due to catalyst influence over the aldol condensation step. Thus, formation of C4 alcohols was promoted, whilst higher alcohol formation was suppressed.
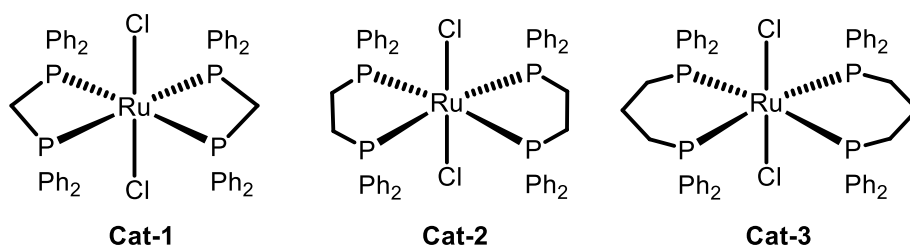
Figure 1.7: Ruthenium bis-chelate complexes for the formation of n-butanol from ethanol[89]

In 2015, the Wass group reported a set of phosphinoamine ligands, which when complexed to ruthenium were also active for *n*-butanol formation from ethanol (Figure 1.8).[90] Once again when these ligands were coordinated to **1.5** in a 1:1 ratio they showed high activity but poor stability, and when the bis-chelate **Cat-4** was preformed, stability was again significantly increased. **Cat-4** was significantly more active than **Cat-1**, the most active catalyst from the previous study, and facilitated the formation of *n*-butanol with a 17.1% yield and 93.5% selectivity over 4 hours. The presence of an N-H moiety (**L4/L5**) was found to aid reactivity; much lower yields were reported when the dimethylated ligand **L6** was used instead (12.1% over 4 hrs). It is postulated that this is because **L4** and **L5** can work *via*

an outer sphere mechanism, whereas **L6** cannot. The **L4**-monochelate complex also shows greater water tolerance than the **L1** complex.
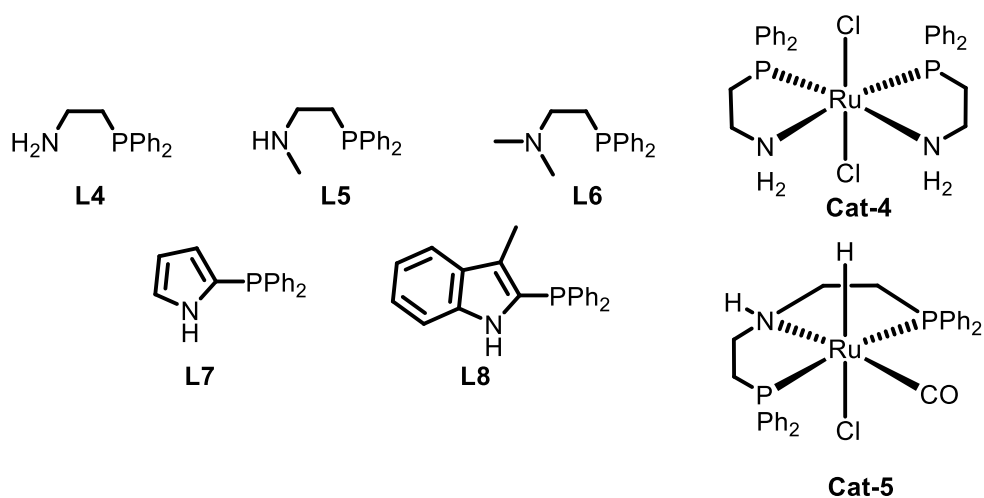
Figure 1.8: A variety of phosphinoamine ligands and Ru complexes used for n-butanol formation from ethanol.[90]

The commercially available tridentate pincer complex Ru-MACHO (**Cat-5**) was also applied to this reaction. This catalyst had previously been used for the production of ethyl acetate from ethanol in an open system at 80 °C.[91] However, under Guerbet conditions (150 °C, sealed reaction vessel) **Cat-5** still favours the formation of ethyl acetate over *n*-butanol (only 12.4% selectivity). This shows the dramatic effect that the ligand can have upon overall activity. Mechanistic work using **L4**, along with **1.5** showed the formation of a Ru-hydride species believed to be the active catalyst.[90]

1.7.3 – *Iso*butanol formation *via* Guerbet chemistry

*Iso*butanol has even more favourable fuel properties than its linear analogue, such as a higher RON and fuel density.[92] Hence, its formation from sustainable feedstocks is also of interest. However, *iso*butanol cannot be formed *via* the simple homocoupling of ethanol, instead it can be made by the heterocoupling of ethanol with two molecules of methanol *via* a Guerbet mechanism (Scheme 1.11).
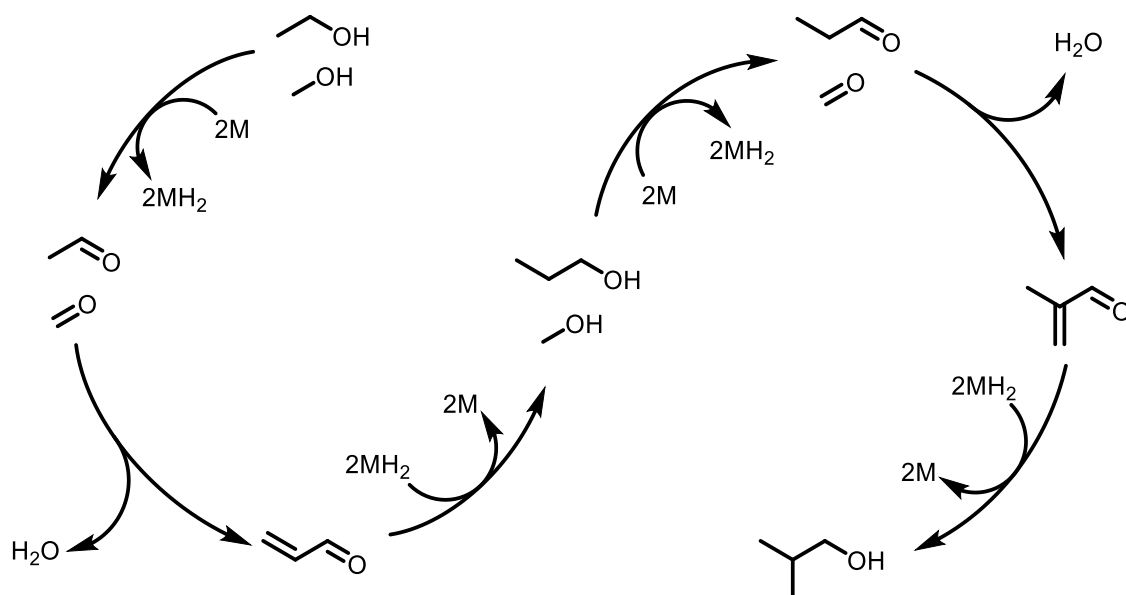
Scheme 1.11: Formation of isobutanol from methanol and ethanol.

In this process methanol and ethanol are dehydrogenated to formaldehyde and acetaldehyde respectively. These then react *via* aldol coupling to form acrylaldehyde, which is subsequently hydrogenated, forming propanol. Propanol can then re-enter the cycle with another molecule of methanol to produce *iso*butanol, which will not react any further as it contains a tertiary β-carbon. The formation of *iso*butanol from methanol requires two Guerbet cycles to form the product, as such, two molecules of water are produced for every molecule of *iso*butanol. Therefore, any catalyst used for this process must exhibit water stability. Much like ethanol, it is also possible to produce methanol from renewable sources using processes such as the pyrolysis of hydrogen and carbon monoxide, or by using methanotrophic bacteria such as *Methylosinus trichosporium* to oxidise methane.[93]

Previous examples of *iso*butanol formation have predominantly revolved around heterogeneous catalysis. In 2003 Carlini *et al.* reported the production of *iso*butanol from ethanol and methanol, and from propanol and methanol. This work predominantly focussed on a heterogeneous copper chromite catalyst, although Raney-Cu was also found to work.[94] Carlini *et al.* also reported a homogeneous system for the coupling of propanol and methanol using a [PdCl$_2$(dppe)] pre-catalyst, which gave a high propanol conversion (84.2%) over just 6 hours at 200 °C under 30 atm N$_2$ along with 160 mol% NaOMe. However,

substantial solid deposition during the reaction was observed and catalytic activity was attributed to both homo- and heterogeneous species.[95]

In 2016, the Wass group reported one of the first truly homogeneous systems for the production of *iso*butanol from ethanol and methanol (Scheme 1.12).[96] It was found that both catalysts **Cat-1** and **Cat-4** were highly active for this conversion, with **Cat-1** giving 66.4% ethanol conversion, along with 98.1% selectivity to *iso*butanol. Complexes **Cat-2** and **Cat-3** were significantly less active, facilitating only 3.3% and 4.7% ethanol conversion respectively. Due to the two Guerbet cycles required to produce *iso*butanol, and the two equivalents of water this produces that hydrolyse the NaOMe base, high base loadings of 200 mol% were required. While such a high base loading in not desirable, reducing base loadings to 100 or 50 mol% led to a significant reduction in the activity of the system therefore high base loadings were maintained. Surprisingly, **Cat-5** which showed little activity for *n*-butanol formation, proved to be an active catalyst for *iso*butanol production giving 48% ethanol conversion over 2 hrs.[97] High selectivity to *iso*butanol over various ethanol homocoupling products is assured by conducting the reaction in a large excess of methanol (14.4:1 molar ratio), and as a result the major by-product observed is propanol. In this system, **Cat-1** showed remarkable water tolerance, with no adverse effect upon reactivity caused by the addition of 200 mol% water before a catalytic run.[96] As such, **Cat-1** could be used for the production of *iso*butanol from ethanol containing beverages, mimicking the environment found in an alcohol fermentation broth.[97]
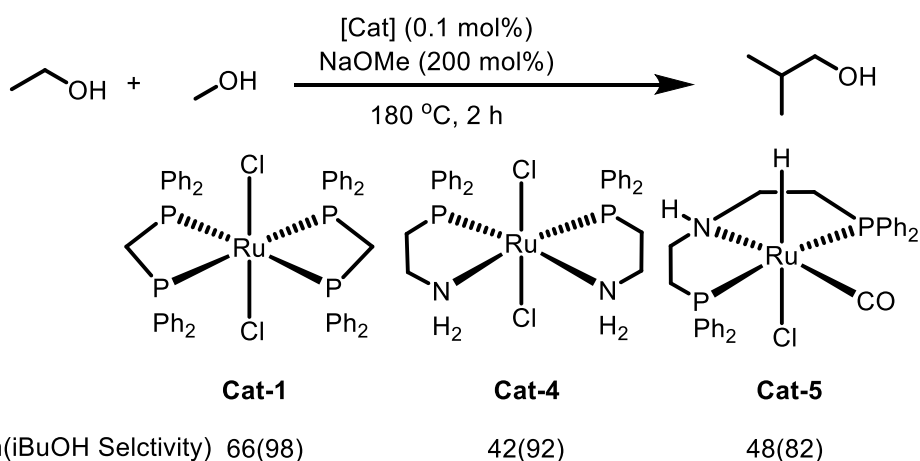
Scheme 1.12: Production of isobutanol using a variety of homogeneous ruthenium(II) catalysts.[96,97]

1.7.4 – More recent Guerbet systems

Since the reporting of the initial Wass system in 2013, several other ruthenium based Guerbet catalysts have been reported. In 2016, Szymczak *et al.* reported a tridentate NNN-ruthenium complex (**1.6**) for *n*-butanol formation (Figure 1.9).[98] This catalyst gave yields up to 38% (84% selectivity) over 2 h and showed impressive air stability, with little change in reactivity seen even when an inert atmosphere was not used. Deactivation of **1.6** was found to occur due to substitution of a PPh$_3$ ligand with CO (generated by ethanol decarbonylation). Phosphine dissociation and therefore deactivation could be suppressed by the addition of an extra equivalent of PPh$_3$ to the reaction mixture.

Milstein *et al.* reported a series of tridentate pincer ligands for *n*-butanol formation from ethanol, the most effective of which, **1.7**, is shown below (Figure 1.9).[99] This complex gave *n*-butanol in a 35.9% yield with 68.1% selectivity over 16 h. While this system is more active than that reported by Szymczak, it is also much less selective, given this poor selectivity hexanol production could be targeted using **1.7**. Using elevated base loadings (20 mol% NaOEt) and long reaction times (40 h), hexanol selectivity could be increased to 31.9%, only 4.4% was produced by a 16 h run with 4 mol% NaOEt. While butanol is still the major product (60.9% selectivity), this is the greatest hexanol selectivity exhibited by any of the discussed systems.

1.6   **1.7**
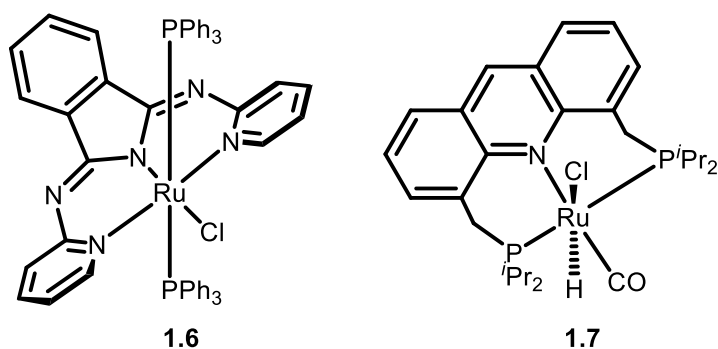
Figure 1.9: Homogeneous catalysts used by Szymczak[98] and Milstein[99] for the formation of n-butanol from ethanol.

Further Guerbet systems using iridium-based catalysts have also been reported. One such system, reported by Jones and Baker, uses catalyst **1.8** with bulky inorganic base **1.9**, producing *n*-butanol with a selectivity >99% along with an ethanol conversion of 37% (Figure 1.10).[100] The inorganic base promotes the coupling of acetaldehyde over longer chain aldehydes and is responsible for the incredibly high selectivity observed. When **1.9**

was applied to the coupling of 1-butanal only trace amounts of the C8 product were observed. If ^{t}BuOK base is used instead this results in a much lower selectivity of only 61%. However, **1.9** was completely inactive for the dehydrogenation of ethanol to acetaldehyde, whereas **1.8** can facilitate this with 21% conversion over 24 h. As such, both complexes are required for *n*-butanol production. The coupling of both ethanol and butanol using immobilised iridium catalysts under aqueous conditions in air has also been reported and this system was later applied to *iso*butanol formation as well.[101,102]

1.8 **1.9**
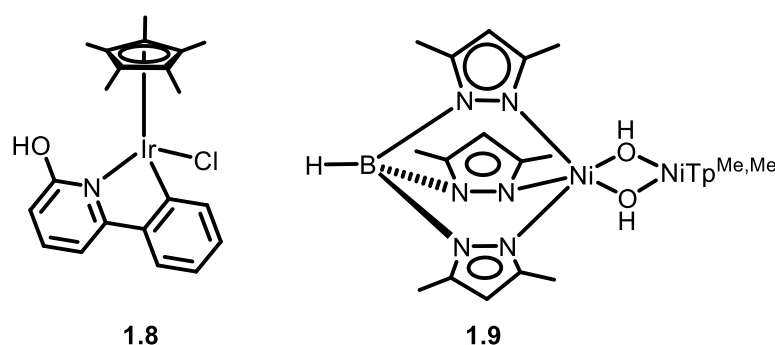
Figure 1.10: Catalyst and inorganic base system used by Jones and Baker for the formation of n-butanol from ethanol.[100]

Recent research into the Guerbet reaction has focused on the selective β-methylation of higher alcohols using methanol, which is a natural development from *iso*butanol formation chemistry. In 2014, Beller *et al.* published the use of **Cat-5** alongside Shvo's catalyst (**1.10**) for the β-methylation of a variety of 2-arylethanols (Scheme 1.13).[103] This system required run times of 45 h to achieve good product yields, and no information about overall selectivity was given. A dual catalyst system was chosen as **1.10** promoted the dehydrogenation of 2-arylethanols, whereas **Cat-5** was able to de/hydrogenate methanol and the aldol coupled product. The venting of hydrogen pressure from the system during reaction was found to be beneficial for overall yield, as in doing so, the equilibrium was shifted towards the aldol product.
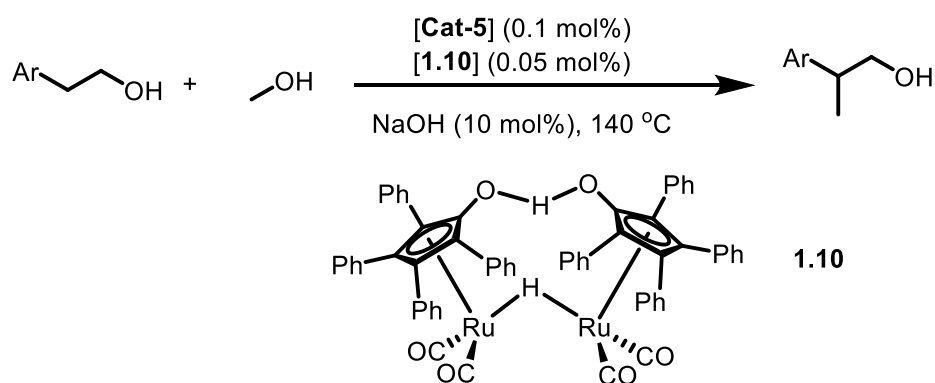
Scheme 1.13: Methylation of 2-arylethanols using a dual catalyst system.[103]

More recently, the Leitner group has expanded upon this, using **Cat-6** in a system that demonstrated TONs of over 18,000 (Figure 1.11).[104] This system could be used for the mono- and di- methylation of a variety of primary and secondary aliphatic and aromatic alcohols. Reaction times were significantly lower than those reported by Beller *et al.* (24 h), and yields were higher. However, it is worth noting that when this system was used for the upgrading of ethanol to *iso*butanol a yield of only 17% was observed, significantly worse than that seen above in the Wass system (Section 1.7.3). DFT studies on the mechanism indicated that rehydrogenation is the rate determining step.[105] Non-noble metal complexes based around manganese (**Cat-7**)[106] and iron (**Cat-8**)[107] (Figure 1.12) have also recently been applied to the β-methylation of alcohols. While this iron complex was effective for the methylation of primary alcohols, when secondary alcohols were used, only low product yields were observed.
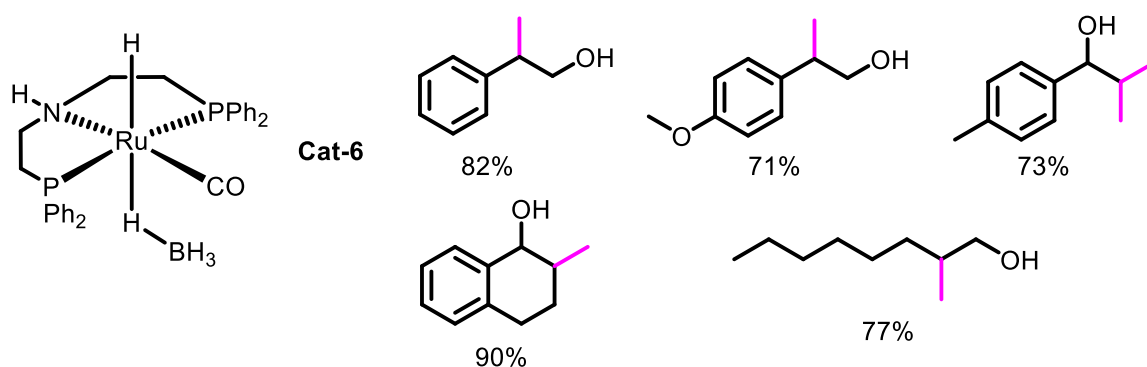
Figure 1.11: Catalyst used for the β-methylation of alcohols, and a variety to the branched alcohols produced with yields (the inserted methyl branch is indicated in pink).[104]
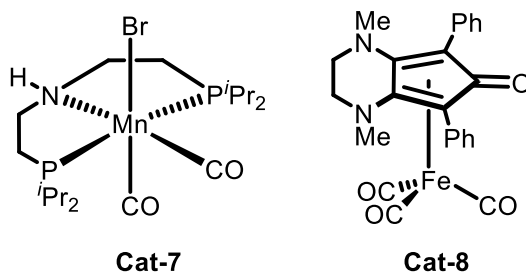
Figure 1.12: Base metal catalysts used for the β-methylation of alcohols.[106,107]

1.8 – Homogeneous manganese catalysts

Much recent homogeneous catalysis research is focused on relieving the dependence on expensive precious metals like ruthenium, rhodium and palladium by replacing them with abundant first row metals, like iron and manganese. Molecular manganese catalysis is currently receiving a lot of attention, where the majority of this work is based around Mn(I) due the diagonal relationship it has with Ru(II) on the periodic table. Ru(II) complexes are some of the most abundant in homogeneous catalysis, particularly for carbonyl hydrogenation reactions (complexes **Cat-1** – **Cat-6** are all based on Ru(II) metal centres). Mn(I) and Ru(II) both have a d^6-electron count, therefore when they are octahedral and low spin, they form diamagnetic complexes; as a result detailed analysis by NMR spectroscopy is possible, which may be a reason why these oxidation states are the most heavily researched.

In 2016, Beller *et al.* reported a series of Mn(I) pincer complexes supported by 'MACHO'-style (bis(phosphino)ethylamine) ligands (**Cat-7**, **1.11**) and their use in the hydrogenation of ketones, aldehydes and nitriles (Figure 1.13).[108] Complexes **1.11 – 1.13** are air stable and highly active allowing for almost quantitative conversion of benzonitrile to benzylamine. It was proposed that catalysis occurs *via* an outer sphere mechanism, and thus that a secondary amine in the backbone was essential for reactivity. Fuelled by the initial success of these complexes, the Beller group used them for ester hydrogenation, the N-alkylation of amines, transfer hydrogenation and the total dehydrogenation of methanol, highlighting the versatility of the catalysts.[109–112] They were also utilised for the α-alkylation of ketones with primary alcohols, displaying their ability to catalyse borrowed hydrogen type reactions, and indicating the potential for their use in Guerbet chemistry.[113] This paper also confirmed the importance of the secondary amine in the ligand backbone, with a

significantly lower product yield recorded when the N-methylated complex **1.13** was used instead.
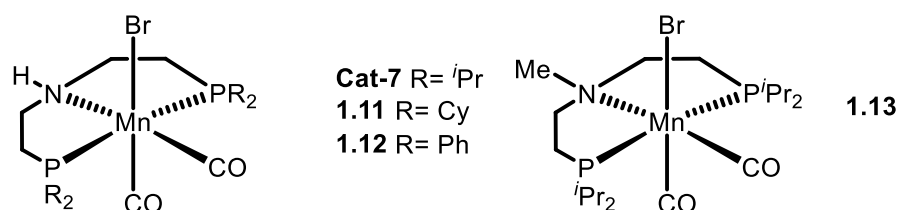
Figure 1.13: Manganese pincer complexes used for a variety of different catalytic processes.[108–113]

Both the Milstein (**1.14**)[114] and Kirchner (**1.15**)[115] groups have also reported the formation of manganese pincer complexes and shown their catalytic ability for the hydrogenation of esters, and the synthesis of quinolines respectively (Figure 1.14). Removal of HBr from **1.14** was possible, forming an unsaturated 5 coordinate complex believed to be the active catalyst. Indeed, this catalyst was active for ester hydrogenation even without the addition of base. It is worth noting that **1.14** showed no activity towards nitrile hydrogenation, whereas **Cat-7** unselectively hydrogenated all CN and CO functional groups trialled. For **1.15**, methylation of the secondary amine pincer linkers completely stopped reactivity, once again showing the importance of the N-H group to catalytic function, even when not directly coordinated to the metal. The synthesis of an assortment of Mn-pincer complexes and their uses in a variety of different catalytic processes are included in a detailed review by Mukherjee and Milstein.[116]
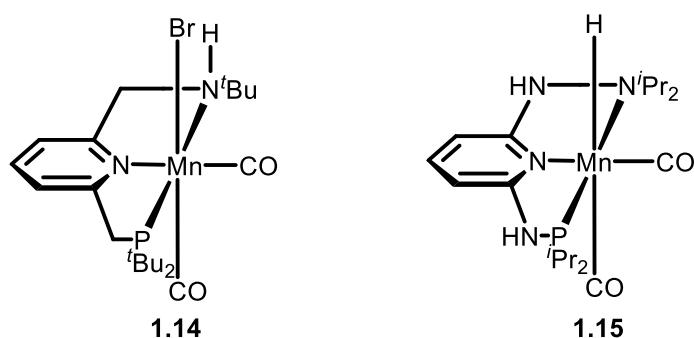
*Figure 1.14: Manganese pincer complexes developed by the Milstein (**1.14**) and Kirchner (**1.15**) groups respectively.*[114,115]

While manganese pincer complexes have been extensively researched, manganese bidentate and bis-chelate catalysts have received much less attention. One of the few recent examples used 2-(diphenylphosphino)ethylamine (dppea, **L4**) ligands with a Mn(I)

centre for ester hydrogenation (Scheme 1.14).[117] Here, **Cat-9** outperformed **Cat-10**, possibly due to the complex still containing a labile bromide ligand making catalyst activation more facile. Of note here, when using the analogous ruthenium complexes, the bidentate derivatives demonstrated superior reactivity. While other manganese bidentate systems are known, far fewer have been reported when compared to pincer systems.[118]

Manganese pincer complexes **Cat-7**, **1.11** and **1.12** have recently been applied to the upgrading of ethanol to *n*-butanol (See Chapter 3 for more details). The recent spike in the popularity of manganese catalysis has led to increased interest in rhenium chemistry as well, and as such, the synthesis and use in catalysis of several rhenium pincer complexes has also recently been reported (See Chapter 4 for more details).
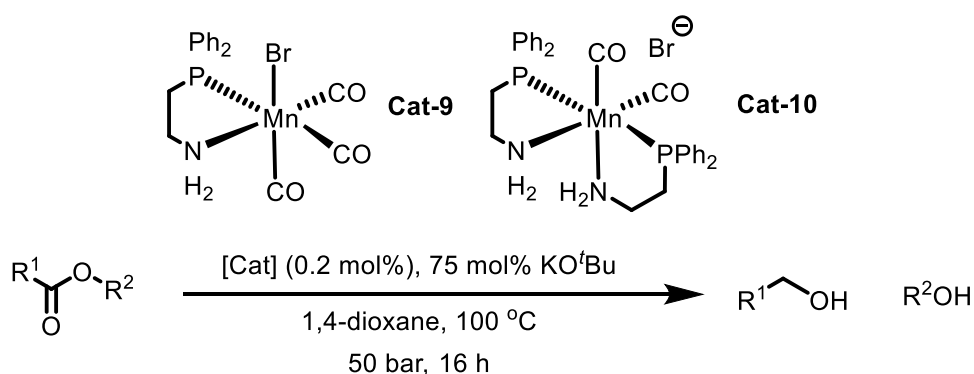
Scheme 1.14: Ester hydrogenation using manganese bidentate and bis-chelate catalysts.[117]

1.9 – Uses for higher Guerbet alcohols

The formation of butanol from ethanol has been extensively discussed, predominantly due to butanol's potential as a fuel replacement, and the challenge that ethanol coupling presents. However, longer chain Guerbet alcohols have a variety of uses outside of the fuel industry. For example, 2-ethylhexanol is used in the polymerisation of acrylates for latex production,[83] and it is also an important precursor in the preparation of bis(2-ethylhexyl)phthalate, a commonly used plasticiser for PVC.[119] Longer chain Guerbet alcohols are also used in the cosmetic industry due to their low irritation potential. Due to their branched structure, Guerbet alcohols melt at much lower temperatures than their linear analogues (Table 1.2), which allows them to be used as low temperature lubricants where the linear alcohols would not be suitable.[120]

Table 1.2: Melting points of various linear and branched (Guerbet) alcohols.[120]

Carbon Number	Linear alcohol mp (°C)	Guerbet Alcohol mp (°C)
C12	24	-30
C16	50	-18
C18	58	-8
C20	69	0

The alcohol functionality in Guerbet products allows for post-coupling functionalisation to produce sulphates. Guerbet sulphates are highly desired as surfactants. Due to the effect that branching has upon a surfactants Krafft point (a measurement of an ionic surfactants water solubility), they are much less soluble than their linear isomers. Owing to their twin tail structure, Guerbet sulphates are also much more effective at micellisation of the oil phase.[120]

1.10 – Hydrogenation of triglycerides

A key step in the conversion of triglycerides to value-added chemicals is their hydrogenation to long chain alcohols and glycerol. The glycerol can then be removed, and the pure alcohol functionalised further. One such way of achieving this is to convert the triglyceride to a fatty acid methyl ester *in situ,* using a basic catalyst and an alcohol solvent, prior to hydrogenation (see Chapter 2 for more details). This removes the need for direct triglyceride hydrogenation. However, hydrogenation of triglycerides directly is possible, and has been reported with a variety of different catalysts.[121]

In 2012, Gusev *et al.* reported the first direct triglyceride to fatty alcohol hydrogenation, without having to go *via* the fatty acid methyl ester, using an osmium-based catalyst (Scheme 1.15).[122] Here, 90% conversion is achieved over 24 h and no base is required, although neat hydrogenation is not possible and thus a toluene solvent must be used. While this system was active for C=C bond hydrogenation, no ester reduction is observed after alkene hydrogenation. As such, for unsaturated triglycerides an initial alkene hydrogenation step using a heterogenous catalyst was required prior to ester hydrogenation using **1.16**. It is proposed that the success of this osmium complex in

triglyceride hydrogenation may be due to its higher thermal stability than the analogous ruthenium complex, thus allowing higher temperatures to be used.
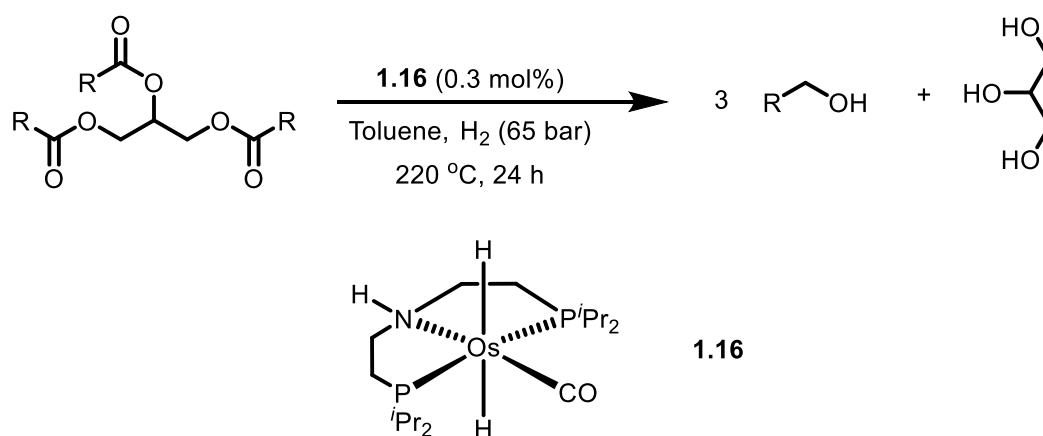
Scheme 1.15: Hydrogenation of triglycerides to fatty alcohols using an osmium-based catalyst.[122]

Subsequently, Gusev *et al.* reported an osmium dimer system (**1.17**) for triglyceride hydrogenation (Figure 1.15).[123] This system required significantly shorter reaction times (6.5 h) at 100 °C, and was tolerant to the presence of C=C bonds in the fatty acid chain. As such, **1.17** could be used for the production of fatty alcohols directly from olive oil.
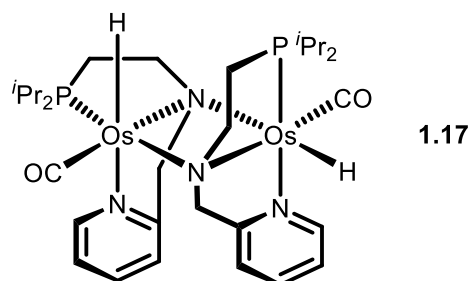
Figure 1.15: A dimeric osmium catalyst for the direct hydrogenation of olive oil.[123]

In 2015, the first example of ruthenium catalysed triglyceride hydrogenation was published, with several different catalysts reported (Figure 1.16).[121] Of these, **1.18** was the most effective giving 91% alcohol yield from the hydrogenation of coconut oil over 6 h. Furthermore, this catalyst was active under neat conditions with no additional solvent required. When **1.19** was used with NaOMe (2.5 eqv.), alcohol yields of only 11% were observed. This decrease in activity is attributed to a lack of catalyst activation, as the NaOMe added is consumed by transesterification rather than by catalyst activation. **Cat-6** was also tested and while this gave poor yields (2%) over 6 h, when reaction times were extended to 24 h yields comparable with catalyst **1.18** were achieved (84%).
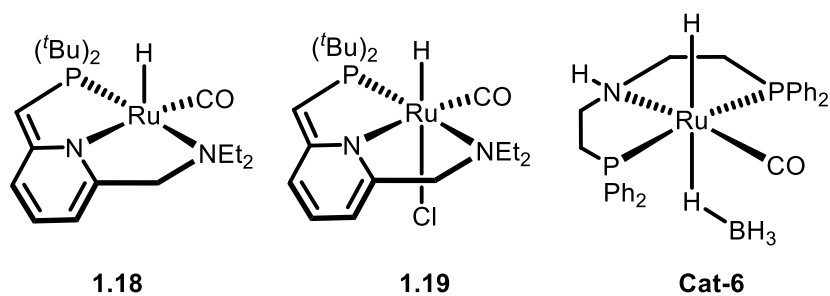
Figure 1.16: Ruthenium catalysts used for the direct hydrogenation of coconut oil.[121]

1.11 – Project aims

The aims of this project are threefold: To increase the general applicability of biodiesel by improving its low temperature flow properties, to investigate complexes based on the group 7 metals manganese and rhenium for *iso*butanol production, and to expand the substrate scope of previously established Wass catalysts towards longer chain alcohols.

Current biodiesel production relies on the simple transesterification of triglycerides to produce fatty acid methylesters (FAMEs), which can then be used directly as a fuel. Utilising this method produces biodiesel in a manner that is inexpensive and readily available, however, a high cloud point (when the fuel begins to solidify) and pour point (when the fuel can no longer be poured) mean it can only be used in warm climates. Insertion of a methyl branch into the fatty acid chain using Guerbet chemistry could improve low temperature flow characteristics, and this functionalisation could be mediated *via* homogenous transition metal catalysis.

One current issue with advanced biofuel production is its reliance on precious metal catalysts, but manganese has recently emerged as a viable substitute due to its low cost and high abundance. As such, the ability of manganese-based complexes to catalyse *iso*butanol production should be investigated. Much of the literature has focused on pincer complexes, with bidentate ligands receiving little attention. However, some of the most effective complexes for ethanol coupling utilise bidentate ligands, therefore both pincer and bis-chelate complexes warrant further investigation.

Unlike manganese, very few molecular rhenium catalysts have been reported, and those that have are all supported by pincer ligands. To date, there are no reported examples of rhenium catalysts for the Guerbet reaction, hence rhenium complexes, supported by the same ligands as those used for manganese, merit investigation.

The Wass group has established several active systems for the homocoupling of ethanol in recent years (see **Cat-1**-**4**). However, currently these catalysts have not been applied to higher alcohol coupling. Given the plethora of potential uses for Guerbet alcohols, the ability of these complexes to produce higher Guerbet products needs to be established.

A more succinct list of project aims has been included below:

- To find catalysts for the production of advanced biofuels, engine oils and synthetic lubricants from cheap, readily available materials such as bioethanol and triglycerides.
- Investigate the production of β-methylated alcohols from triglycerides using a '1-pot' system. To probe the scope and limitations of this system for potential advanced biofuel production.
- To synthesise and test manganese catalysts supported by bidentate ligands for *iso*butanol production, and to establish how these compare to manganese complexes supported by tridentate ligands.
- To perform a preliminary investigation into rhenium-based catalysts for *iso*butanol production, and to compare these to their manganese analogues.
- To investigate Guerbet catalysts previously reported by the group for the coupling of higher alcohols and to establish how these systems compare to ethanol homocoupling.
- Establish if *ortho*-alkylated dppm ligands show any potential for the stabilisation of ruthenium-cymene catalysts through cyclometallation.

1.12 – References

1   IPCC, *Climate Change 2014 Synthesis Report Summary for Policymakers*, Cambridge, 2014.

2   J. Hansen, M. Sato, R. Ruedy, K. Lo, D. W. Lea and M. Medina-Elizade, *Proc. Natl. Acad. Sci. U. S. A.*, 2006, **103**, 14288–14293.

3   IPCC, *IPCC, 2014: Summary for Policymakers. In: Climate Change 2014: Mitigation of Climate Change. Contribution of Working Group III to the Fifth Assessment Report of the Intergovernmental Panel on Climate Change*, Cambridge, 2014.

4   Global Monitoring Laboratory - Carbon Cycle Greenhouse Gases, https://www.esrl.noaa.gov/gmd/ccgg/trends/, (accessed 24 April 2020).

5   R. Lindsey, Climate Change: Atmospheric Carbon Dioxide | NOAA Climate.gov,

https://www.climate.gov/news-features/understanding-climate/climate-change-atmospheric-carbon-dioxide, (accessed 24 April 2020).

6   C. Kuo, C. Lindberg and D. J. Thomson, *Nature*, 1990, **343**, 709–714.

7   UNFCC, *Adoption of the Paris Agreement*, Paris, 2015.

8   National Aeronautics and Space Anministration and Goddard Institute for Space Studies., GISS Surface Temperature Analysis: Analysis Graphs and Plots, https://data.giss.nasa.gov/gistemp/graphs_v4/, (accessed 24 April 2020).

9   BP, *BP Statistical Review of World Energy, 69th edition*, 2020.

10   OPEC, OPEC Share of World Crude Oil Reserves, https://www.opec.org/opec_web/en/data_graphs/330.htm, (accessed 24 April 2020).

11   Oil Production by Country - Worldometer, https://www.worldometers.info/oil/oil-production-by-country/, (accessed 24 April 2020).

12   D. Ansari, *Energy Policy*, 2017, **111**, 166–178.

13   G. E. Batley and R. S. Kookana, *Environ. Chem.*, 2012, **9**, 425–428.

14   B. Warner and J. Shapiro, *Publius J. Fed.*, 2013, **43**, 474–496.

15   Renewable Energy Policy Network for the 21st Century, *Renewable Energy Policy Network for the 21st Century- REN21.2015 Renewables 2015 Global Status Report*, 2015.

16   RenewableUK, Wind Energy Statistics - UKWED, https://www.renewableuk.com/page/UKWEDhome, (accessed 27 April 2020).

17   Y. Kumar, J. Ringenberg, S. S. Depuru, V. K. Devabhaktuni, J. W. Lee, E. Nikolaidis, B. Andersen and A. Afjeh, *Renew. Sustain. Energy Rev.*, 2016, **53**, 209–224.

18   D. Shepherd, D. McBride, D. Welch, K. N. Dirks and E. M. Hill, *Noise Heal.*, 2011, **13**, 333–339.

19   Interation Renewable Energy Agency, *Estimating the Renewable Energy Potential in Africa: A GIS-based approach*, 2014.

20   K. J. Hancock and B. K. Sovacool, *Int. Stud. Rev.*, 2018, **20**, 615–632.

21   B. Pandey and A. Karki, *Hydroelectric energy: Renewable energy and the environment*, CRC Press, 2016.

22   M. A. Rosen and S. Koohi-Fayegh, *Geothermal Energy: Sustainable Heating and Cooling Using the Ground*, 2017.

23   J. Cheng, *Biomass to renewable energy processes, second edition*, CRC Press, 2017.

24   A. V. Bridgwater, *Chem. Eng. J.*, 2003, **91**, 87–102.

25   S. V. Vassilev, C. G. Vassileva and V. S. Vassilev, *Fuel*, 2015, **158**, 330–350.

26   London buses to be powered by coffee - BBC News,

https://www.bbc.co.uk/news/uk-england-london-42044852, (accessed 27 April 2020).

27   S. S. Ho and S. Kristainsen, *Environ. Commun.*, 2019, **13**, 431–439.

28   L. Bernardi, L. Morales, M. Lühiste and D. Bischof, *Env. Polit.*, 2018, **27**, 42–68.

29   *Interational Energy Agency, CO₂ Emissions from Fuel Combustion 2018 Highlights*, 2018.

30   Best electric cars to buy 2020: the complete guide | Auto Express, https://www.autoexpress.co.uk/best-cars/electric-cars/86169/best-electric-cars-to-buy-2020, (accessed 24 April 2020).

31   A. Targonya, A. Khmeluk and I. Bankovskaya, *Electric cars: Advantages and Disadvantages*, Minsk, Belarus, 2019.

32   • Global plug-in electric light vehicle sales 2020 | Statista (Accessed 10/03/2021), https://www.statista.com/statistics/665774/global-sales-of-plug-in-light-vehicles/, (accessed 19 March 2021).

33   J. Wind, in *Compendium of Hydrogen Energy*, Elsevier, 2016, pp. 3–21.

34   S. N. Naik, V. V. Goud, P. K. Rout and A. K. Dalai, *Renew. Sustain. Energy Rev.*, 2010, **14**, 578–597.

35   G. Chavanne, *Procédé de transformation d'huiles végétales en vue de leur utilisation comme carburants, BE422877*, 1937.

36   F. J. C. Hugo, *Plant Oils as a Fuel for Diesel Engines: Experience with Sunflower Oil*, 1982.

37   CEN (European committee for Standardisation), *Automotive fuels-Fatty acid methyl esters (FAME) for diesel engines-Requirements and test methods EN 14214*, CEN, 2010.

38   V. K. Mishra and R. Goswami, *Biofuels*, 2018, **9**, 273–289.

39   S. Jain and M. P. Sharma, *Renew. Sustain. Energy Rev.*, 2010, **14**, 763–771.

40   T. W. Jeffries, *Nat. Biotechnol.*, 2005, **23**, 40–41.

41   H. Alper, J. Moxley, E. Nevoigt, G. R. Fink and G. Stephanopoulos, *Science.*, 2006, **314**, 1565–1568.

42   M. W. Rosegrant and S. Msangi, *Annu. Rev. Environ. Resour.*, 2014, **39**, 271–294.

43   S. Kumar, S. P. Singh, I. M. Mishra and D. K. Adhikari, *Chem. Eng. Technol.*, 2009, **32**, 517–526.

44   M. Vohra, J. Manwar, R. Manmode, S. Padgilwar and S. Patil, *J. Environ. Chem. Eng.*, 2014, **2**, 573–584.

45   H. B. Aditiya, T. M. I. Mahlia, W. T. Chong, H. Nur and A. H. Sebayang, *Renew. Sustain. Energy Rev.*, 2016, **66**, 631–653.

46   A. A. Houfani, N. Anders, A. C. Spiess, P. Baldrian and S. Benallaoua, *Biomass Bioenerg.*, 2020, **134**, 105481.

47   A. Gupta and J. P. Verma, *Renew. Sustain. Energy Rev.*, 2015, **41**, 550–567.

48   S. K. Thangavelu, A. S. Ahmed and F. N. Ani, *Renew. Sustain. Energy Rev.*, 2016, **56**, 820–835.

49   U.S. Energy Information Administration, U.S. fuel ethanol production continues to grow in 2017 - Today in Energy - U.S. Energy Information Administration (EIA), https://www.eia.gov/todayinenergy/detail.php?id=32152, (accessed 28 April 2020).

50   M. Balat, *Energy Convers. Manag.*, 2011, **52**, 858–875.

51   A. K. Agarwal, *Prog. Energy Combust. Sci.*, 2007, **33**, 233–271.

52   C. Hammel-Smith, J. Fang, M. Powders and J. Aabakken, *Issues Associated with the Use of Higher Ethanol Blends (E17-E24)*, 2002.

53   C. N. Hamelinck and A. P. C. Faaij, *Energy Policy*, 2006, **34**, 3268–3283.

54   K. R. Szulczyk, *Int. J. Energy Environ.*, 2010, **1**, 501–512.

55   P. Dürre, *Biotechnol. J.*, 2007, **2**, 1525–1534.

56   J. Yanowitz, E. Christensen and R. McCormick, *Utilization of renewable oxygenates as gasoline blending components*, 2011.

57   T. Riittonen, E. Toukoniitty, D. K. Madnani, A. R. Leino, K. Kordas, M. Szabo, A. Sapi, K. Arve, J. Wärnå and J. P. Mikkola, *Catalysts*, 2012, **2**, 68–84.

58   C. Jin, M. Yao, H. Liu, C. F. F. Lee and J. Ji, *Renew. Sustain. Energy Rev.*, 2011, **15**, 4080–4106.

59   V. F. Andersen, J. E. Anderson, T. J. Wallington, S. A. Mueller and O. J. Nielsen, in *Energy and Fuels*, 2010, vol. 24, pp. 3647–3654.

60   G. D. Frey, *J. Organomet. Chem.*, 2014, 754, 5–7.

61   C. E. Adams and D. E. Burney, *Oxo Process, US2464916*, 1949.

62   E. R. Tucci, *Oxo Process, US3631111A*, 1971.

63   C. R. Greene, *Oxo process using cobalt carbonyl and tertiary phosphine under basic conditions, US3278612A*, 1966.

64   F. E. Paulik, *Catal. Rev.*, 1972, **6**, 49–84.

65   E. Billig and D. R. Bryant, in *Kirk-Othmer Encyclopedia of Chemical Technology*, John Wiley & Sons, Inc., Hoboken, NJ, USA, 2000.

66   A. Kujawska, J. Kujawski, M. Bryjak and W. Kujawski, *Renew. Sustain. Energy Rev.*, 2015, **48**, 648–661.

67   A. P. Mariano, N. Qureshi, R. Maciel Filho and T. C. Ezeji, *J. Chem. Technol. Biotechnol.*, 2012, **87**, 334–340.

68   H. Huang, H. Liu and Y. R. Gan, *Biotechnol. Adv.*, 2010, **28**, 651–657.

69   P. Dürre, in *Annals of the New York Academy of Sciences*, Blackwell Publishing Inc., 2008, vol. 1125, pp. 353–362.

70   N. R. Baral and A. Shah, *Appl. Microbiol. Biotechnol.*, 2014, **98**, 9151–9172.

71   F. Raganati, G. Olivieri, P. Götz, A. Marzocchella and P. Salatino, *Anaerobe*, 2015, **34**, 146–155.

72   M. C. R. Guerbet, *C. R. Hebd. Seances Acad. Sci.*, 1899, **128**, 1002–1004.

73   C. A. Carter, *Condensation of Alcohols, US2457866A*, 1949.

74   E. F. Pratt and D. G. Kubler, *J. Am. Chem. Soc.*, 1953, **1**, 52–56.

75   S. Veibel and J. I. Nielsen, *Tetrahedron*, 1967, **23**, 1723–1733.

76   M. H. S. A. Hamid, P. A. Slatford and J. M. J. Williams, *Adv. Synth. Catal.*, 2007, **349**, 1555–1575.

77   M. H. S. A. Hamid, C. L. Allen, G. W. Lamb, A. C. Maxwell, H. C. Maytum, A. J. A. Watson and J. M. J. Williams, *J. Am. Chem. Soc.*, 2009, **131**, 1766–1774.

78   D. Wang and D. Astruc, *Chem. Rev.*, 2015, **115**, 6621–6686.

79   G. R. M. Dowson, *Transformations of Ethanol by Homogeneous Catalysis for Creation of Advanced Biofuels, Ph. D. Thesis, Univeristy of Bristol*, 2012.

80   R. Miller and G. Bennett, *Ind. Eng. Chem.*, 1961, **53**, 33–36.

81   G. Gregorio, G. F. Pregaglia and R. Ugo, *J. Organomet. Chem.*, 1972, **37**, 385–387.

82   P. L. Burk, R. L. Pruett and K. S. Campo, *J. Mol. Catal.*, 1985, **33**, 1–14.

83   C. Carlini, A. Macinai, A. M. Raspolli Galletti and G. Sbrana, *J. Mol. Catal. A Chem.*, 2004, **212**, 65–70.

84   T. Matsu-ura, S. Sakaguchi, Y. Obora and Y. Ishii, *J. Org. Chem.*, 2006, **71**, 8306–8308.

85   K. Koda, T. Matsu-ura, Y. Obora and Y. Ishii, *Chem. Lett.*, 2009, **38**, 838–839.

86   H. Aitchison, R. L. Wingad and D. F. Wass, *ACS Catal.*, 2016, **6**, 7125–7132.

87   P. A. Slatford, M. K. Whittlesey and J. M. J. Williams, *Tetrahedron Lett.*, 2006, **47**, 6787–6789.

88   Y. Tanaka and M. Utsunomiya, *Process of Producing Alcohol, US8318990B2*, 2010.

89   G. R. M. Dowson, M. F. Haddow, J. Lee, R. L. Wingad and D. F. Wass, *Angew. Chem. Int. Ed.*, 2013, **52**, 9005–9008.

90   R. L. Wingad, P. J. Gates, S. T. G. Street and D. F. Wass, *ACS Catal.*, 2015, **5**, 5822–5826.

91   M. Nielsen, H. Junge, A. Kammer and M. Beller, *Angew. Chem. Int. Ed.*, 2012, **51**, 5711–5713.

92   A. M. Brownstein, *Renewable motor fuels : the past, the present, and uncertain future*, Butterworth-Heinemann, 2014.

93   N. S. Shamsul, S. K. Kamarudin, N. A. Rahman and N. T. Kofli, *Renew. Sustain. Energy Rev.*, 2014, **33**, 578–588.

94   C. Carlini, M. Di Girolamo, A. Macinai, M. Marchionna, M. Noviello, A. M. Raspolli Galletti and G. Sbrana, *J. Mol. Catal. A Chem.*, 2003, **200**, 137–146.

95   C. Carlini, M. Di Girolamo, A. Macinai, M. Marchionna, M. Noviello, A. M. Raspolli Galletti and G. Sbrana, *J. Mol. Catal. A Chem.*, 2003, **204**–**205**, 721–728.

96   R. L. Wingad, E. J. E. Bergström, M. Everett, K. J. Pellow and D. F. Wass, *Chem. Commun.*, 2016, **52**, 5202–5204.

97   K. J. Pellow, R. L. Wingad and D. F. Wass, *Catal. Sci. Technol.*, 2017, **7**, 5128–5134.

98   K. N. T. Tseng, S. Lin, J. W. Kampf and N. K. Szymczak, *Chem. Commun.*, 2016, **52**, 2901–2904.

99   Y. Xie, Y. Ben-David, L. J. W. Shimon and D. Milstein, *J. Am. Chem. Soc.*, 2016, **138**, 9077–9080.

100   S. Chakraborty, P. E. Piszel, C. E. Hayes, R. T. Baker and W. D. Jones, *J. Am. Chem. Soc.*, 2015, **137**, 14264–14267.

101   G. Xu, T. Lammens, Q. Liu, X. Wang, L. Dong, A. Caiazzo, N. Ashraf, J. Guan and X. Mu, *Green Chem.*, 2014, **16**, 3971–3977.

102   Q. Liu, G. Xu, X. Wang and X. Mu, *Green Chem.*, 2016, **18**, 2811–2818.

103   Y. Li, H. Li, H. Junge and M. Beller, *Chem. Commun.*, 2014, **50**, 14991–14994.

104   A. Kaithal, M. Schmitz, M. Hölscher and W. Leitner, *ChemCatChem*, 2019, **11**, 5287–5291.

105   A. Kaithal, M. Schmitz, M. Hölscher and W. Leitner, *ChemCatChem*, 2020, **12**, 781–787.

106   A. Kaithal, P. Bonn, M. Hölscher and W. Leitner, *Angew. Chem. Int. Ed.*, 2020, **59**, 215–220.

107   K. Polidano, J. M. J. Williams and L. C. Morrill, *ACS Catal.*, 2019, **9**, 8575–8580.

108   S. Elangovan, C. Topf, S. Fischer, H. Jiao, A. Spannenberg, W. Baumann, R. Ludwig, K. Junge and M. Beller, *J. Am. Chem. Soc.*, 2016, **138**, 8809–8814.

109   S. Elangovan, M. Garbe, H. Jiao, A. Spannenberg, K. Junge and M. Beller, *Angew. Chem. Int. Ed.*, 2016, **55**, 15364–15368.

110   S. Elangovan, J. Neumann, J. B. Sortais, K. Junge, C. Darcel and M. Beller, *Nat. Commun.*, 2016, **7**, 1–8.

111   M. Perez, S. Elangovan, A. Spannenberg, K. Junge and M. Beller, *ChemSusChem*, 2017, **10**, 83–86.

112   M. Andérez-Fernández, L. K. Vogt, S. Fischer, W. Zhou, H. Jiao, M. Garbe, S. Elangovan, K. Junge, H. Junge, R. Ludwig and M. Beller, *Angew. Chem. Int. Ed.*, 2017, **56**, 559–562.

113   M. Peña-López, P. Piehl, S. Elangovan, H. Neumann and M. Beller, *Angew. Chem. Int. Ed.*, 2016, **55**, 14967–14971.

114   N. A. Espinosa-Jalapa, A. Nerush, L. J. W. Shimon, G. Leitus, L. Avram, Y. Ben-David and D. Milstein, *Chem. Eur. J.*, 2017, **23**, 5934–5938.

115   M. Mastalir, M. Glatz, E. Pittenauer, G. Allmaier and K. Kirchner, *J. Am. Chem. Soc.*, 2016, **138**, 15543–15546.

116   A. Mukherjee and D. Milstein, *ACS Catal.*, 2018, **8**, 11435–11469.

117   R. van Putten, E. A. Uslamin, M. Garbe, C. Liu, A. Gonzalez-de-Castro, M. Lutz, K. Junge, E. J. M. Hensen, M. Beller, L. Lefort and E. A. Pidko, *Angew. Chem. Int. Ed.*, 2017, **56**, 7531–7534.

118   S. Weber, B. Stöger, L. F. Veiros and K. Kirchner, *ACS Catal.*, 2019, **9**, 9715–9720.

119   D. W. Cadogan, C. J. Howick, J. I. Kroschwitz and M. Howe-Grant (eds), *Kirk-Othmer Encycl. Chem. Technol. vol. 19, 4th ed*, 1991, 258.

120   A. J. O'Lenick, *J. Surfactants Deterg.*, 2001, **4**, 311–315.

121   N. T. Fairweather, M. S. Gibson and H. Guan, *Organometallics*, 2015, **34**, 335–339.

122   A. Acosta-Ramirez, M. Bertoli, D. G. Gusev and M. Schlaf, *Green Chem.*, 2012, **14**, 1178–1188.

123   D. Spasyuk, S. Smith and D. G. Gusev, *Angew. Chem. Int. Ed.*, 2012, **51**, 2772–2775.

Chapter 2: Functionalisation of triglycerides towards β-methylated alcohols

2.1 – Introduction

2.1.1 – Triglycerides in biofuels

Triglycerides, most commonly found in vegetable oils, are a readily available and low cost feedstock with over 203 million metric tonnes being produced from 2018 – 2019 alone.[1] Given their abundance, they have already been considered as a possible precursor to biofuels. While triglycerides alone can be used as fuels (some of the earliest diesel engines were reported to run on peanut oil),[2] they are much more viscous than regular diesel. Triglycerides have a kinematic viscosity range at 40 °C of 17.3 – 32.9 mm^2s^{-1} compared to 1.9 – 4.1 mm^2s^{-1} for regular petrodiesel (ASTM, D975).[3] This higher viscosity can lead to incomplete combustion, causing coking and carbon deposition in engines.[4] As such, triglycerides are usually converted into fatty-acid methyl esters (FAMEs), *via* transesterification with methanol under basic conditions, before use as fuels (Scheme 2.1).[2] These FAMEs exhibit much lower viscosities than the triglycerides they are derived from (1.9-6.0 mm^2s^{-1}, ASTM D6751), and even show a comparable heat of combustion to regular diesel.[3]
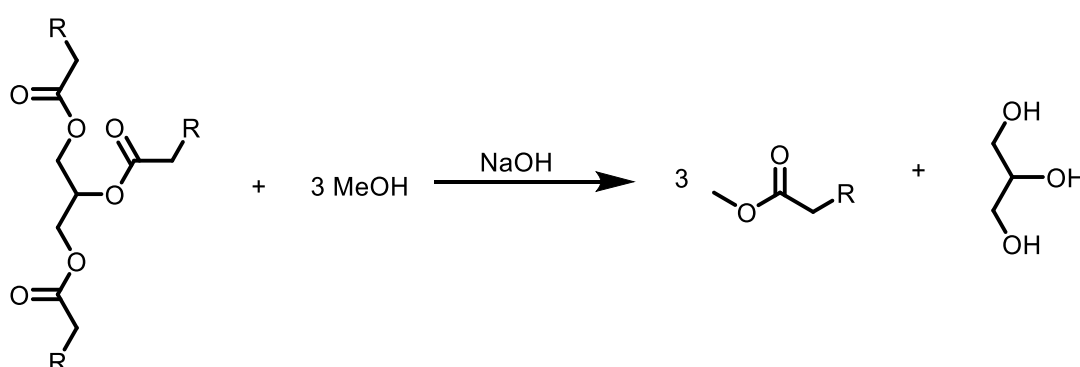
Scheme 2.1: Formation of fatty-acid methyl esters from triglycerides using a basic catalyst.

Despite their ease of production, biofuels only accounted for 1.6% of EU diesel fuel consumption in 2005.[5] One of the factors contributing to FAMEs low adoption rate may be their poor cold temperature properties. When fuels cool fine crystals begin to precipitate, the temperature at which this occurs is known as the cloud point (CP). These crystals can cause problems with engine function by blocking fuel lines. Cooling further allows the fuel

to form into a gel that cannot be poured, this temperature is known as the pour point (PP). The cloud point of soybean derived biodiesel is as high as 0 °C.[5] These high cloud and pour points make use of FAME biofuels impossible in cold climates. Proposed methods of reducing the CP and PP of FAMEs include: esterification with branched alcohols (such as *iso*propanol, or 2-butanol), and altering the fatty acid composition of the input oil.[6,7] The use of unsaturated fatty acid chains was found to have a positive effect upon cold temperature properties.[8] However, increasing the degree of unsaturation in the fatty-acid chain also increases the rate of oxidation. Oxidation causes a build-up of hydroperoxides which polymerise to form insoluble sediments, this can cause blockages in engines and have a negative effect on performance.[9]

An ideal triglyceride derived biofuel requires: the low viscosity associated with FAMEs, coupled with the cold-temperature properties of unsaturated fatty-acid chains and the oxidative stability seen in saturated fatty chains. With the aim of producing biofuels with such favourable properties, this chapter will focus on the production of β-methylated alcohols *via* cascade catalysis from triglyceride feedstocks. (Scheme 2.2). Hydrogenation of the ester group followed by the addition of a methyl branch can decrease the freezing point of compounds and therefore CPs and PPs. The positive effect of adding a methyl branch, albeit in the *iso* not the β-position, has already been noted in FAMEs derived from lanolin for use as biolubricants.[10] Moving the methyl branch from the *iso* to the anteiso position led to greater depression of melting point, showing the benefit of branching closer to the ester. The favourable fuel properties associated with long chain alcohol-based biofuels are well documented, with the energy density of even C4 alcohols approaching that of gasoline.[11] The effect that the overall process would have on fuel freezing point can be observed using short chain fatty acids. For a C3 triglyceride, the fuel produced in Scheme 2.2 (*iso*butanol) would have a freezing point 20 °C lower than the fuel produced in Scheme 2.1 (methyl propanoate).
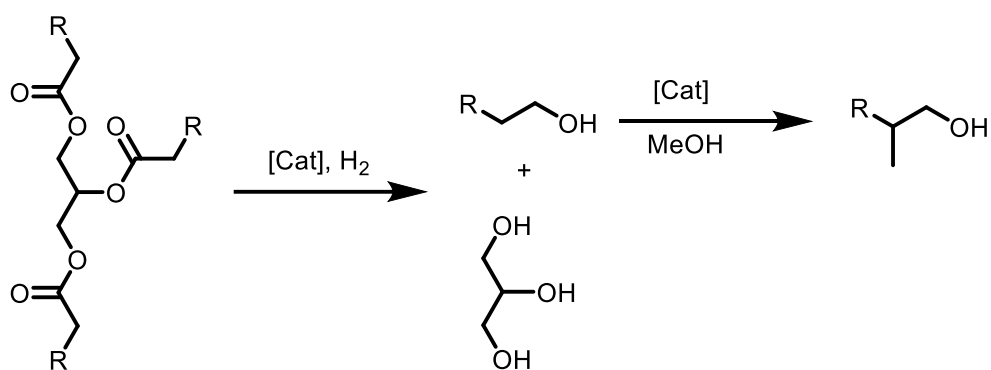
Scheme 2.2: Production of β-methylated alcohols from triglycerides for use as advanced biofuels.

2.1.2 – Choice of catalyst

For this cascade catalysis to be possible with a single catalyst, the use of a complex known for both ester hydrogenation and Guerbet chemistry is required. RuMACHO (**Cat-5**), a well-studied, commercially available catalyst has been reported for both processes (Figure 2.1). **Cat-5** gives 36% *iso*butanol in 82% selectivity over 2 hours from an ethanol substrate,[12] and has been shown to hydrogenate the long chain ester methyl dodecanoate in 90% yields over 16 hours under 50 bar of hydrogen.[13] It is also known for other reactions such as the N-monomethylation of amines,[14] and the acceptorless dehydrogenative coupling of alcohols.[15] Recent studies have also used similar compounds for the β-methylation of a variety of different aromatic and aliphatic alcohols.[16,17] Owing to its proven versatility and commercial availability, **Cat-5** was chosen as the benchmark catalyst for this study.

Cat-5
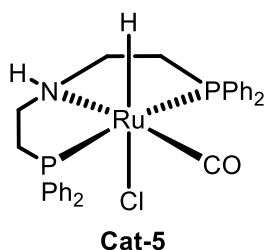
Figure 2.1: Commercially available catalyst RuMACHO.

2.2 – Proof of concept: *iso*butanol formation from methyl propanoate

Whether hydrogenation followed by Guerbet chemistry cascade catalysis was possible needed to be established before this process could be applied to triglycerides. As such, methyl propanoate was chosen as a model substrate. This can be hydrogenated to *n*-propanol, the intermediate in the formation of *iso*butanol from ethanol and methanol. Given RuMACHO catalysed *iso*butanol formation has already been established,[12] this made

analysis of the product mixture significantly simpler. Both steps were investigated separately before being combined to directly investigate the possibility of cascade catalysis.

2.2.1 – Step 1: Methyl propanoate hydrogenation

Conditions for hydrogenation were altered to be in line with those used for Guerbet chemistry with RuMACHO.[12] Catalyst loading (0.1 mol%) was maintained and a 10:1 volumetric ratio of solvent (methanol) to substrate was used. While loadings as low as 10 mol% NaOMe have been used for ester hydrogenation previously, and low base loadings are needed for alcohol homocoupling, large amounts of base are required for *iso*butanol formation *via* Guerbet chemistry.[18] As such, 200 mol% NaOMe was used throughout both catalytic steps.

In order to explore the activity of **Cat-5** for the hydrogenation of methyl propanoate catalytic tests were carried out in a 100 mL Parr stainless steel autoclave to explore the role of pressure, temperature and other factors on catalytic performance. The results of this are reported in Table 2.1.

RuMACHO is highly active for the hydrogenation of methyl propanoate to *n*-propanol and methanol (Table 2.1). This is perhaps unsurprising given the efficiency it has already shown for the hydrogenation of long chain aliphatic esters, among other challenging functional groups.[13]

Table 2.1: Hydrogenation of methyl propanoate to n-propanol condition screen (optimised conditions in bold).
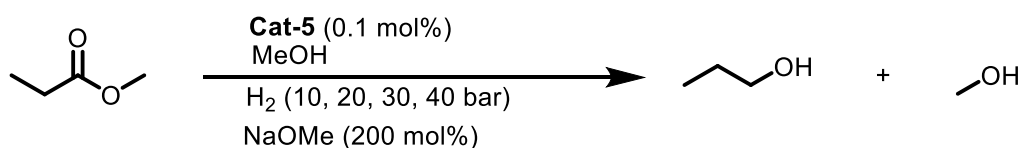
Entry[a]	Temperature (°C)	Pressure (Bar)	Time (h)	n-propanol Yield (%)[b]
1	**100**	**40**	**16**	**96**
2	100	30	16	86
3	100	20	16	69
4	100	10	16	47
5	70	30	16	58
6	120	30	16	97
7	120	40	16	97
8	100	30	64	94
9	120	30	65	74
10[c]	100	40	16	95
11[d]	100	40	16	0

[a] Conditions: methanol (10 mL), methyl propanoate (1 mL, 10.39 mmol), **Cat-5** (0.1 mol%, 0.0104 mmol, 6.3 mg), H_2 (10-40 bar), NaOMe (200 mol%, 1.122 g), [b] determined by GC, [c] 100 mol% NaOMe, [d] no catalyst used.

While ester hydrogenation has previously been conducted under 50 bar H_2,[13] the reduction of pressure to 40 bar was found to make little difference to overall yield, with 96% *n*-propanol given after 16 hours (Table 2.1, Entry 1). A further reduction to 30 bar resulted in a noticeable decrease in yield to 86% *n*-propanol (Entry 2). Further decreases to 20 and 10 bar caused a more significant reduction in yield to 69% and 47%, respectively (Entries 3 and 4).

Lowering the reaction temperature to 70 °C caused a significant decrease in yield (58%, Entry 5). Increasing the reaction temperature to 120 °C gives comparable yields to 100 °C, although at this higher temperature a hydrogen pressure of 30 bar is sufficient to give almost quantitative yields of propanol (Entries 6 and 7). A small amount of solid by-product is also produced when higher temperatures and lower pressures are used (Entry 6). Given that comparable yields of propanol are produced at both 100 and 120 °C, and at lower

temperatures the reaction remains fully homogeneous, the conditions used in Entry 1 were considered optimal. Increasing reaction times does not have a positive effect upon *n*-propanol yield (Entries 8 and 9). Decreasing the base loading to 100 mol% had no effect upon overall reaction yield (Entry 10). Once the activity of RuMACHO towards methyl propanoate hydrogenation had been established, its ability to catalyse *iso*butanol formation from *n*-propanol was investigated.

2.2.2 – Step 2: *iso*butanol formation from *n*-propanol

To probe the formation of *iso*butanol from propanol using **Cat-5**, a 100 mL Parr stainless steel autoclave was used once again. Results are reported in Table 2.2.

Unsurprisingly, *n*-propanol conversion to *iso*butanol proceeded in high yields over short reaction times when catalysed by **Cat-5** (Table 2.2, Entry 1). Yields were significantly higher than those reported for the formation of *iso*butanol from ethanol (59% compared to 36%).[12] This is to be expected, given that one Guerbet cycle has to be completed instead of two. Increasing the run time to 5 hours led to total propanol conversion, along with an increased *iso*butanol yield of 69% (Entry 2). It was proposed that as fewer Guerbet cycles were required to form the desired product (and thus less water produced) that base loadings could be lowered to 100 mol% (Entry 3). While *iso*butanol formation was still possible, both *n*-propanol consumption and product yield decreased (by 21% and 12% respectively). As such, a high base loading was maintained. The reaction was also performed under a 30 bar hydrogen atmosphere (Entry 4) to ascertain whether hydrogenation and Guerbet could occur simultaneously. While *iso*butanol was still produced (30%), it was in significantly lower yields than when no hydrogen atmosphere was used. It is of note however, that the discrepancy between propanol conversion and *iso*butanol yield is significantly lower (only 8%, compared to 39% for Entry 1). This has been attributed to the suppression of Tishchenko chemistry, which leads to the production of alkylate salts, along with a molecule of H_2, under normal Guerbet conditions (see Section 4.2.3 for more details).[19]

Table 2.2: isobutanol formation from n-propanol and methanol.
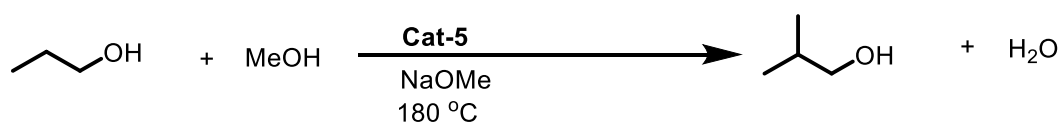
Entry[a]	Base Loading (mol%)	Reaction time (h)	*n*-propanol consumption (%)[b]	*Iso*butanol Yield (%)[b]
1	200	2	98	59
2	200	5	100	69
3	100	2	77	47
4[c]	200	2	37	29

[a] Conditions: *n*-propanol (1 mL, 13.38 mmol), methanol 10 mL, **Cat-5** (0.1 mol%, 0.0134 mmol, 8.12 mg), 180 °C, NaOMe (100-200 mol%), 2h, [b] Determined by GC, [c] H_2 (30 bar) added before reaction.

2.2.3 – Catalyst screen

Once workable conditions had been established for both steps using **Cat-5**, attention was directed towards other potential catalysts. **Cat-11** (Figure 2.2) has previously been used for the hydrogenation of dimethyl oxalate to ethylene glycol,[20] and its ability to catalyse Guerbet chemistry shown recently within the Wass group.[21] **Cat-4** has been used for the stereoselective hydrogenation of chiral esters to alcohols.[22–24] It has also displayed high activity for both the homocoupling of ethanol to form *n*-butanol and the coupling of ethanol and methanol to make *iso*butanol.[18,19] As such, both complexes were identified as possible catalysts for cascade catalysis alongside **Cat-5**.
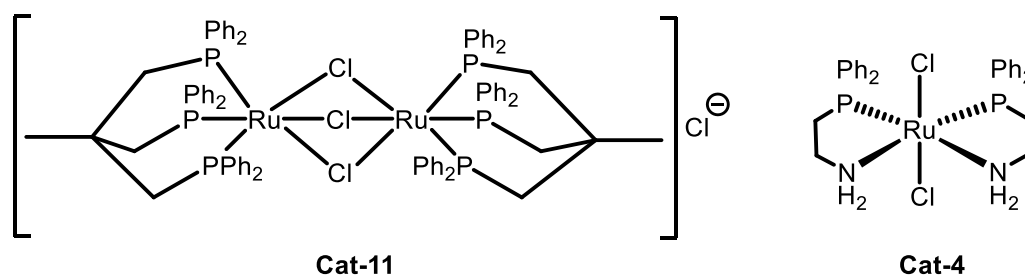
Figure 2.2: Other potential catalysts for isobutanol formation from methyl propanoate.

Unfortunately, neither **Cat-11** nor **Cat-4** showed any appreciable activity for methyl propanoate hydrogenation, with yields not exceeding 10% (Table 2.3); under the same conditions **Cat-5** gave almost total conversion. This result is surprising considering that **Cat-11** has previously been used for the hydrogenation of challenging diesters.[25] For **Cat-11**,

increasing reaction temperature to 180 °C (reaction temperature for the Guerbet reaction) appeared to favour the dehydrogenation reaction. The post reaction mixture contained a large amount of solid and thus GC analysis was not possible. As both **Cat-11** and **Cat-4** displayed little activity for step 1, their efficiency for step 2 was not investigated. Instead, **Cat-5** alone was used for the '1-pot-2-step' synthesis of *iso*butanol from methyl propanoate *via* cascade catalysis.

*Table 2.3: Catalyst screen for methyl propanoate hydrogenation. Results with **Cat-5** included again for comparison.*

Entry[a]	Catalyst	Temperature (°C)	*n*-propanol Yield (%)
1	**Cat-5**	100	96
2[b]	**Cat-11**	100	6
3	**Cat-4**	100	7
4[b,c]	**Cat-11**	180	-

[a] Conditions: methanol (10 mL), methyl propanoate (1 mL, 10.39 mmol), [cat] (0.1 mol%, 0.0104 mmol), H_2 (40 bar), NaOMe (200 mol%, 1.122 g), 16 h, [b] 0.05 mol% [cat], [c] too much solid produced unable to analyse.

2.2.4 – Combining steps 1 and 2: *iso*butanol formation from methyl propanoate

Once the ability of **Cat-5** to catalyse both steps had been fully investigated, and optimum conditions established, the combined process was examined. Two different processes were proposed for this combination. Method A: a 1-step process (Scheme 2.3), where hydrogenation of methyl propanoate and Guerbet coupling of *n*-propanol were occurring in tandem, and Method B: a '2-step-1-pot' reaction (Scheme 2.4), where hydrogenation was conducted first, under optimal conditions, followed by Guerbet. All reactions were carried out in a 100 mL Parr stainless steel autoclave.
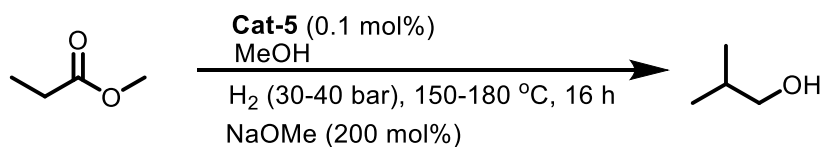
Scheme 2.3: Method A: A 1-step process for the formation of isobutanol from methyl propanoate.
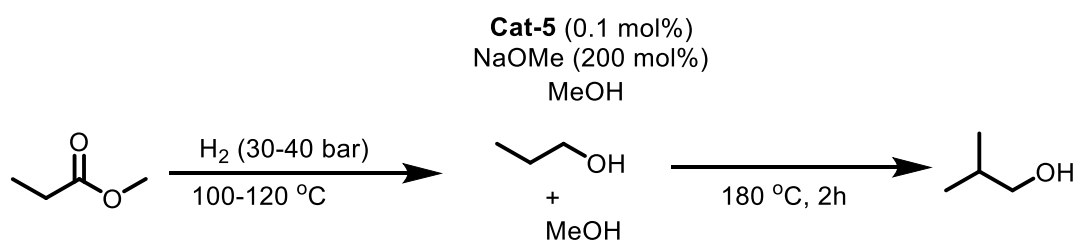
Scheme 2.4: Method B: A 2-step-1-pot process for the production of isobutanol from methyl propanoate.

*Iso*butanol formation from ethanol is reported to be optimal at 180 °C, with formation still being significant at 150 °C. However, when the temperature is decreased further to 120 °C, both ethanol conversion and *iso*butanol selectivity are significantly reduced.[18] As such, for method A reaction temperatures of both 150 °C and 180 °C were investigated. This should allow for both ester hydrogenation and Guerbet chemistry to occur. As alcohol dehydrogenation and propanoate salt formation occurs more rapidly at higher temperatures, it was postulated that running the reactions at 150 °C would give the best balance between hydrogenation and Guerbet and thus give the greatest *iso*butanol yield.

Method B combines the optimal reaction conditions for both individual steps. This allows for hydrogenation to take place selectively, in order to maximise the *n*-propanol yield before this is converted to *iso*butanol. This should maximise selectivity to *iso*butanol over any undesired side products. Between step 1 and 2, the autoclave was immersed in ice-water and the hydrogen removed, but the reaction mixture kept under an inert atmosphere.

Table 2.4: Formation of isobutanol from methyl propanoate using methods A and B.

Entry[a]	Method[b,c]	Step	Temperature (°C)	*n*-propanol Yield (%)	*Iso*butanol Yield (%)	*Iso*butanol selectivity (%)[d]
1	A	-	180	16	28	64
2	A	-	150	75	4	5
3[e]	A	-	150	60	2	3
4[f]	B	1	120	74	-	-
	-	2	180	32	19	37
5	B	1	100	94	-	-
	-	2	180	9	40	83

[a] Conditions: methanol (10 mL), methyl propanoate (1 mL, 10.39 mmol), **Cat-5** (0.1 mol%, 0.0104 mmol), NaOMe (200 mol%, 1.122 g), [b] Method A: H_2 (30 bar) 16 h, [c] Method B: Step 1: H_2 (40 bar), 16 h, Step 2: 180 °C, 2h, [d] selectivity calculated from observed products in the liquid fraction, [e] H_2 (40 bar), [f] Step 1: 65 h, H_2 (30 bar).

When method A was employed, the highest *iso*butanol yield was recorded when the reaction was conducted at 180 °C (Table 2.4, Entry 1). When the temperature was decreased to 150 °C, *n*-propanol yields remained high, but *iso*butanol yields decreased significantly (28% to 4%, Entries 1 and 2). While the Guerbet reaction will proceed smoothly at 150 °C without a hydrogen atmosphere,[18] under 30 or 40 bar H_2 it occurs far more slowly and therefore little *iso*butanol is produced. A maximum *iso*butanol selectivity of 64% was observed, with *n*-propanol being the major by-product. Again, this is due to the Guerbet reaction being slow under a hydrogen atmosphere, and thus *iso*butanol formation being suppressed.

When method B was used, step 1 produced *n*-propanol in a high yield (94%, Entry 5), as observed in Section 2.2.1. Although, increasing the temperature above 100 °C disfavoured *n*-propanol production. Subsequent coupling of *n*-propanol with methanol at 180 °C gave *iso*butanol in a moderate yield and high selectivity (40% and 83% respectively). *Iso*butanol yields were highly dependent on the amount of *n*-propanol produced in Step 1. In Entry 4 only 74% *n*-propanol was observed, this led to a significant reduction in *n*-propanol conversion and *iso*butanol selectivity in step 2, despite the same conditions being used in both Entries 4 and 5. It is therefore essential to use conditions which favour selective ester

hydrogenation in step 1, otherwise this can have a significant knock-on effect for the final product yield. Method B can clearly be identified as the superior method, with both higher *iso*butanol yields and selectivity being observed.

The ability of **Cat-5** to catalyse the production of β-methylated alcohols from methyl esters *via* cascade catalysis had been established, and a '2-step-1-pot' process gave the greatest yield and selectivity of the desired final product. With optimal conditions in hand this process was applied to the functionalisation of triglycerides.

2.3 – Formation of *iso*butanol from C3 triglyceride tripropionin

Tripropionin was chosen as the initial triglyceride target as its fatty acid chains were 3 carbons long, and therefore upon hydrogenation will produce *n*-propanol. Given the model substrate methyl propanoate is also hydrogenated to *n*-propanol, this makes analysis of the product mixture much easier.

The conversion of triglycerides to FAMEs is usually conducted in methanol with the use of a basic catalyst (most often this is sodium hydroxide due to its low cost, but sodium methoxide is reported to be much more effective) (see Section 2.1).[26] With a basic catalyst, conversion from the triglyceride to the FAME is rapid, taking only 30 – 60 minutes (Scheme 2.5). Acid catalysts can also be used, but are much slower. Given that both hydrogenation and Guerbet catalysis are conducted in methanol with an excess of NaOMe, triglycerides will undergo transesterification giving 3 equivalents of the corresponding FAME. This can be rapidly hydrogenated by **Cat-5** to the corresponding alcohol. While direct hydrogenation of triglycerides is known, mostly with heterogeneous catalysts or under neat conditions,[27,28] the hydrogenation of methyl esters is much more widely studied.[29–31]
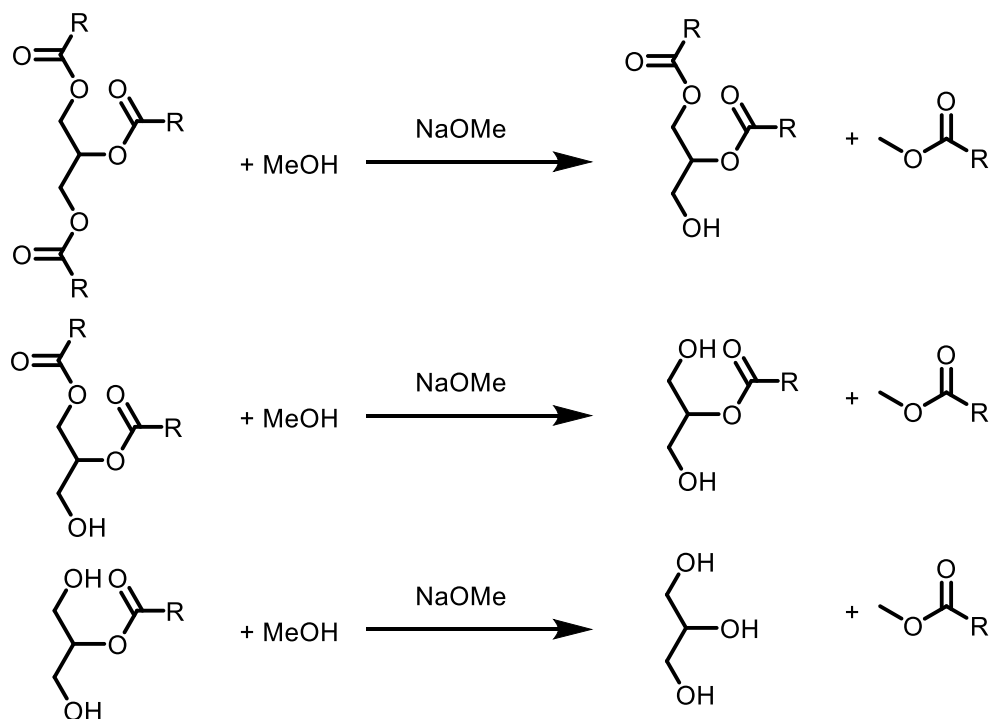
Scheme 2.5: Formation of glycerol, and 3 equivalents of FAME from the transesterification of a triglyceride.

After tripropionin was added to the pre-reaction mixture, the reaction was allowed a 45 – 60 min pre-hydrogenation period to give time for complete conversion to the methyl ester. After this, steps 1 and 2 were conducted using the optimal conditions established in Section 2.2.4. Both catalyst and base loading were increased to 0.3 and 600 mol% respectively relative to tripropionin. This is to account for the 3 equivalents of methyl ester produced for every equivalent of triglyceride. Despite its inferiority to method B for the conversion of methyl propanoate to *iso*butanol, method A was also tested with tripropionin as the substrate. For this method, a shorter 10-minute pre-hydrogenation period was used.

n-Propanol can be formed in high yields from the hydrogenation of tripropionin, although these yields are significantly lower than when methyl propanoate is used as a substrate (79% compared to 95%, Table 2.5, Entry 1). In turn this can be converted into *iso*butanol in a 36% yield with 76% selectivity. Surprisingly, these numbers are comparable to when *iso*butanol is formed from the methyl ester, despite the lower hydrogenation yield. Direct conversion from the triglyceride to *iso*butanol is possible, although once again this is to the detriment of both the yield and selectivity of *iso*butanol (15% and 37% respectively, entry 3). When method A is used *n*-propanol is the major product. Given the lower *n*-propanol yields after step 1, and the large amount of remaining *n*-propanol after step 2, it was

proposed that extending reaction times would improve the *iso*butanol yield. As such the pre-hydrogenation period was extended by 15 minutes, step 1 by 2 hours and step 2 by 3 hours (entry 2). This had a significant effect, with the *n*-propanol yield after step 1 rising to 90% and the final *iso*butanol yield and selectivity increasing to 46%, and 85% respectively. This yield is greater than that reported when **Cat-5** is used for the direct conversion of ethanol to *iso*butanol, even if extended run times of 20 hours are used.[12] This is proposed to be because only one Guerbet cycle rather than two is needed for formation of the final product. Neither glycerol nor any glycerol Guerbet products were observed by GC analysis of the liquid phase, as such, it was postulated that the solid residue generated during reaction must contain any glycerol products produced. This is explored further in Section 2.5.

Table 2.5: Formation of isobutanol from tripropionin (Method B detailed below).
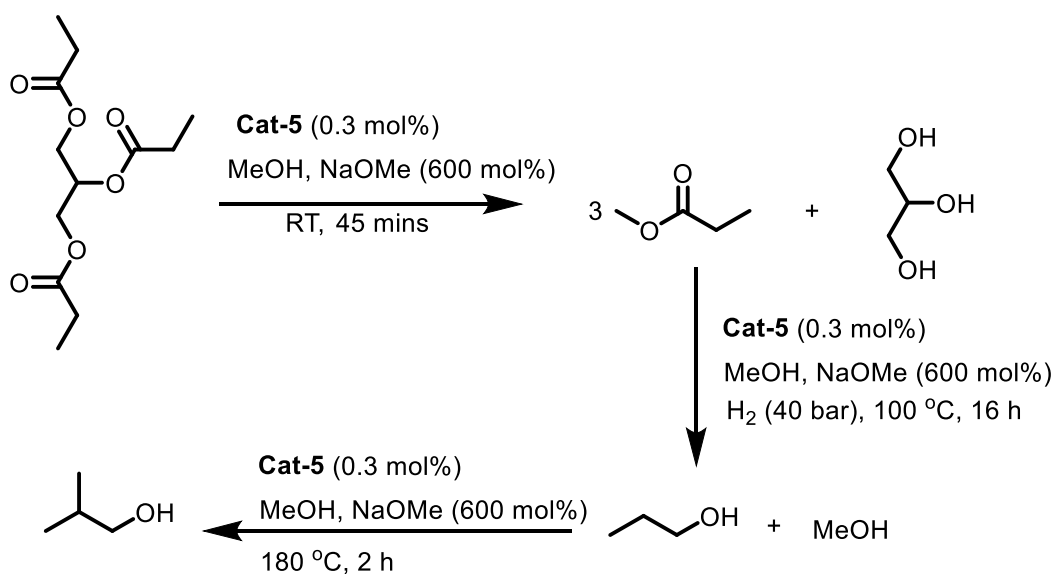
Entry[a]	Method[b,c]	Step	*n*-propanol Yield (%)[d]	*Iso*butanol Yield (%)[d]	*Iso*butanol selectivity (%)[e]
1	B	1	79	-	-
	-	2	9	36	76
2[f]	B	1	90	-	-
	-	2	8	46	85
3	A	-	26	15	37

[a] Conditions: methanol (10 mL), tripropionin (1 mL, 4.15 mmol), **Cat-5** (0.3 mol%, 0.0125 mmol, 7.56 mg), NaOMe (600 mol%, 1.345 g), [b] Method A: 10 min pre-hydrogenation period, H_2 (30 bar), 17 h, 180 °C, [c] Method B: 45 min pre-hydrogenation period, Step 1: 100 °C, H_2 (40 bar), 16 h, Step 2: 180 °C, 2h, [d] Yields as a % of the amount of tripropionin added [e] Selectivity calculated from observed products in the liquid fraction [f] 1 hr pre-hydrogenation period, Step 1: 18 h, Step 2: 5h.

2.3.1 – A dual catalyst system

While extending run times allowed this system to outperform previous systems where **Cat-5** had been used for *iso*butanol production. Other ruthenium complexes reported by the Wass group still outperform **Cat-5** in terms of *iso*butanol production from ethanol. For example, **Cat-1** (Figure 2.3) produced *iso*butanol in 65% yield over just 2 hours, almost double that seen for **Cat-5** under the same conditions.[18] When *n*-propanol is used as the substrate instead of ethanol, the yield of *iso*butanol increases to 70%, with 78% conversion (1 mL *n*-propanol, 10 mL methanol, 180 °C, 2h, 200 mol% NaOMe). This increase in yield is

due to only one Guerbet cycle being required for *iso*butanol formation, instead of the two required when ethanol is used as a substrate.
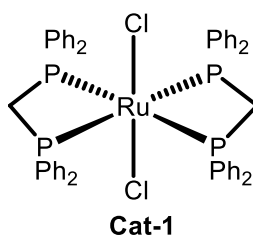
Cat-1

Figure 2.3: The most effective catalyst for isobutanol production from ethanol reported by the Wass group.

As **Cat-1** is very effective for Guerbet processes it was investigated as a catalyst for converting triglycerides to *iso*butanol. However, when benchmarking the ability of **Cat-1** to hydrogenate tripropionin, using conditions optimised for **Cat-5**, no activity was observed. As such, **Cat-1** alone cannot be used as a catalyst for this reaction. Instead, **Cat-1** was used in a dual catalyst system with **Cat-5**. Here, **Cat-5** is active for hydrogenation, whereas **Cat-1** is the dominant catalyst in the Guerbet reaction (Table 2.6).

The addition of **Cat-1** had a massive impact, with the *iso*butanol yield increasing to 63% with 93% selectivity. The rapid Guerbet catalyst clearly making step 2 significantly quicker. Unsurprisingly, step 1 was completely unaffected by **Cat-1**. When the dual catalyst system was used with method A, no improvement in performance was observed. It therefore postulated that while **Cat-5** can still work, albeit slowly, under high hydrogen pressure, the effect on **Cat-1** is much more severe. This dual catalyst system gives *iso*butanol yields comparable to those reported when **Cat-1** produces *iso*butanol directly from ethanol.[18] This dual catalyst system can also be applied to the production of β-methylated alcohols from non-triglyceride esters.

Table 2.6: Formation of isobutanol using a dual catalyst system, dominant catalyst for each step shown in bold.
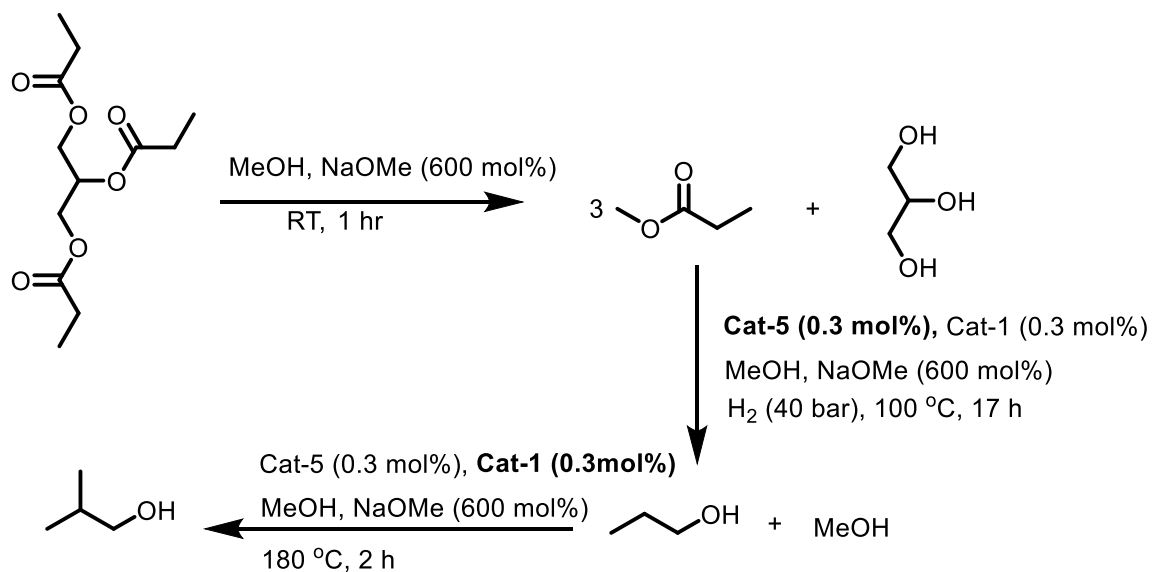
Entry[a]	Method[b,c]	Step	*n*-propanol Yield (%)	*Iso*butanol Yield (%)	*Iso*butanol selectivity (%)[d]
1	B	1	82	-	-
	-	2	4	63	93
2	A	1	23	12	35

[a] Conditions: methanol (10 mL), tripropionin (1 mL, 4.15 mmol), **Cat-5** (0.3 mol%, 0.0125 mmol, 7.56 mg), **Cat-1** (0.3 mol%, 0.0125 mmol, 11.7 mg), NaOMe (600 mol%, 1.345 g), [b] Method A: H_2 (30 bar), 20 h, 180 °C, [c] Method B: 1 hr pre-hydrogenation period, Step 1: 100 °C, H_2 (40 bar), 17 h, Step 2: 180 °C, 2h, [d] selectivity calculated from observed products in the liquid fraction.

2.3.1.1 – Production of *iso*butanol from ethyl acetate (an aside)

The above dual catalyst system can also be used for the production of *iso*butanol from ethyl acetate. Under non-pressurised conditions, **Cat-5** can produce ethyl acetate from ethanol.[15] However, under 40 bar of H_2 in a sealed reaction vessel the equilibrium is forced towards the hydrogenation reaction. A subsequent Guerbet step forms *iso*butanol, albeit in low yields (Table 2.7). This is likely because for every equivalent of ethyl acetate, two equivalents of ethanol are produced. Therefore, the reaction is conducted in 0.05 mol% **Cat-5** and **Cat-1**, and 100 mol% NaOMe with respect to ethanol. Despite its low yield, this reaction shows greater turnover numbers for the Guerbet reaction than the equivalent reaction with tripropionin (920 compared to 630); this is due to the low catalyst loadings

and that two Guerbet cycles are needed to form the desired product. This provides a useful example of the versatility of this process towards ester functionalisation.

Table 2.7: Formation of isobutanol from ethyl acetate using a dual catalyst system.
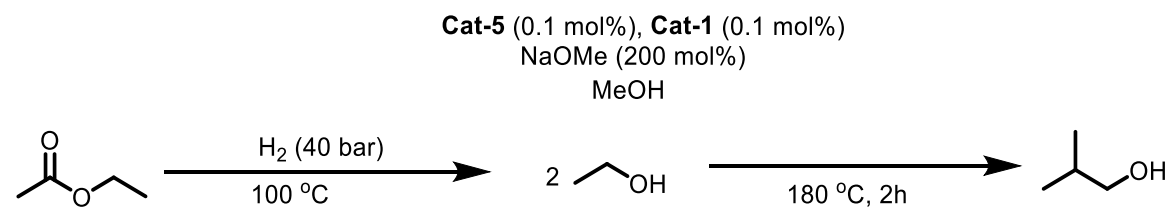
Entry	Method[a]	Step	Ethanol Yield (%)	*Iso*butanol Yield (%)	*Iso*butanol selectivity (%)[b]
1	B	1	97	-	-
	-	2	33	23	41

[a] Method B: methanol (10 mL), ethyl acetate (1 mL, 10.2 mmol), **Cat-5** (0.1 mol%, 0.0102 mmol, 6.2 mg), **Cat-1** (0.1 mol%, 0.0102 mmol, 9.6 mg), NaOMe (200 mol%, 1.106 g), Step 1: 100 °C, H_2 (40 bar), 17 h, Step 2: 180 °C, 2h [b] selectivity calculated from observed products in the liquid fraction

2.3.2 – Effect of base loading on *iso*butanol yield

While it has previously been established that higher base loading gives greater Guerbet reaction products (see section 2.2.2), the effect of base on the reaction as a whole is unclear. Given that hydrogenation of methyl esters with **Cat-5** can proceed with base loadings as low as 10 mol%,[13] and hydrogenation of methyl propanoate is unaffected by using 100 mol% NaOMe, it is possible that this step can proceed with low base loading and additional base can be added for step 2. This addition of fresh base to the reaction when it is required could help to increase catalytic activity and therefore product yield. To investigate this, the effect of base loading on catalytic performance was investigated (Table 2.8).

This investigation was performed on the monocatalyst system (Section 2.3). The use of this simpler system meant that fewer variables had to be controlled, also, it was the first step that was primarily under investigation for which **Cat-1** is inactive. Surprisingly, upon the reduction of base to 300 mol% (100 mol% relative to the methyl ester produced) a large decrease in *n*-propanol yield was seen (19%, Entry 2). The subsequent *iso*butanol yield produced during step 2 was also very low (4%). Reducing the base loading further to 150 mol% (Entry 3) gave comparable *n*-propanol yields to entry 2. However, a further reduction

in the final *iso*butanol yield was observed. While a high base loading is required for optimal activity in step 1, it appears that a baseline level of hydrogenation will occur with a lower amount of base present. Step 2 on the other hand is much more directly affected, with changes in base loading always reflected in the *iso*butanol yield.

The role of base in this reaction is twofold: firstly, it catalyses the transesterification of triglycerides to the corresponding FAME. Secondly, it allows for the conversion of **Cat-5** to its active catalytic form.[32] When methyl esters are used as a starting material transesterification prior to reaction is not necessary, hence the role of the base is only to activate the catalyst, and thus the loading can be lower. The dual use of base in this reaction, along with the low concentration of **Cat-5** compared to tripropionin, is likely why such large amounts of base are needed for high alcohol yields to be recorded.

Table 2.8: Effect of base loading on isobutanol formation from tripropionin using method B.

Entry[a]	Base loading (mol%)	Step	*n*-propanol yield (%)	*Iso*butanol Yield (%)	*Iso*butanol selectivity (%)[b]
1	600	1	79	-	-
		2	9	36	76
2	300	1	19	-	-
		2	13	4	22
3	150	1	23	-	-
		2	19	2	11

[a] Method B: methanol (10 mL), tripropionin (1 mL, 4.15 mmol), **Cat-5** (0.3 mol%, 0.0125 mmol, 7.56 mg), NaOMe loading as stated, 45 min pre-hydrogenation period, Step 1: 100 °C, H_2 (40 bar), 17 h, Step 2: 180 °C, 2h, [b] selectivity calculated from observed products in the liquid fraction

2.4 – Effect of pre-hydrogenation period

Cat-5 appears to be a spectator through this process, with little change in $^{31}P\{^{1}H\}$ NMR spectra observed during pre-hydrogenation. The interaction of **Cat-5** with base has been extensively studied by Schaub *et al.* and a variety of different ruthenium species identified, however, none of these were observed in this study upon the addition of NaOMe.[32]

When tripropionin was added to a 600 mol% solution of NaOMe in methanol a white precipitate began to form after ~2 minutes. Isolation of this solid and ^{1}H NMR spectroscopic analysis confirmed this to be a sodium glyceroxide salt (Scheme 2.6), while the liquid

fraction contained predominantly methoxide and methyl propanoate. Interestingly, while solid formed quickly when using 600 mol% base, formation was much slower (~2.5 hrs) when 300 mol% was used and no solid was seen overnight for 150 mol% base. The formation of this glyceroxide base may indicate why a high base loading is so vital for acceptable catalytic performance to be seen.
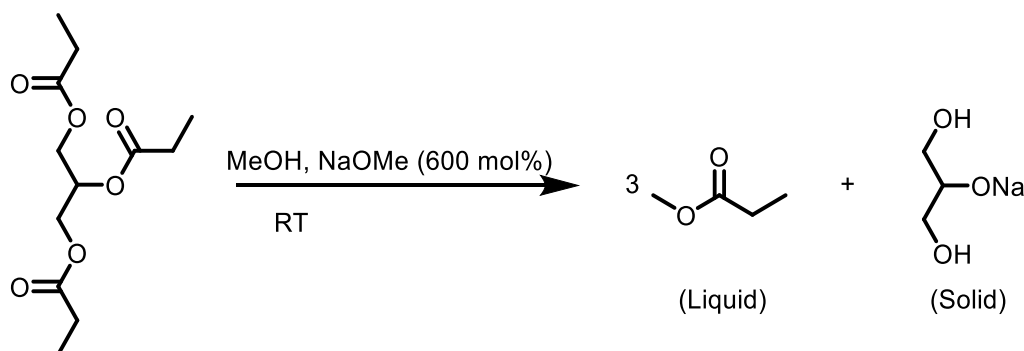
Scheme 2.6: Production of sodium glyceroxide via transesterification of tripropionin.

To establish the importance of this base, transesterification was allowed to proceed for one hour, after which all solid was removed by filtration and the liquid fraction was used for catalysis. Surprisingly, superior performance compared to when the solid was not removed was observed, indicating that its formation is detrimental to the reaction (Table 2.9, Entry 2). In all previous experiments a 45 – 60 min 'pre-hydrogenation period' had been allowed to give transesterification time to proceed. However, as solid glyceroxide begins to form during this period, a catalytic run without this additional time was also performed. Again, this showed superior performance to a standard catalytic run (Table 2.9, Entry 3). These initial experiments indicate that formation of the glyceroxide base is detrimental to catalytic activity.

Table 2.9: Investigating the effect of solid formation upon catalytic activity.

Entry[a]	Step	*n*-propanol yield (%)	*Iso*butanol yield (%)	*Iso*butanol selectivity (%)[b]
1	1	79	-	-
	2	9	36	76
2[c]	1	79	-	-
	2	11	45	80
3[d]	1	83	-	-
	2	13	44	78

[a] Conditions: methanol (10 mL), tripropionin (1 mL, 4.15 mmol), **Cat-5** (0.3 mol%, 0.0125 mmol, 7.56 mg), NaOMe (600 mol%, 1.345 g), 45 min pre-hydrogenation period, Step 1: 100 °C, H_2 (40 bar), 16 h, Step 2: 180 °C, 2h, [b] selectivity calculated from observed products in the liquid fraction [c] transesterification allowed to occur for 1 hr then mixture filtered and added to autoclave, [d] no prehydrogenation period used.

To investigate this further, sodium glyceroxide was synthesised from glycerol and sodium hydride and used as the base in the reaction. For ease of analysis, both steps were investigated in isolation and methyl propanoate was used as the substrate instead of tripropionin. The results of these experiments are shown in Table 2.10. Alongside usual base loadings (200 mol%), a base loading of 33 mol% was also investigated to replicate the complete conversion of glycerol to sodium glyceroxide when tripropionin is used as a substrate. When sodium glyceroxide was used as a base, the system was active for the hydrogenation of methyl propanoate, albeit at ~50% efficiency compared to NaOMe. Even at lower loadings some activity was seen (Entry 2). This indicates that NaOGly is sufficiently basic to activate the pre-catalyst **Cat-5**. This base showed no activity for Guerbet chemistry at either loading, although these runs do produce a lot of gas (28 bar after reaction for Entry 1) indicating that dehydrogenation was occurring but that the base was not sufficient to catalyse the Guerbet reaction.

Table 2.10: Use of sodium glyceroxide as a base for hydrogenation and Guerbet steps.

Entry	Step	Base loading (mol%)	*n*-propanol yield (%)	*n*-propanol conversion (%)	*Iso*butanol yield (%)
1	1	200	50	-	-
2	1	33	33	-	-
3	2	200	-	13	0
4	2	33	-	5	1

[a] Conditions: methanol (10 mL), **Cat-5** (0.1 mol%, 0.0104 mmol), NaOGly, Step 1: methyl propanoate (1 mL, 10.39 mmol), H_2 (40 bar), 16 h, Step 2: *n*-propanol (1 mL, 13.38 mmol), NaOGly, 180 °C, 2h

These results indicate why catalytic runs at lower base loadings perform so poorly. If much of the available base is converted sodium glyceroxide, a base which is much less effective for activating the pre-catalyst and catalysing the Guerbet reaction, this will have a hugely detrimental effect upon reactivity. Furthermore, as this base appears significantly less soluble than methoxide, precipitation during reaction will lower the concentration of base in solution.

2.5 – Solid analysis

As the solid produced at the beginning of the reaction had now been identified, attention was directed towards the post-reaction solid. When the Guerbet reaction is used to make *iso*butanol from ethanol a large amount of solid by-product is produced.[12] When the starting material is changed to tripropionin solid products are also observed; analysis of this can give insight into what side reactions are occurring during catalysis. It may also help to account for the final fate of the glycerol, given that none is observed during GC analysis of the reaction solution it seems likely that any glycerol products formed are in the solid residue. Isolation of the solid *via* filtration followed by drying *in vacuo* gave 0.72 g of a fine white powder. This was dissolved in D_2O and analysed by ^1H and $^{13}C\{^1H\}$ NMR spectroscopy. ^1H NMR analysis shows the sample is predominantly sodium formate, produced from the dehydrogenation of methanol (See Chapter 3, Section 3.6), there is also a significant amount of unreacted sodium methoxide still present. These results are unsurprising given formate production is noted when **Cat-5** is used in the direct production of *iso*butanol from ethanol.[12]

A small amount of propanoate is also produced from *n*-propanol *via* the Tishchenko reaction (Figure 2.4).[33] This is to be expected, as some acetate is produced when ethanol is used as the substrate. This solid also gives some indication as to the fate of the glycerol, with the doublet at 1.32 ppm and quartet at 4.15 ppm indicating the presence of sodium lactate. This is formed when glycerol is dehydrogenated to glyceraldehyde, which is subsequently dehydrated and then undergoes the Cannizzaro reaction forming lactic acid (Scheme 2.7). Lactic acid then reacts with NaOH (formed by the reaction of NaOMe with water) to produce sodium lactate which precipitates from the solution.[34] **Cat-5** has been used previously for the dehydrogenation of glycerol, producing lactic acid and molecular hydrogen, under much less forcing conditions than those used here (125 °C, 108 mol% KOH).[35] The formation of these products is unsurprising given that sodium formate also forms *via* Cannizzaro chemistry and **Cat-5**, along with other ruthenium catalysts, is already known for this transformation.[36] The cause of the singlet at 1.35 ppm is as yet unexplained; it has been proposed this could be caused by formation of a glycerol Guerbet product where the central 3° carbon is methylated. However, to date, the addition of a methyl group to a 3° carbon centre by Guerbet chemistry has not been observed, therefore this does not appear to be a likely product. As glycerol dehydrogenation seems to compete with Guerbet chemistry this could explain why removal of the pre-hydrogenation solid improved the *iso*butanol yield.
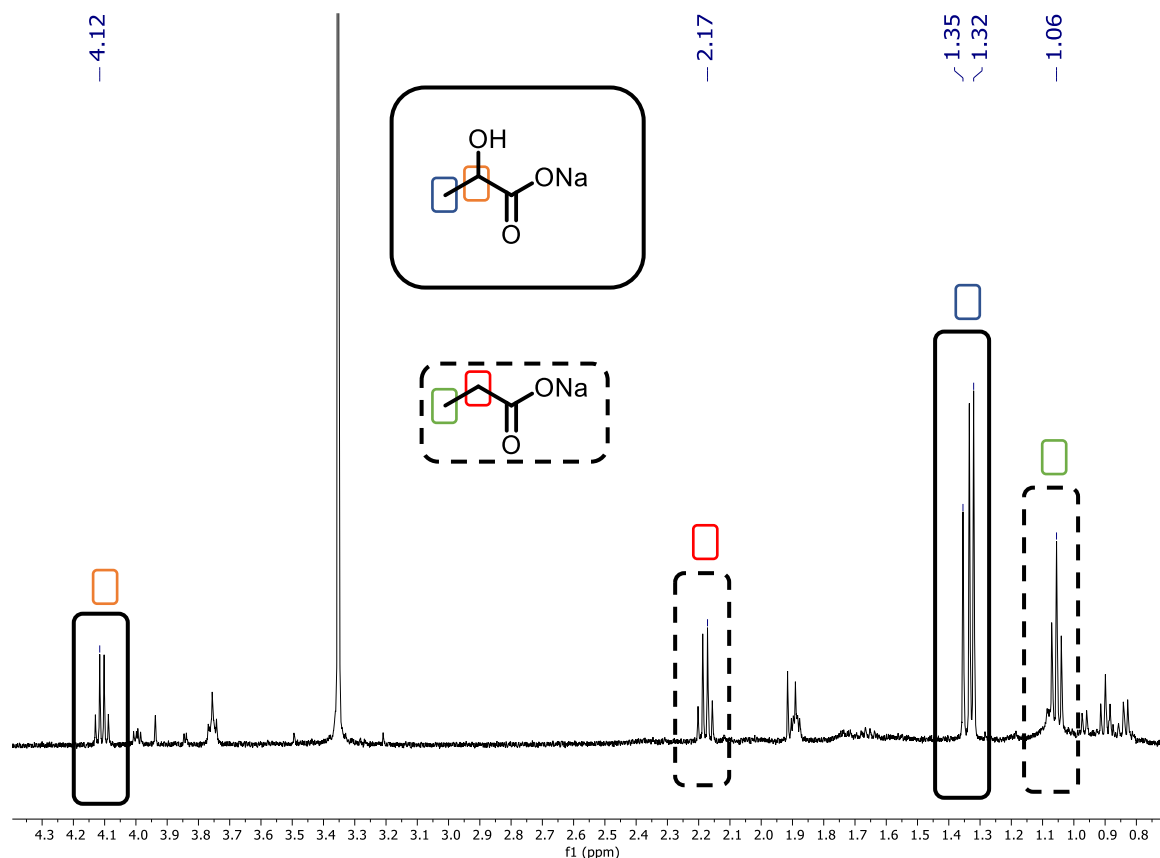
Figure 2.4: ^{1}H (500 MHz, D$_2$O) NMR spectrum of solid residue produced during isobutanol formation from tripropionin (Table 2.5, Entry 2). Small amount of THF visible at 1.90 and 3.75 ppm- this is an impurity in the NMR solvent.
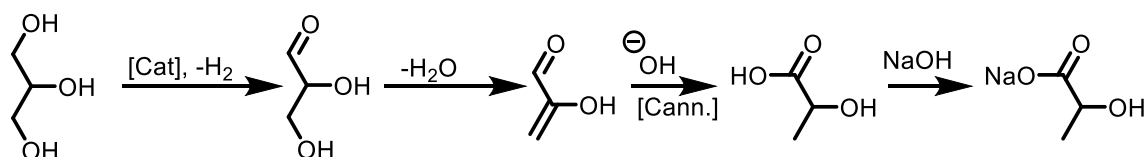
Scheme 2.7: Formation of sodium lactate from glycerol via Cannizzaro chemistry. [Cann.] indicates the Cannizzaro reaction step.

The ^{13}C{^{1}H} NMR spectrum (Figure 2.5) shows the presence of both sodium formate (171 ppm) and sodium carbonate (168 ppm) in the solid residue. Again, this is to be expected, as both are produced from methanol and are seen in the solid analysis of methanol and ethanol coupling reactions.[12]
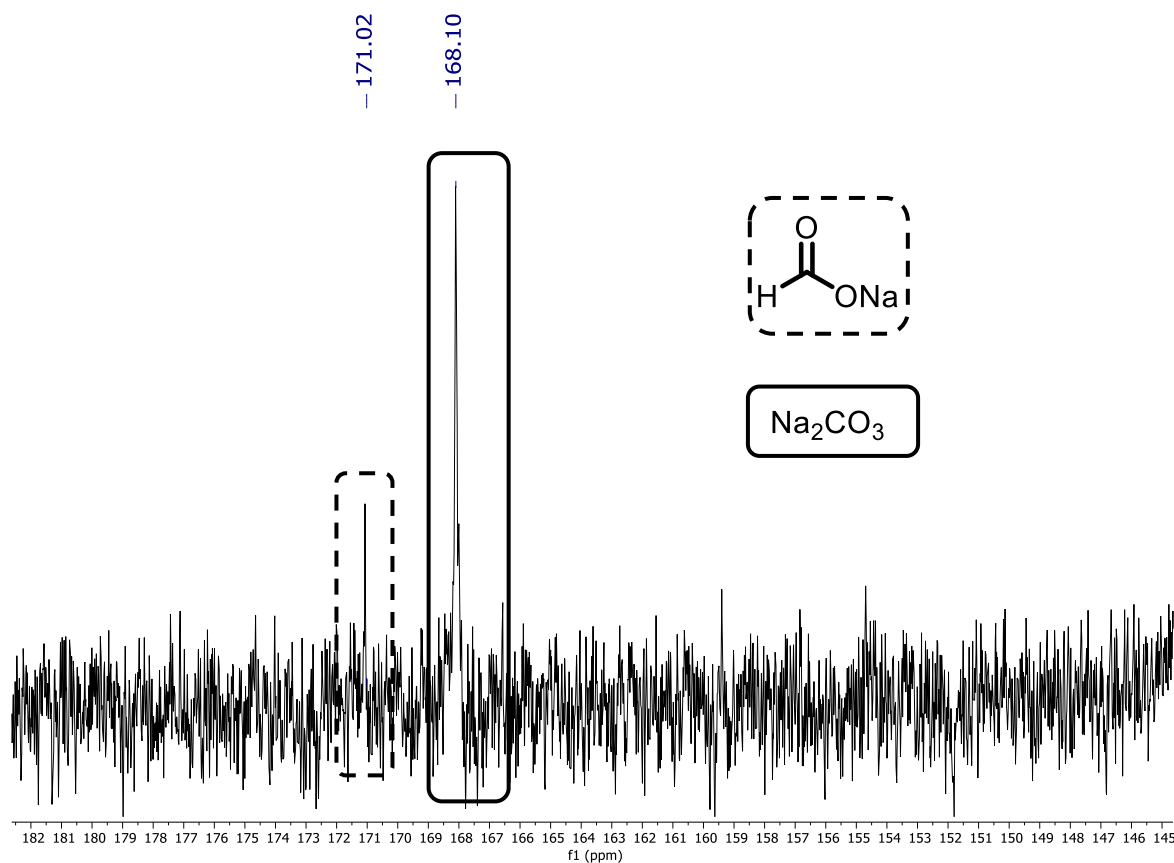
Figure 2.5: $^{13}C\{^1H\}$ (126 MHz, D_2O) NMR spectrum of solid residue produced during isobutanol formation from tripropionin (Table 2.5, Entry 2).

This solid analysis shows once again that in Guerbet chemistry the two main competing side processes are the Tishchenko and Cannizzaro reactions, with formate and carbonate making up most of the solid produced. However, it does give key insight into the fate of the glycerol in these reactions, which hitherto had not been investigated. Crude glycerol, predominantly formed as a by-product during biodiesel production, is developing into an important chemical feedstock due to its low cost and high availability.[37,38] If glycerol can be removed from the reaction before it is converted to lactate, it could find uses in other areas of chemistry.
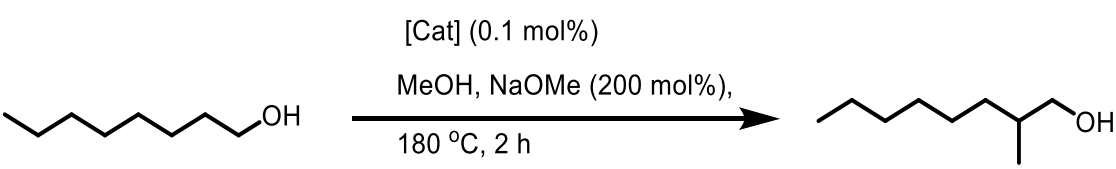
2.6 – Functionalisation of longer chain triglycerides towards β-methylated alcohols

Now that the possibility of producing β-methylated alcohols from triglycerides using **Cat-5**, or a dual catalyst system of **Cat-5** and **Cat-1,** had been established. Focus was changed to expanding the substrate scope of the reaction, primarily by extending the length of the fatty acid chain. As such, triglycerides with C8 and C12 chains were chosen for further investigation.

2.6.1 – Choice of catalytic system

With the dual catalyst system employed above, **Cat-5** is used for the hydrogenation of the triglyceride to the alcohol, and **Cat-1** is used for the subsequent coupling of the linear alcohol with methanol to give the β-methylated alcohol. The ability of both **Cat-5** and **Cat-1** to catalyse the coupling of methanol and octanol was investigated before conversion from the triglyceride was attempted (Table 2.11). Surprisingly, while **Cat-1** is very active for the coupling of *n*-propanol and methanol (70% *iso*butanol yield) it becomes significantly less active when the alcohol chain length is increased, giving a methylated alcohol yield of only 2.3%. **Cat-5** was also very active for *iso*butanol production (59%), and the effect of decreasing yield with increasing chain length was not observed with 82% octanol conversion, along with 57% of the β-methylated alcohol observed. Production of 2-methyloctanol as the major product was confirmed by GC-MS. As **Cat-5** is the superior catalyst for Guerbet coupling of higher alcohols with methanol, the mono catalyst system was used with long chain triglyceride substrates.

Table 2.11: Conversion of octanol to 2-methyl-octanol.

[Cat] (0.1 mol%)

MeOH, NaOMe (200 mol%),

180 °C, 2 h

Entry[a]	Catalyst	Octanol Conversion (%)	2-methyloctanol yield (%)[b]
1	Cat-5	82	57
2	Cat-1	6	2.3

[a] Conditions: methanol (10 mL), Octanol (1 mL, 6.3 mmol), [cat] (0.0063 mmol, 0.1 mol%), NaOMe (0.68 g, 200 mol%), 180 °C, 2h, [b] Yield as a percentage of all products in the the organic fraction

2.6.2 – Formation of β-methylated alcohols from C8 and C12 triglyceride feedstocks

Initial experiments into the functionalisation of glyceryl trioctanoate were performed in the same reaction vessel using the same volumetric ratio of solvent to substrate as had been used for previous reactions with both ethanol and tripropionin (10:1).[18] However, this gave very little hydrogenation to octanol and only trace amounts of 2-methyloctanol *via* both methods A and B (Table 2.12, Entries 1 and 2). As the substrates get heavier, maintaining the same volumetric ratio decreases the molar ratio of substrate to methanol (14.4:1 for ethanol, 19.9:1 for tripropionin and 40.6:1 for glyceryl trioctanoate). This decrease in

substrate-, and therefore catalyst-, loading has little effect for short chain triglycerides. However, for larger triglycerides, catalyst and substrate concentrations were too low for appreciable product yield to be observed at a 10:1 solvent:substrate volumetric ratio. As such, the solvent:substrate molar ratio was increased to match that used in methanol-ethanol coupling chemistry (14.4:1).[18] This gave octanol yields of 80% after hydrogenation (Entry 3, step 1), significantly greater than those observed previously. The subsequent Guerbet step resulted in 63% octanol consumption, and significant amounts of 2-methyloctanol, 62% of the organic soluble fraction. Small amounts of non-hydrogenated methyloctanoate (2.5%) and 2-methyloctene (from the dehydration of 2-methyloctanol) are also observed. A significant amount of octanoic acid was also present, generated by dehydrogenation of octanol by **Cat-5**. Carboxylic acid salts are usually observed in the solid by-product after Guerbet chemistry. However, the presence of glycerol-based salts in the solid indicates that these may have exhausted the supply of sodium ions, allowing some acid to remain in solution.

Table 2.12: Conversion of glyceryl trioctanoate to 2-methyloctanol.
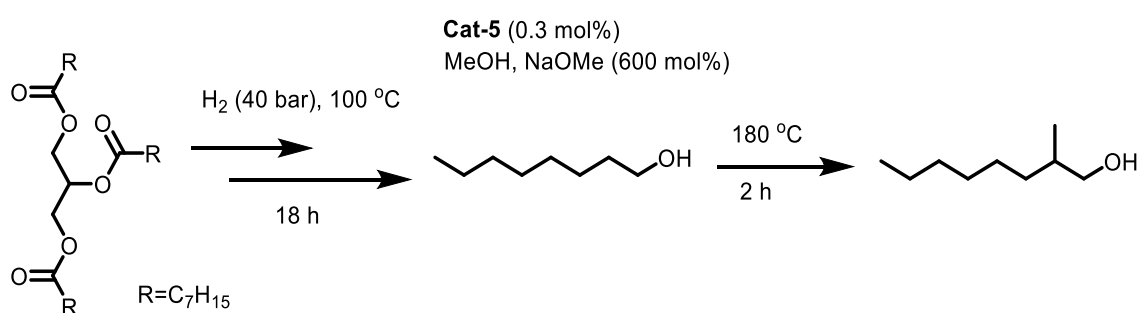
Entry[a]	Method[b,c]	Step	Octanol Yield (%)[d]	2-methyloctanol yield (%)
1	B	1	12	-
	-	2	7	Trace
2	A	-	5	Trace
3[e]	B	1	80	-
	-	2	17	62[f]

[a] Conditions: Methanol (10 mL), glyceryl trioctanoate (1 mL, 2.03 mmol), **Cat-5** (6 mg, 0.0037 mmol, 0.3 mol%), NaOMe (0.66 g, 600 mol%), [b] Method A: 180 °C, H_2 (30 bar), 18 h, [c] Method B: 45 minute pre-hydrogenation period Step 1: 100 °C, H_2 (40 bar), 17 h, Step 2: 180 °C, 2 h, [d] Calculated by GC, [e] glyceryl trioctanoate (2.81 mL, 5.71 mmol), **Cat-5** (17 mg, 0.0104 mmol, 0.3 mol%), NaOMe (1.85 g, 600 mol%), [f] Yield as a percentage of all products in the organic fraction.

With the importance of a moderate solvent:substrate molar ratio now established, trilaurin, a triglyceride produced in laurel leaves, was investigated. At high solvent:substrate ratios, (14.4:1) excessive solid build up made GC analysis challenging, this was easily avoided by reducing substrate loading slightly to a 20:1 molar ratio. Production of 2-methyldodecanol (Scheme 2.8) was possible under the previously established reaction conditions, with product formation confirmed by GC-MS. Neutralisation of the post reaction mixture with 1 M HCl, in order to allow for analysis of any sodium salts produced during reaction, followed by extraction with toluene showed that 2-methyldodecanol is the major product making up 54% of the organic fraction. A small amount of the dehydrated product 2-methyldodecene along with dodecanoic acid is also observed. This is this first example of β-methylated alcohols being produced directly from naturally occurring triglycerides.
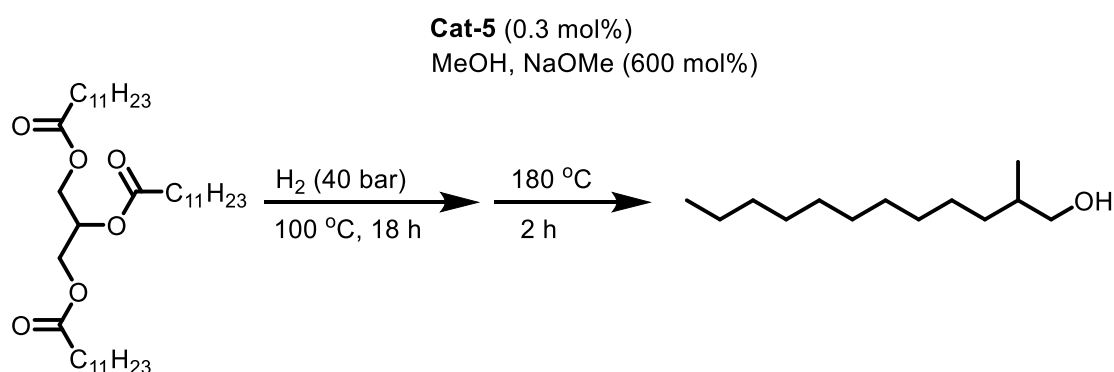
Scheme 2.8: Formation of 2-methyldodecanol from trilaurin.

2.7 – Alkene hydrogenation

While trilaurin is a saturated naturally occurring triglyceride, most readily available triglycerides contain one or more unsaturated C=C bonds (Figure 2.6). Hydrogenation of these double bonds is shown to improve fuel stability, whereas maintaining them can improve low temperature flow characteristics. Previous ruthenium catalysts have shown little selectivity in the hydrogenation of methyl oleate with the saturated alcohol being the major product.[39] However, these experiments were carried out using a dimeric ruthenium catalyst supported by a PNN pincer ligand. In many long chain triglycerides, the unsaturated C=C bonds are located some distance from the ester functionality and there is no

conjugation between them. As such, to establish the activity of **Cat-5** towards alkene hydrogenation, 1- and 2-hexene were chosen as model substrates (Scheme 2.9).
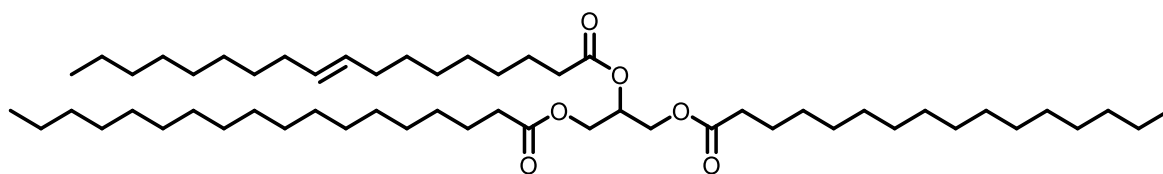
Figure 2.6: Cocoa butter: a commonly used, readily available triglyceride containing an unsaturated fatty acid chain.
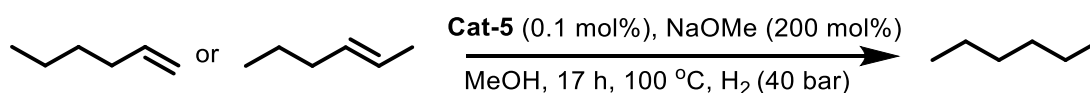
*Scheme 2.9: Hydrogenation of 1-hexene and 2-hexene by **Cat-5**.*

Hydrogenation was conducted under analogous conditions to method B, step 1, and the post reaction mixture was analysed by ^{1}H NMR spectroscopy (Figure 2.7). This indicated that 1-hexene was smoothly hydrogenated to the saturated alkene, with a small amount of 2-hexene also being observed due to isomerisation. However, 2-hexene showed significantly less hydrogenation, with only a small amount of hexane observed by ^{1}H NMR spectroscopy. As slow isomerisation occurs under the reaction conditions it seems likely that 2-hexene is converted to 1-hexene, which can readily undergo hydrogenation. However, 2-hexene itself cannot be hydrogenated under these conditions without being isomerised beforehand. Unfortunately, as hexane, and 2-hexene peaks overlap in the ^{1}H NMR spectrum, exact conversions and yields could not be calculated.

Given that hydrogenation of internal C=C bonds is slow under the chosen reaction conditions, and C=C bonds in most common triglycerides are internal (most vegetable oils contain oleic, linoleic and linolenic fatty acid chains). It seems likely that method B can be used for the selective production of unsaturated β-methylated alcohols.
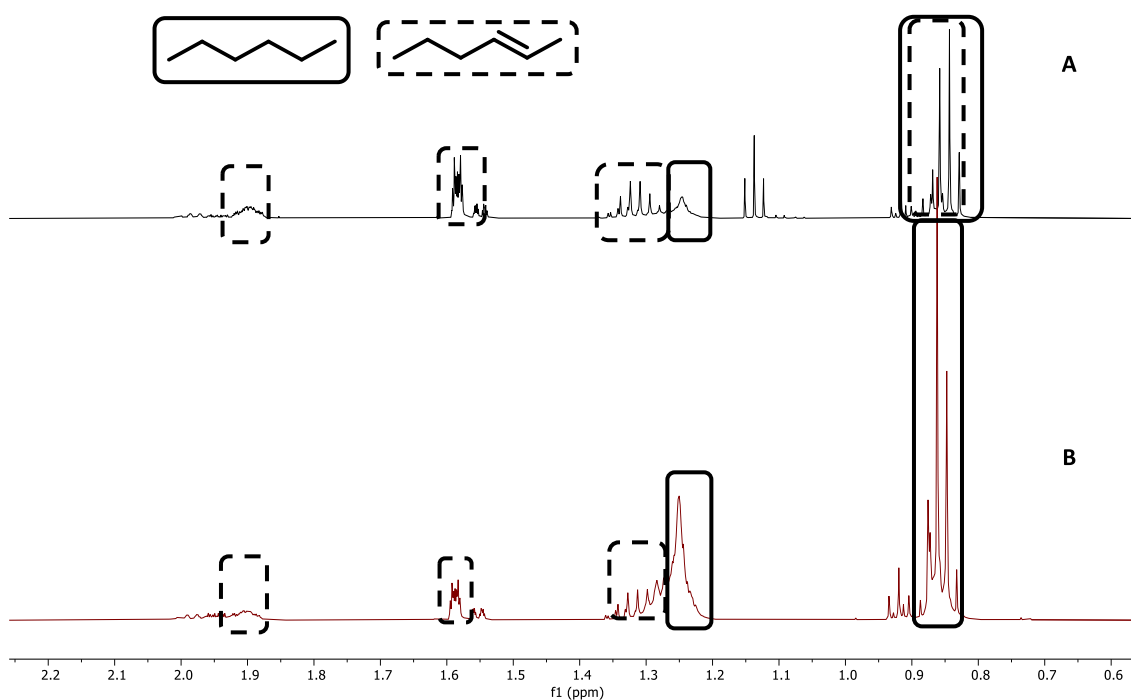
Figure 2.7: ^{1}H NMR (500 MHz, MeOH) spectra of the post reaction mixture of (A) 2-hexene hydrogenation (B) 1-hexene hydrogenation. Triplet at 1.15 ppm in (A) due to diethyl ether impurity.

For further investigation methyl oleate was chosen as a model substrate (Scheme 2.10). Many commercially available triglycerides contain oleyl fatty acid chains and as such this was considered an ideal starting point. Analysis of the post reaction mixture by GC-MS showed the presence of both oleyl alcohol and octadecanol, indicating that both C=C and C=O bond hydrogenation is possible. As the unsaturated alcohol is present in higher quantities than its saturated analogue this result suggests that **Cat-5** is still more selective for carbonyl hydrogenation. After performing the Guerbet step β-methylated products of both the saturated and unsaturated alcohol were observed, thus showing that the double bond had no detrimental effect upon Guerbet chemistry. The post reaction mixture after hydrogenation contained a large amount of solid, likely due to the formation of octadecanol which is a solid at room temperature. Unusually, performing the Guerbet step reduces the amount of solid observed. This is attributed to the effect of β-methylation, causing the melting point to decrease. Qualitative analysis of the post reaction mixture has

confirmed the presence of the expected products; however, quantitative analysis has to date not been possible.
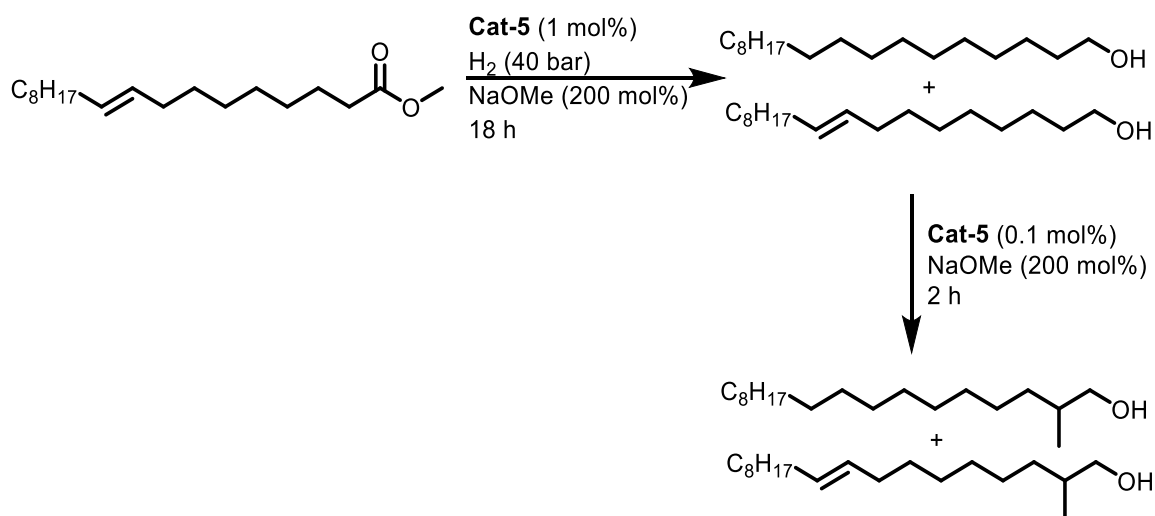
Scheme 2.10: Formation of β-methylated alcohols from methyl oleate.

2.8 - Formation of β-methylated alcohols from coconut oil

Now that the ability of this system to form β-methylated alcohols from triglycerides containing a variety of different fatty-acid chain lengths had been established, and its interaction with C=C bonds investigated, attention was turned to more readily available triglycerides. Coconut oil from *Cocos nucifera* contains a variety of different fatty acid chain lengths (Figure 2.8),[40] meaning that by hydrogenation a variety of different alcohols would be produced, and the final product would be a mixture of alcohol chain lengths. This should give insight into how this system deals with a mixture of substrates, and how this affects reactivity.
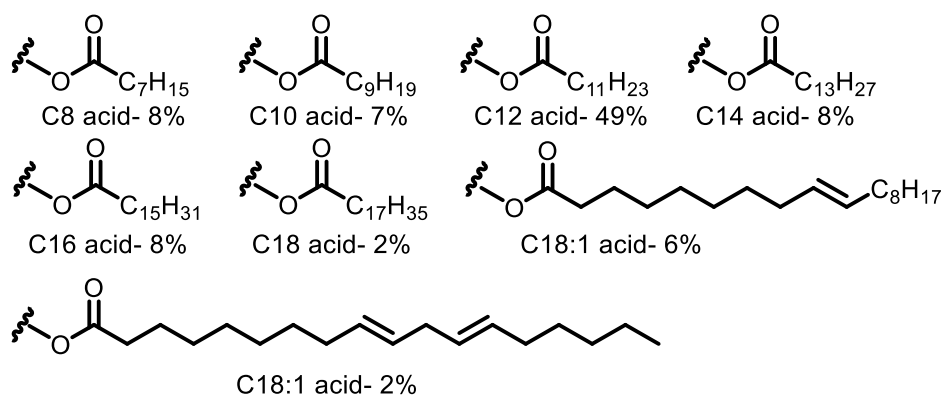
Figure 2.8: Fatty acid chain lengths in coconut oil.

Analysis of the post reaction mixture by GC-MS showed a variety of different chain length alcohols present, indicating that hydrogenation was unselective towards a particular carbon chain length, as has been observed before. This GC-MS trace also showed the presence of many methyl-branched alcohols indicating that the Guerbet reaction had also been successful. As expected, 2-methydodecanol was present in the highest proportion, but appreciable amounts of a variety of other carbon lengths were also detected. Unlike the hydrogenation step the Guerbet reaction did not proceed to completion, as shown by the presence of a large amount of linear alcohol. While qualitative analysis of the post reaction mixture was possible, detailed quantitative analysis has not yet been performed, which would give exact yields of each of the respective linear and branched alcohols. This work has been an exciting 'proof of concept' of the functionalisation of readily-available triglycerides to β-methylated alcohols.

2.9 – Heterogeneous catalysts for β-methylated alcohol production from triglycerides

As a homogeneous catalyst, separation of **Cat-5** from the post reaction mixture would present a serious challenge in the industrialisation of this process. In Industry, the Guerbet reaction is performed with heterogeneous copper chromite or Raney-Ni catalysts.[41] Carlini *et al.* have also used a variety of copper chromite and Raney-Cu catalysts for the production of *iso*butanol from *n*-propanol, later showing the activity of Mg/Al mixed metal oxides for the same process.[42–44] Several precious metals supported on activated carbon, including ruthenium, are also known to catalyse Guerbet chemistry.[41] Given the advantages heterogenous catalysts offer in terms of separation, the potential of replacing **Cat-5** with a heterogenous catalyst was investigated (Table 2.13). Tripropionin was chosen as the model substrate for these investigations to allow for ease of analysis.

Table 2.13: Heterogeneous catalysts for the production of isobutanol from tripropionin.

Entry[a]	Step	Catalyst	*n*-propanol Yield (%)	*Iso*butanol Yield (%)
1	1	Ru/C (5 wt%)	0	0
	2	-	0	0
2	1	$2CuO.Cr_2O_3$	0	0
	2	-	0	0

[a] Method B: methanol (10 mL), tripropionin (1 mL, 4.15 mmol), [cat] (0.3 mol%, 0.0125 mmol), NaOMe (600 mol%, 1.345 g), 45 min pre-hydrogenation period, Step 1: 100 °C, H_2 (40 bar), 17 h, Step 2: 180 °C, 2h

Unfortunately, neither catalyst produced any *n*-propanol or *iso*butanol. Analysis of the post reaction mixture by ^{1}H NMR spectroscopy showed only methyl propanoate. While both these catalysts are active for Guerbet chemistry, they show no activity towards ester hydrogenation under these reaction conditions. Copper chromite ($2CuO.Cr_2O_3$) is used industrially for the hydrogenation of FAMEs, however, harsh conditions (40-300 bar H_2, 170-300 °C) are required.[45] Moreover, copper chromite catalysts are poisoned by the presence of glycerol or glycerol decomposition products in the reaction mixture.[46] As such, these catalysts could not be used for the hydrogenation of triglycerides without first removing the glycerol from the solution after transesterification.

While these catalysts were inactive for ester hydrogenation, there remain a multitude of commercially available heterogeneous catalysts which are active for Guerbet coupling which could be tested for the above reaction.

2.10 – Neat hydrogenation of triglycerides

Direct hydrogenation of coconut oil under neat conditions without prior formation of the FAME was recently reported by the Guan group. This process primarily used a homogeneous ruthenium catalyst supported by a PNN ligand. However, this publication also showed the ability of the preactivated Ru-MACHO **Cat-6** to promote the same reaction.[28] Inspired by this, direct hydrogenation of glyceryl trioctanoate to octanol was attempted with **Cat-5** (Table 2.14). If this were possible, subsequent octanol homocoupling to the C16 alcohol could be attempted.

Unfortunately, **Cat-5** only produced trace amounts of octanol, with the ester octyl octanoate instead being the major product. Changing the base from NaOOct to NaOMe

made little difference to the reaction. It was initially proposed that these low octanol yields may be due to slow catalyst activation caused by low base loadings (see Section 2.3.2). However, using the preactivated catalyst **Cat-6** (Figure 2.9) gave comparable results, ruling this out as the cause. **Cat-5** is a very active catalyst for the dehydrogenative coupling of alcohols to esters.[15] It therefore seems likely that while **Cat-5** is active for triglyceride hydrogenation, the alcohol produced is rapidly converted to the ester, thus giving octyloctanoate as the major product. When **Cat-5** is used for the homocoupling of octanol, octyloctanoate is seen as the major product, with selectivity for the Guerbet product being only 11%. Due to its poor selectivity for Guerbet chemistry under neat alcohol conditions, it seems unlikely that **Cat-5** could be used to produce long chain branched alcohols from neat triglycerides.

Cat-6
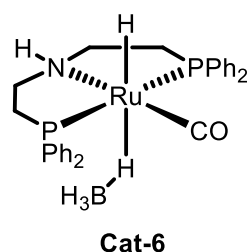
*Figure 2.9: An analogue of **Cat-5** that does not require base for activation.*

Table 2.14: Neat hydrogenation of glyceryl trioctanoate.
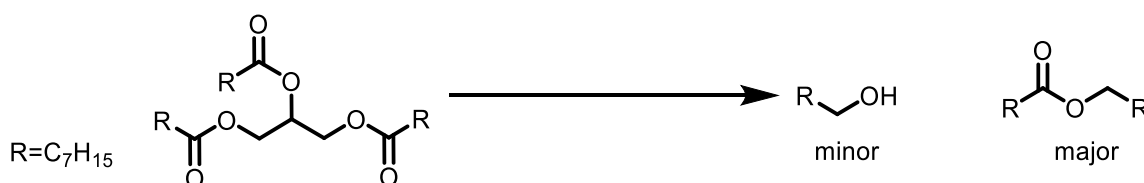
Entry	Base	Catalyst	Octanol Yield (%)	Octyloctanoate Yield (%)
1	NaOOct	1	0.4	23
2	NaOMe	1	0.7	22
3	NaOMe	5	0.8	26

[a] Conditions: glyceryl trioctanoate (10 mL, 20.3 mmol), base (15 mol%, 3 mmol), [cat] (0.3 mol%, 37 mg), H_2 (40 bar), 100 °C, 18 h.

Guan *et al.* reported high alcohol yields (84%) when **Cat-6** was used for neat triglyceride hydrogenation, with little mention of ester formation.[28] This is likely as a result of the elevated reaction temperatures (135 °C) and hydrogen pressures (52 bar). If ester

formation could be suppressed, the use of the dual catalyst system could maximise the yield of the homocoupled alcohol. However further research is required to establish the viability of this process.

2.11 – Summary

The ability of **Cat-5** to produce *iso*butanol from methyl propanoate *via* cascade catalysis has been established. This process has also been applied to triglycerides, with *iso*butanol also being formed from tripropionin. For these reactions high base loadings are still required in order to form product in a reasonable yield. Decreasing base loading reduces the efficiency of both the hydrogenation and the Guerbet steps due to the formation of a sodium glyceroxide precipitate. For tripropionin, the use of a dual catalyst system containing both **Cat-5** and **Cat-1** was found to give the greatest product yields. However, this system could not be applied to longer triglycerides as **Cat-1** was largely inactive for the heterocoupling of higher alcohols and methanol. The monocatalyst system was active for the production of β-methylated alcohols from glyceryl trioctanoate and trilaurin. Although a balance in substrate concentration needed to be found to allow for reaction without excessive solid build-up. This system can be applied to methyl oleate hydrogenation with both C=C and C=O bond hydrogenation observed. Coconut oil could also be functionalised with a complex mixture of linear and β-methylated alcohols being produced. Several heterogeneous systems have been investigated but have shown no activity towards ester hydrogenation. Attempts to use **Cat-5** for the neat hydrogenation of triglycerides have shown some potential. However, as **Cat-5** is a very active acceptorless dehydrogenation catalyst, it quickly forms esters from any alcohol produced. As such, a larger catalyst and/or condition screen is needed for this reaction.

2.12 – Future work

While this process has shown pleasing activity towards the functionalisation of simple, symmetrical, short chain triglycerides, its activity towards more complicated triglycerides (with the exception of coconut oil) remains as yet under investigated. Many naturally occurring triglycerides contain three separate fatty acids of different lengths and degrees of unsaturation (Figure 2.10). It is possible that these longer more complicated triglycerides may not be so amenable to this process. Given the plethora of different products it is possible to make during this reaction, depending on the degree of hydrogenation (14 for

rapeseed oil, pictured below), analyses of these reactions are likely to be significantly more challenging. Furthermore, the production of many long chain alcohols can lead to issues with solid build-up, thus making analysis complicated.
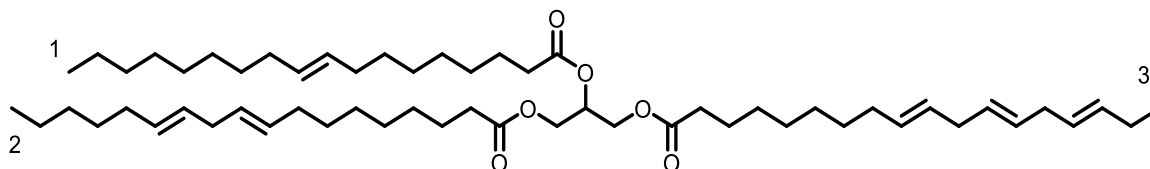
Figure 2.10: Chemical structure of rapeseed oil containing (1) oleic (2) linoleic and (3) linolenic fatty acid chains.

Quantification of the selectivity of C=C vs. C=O hydrogenation in methyl oleate needs to be conducted, and greater investigation into the tuning of this selectivity should be undertaken. It is possible using less forcing reaction conditions (lower H_2 pressures/temperatures) along with longer reaction times may help to keep the olefin bond intact, leading to the formation of alcohols with greater cold-flow properties. Conversely, the use of more forcing conditions could lead to complete dehydrogenation of methyl oleate, giving a product with greater stability.[2]

Two of the key issues with this reaction are the high base loadings required and the large amount of solid produced. While these issues are not too significant in a lab scale reaction, they would make scale up to an industrial process challenging and costly, as such solutions need to be found before commercialisation could be considered. For *n*-butanol formation it was found that using the corresponding alkoxide base gave the best yields.[47] However, no further base screen has been conducted for this reaction with hydrogenation included. It is possible that a base which showed inferior performance for Guerbet chemistry alone may be more effective, or require lower loadings, when used in cascade catalysis. Solid is predominantly produced by the dehydrogenation of alcohols to form carboxylic acid salts like formate and propanoate. Therefore, to reduce solid production a catalyst which is less active for alcohol dehydrogenation must be used. As such, a wider catalyst screen is required.

Another key step towards commercialisation would be the discovery of an active heterogeneous catalyst, as this makes purification of the final product significantly easier. Supporting a homogeneous catalyst on silica or alumina could also be a potential route to

heterogenisation. Initially a catalyst which is active for ester hydrogenation must be found, as this has been the issue with all previously tested systems. The doping of rhenium onto Raney catalysts has been shown to reduce the temperatures and pressures needed for hydrogenation of FAMEs (200 °C, 80 bar H_2).[48] Rhenium doped Ru/SiO_2 or Rh/C is also been shown to hydrogenate FAMEs at pressures of only 35 bar H_2.[49] As both Raney metals and Ru/C are known to catalyse the Guerbet coupling of alcohols, investigating these catalytic systems may be a useful starting point.

Finally, further investigation should be conducted into catalysts that can hydrogenate neat triglyceride without subsequently dehydrogenating the product alcohol back to an ester. These alcohols can then be homocoupled to give long chain branched alcohol products. Catalyst **1.19** has been noted for triglyceride hydrogenation (Figure 2.11), and is known for the homocoupling of ethanol *via* the Guerbet reaction.[28,50] Milstein *et al.* have also reported other effective Guerbet catalysts that have yet to be investigated for triglyceride hydrogenation (e.g. **1.7**). These complexes show potential for the neat functionalisation of triglycerides to β-branched alcohols.

1.19   **1.7**
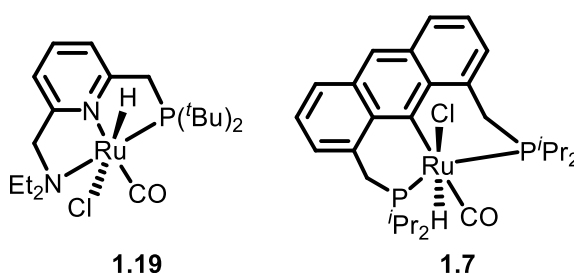
Figure 2.11: Potential catalysts for the production of β-branched alcohols from triglycerides.

2.13 – References

1   Statista, World vegetable oil production 2020, https://www.statista.com/statistics/263978/global-vegetable-oil-production-since-2000-2001/, (accessed 10 April 2020).

2   T. P. Durrett, C. Benning and J. Ohlrogge, *Plant J.*, 2008, **54**, 593–607.

3   G. Knothe and K. R. Steidley, *Fuel*, 2005, **84**, 1059–1065.

4   T. W. Ryan, L. G. Dodge and T. J. Callahan, *J. Am. Oil Chem. Soc.*, 1984, **61**, 1610–1619.

5   Commission of the European Communities, *Report on the progress made in the use of biofuels and other renewable fuels in the Member States of the European Union*, 2007.

6   I. Lee, L. A. Johnson and E. G. Hammond, *J. Am. Oil Chem. Soc.*, 1995, **72**, 1155–1160.

7   R. O. Dunn, M. W. Shockley and M. O. Bagby, *J. Am. Oil Chem. Soc.*, 1996, **73**, 1719–1728.

8   A. Serdari, E. Lois and S. Stournas, *Ind. Eng. Chem. Res.*, 1999, **38**, 3543–3548.

9   G. Knothe and R. O. Dunn, *J. Am. Oil Chem. Soc.*, 2003, **80**, 1021–1026.

10   L. Yao and E. G. Hammond, *J. Am. Oil Chem. Soc.*, 2006, **83**, 547–552.

11   B. G. Harvey and H. A. Meylemans, *J. Chem. Technol. Biotechnol.*, 2011, **86**, 2–9.

12   K. J. Pellow, R. L. Wingad and D. F. Wass, *Catal. Sci. Technol.*, 2017, **7**, 5128–5134.

13   W. Kuriyama, T. Matsumoto, O. Ogata, Y. Ino, K. Aoki, S. Tanaka, K. Ishida, T. Kobayashi, N. Sayo and T. Saito, *Org. Process Res. Dev.*, 2012, **16**, 166–171.

14   O. Ogata, H. Nara, M. Fujiwhara, K. Matsumura and Y. Kayaki, *Org. Lett.*, 2018, **20**, 3866–3870.

15   M. Nielsen, H. Junge, A. Kammer and M. Beller, *Angew. Chem. Int. Ed.*, 2012, **51**, 5711–5713.

16   A. Kaithal, M. Schmitz, M. Hölscher and W. Leitner, *ChemCatChem*, 2019, **11**, 5287–5291.

17   A. Kaithal, M. Schmitz, M. Hölscher and W. Leitner, *ChemCatChem*, 2020, **12**, 781–787.

18   R. L. Wingad, E. J. E. Bergström, M. Everett, K. J. Pellow and D. F. Wass, *Chem. Commun.*, 2016, **52**, 5202–5204.

19   R. L. Wingad, P. J. Gates, S. T. G. Street and D. F. Wass, *ACS Catal.*, 2015, **5**, 5822–5826.

20   H. T. Teunissen and C. J. Elsevier, *Chem. Commun.*, 1997, 667–668.

21   A. Riley, Ph.D. Thesis, Univeristy of Bristol, 2020.

22   W. Kuriyama, Y. Ino, O. Ogata, N. Sayo and T. Saito, *Adv. Synth. Catal.*, 2010, **352**, 92–96.

23   S. Werkmeister, K. Junge and M. Beller, *Org. Process Res. Dev.*, 2014, **18**, 289–302.

24   L. A. Saudan, C. M. Saudan, C. Debieux and P. Wyss, *Angew. Chemie*, 2007, **119**, 7617–7620.

25   H. T. Teunissen and C. J. Elsevier, *Chem. Commun.*, 1998, 1367–1368.

26   A. E. Atabani, A. S. Silitonga, I. A. Badruddin, T. M. I. Mahlia, H. H. Masjuki and S. Mekhilef, *Renew. Sustain. Energy Rev.*, 2012, **16**, 2070–2093.

27   D. M. Singleton and B. D. Murray, *Process for the direct hydrogenation of triglycerides, US5475160A*, 1994.

28   N. T. Fairweather, M. S. Gibson and H. Guan, *Organometallics*, 2015, **34**, 335–339.

29   T. Fleckenstein, J. Pohl and F. J. Carduck, *Process for the hydrogenation of fatty acid methyl esters, US5124491A*, 1992.

30   R. D. Rieke, D. S. Thakur, B. D. Roberts and G. T. White, *J. Am. Oil Chem. Soc.*, 1997, **74**, 333–339.

31   T. Chen, H. Li, S. Qu, B. Zheng, L. He, Z. Lai, Z. X. Wang and K. W. Huang, *Organometallics*, 2014, **33**, 4152–4155.

32   A. Anaby, M. Schelwies, J. Schwaben, F. Rominger, A. S. K. Hashmi and T. Schaub, *Organometallics*, 2018, **37**, 2193–2201.

33   S. R. Waldvogel, in *Comprehensive Organic Name Reactions and Reagents*, John Wiley & Sons, Inc., Hoboken, NJ, USA, 2010, pp. 2782–2788.

34   R. H. Crabtree, *ACS Sustain. Chem. Eng.*, 2019, **7**, 15845–15853.

35   Y. Li, M. Nielsen, B. Li, P. H. Dixneuf, H. Junge and M. Beller, *Green Chem.*, 2015, **17**, 193–198.

36   J. M. Heltzel, M. Finn, D. Ainembabazi, K. Wang, A. M. Voutchkova-Kostal, R. Li, / Chemcomm and C. Communication, *Chem. Commun*, 2018, **54**, 16–28.

37   F. Yang, M. A. Hanna and R. Sun, *Biotechnol. Biofuels*, 2012, **5**, 13.

38   S. Fernando, S. Adhikari, K. Kota and R. Bandi, *Fuel*, 2007, **86**, 2806–2809.

39   D. Spasyuk, S. Smith and D. G. Gusev, *Angew. Chem. Int. Ed.*, 2012, **51**, 2772–2775.

40   L. Boateng, R. Ansong, W. B. Owusu and M. Steiner-Asiedu, *Ghana Med. J.*, 2016, 50, 189–196.

41   M. Matsuda and M. Horio, *Process for the preparation of Guerbet alcohols, US4518810A*, 1983.

42   C. Carlini, M. Di Girolamo, M. Marchionna, M. Noviello, A. M. R. Galletti and G. Sbrana, *J. Mol. Catal. A Chem.*, 2002, **184**, 273–280.

43   C. Carlini, M. Di Girolamo, A. Macinai, M. Marchionna, M. Noviello, A. M. Raspolli Galletti and G. Sbrana, *J. Mol. Catal. A Chem.*, 2003, **200**, 137–146.

44   C. Carlini, C. Flego, M. Marchionna, M. Noviello, A. M. Raspolli Galletti, G. Sbrana, F. Basile and A. Vaccari, *J. Mol. Catal. A Chem.*, 2004, **220**, 215–220.

45   K. Noweck and W. Grafahrend, in *Ullmans Encyclopedia of Industrial Chemistry*, Wiley-VCH, Weinheim, Germany, 2006, vol. 262, p. 18.

46   D. S. Thakur, B. D. Roberts, G. T. White and R. D. Rieke, *J. Am. Oil Chem. Soc.*, 1999, **76**, 995–1000.

47   G. R. M. Dowson, *Transformations of Ethanol by Homogeneous Catalysis for Creation of Advanced Biofuels, Ph. D. Thesis, Univeristy of Bristol*, 2012.

48   D. Ostgard, K. Moebus, M. Berweiler, B. Bender and G. Stein, *Fixed Bed Catalysts,*

US6489521B2, 2002.

49 B. C. Trivedi, D. Grote and T. O. Mason, *J. Am. Oil Chem. Soc.*, 1981, **58**, 17–20.

50 Y. Xie, Y. Ben-David, L. J. W. Shimon and D. Milstein, *J. Am. Chem. Soc.*, 2016, **138**, 9077–9080.

Chapter 3: Manganese based catalysts for the production of advanced biofuels

Declaration: This chapter is reproduced from '*Manganese Diphosphine and Phosphinoamine Complexes Are Effective Catalysts for the Production of Biofuel Alcohols via the Guerbet Reaction*', Ashley M. King, Hazel A. Sparkes, Richard L. Wingad and Duncan F. Wass, *Organometallics*, 2020, **39**, 3873–3878.

3.1 - Introduction

The formation of *n*-butanol from ethanol *via* the Guerbet reaction, using a manganese catalyst, was recently reported by both the Jones and Lui groups.[1, 2] These catalysts contained 'MACHO-style' (bis(phosphino)ethylamine) pincer ligands and gave *n*-butanol yields of up to 31% over 48 hours, using 0.5 mol% catalyst and 25 mol% NaOEt. A variety of different phosphine substituents were tested, and *iso*propyl groups (**Cat-7**) were found to give the most effective catalyst (Figure 3.1). A secondary amine in the backbone was also vital for catalytic activity, with yields decreasing significantly upon methylation. The Jones group also report that when NaOMe was used as a base a small amount of *n*-propanol was formed (4%). Given that *n*-propanol is the key intermediate in the formation of *iso*butanol from methanol and ethanol (See Section 1.7.3), it was hypothesised that these catalysts could also be used in the production of this advanced biofuel. Most ligands used with manganese catalysts to date have been PNP-pincer ligands, with comparatively little published work on bischelate and bidentate complexes.[3,4] Much advanced biofuel formation previously undertaken in the Wass group was centred around bidentate ligands bound to a ruthenium centre.[5–8] Investigations were performed to determine if these ligands could show catalytic competence when complexed to manganese.

Cat-7 R= *i*Pr
1.11 R= Cy
1.12 R= Ph
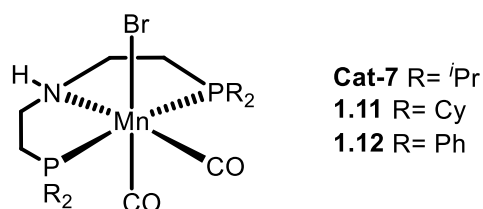
Figure 3.1: Manganese pincer catalysts used for the formation of n-butanol from ethanol.

3.2 - *Iso*butanol formation using Cat-7

Cat-7, the most effective catalyst for *n*-butanol formation reported in the literature was used as the model catalyst to establish optimum reaction conditions for *iso*-butanol

synthesis. Initially, the same conditions as those used previously in the Wass group for ruthenium catalysts were tested and a conditions scope was carried out in a 100 mL Parr stainless steel autoclave (Table 3.1).[7] While it was quickly established that catalyst **Cat-7** could be used for *iso*butanol formation, it was also shown to be significantly slower than many of the ruthenium catalysts previously tested. Yields of only 7% *iso*butanol were seen over 2 hrs using 0.1 mol% catalyst (Entry 1), although this could be improved by increasing catalyst loadings five-fold (Entry 4). Lengthening reaction times to 24 hrs also increased both yield and selectivity (Entry 6). The main by-product seen in all runs was *n*-propanol, so increases in selectivity with time were attributed to the conversion of this into *iso*butanol. Once formed, *iso*butanol will not undergo any subsequent Guerbet reactions. A large rise in pressure was also seen during reactions (42 bar after reaction, 17 bar after cooling, Entry 3). This is caused by hydrogen evolution from the formation of formate and carbonate, along with a small amount of acetate.[8] Owing to the large sodium methoxide base loadings (200 mol%) these often precipitate as sodium salts, leading to a large amount of solid product. In some cases (Entry 4) this solid build up made preparation of GC samples challenging and filtration of reaction mixtures before analysis was required. Strangely, this was not an issue over longer run times.

*Table 3.1: Condition screen for isobutanol formation from methanol and ethanol using **Cat-7***
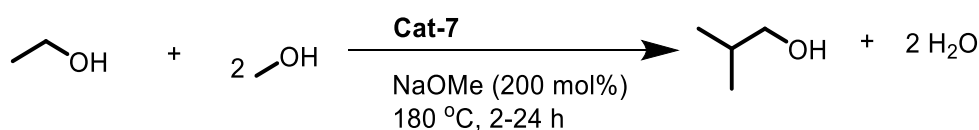
Entry[a]	Catalyst loading (mol%)	Time (h)	Ethanol consumption (%)	*Iso*butanol yield (%)	*Iso*butanol selectivity (%)[b]
1	0.1	2	68	7	64
2	0.1	4	78	10	79
3	0.1	20	77	17	86
4[c]	0.5	2	70	22	84
5	0.5	4	69	24	83
6	0.5	24	71	27	82

[a] Conditions: 1 mL (17.13 mmol) EtOH, 10 mL MeOH, [b] selectivity calculated from observed products in the liquid fraction [c] large amount of solid produced

While this work was being under-taken a further paper by the Lui group was published detailing the use of **Cat-7,** among others, for *iso*butanol formation.[9] This paper reported yields of up to 40% at runtimes of 48 hours and with elevated base loadings of 350 mol%. Owing to this paper's publication, focus was shifted towards investigating manganese bischelates for advanced biofuel formation.

3.3 - *Iso*butanol formation *via* manganese bischelate catalysis

3.3.1 – Identification of target manganese mono and bischelates

The most effective catalyst for *iso*butanol formation from the Wass group thus far is a ruthenium centre with two 1,1-bis(diphenylphosphino)methane (dppm) ligands (**Cat-1**).[7] The equivalent Mn(I) complex (**Cat-12**) was targeted for investigation (Figure 3.2). The related complex featuring 1,2-bis(diphenylphosphino)ethane (dppe) ligands (**Cat-13**) was also chosen. With ruthenium catalysts, the change from dppm to dppe was accompanied by a significant drop in both conversion and yield,[7] so a comparison to see if the same happens with a manganese centre would be useful. The formation of complexes **Cat-9** and **Cat-10**, incorporating 2-(diphenylphosphino)ethylamine (dppea, **L4**) as a supporting ligand, has recently been reported and their competence for ester hydrogenation established.[4] For

this use, **Cat-9** significantly outperforms **Cat-10**; both complexes were synthesised for catalytic testing. Previous work with manganese pincer complexes had established the importance of the N-H moiety for catalytic performance,[10] it was therefore hypothesised that substituting the –(CH$_2$)- unit in dppm for a -N(H)- may produce a more effective catalysts. As such, **Cat-14** and **Cat-15** with N,N-bis(diphenylphosphino)amine (dppa) ligands were also synthesised.
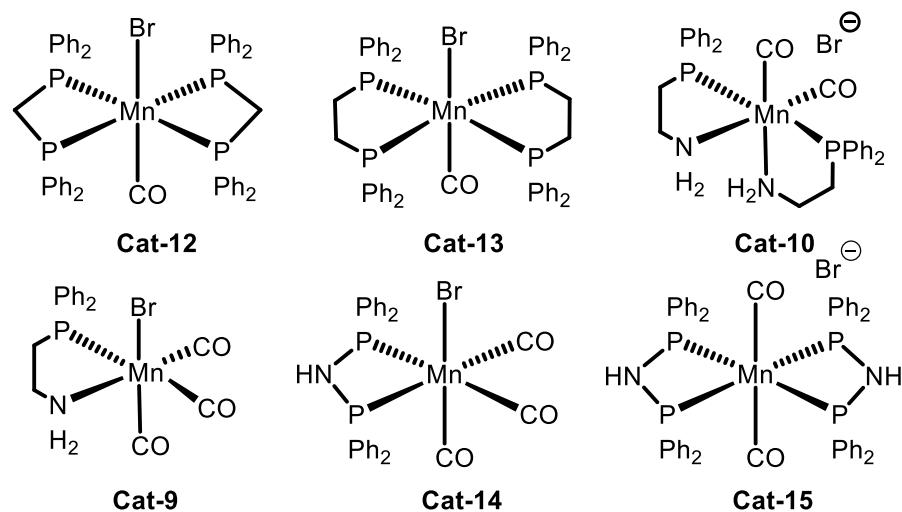
Figure 3.2: Manganese complexes targeted for testing in isobutanol formation.

3.3.2 – Synthesis of complexes

Cat-12 was synthesised by irradiation of a benzene solution of the ligand and manganese precursor, [Mn(CO)$_5$Br], under long-wave UV light (Scheme 3.1).[11] Benzene has previously been established as one of the most effective solvents for the photochemical preparation of manganese phosphorous complexes,[12] and attempts to use toluene instead for the formation of **Cat-12** gave very poor yields and product purity. Synthesis of **Cat-12** was also not possible by simply refluxing the ligand and catalyst precursor in toluene. Under these conditions the pendant complex **Cat-12b** was formed instead (Scheme 3.1). Given the comparatively simple formation of **Cat-12b,** and the possibility that under reaction conditions both **Cat-12b** and **Cat-12** could form the same active catalyst, **Cat-12b** was also isolated for testing. **Cat-13** was synthesised *via* irradiation in benzene as well, with the desired product precipitating at room temperature over 2 days.[11] The ^{31}P{^{1}H} NMR spectrum of this product matched well with that reported in literature and was thus used without further purification.[13] Crystals of **Cat-13** suitable for X-ray analysis were grown from a cooled chloroform-*d* solution.
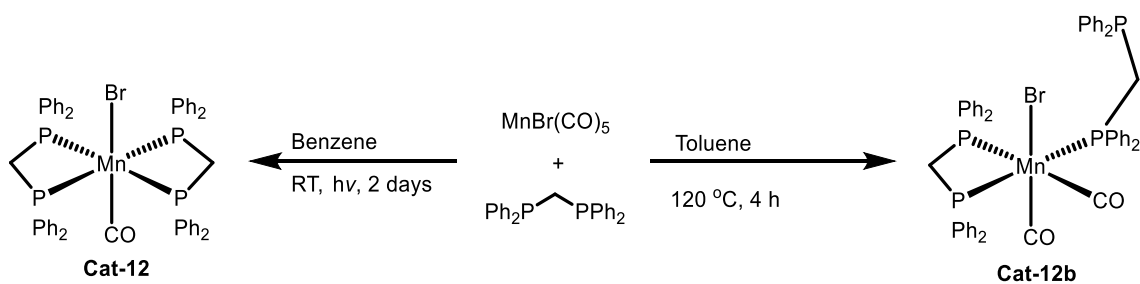
*Scheme 3.1: Formation of **Cat-12** and **Cat-12b***

The complex crystallised in a triclinic space group and was in the *trans* configuration, displaying a slightly distorted octahedral geometry (Figure 3.3). This complex, with an average Mn-P bond length of 2.3425 Å, has slightly longer Mn-P bonds than the related manganese complex [*trans*-Mn(CO)(dppe)$_2$(H$_2$)][Cl{Ga(C$_6$F$_5$)$_3$}$_2$] reported by Kubas *et al.* with an average P-C bond length of 2.3160 Å.[14] However, **Cat-13** has a significantly shorter Mn-C bond indicating a much more electron rich metal centre; this is unsurprising given it the complex reported by Kubas is cationic. The intra-ligand P-Mn-P bond angles are very similar between the two complexes, differing only by 0.12°. The inter-ligand P-Mn-P bond angles differ by 1.45° between the complexes.
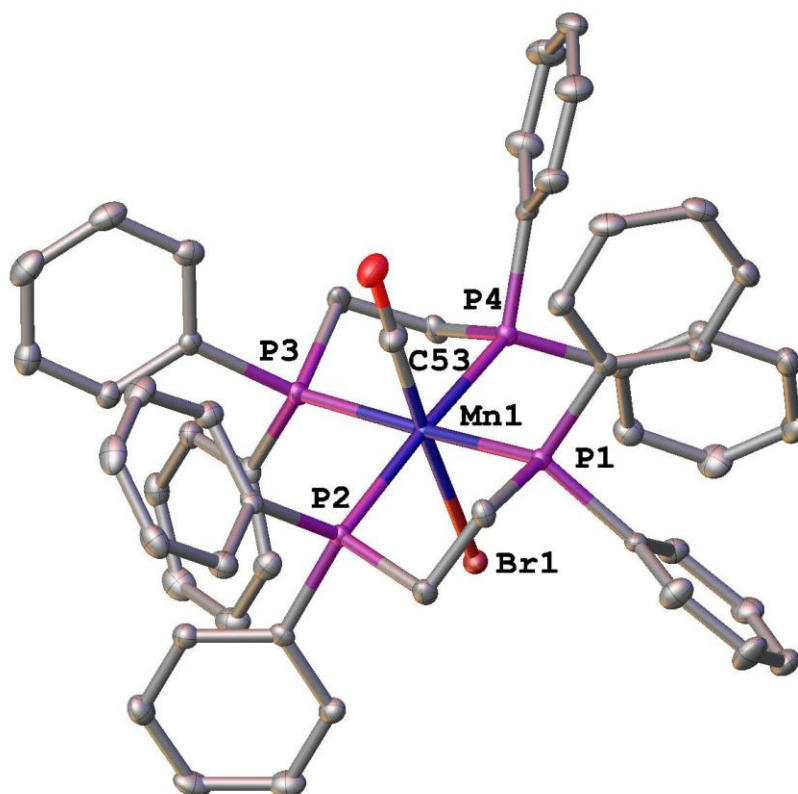
*Figure 3.3: Structure of **Cat-13**. Hydrogen atoms omitted for clarity. Selected bond lengths (Å) and angles (°): Mn1-P1 2.3482(8), Mn1-P2 2.3318(10), Mn1-P3 2.3500(8), Mn1-P4 2.340(1), Mn-C53 1.688(6), Mn-Br1 2.5458(10), P1-Mn1-P2 83.62, P1-Mn1-P4 97.95.*

Cat-10 and **Cat-9** were synthesised by refluxing a 2:1 or 1:1 mixture of the ligand and manganese precursor in toluene.[4] After workup, this gave both complexes as yellow powders in 54% and 23% yields respectively. Synthesis of the *trans* isomer, **Cat-10b**, was also possible *via* irradiation of a benzene solution followed by recrystallisation from a layered solution of benzene and ethanol (Scheme 3.2). This complex displayed a signal with a significantly different chemical shift in the ^{31}P{^{1}H} NMR spectrum compared to **Cat-10**, 89.2 ppm compared to 79.3 ppm. A single peak at 1869 cm^{-1} in the carbonyl region of the IR spectrum was also seen, **Cat-10** meanwhile showed 2 peaks at 1919 and 1836 cm^{-1} in this region. Finally, crystals suitable for X-ray diffraction were grown from a layered solution of benzene and ethanol. This allowed determination of the absolute structure of the complex, confirming a *trans* geometry (Figure 3.4). While **Cat-10b** could only be produced in very poor yields (17%), enough was produced to allow for catalytic testing. It was therefore possible to establish if use of a distinct isomer affected catalytic performance.
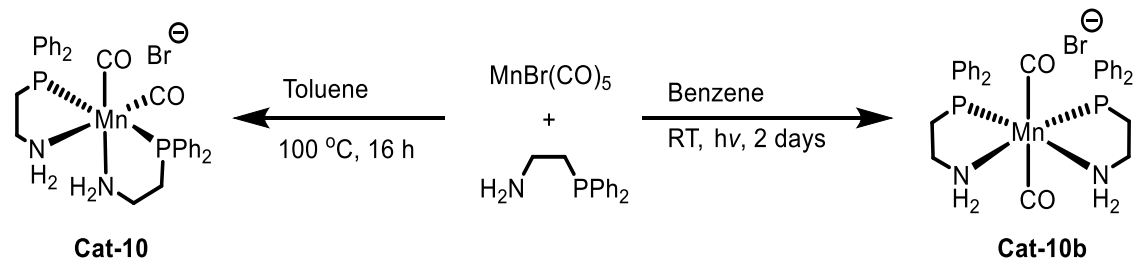
Scheme 3.2: Formation of cis and trans isomers of [Mn(CO)$_2$(dppea)$_2$]Br.

Cat-10b crystallised in a triclinic space group and displays a distorted octahedral geometry. The phosphine groups are *cis* to one another whereas in **Cat-10** they are *trans*.[4] When compared to **Cat-10** (Table 3.2), all Mn-P and Mn-N bonds are shorter, by 0.02545 Å and 0.0185 Å on average respectively. Mn-C bonds on the other hand are slightly longer (0.0595 Å on average).[4] Conversely, the C-O bonds in **Cat-10** and **Cat-10b** not significantly different from one another. Carbonyl ligands bond to metal centres *via* two interactions. The first is a σ-type interaction from the lone pair on the carbonyl carbon into a vacant metal d-orbital. The second involves π-back donation from the metal into a C-O π* orbital. The more electron rich the metal centre, the greater π-back donation, and the stronger the M-C bond. Conversely, as back-donation into the π* orbital increases the C-O bond gets weaker.[15] As the Mn-C bonds are shorter in **Cat-10** but the C-O bonds are statistically similar this implies that the short Mn-C bonds are due to the *trans* effect and not a more electron rich metal centre.

*Table 3.2: Table comparing bond lengths and angles between **Cat-10** and **Cat-10b***

Bond length/ angle	Cat-10	Cat-10b
Mn1-P1	2.2898(7)	2.2542(8) Å
Mn1-P2	2.2714(7)	2.2561(8) Å
Mn1-N1	2.134(2)	2.113(2) Å
Mn1-N2	2.129(2)	2.113(2) Å
Mn1-C(average)	1.772(3)	1.832(3) Å
C-O(Average)	1.164(3)	1.153(3) Å
P2-Mn1-N2	82.58(6) °	83.00(7) °
P1-Mn1-N1	82.26(7) °	83.83(6) °
P2-Mn1-P1	175.59(3) °	109.37(3) °
P2-Mn1-N1	96.25(7) °	166.42(6) °

P-Mn-N bond angles between the same ligand are slightly larger in **Cat-10b** at 83.83 °. The *cis* P-Mn-P bond angle in **Cat-10b** is significantly larger than any *cis* angles in **Cat-10**, this is attributed to the steric hindrance between the two large phosphine groups. Interestingly, **Cat-10b** is cationic whereas the analogous complex prepared using a diphosphine ligand (**Cat-13**) is a neutral complex. Amines are considered much harder ligands than phosphines, and so may preferentially bind to a cationic metal centre with a higher charge density, leading to the formation of the charged **Cat-10b** over the neutral complex.
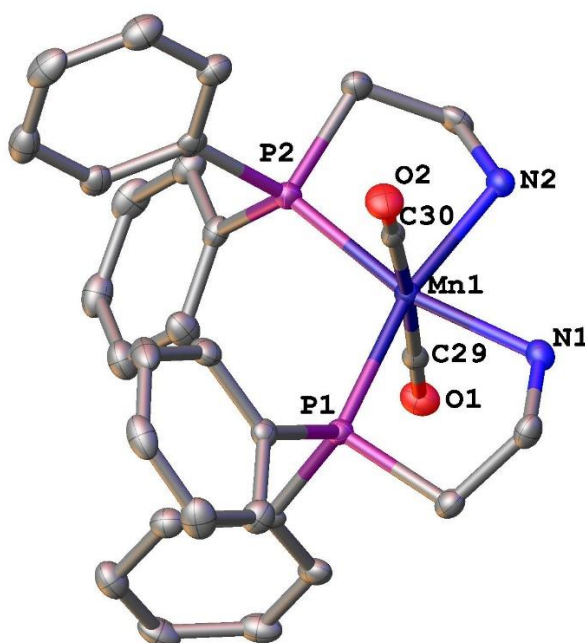
*Figure 3.4: Structure of **Cat-10b**. Hydrogen atoms and bromide counterion omitted for clarity. Selected bond lengths (Å) and angles (°): Mn1-P1 2.2542(8), Mn1-P2 2.2561(8), Mn1-N1 2.113(2), Mn1-N2 2.113(2), Mn1-C29 1.828(3), Mn1-C30 1.835(3), C29-O1 1.154(3), C30-O2 1.152(3), P2-Mn1-N2 83.00, P1-Mn1-N1 83.83, P2-Mn1-P1 109.37, P2-Mn-N1 166.42.*

The novel complexes **Cat-14** and **Cat-15** were prepared by refluxing the ligand and complex precursor in toluene for 16 hours (Scheme 3.3). Yields of **Cat-14** were significantly higher than those seen for **Cat-15** (67% compared to 7%). It was found that complex **Cat-15** formed irrespective of whether the irradiation or reflux technique was used. Both methods gave an orange powder with the $^{31}P\{^1H\}$ NMR spectra showing a single peak at 105 ppm. Reflux in toluene was chosen as the main method of preparation as it gave a higher purity product, albeit in low yields. A single peak at 1839 cm^{-1} in the carbonyl region of the IR spectrum was observed, indicating a *trans* geometry. IR spectrum bands occur when a bond stretch causes a change in a molecule's dipole moment. For a *trans* dicarbonyl complex a

symmetrical stretch will not cause a change in dipole moment, but an asymmetrical stretch will, hence only one peak in seen in the IR spectrum. If the isomeric *cis* product had formed, then both the symmetric and asymmetric stretch would cause changes in dipole moment and thus two IR stretching bands would be observed. This was confirmed when crystals of **Cat-15** were grown from a layered solution of dichloromethane and pentane (Figure 3.5).
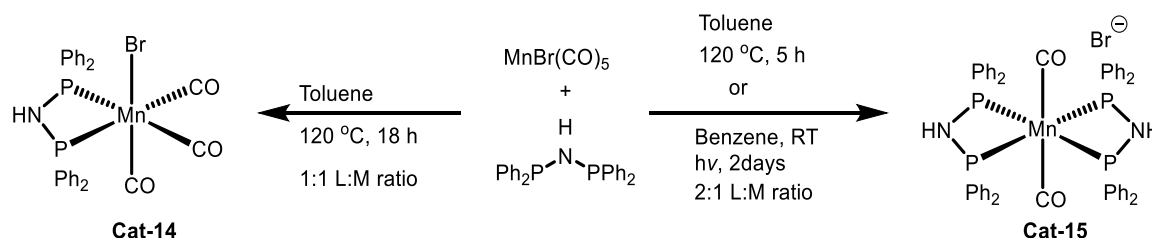
*Scheme 3.3: Formation of **Cat-14** and **Cat-15**.*

Cat-15 crystallised in a monoclinic space group. Much like both **Cat-13** and **Cat-10b** shown above, **Cat-15** displays a distorted octahedral geometry, and the phosphine ligands are *trans* to each other. It is worth noting that like **Cat-10b** this complex preferentially forms the cationic, dicarbonyl bischelate, rather than the neutral bischelate or pendant complex seen when dppm complexes are made (**Cat-12/ Cat-12b**). With P1-Mn1-P2 and P1-N1-P2 angles of only 70.23 ° and 101.76 ° respectively, this complex is highly strained. The P-N-P angle in the free ligand being 118.91 ° (calculated from crystal structure collected for the Cambridge Structural Database (CSD)),[16] this may explain why its formation is slow, and yields are low. The main side product from formation *via* irradiation is the monochelate **Cat-14**; the chelation of only one ligand may significantly reduce the strain and therefore yields are much higher.
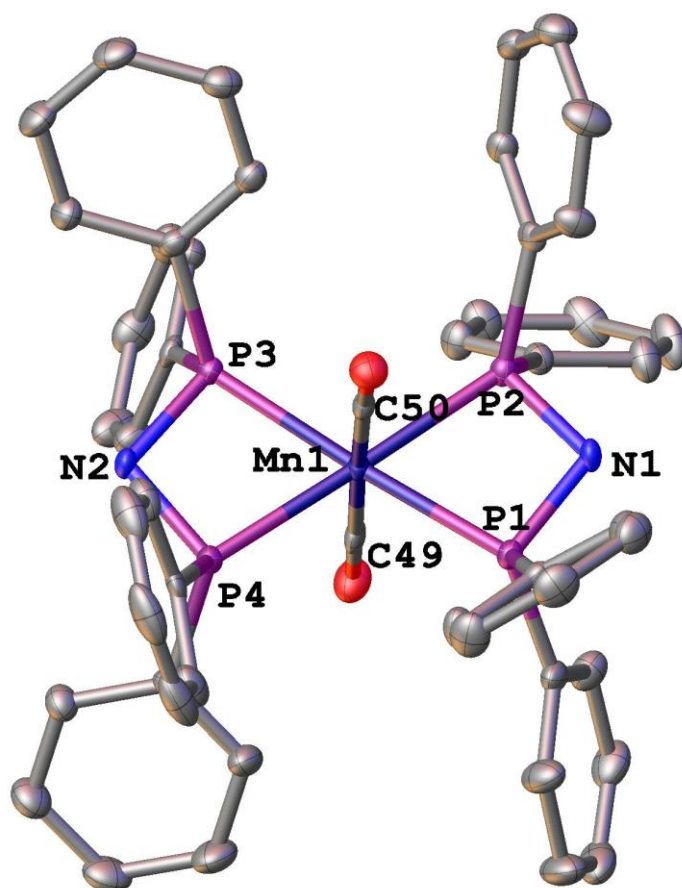
*Figure 3.5: Structure of **Cat-15**. Hydrogen atoms and bromide counterion omitted for clarity. Selected bond lengths (Å) and angles (°): Mn1-P1 2.2689(9), Mn1-P2 2.2606(6), Mn1-P3 2.2652(9), Mn1-P4 2.2748(9), Mn1-C49 1.824(3), Mn1-C50 1.824(3), P2-Mn1-P1 70.23, P1-Mn-P4 111.22, P1-N1-P2 101.76.*

3.3.3 – Testing of complexes for *iso*butanol formation

Experiments to test the activity of manganese complexes for the formation of *iso*butanol from methanol and ethanol were performed in a 100 mL Parr stainless steel autoclave under previously established conditions (Table 3.3) A preliminary screen of catalysts using short run times (overnight, 18 h) showed little promise for *iso*butanol formation. While ethanol consumption rates varied, *iso*butanol yields remained around 1-2%, little above the background level for control runs using only base. Increasing the base loading to 350 mol%, as used for the manganese pincer complex[9] had no effect upon *iso*butanol yields, although it did increase the rate of ethanol consumption in the case of **Cat-12** (Entries 3 and 4). It was proposed that these catalysts were thermally degrading upon being subjected to high reaction temperatures (180 °C), and that lowering the temperatures to 150 °C would help with catalytic activity (Entry 5). However, this resulted in total suppression of *iso*butanol formation. Slightly higher ethanol consumptions were observed for **Cat-13**, **Cat-**

9, and **Cat-10** (Entries 6-8), however no significant increase in *iso*butanol yield was observed. Unfortunately, it appeared that these complexes showed little promise for Guerbet type chemistry under the same conditions as those used for the analogous ruthenium complexes.[7]

Table 3.3: Initial catalyst screen for isobutanol formation from ethanol and methanol.

Entry[a]	Catalyst	Base loading (mol%)	Ethanol consumption (%)	*Iso*butanol yield (%)
1	12/12b	200	7	1
2	12b	200	-	trace
3	12	350	18	1
4	12b	350	2	1.5
5[b]	12b	200	5	0
6	13	200	11	2
7	10	200	7	1
8	9	200	7	1

[a] Conditions: 1 mL (17.13 mmol) EtOH, 10 mL MeOH, NaOMe (1.85 g, 34.26 mmol, 200 mol%), [cat] (0.01713 mmol, 0.1 mol%), 180 °C, 18 h runtime, [b] 150 °C

3.3.4 – *Iso*butanol formation by manganese catalysts over extended runtimes

It was proposed that the catalysts were not completely ineffectual for *iso*butanol formation, but that they were instead significantly slower than their ruthenium analogues. This was tested by extending run times up to 90 hours (Table 3.4). Pleasingly, this did give some formation of *iso*butanol. Both **Cat-12** and **Cat-12b** gave yields in excess of 10% over this time (Entries 1 and 3). While there is a large discrepancy between their respective ethanol conversions, it is not clear if this is because a different active catalyst is forming, or that **Cat-12** forms the active catalyst quicker and in a greater yield than **Cat-12b.** Loadings of **Cat-12b** could be lowered to 0.1 mol% with no visible effect upon conversion or yield (Entry 1), giving a turnover number in excess of 100. The dppe supported complex is essentially inactive, even over extended runtimes, displaying that small bite-angle diphosphine ligands are vital for catalytic activity with both ruthenium and manganese (entry 6). Although, **Cat-12** performed significantly better at higher catalyst loadings (Entry 3), it is possible that **Cat-13** would show the same effect if loadings were increased. Dppea-supported complexes are active but significantly less efficient than complexes bearing

dppm ligands (entries 7 and 8). **Cat-14** showed almost no activity towards *iso*butanol formation (Entry 9), while **Cat-15** performed comparably with **Cat-10b** indicating that bis-chelation is important for catalytic activity.

It is worth noting that while both the *cis* **Cat-10** and *trans* **Cat-10b** dppea isomers are active (entries 7 and 8), the *cis* species marginally outperforms the *trans*. However, this is only by 3%, easily within experimental error, and therefore gives little information as to whether two distinct catalytic species are forming. A surprising feature is the extent to which structure-activity relationships for these manganese complexes mimic those for the analogous ruthenium complexes, with complexes featuring the dppm ligand the most effective catalysts of those screened.

Table 3.4: Longer run time catalyst screening for isobutanol formation.

Entry[a]	Time (h)	Catalyst	EtOH Consumption (%)	iBuOH yield (%)	iBuOH selectivity (%)[b]	Turn over numbers[c]
1	90	**12b**	27	11	69	113
2[d]	90	**12b**	19	11	68	38
3[e]	90	**12**	42	14	74	58
4	90	**12**	10	2	52	22
5	66	**12**	9	3	57	32
6	90	**13**	19	3	58	26
7	90	**10b**	23	6	59	61
8	90	**10**	20	9	62	87
9	90	**14**	9	1	44	12
10	90	**15**	18	5	59	50
11	90	Mn tainted sleeve	-	1	54	-
12	90	-	-	1	49	-

[a] Conditions: 1 mL (17.13 mmol) EtOH, 10 mL MeOH, NaOMe (1.85 g, 34.26 mmol, 200 mol%), [cat] (0.01713 mmol, 0.1 mol%,), 180 °C, 90 h runtime, [b] Selectivity calculated from observed products in the liquid fraction, [c] Turnover number (TON) based on mmol of ethanol converted to *iso*butanol per mmol of Mn, [d] 0.3 mol% catalyst, [e] 0.25 mol% catalyst.

For **Cat-12**, shorter run times of 66 hours (Entry 5) also generate very little *iso*butanol. It therefore seems that one of the issues with these catalysts is the time it takes for the active catalyst to form, necessitating a long pre-activation time. Another possible explanation is that **Cat-12** rapidly generates an off-cycle species which is inactive for *iso*butanol formation, and only when high catalyst loadings are used is a sufficient amount of the active catalyst generated to give appreciable *iso*butanol yields. Hence why **Cat-12** only appears to be active at 0.25 mol% catalyst loading (Entry 3). It was considered that over such long times either the methoxide base alone, or manganese nano particles impregnated into the teflon sleeves from previous runs could being performing the catalysis, instead of the complexes being studied. However, extended run times with both a tainted sleeve and a

clean sleeve, with only base present, gave just trace amounts of the *iso*butanol product (Entries 11 & 12). It was therefore concluded that these were not affecting the observed yields for other catalysts.

Once the potential for manganese bischelate complexes to catalyse the formation of *iso*butanol had been established, with **Cat-12** giving the greatest *iso*butanol yield at high catalyst loadings and **Cat-12b** performing best at lower loadings, variations on the catalyst structure were investigated in order to try and maximise production of *iso*butanol.

3.3.5 – Attempted synthesis of analogues of Cat-12

Cat-12 has been established as a competent catalyst for *iso*butanol formation and was the most effective of those screened above. Several variations upon the structure of **Cat-12** were identified, to attempt to optimise performance and identify features necessary for catalytic activity. Several recent papers have established that manganese pincer complexes bearing electron donating phosphine substituents, such as *iso*propyl or cyclohexyl, are still effective catalysts.[17–19] Indeed, for *iso*butanol formation using Mn-PNP pincer catalysts, the *iso*propyl and cyclohexyl analogues were found to give higher yields and selectivities than their phenyl counterpart.[9] It seemed possible therefore that changing the bis(diphenylphosphino)methane ligands for 1,1-bis(dicyclohexylphosphino)methane (dcypm) may produce a superior catalyst. Both irradiation and reflux in toluene were attempted to make the cyclohexyl analogue, however neither syntheses were successful (Scheme 3.4). After irradiation for 3 days an orange powder started to form, this was isolated by filtration but showed no resonance in the $^{31}P\{^{1}H\}$ NMR spectrum so was attributed to precipitated starting complex. The resulting orange filtrate only showed a $^{31}P\{^{1}H\}$ NMR resonance for the free ligand. Similar results were found after reflux in toluene; after 5 hours a white powder was isolated and identified as uncoordinated ligand. The $^{31}P\{^{1}H\}$ NMR spectrum of the solution also showed almost entirely uncoordinated ligand as well. It is possible that ligand coordination is hampered by the increase bulk of the cyclohexyl substituents.
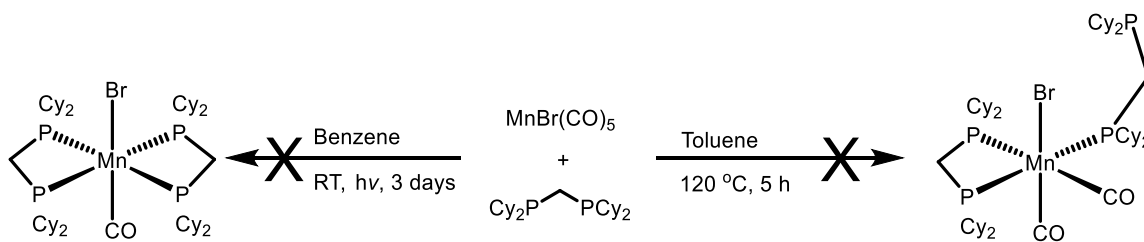
Scheme 3.4: Attempted reaction of dcypm with Mn(CO)$_5$Br.

The vast majority of recently reported manganese catalysts have a Mn(I) metal centre, with comparatively few examples of Mn(0) or Mn(II).[20–22] A range of complexes in these oxidation states can easily be prepared from inexpensive and widely available precursors including manganese dihalides, such as MnCl$_2$, or manganese acetates. As such, Mn(II) catalysis with the aid of diphosphine ligands is a very under developed area. The Mn(II) analogue of **Cat-12** was identified as a promising starting point, given the activity **Cat-12** had already shown for *iso*butanol formation. This complex was also very similar to the current most effective catalyst for this process, replacing a ruthenium centre for manganese. Similar ruthenium complexes are produced with a ruthenium(II) precursor in a 2:1 ratio with the ligand under reflux in toluene.[23] However, when this was attempted with the manganese precursor, solid was still present after being left under reflux overnight, suggesting poor solubility of this precursor in toluene (Scheme 3.5). ^{31}P{^{1}H} NMR spectroscopic analysis of the solution showed only the presence of uncoordinated ligand. Recent publications have found that coordination of monodentate phosphine groups, with pendant aryl substituents, to MnCl$_2$ is possible using THF as a solvent. These complexes form homo-binuclear species, although mononuclear species can be formed in the presence of 18-crown-6.[24] However, when THF was tested as a solvent for the below complexation, no complex was formed. After 2 days a white solid and clear solution were observed. Isolation *via* filtration, and ^{31}P{^{1}H} NMR analysis of the solution again showed the presence of only uncoordinated ligand. The THF solution was reduced to dryness leaving a white powder, which was analysed by mass spectrometry, showing only free ligand, with no sign of any complexation.

MnCl$_2$

+

2 Ph$_2$P⌢PPh$_2$

Toluene, reflux, 16 h ✗→

THF, reflux, 2 days ✗→

[Mn complex: Ph$_2$P, Cl, Ph$_2$P, Mn, P, P, Ph$_2$, Cl, Ph$_2$]
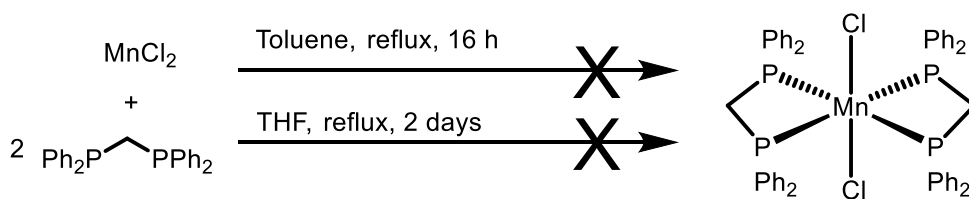
Scheme 3.5: Attempted synthesis of an Mn(II) bischelate.

Mn(II) complexes have a d^5 electron count and are therefore paramagnetic, this means that getting well resolved NMR spectra of the complexes is challenging. This may explain why no signs of any complexation was seen by $^{31}P\{^1H\}$ NMR spectroscopy. Given the phosphine groups are bound directly to the Mn(II) centre, line broadening is sufficiently large that no peak for these complexes can be seen in the $^{31}P\{^1H\}$ NMR spectrum. The manganese precursor and ligand were reacted in stoichiometric amounts. Therefore, if complexation was occurring reduction in the free-dppm resonance should be seen. Other methods of analysis are usually used for paramagnetic complexes, such as IR spectroscopy, EPR, and X-ray crystallography. Mass spectrometry would still show the presence of any paramagnetic species, and as only free ligand (m/z= 385.2) was observed, formation of the Mn(II) bis chelate was unsuccessful *via* this route.

3.4 – *n*-Butanol formation using manganese catalysts

Most previous studies into Guerbet chemistry using manganese catalysts have focussed on *n*-butanol production.[1,2] Therefore, formation of *n*-butanol from a neat solution of ethanol was attempted with two of the catalysts that proved to be most effective for *iso*butanol formation, **Cat-12b** and **Cat-10** (Table 3.5). This allowed for direct comparison between pincer and bischelate complexes.

Previous experiments using ruthenium catalysts had used 10 mL ethanol and 0.1 mol% catalysts loading.[6] However, the manganese complexes used could only be produced on a much smaller scale and therefore loadings were decreased to ~0.05 mol%. For ruthenium complexes base loadings as low as 5 mol% are commonly used, but for manganese catalysts increasing the base loading had been found to have a significant effect upon *n*-butanol yields (14.1%, at 12 mol% NaOEt, compared to 8.4% at 6 mol%).[2] Therefore, for these experiments, base loading was increased to 10 mol%. Owing to the low turnover frequency of these catalysts in *iso*butanol chemistry (~1 TON h^{-1} for **Cat-10**), 90 hour run times were

used again. This is also in line with work performed by the Lui group on *n*-butanol formation, where run times up to 168 hours were used.[2]

Table 3.5: Screen of catalysts for n-butanol formation from ethanol.
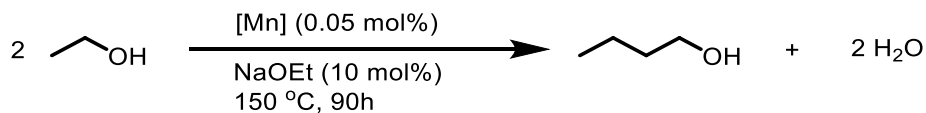
Entry[a]	Catalyst	Loading (mol%)	EtOH Conversion (%)	Yield nBuOH (%)	Selectivity nBuOH (%)[b]	TON[c]
1	12b	0.045	0.73	0.7	100	16
2	10	0.049	15.5	4.8	93	97

[a] Conditions 10 mL (171.3 mmol) ethanol [b] Total selectivity to n-butanol in the liquid fraction determined by gas chromatography, [c] Turnover number (TON) based on mmol of ethanol converted to *iso*butanol per mmol of Mn

Pleasingly it appears **Cat-10** is also active for *n*-butanol formation with nearly 100 turnover numbers over 90 hrs (Table 3.4, entry 2). Catalyst **Cat-12b**, however shows little activity for this reaction. This is attributed to lack of catalyst stability under these conditions. The post reaction mixture of **Cat-12b** is dark brown, implying that the catalyst decomposes giving elemental manganese, which is not an active catalyst. A similar process is seen in early ruthenium catalysts used for this reaction, with a large amount of ruthenium-black observed at the end of the reaction as a metallic solid.[5] Given these ruthenium catalysts have a significantly higher turnover frequency than their manganese analogues, they manage to produce appreciable amounts of *n*-butanol before degradation occurs. The slow manganese catalysts on the other hand give negligible *n*-butanol yields before decomposing. The post reaction mixture using catalyst **Cat-10** is still bright yellow, and predominantly homogeneous, indicating that little catalyst decomposition has occurred. This does fade to brown over 5 minutes once exposed to air, so the active catalyst appears to be highly air sensitive. High selectivity to *n*-butanol (97%) is observed, with only small amounts of ethyl acetate and higher alcohols, such as 2-ethylbutanol and *n*-hexanol, produced. No alcohols with carbon numbers higher than 6 are observed by GC. This high selectivity is likely a by-product of the low conversion, the large amount of unreacted ethanol present increasing the likelihood of butanol formation over higher alcohols.

While **Cat-10** is a competent catalyst for *n*-butanol formation, it is still outperformed by manganese pincer complex **Cat-7**. This gives 14.5% *n*-butanol over 96 hours with only 0.02 mol% catalyst. However, slightly higher NaOEt loadings of 12 mol% are needed.

3.5 – Interaction of manganese complexes with base

When ruthenium catalysts are used for Guerbet chemistry, base is required not only for the aldol coupling, but also for catalyst activation. In *n*-butanol chemistry when sodium ethoxide is used, the dihydride species (believed to be the active catalyst) forms by ethoxide coordination to the ruthenium centre followed by β-hydride elimination.[5] This activation is proposed to proceed *via* a classical inner sphere route.[25] Ruiz *et al.* found that when a manganese dicarbonyl cation was exposed to sodium methoxide, selective deprotonation of the backbone was seen, giving two multiplets in the $^{31}P\{^{1}H\}$ NMR spectrum at 44.9 and 15.4 ppm (Scheme 3.6).[26] With **Cat-12** and **Cat-12b** it was proposed a similar product could be seen, along with possible substitution of the bromide ligand for a hydride (Scheme 3.7).
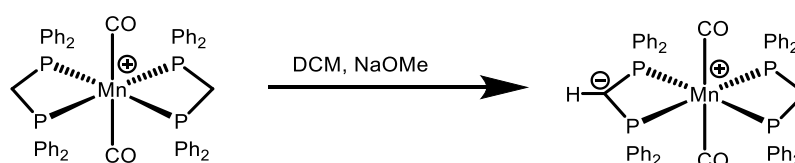
Scheme 3.6: Deprotonation of the dppm backbone on [Mn(CO)₂(dppm)₂] with NaOMe.
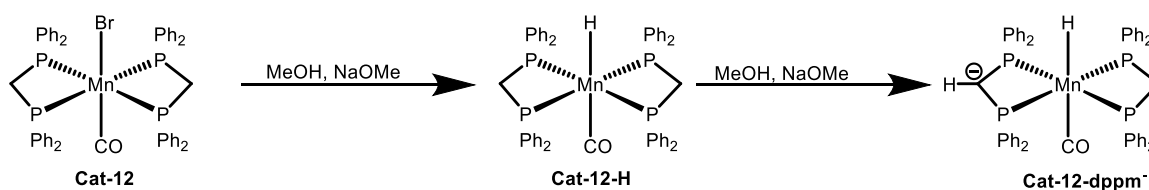
*Scheme 3.7: Proposed formation of the active catalyst generated by reaction of **Cat-12** with NaOMe.*

3.5.1 – Reaction of Cat-12 with sodium methoxide
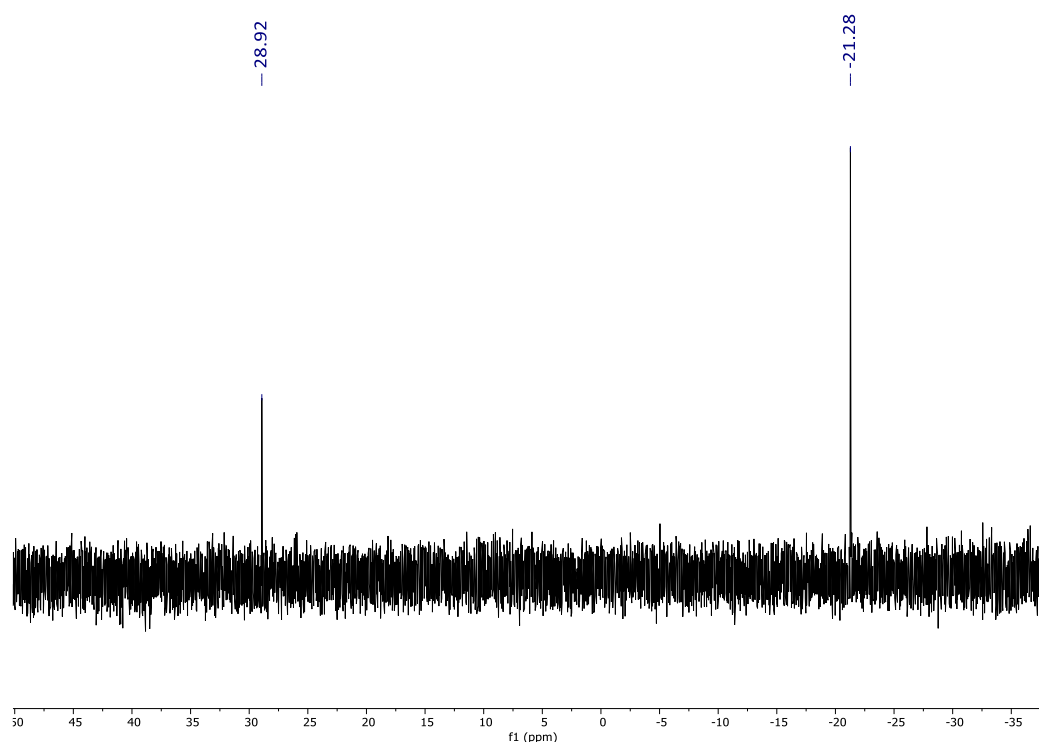
*Figure 3.6: $^{31}P\{^1H\}$ (188 MHz, MeOH) NMR spectrum of the addition of NaOMe to **Cat-12**.*

When a suspension of **Cat-12** (which gives a singlet at 32.5 ppm in the $^{31}P\{^1H\}$ NMR spectrum) in methanol was prepared and an excess of base (NaOMe) added, a large amount of free ligand (δ_P -21.3 ppm) was observed immediately (Figure 3.6). While solubility of **Cat-12** in methanol was initially an issue, dissolution does begin to occur once base is added, likely due to the formation of a cationic species. The resonances that Ruiz reported are not seen and there is no evidence of hydride formation in the ^1H NMR spectrum. When this solution was re-examined after 3 days the resonance at 28.9 ppm had disappeared and only free ligand was seen. A large amount of orange precipitate was still observed in the NMR tube, which is likely to be unreacted **Cat-12**. The reactivity of this complex with base is very different from both its ruthenium, and dicarbonyl analogues.[5] Given these observations it seems unlikely that the bischelate hydride complex proposed above is the active catalyst.

A similar effect was seen upon the mixing of **Cat-13** with NaOMe, with a large amount of free ligand observed almost immediately.

3.5.2 – Reaction of Cat-12b with sodium methoxide

To try and gain more insight into the active catalyst, and mechanism of activation, the interactions of **Cat-12b** with base were examined (Figure 3.7). In chloroform-*d* with no base present, **Cat-12b** gives a complex $^{31}P\{^1H\}$ NMR spectrum containing three broad resonances at 50.7, 36.0 and 2.5 ppm, along with a sharp doublet of doublets at -27.4 ppm. Upon the addition of base, a large amount of free ligand was seen once again along with three weak, broad peaks. Phosphines complexed to manganese often exhibit slight line broadening, so this spectrum suggests the presence of several manganese complexes in solution.
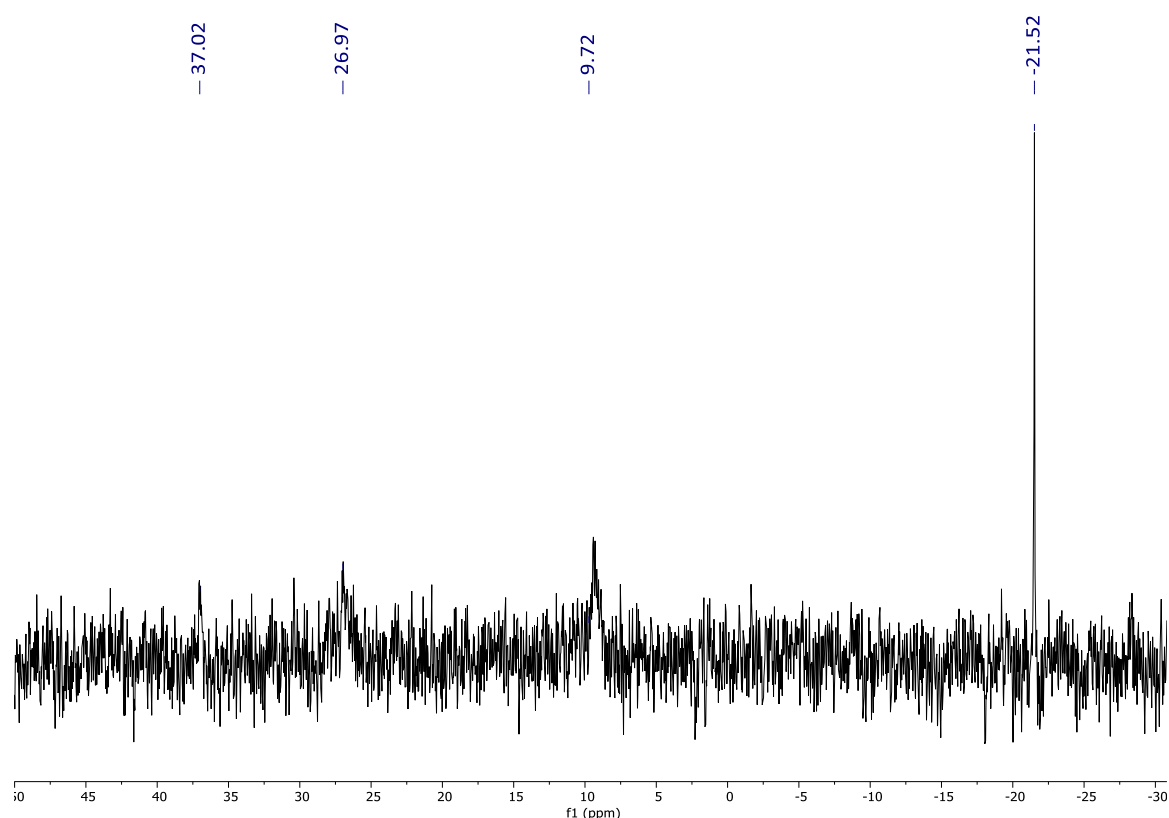
*Figure 3.7: $^{31}P\{^1H\}$ (188 MHZ, MeOH) NMR spectrum from the reaction of **Cat-12b** with NaOMe.*

The doublet of doublets at -27.4 ppm in **Cat-12b** is due to the pendant phosphine group, as this is no longer observed either chelation or complete ligand dissociation has occurred. Previous papers have shown that the addition of a halide abstraction agent such as TlPF$_6$ to complex **Cat-12b** can generate the *cis* bischelate dicarbonyl **Cat-12c** (Scheme 3.8), and addition of a base potentially has the same effect.[27] This complex, with a non-coordinating counter ion like [PF$_6$]$^-$ gives $^{31}P\{^1H\}$ NMR resonances of 27.4 and 9.9 ppm, so appears to be the primary species formed by base addition to **Cat-12b**.[28] The *trans* isomer, **Cat-12d**, has a reported resonance of 37.9 ppm, so may also be present, but in smaller amounts. The

large amount of free dppm present comes from total ligand dissociation from the manganese centre, also generating the corresponding manganese monochelate complex. The manganese-dppm monochelate **Cat-16** has a $^{31}P\{^1H\}$ NMR resonance of 10.6 ppm in CDCl$_3$.[29] Given how similar this is to resonances reported for **Cat-12c**, and the line broadening seen on manganese coordination, it is possible that these resonances are overlapping and both species are present in solution. Complex **Cat-12e** is drawn with a coordinated solvent molecule, to give the neutral Mn(I) complex. Unlike the product solution obtained from base with **Cat-12**, these complexes are stable in solution for several days, with little change seen in the $^{31}P\{^1H\}$ NMR spectra over this time. With several different complexes generated upon the addition of base it is impossible to know which are the active species.
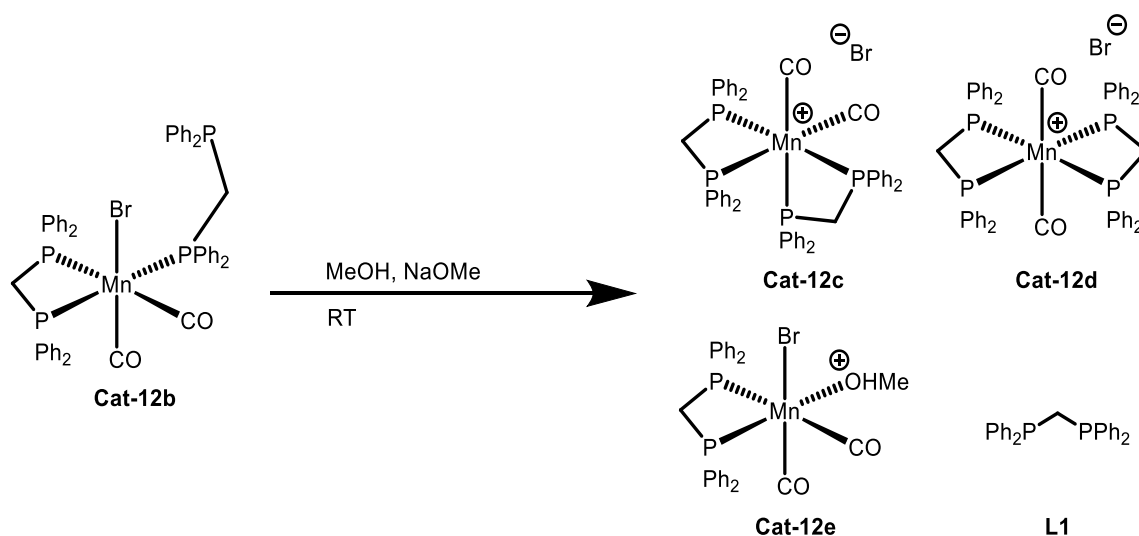
*Scheme 3.8: Species generated by the reaction of **Cat-12b** with NaOMe at room temperature*.

When **Cat-12b** is suspended in methanol along with 100 equivalents of NaOMe and heated to 180 °C for 20 hours, no manganese phosphine complexes are observed in the $^{31}P\{^1H\}$ NMR spectrum. However, mass spectrometric analysis of the post reaction mixture shows a species with m/z= 528.5. Given the presence of a large amount of free ligand in solution as well, this is believed to correspond to **Cat-12f** (Figure 3.8). This species contains a paramagnetic Mn(II) metal centre which explains why no evidence of it is seen by NMR spectroscopy. The presence of formate from methanol dehydrogenation in the post reaction mixture confirms that the active catalyst has indeed been formed, therefore **Cat-**

12f is tentatively assigned as a resting state with the methoxide dissociating to regenerate the active catalyst.
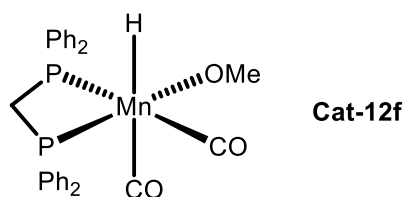
Figure 3.8: A potential manganese catalyst resting state identified by mass spectrometry.

The reaction of **Cat-12b** with base produces a variety of stable complexes which under reaction conditions (180 °C, autoclave) appear to form the active catalyst. Conversely, **Cat-12** does not form the same group of stable complexes with any manganese species present precipitating from methanol over several days. This may explain why the turnover numbers seen for **Cat-12b** are far superior.

3.5.3 – Formation of the monochelate and catalytic testing

Given the free ligand seen upon the addition of base to both **Cat-12** and **Cat-12b**, and the identification of **12f** as a possible catalyst resting state, it seems likely that the active catalyst is a monochelate complex. In order to test this the monochelate species **Cat-16** was synthesised and tested for *iso*butanol formation.
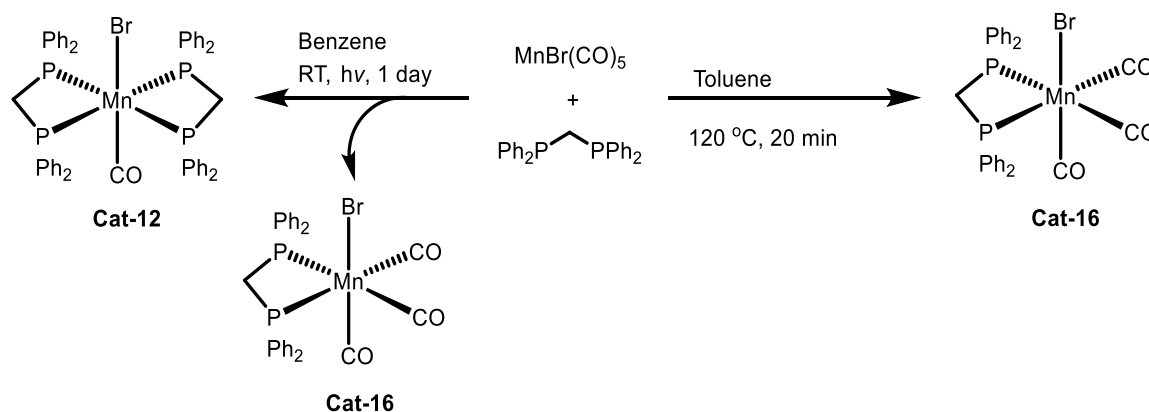
Scheme 3.9: Formation of manganese-dppm monochelate via two separate routes.

Cat-16 was recovered as the main by-product during the synthesis of **Cat-12**, precipitating from a stirred benzene solution overnight. This was confirmed as the monochelate by $^{31}P\{^{1}H\}$ NMR spectroscopy and mass spectrometry ([M-Br]$^+$ m/z=523.4). **Cat-16** can also be directly synthesised from a short reflux in toluene (Scheme 3.9).[30]

*Table 3.6: Isobutanol formation using manganese monochelate **Cat-16**, results for **Cat-12b** included again for comparison.*

Entry[a]	Catalyst	EtOH Consumption (%)	iBuOH yield (%)	iBuOH selectivity (%)[b]	TON[c]
1	12b	27	11	69	113
2	16	25	7	62	67
3[d]	16	2	trace	-	-

[a] Conditions: 1 mL (17.13 mmol) ethanol, 10 mL methanol, 0.1 mol% catalyst, 200 mol% NaOMe, 180 °C, 90h. [b] Total selectivity to isobutanol in the liquid fraction determined by gas chromatography, [c] Turnover number (TON) based on mmol of ethanol converted to *iso*butanol per mmol of Mn [d] Run time- 17 h

When tested for *iso*butanol formation it was confirmed that **Cat-16** was indeed a competent catalyst, giving ethanol conversions similar to **Cat-12b** (Table 3.6). However, the TON significantly decreased and the selectivity for *iso*butanol was slightly lower. It is therefore proposed, that while **Cat-16** may be produced under the reaction conditions when **Cat-12b** is used, it is either not the sole active catalyst, or is an off cycle species that can react to form the active complex. Either one or both of **Cat-12c** or **Cat-12d** must also be active, and show higher selectivity for *iso*butanol formation, thus giving **Cat-12b** the observed superior catalytic performance. For similar ruthenium complexes, no difference in catalytic activity is seen between the *cis* and *trans* geometry.[5] This suggest that the same active catalyst is formed regardless. A similar effect could be seen here with **Cat-12c** and **Cat-12d**. Much like all previous catalysts tested, **Cat-16** displays little signs of activity over shorter reaction times (Entry 3).

3.6 – Solid analysis

As ethanol consumption increases for a catalyst, so too does the amount of solid seen in the post-reaction mixture. Analysis of this solid can give insight into what side reactions are also occurring. This solid was isolated by filtration, washed with toluene, and dissolved in D$_2$O before being analysed by ^{1}H and ^{13}C{^{1}H} NMR spectroscopy.

3.6.1 – Analysis of solids produced from *iso*butanol formation

The solid produced during *iso*butanol formation using both **Cat-12b** (Table 3.3, Entry 2) and **Cat-12** (Table 3.3, Entry 3) was analysed. **Cat-12** produced slightly more solid (0.0315 g,

compared to 0.0294 g), this explains the fate of some of the 22% missing ethanol (the discrepancy between ethanol consumption, and product yield).
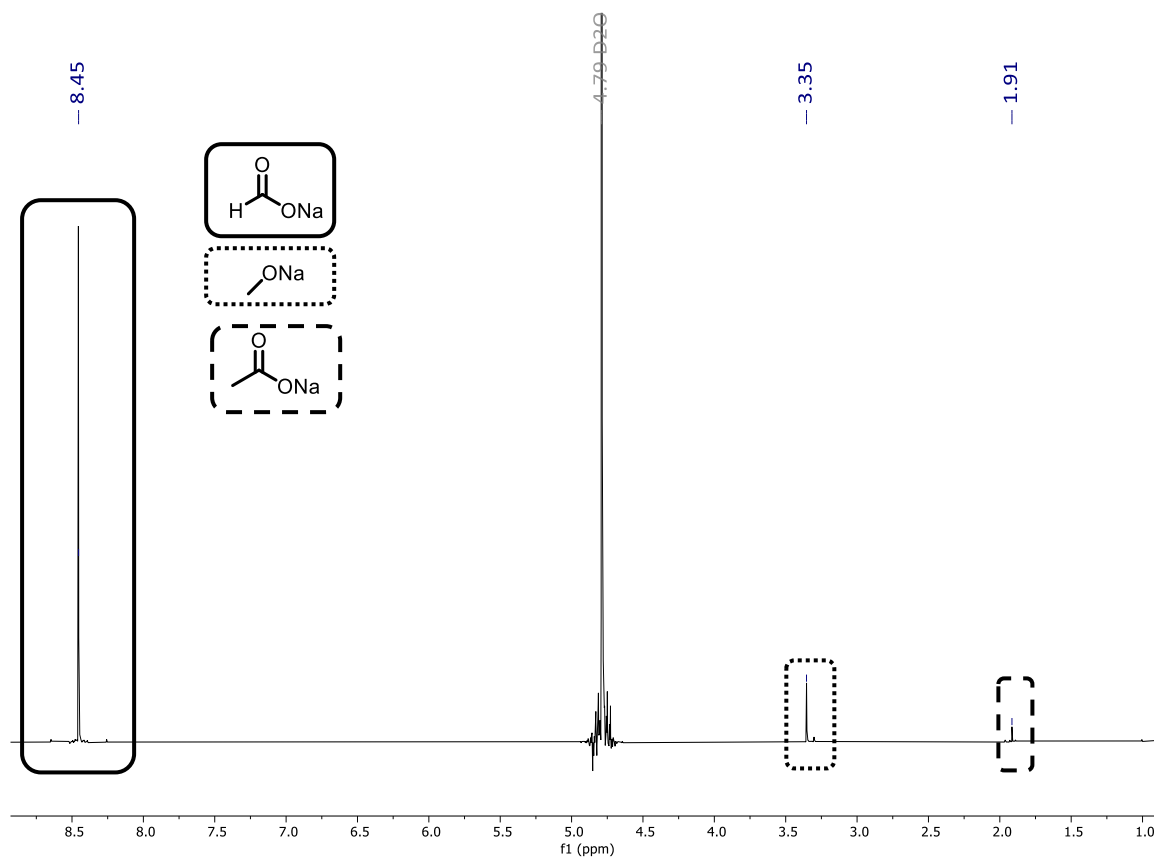
Figure 3.9: ^{1}H NMR (500 MHz, D_2O) spectrum of solid product produced by catalyst **Cat-12b** during isobutanol production (Table 3.3, Entry 2).

The proton spectra show that both solids are made up mostly of sodium formate (roughly 95%), giving a sharp peak at 8.5 ppm (Figure 3.9). A small amount of sodium acetate, produced *via* Tishchenko chemistry, is also seen (1.91 ppm). This is in line with what has been reported in the literature for *iso*butanol formation *via* Guerbet chemistry.[8] A small amount of sodium methoxide is also observed in similar proportions to that seen in the post-reaction solid when a ruthenium catalyst is used. High base loadings are needed as the reaction produces water, which hydrolyses the NaOMe to give methanol and sodium hydroxide (Equation 3.10). Given the low ethanol conversions seen with these catalysts, this NaOMe is attributed to a small amount of unconsumed base.[31]

$$NaOMe \quad + \quad H_2O \longrightarrow MeOH \quad + \quad NaOH$$

Scheme 3.10: Hydrolysis of sodium methoxide by water produced in the Guerbet reaction.

This hydroxide formed can in turn go onto react with formaldehyde, produced by the dehydrogenation of methanol, to give formic acid and methanol. Under the basic reaction conditions this formic acid quickly reacts with NaOMe present to form methanol and sodium formate; this is known as the Cannizzaro reaction (Scheme 3.11). This is yet another pathway for base consumption and shows again why such high loadings are required.
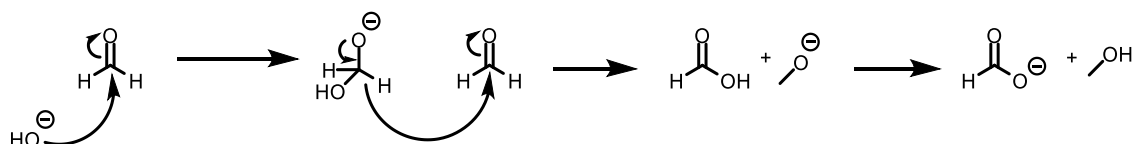
Scheme 3.11: Production of formate via the Cannizzaro reaction.

For ruthenium catalysts the post reaction solid is typically made up predominantly of sodium carbonate, shown by a peak at 168.1 ppm in the ^{13}C NMR spectrum. However, when manganese catalysts are used, no carbonate is detected, with only a sodium formate peak (171.0 ppm) observed (Figure 3.10). Formate can be dehydrogenated to CO_2 by some catalysts, which in turn reacts with NaOH (formed in equation 3.1) to produce sodium carbonate (Scheme 3.12). The use of ruthenium catalysts for the conversion of methanol (and by extension formate) to CO_2 are well known,[32,33] and a recent example has shown the same process is possible with manganese pincer complexes.[34] However, to date there have been no examples of full methanol dehydrogenation using non-pincer manganese complexes. Given the lack of any carbonate seen in these mixtures, it seems likely that **Cat-12** and **Cat-12b** are not active for this conversion. The lack of pressure built up in the autoclave (a maximum of 2 bar after cooling) also indicates no formate dehydrogenation is occurring.
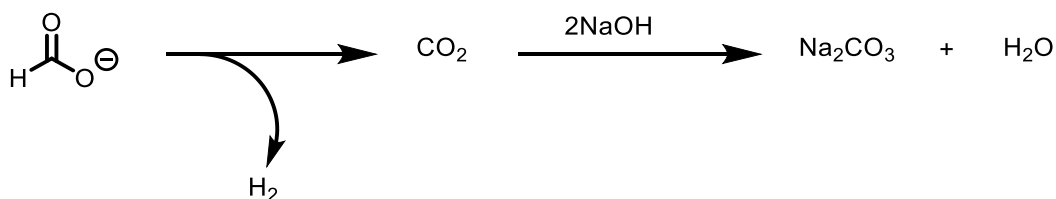
Scheme 3.12: Formation of sodium carbonate.
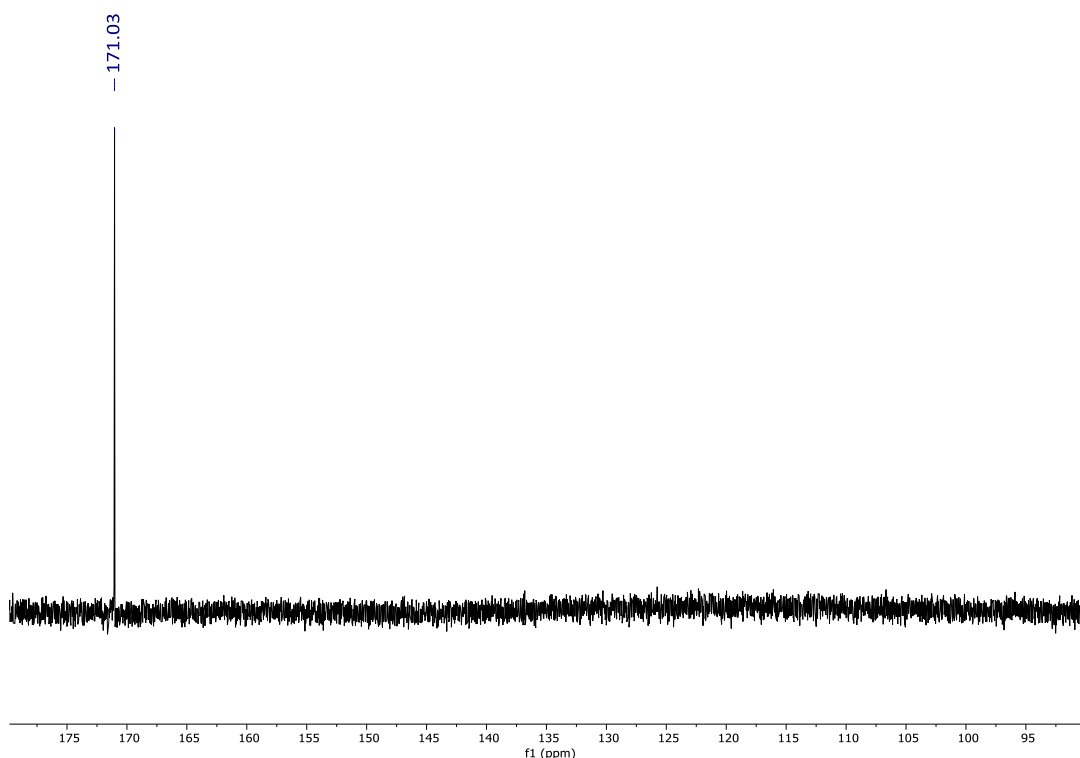
*Figure 3.10: ^{13}C NMR (126 MHz, D_2O) spectrum of solid product produced by **Cat-12b** during isobutanol production (Table 3.3, Entry 2).*

This solid analysis highlights the ability of manganese catalysts to slowly dehydrogenate methanol and ethanol to formate and acetate. This result is unsurprising considering alcohol dehydrogenation is the first step of the Guerbet cycle. However, it does also show the inability of these catalysts to further dehydrogenate formate to carbonate.

3.7 - Substituted dppm ligands for *iso*butanol formation

A recent paper from the Valyaev group showed the first example of dppm acting as a non-innocent ligand on manganese.[35] It was shown that monochelate **Cat-16** can be deprotonated by potassium bis(trimethylsilyl)amide in toluene at room temperature to produce **Cat-16b**, a highly strained complex containing two 3-membered metallocycles. Complex **Cat-16b** can further be reacted with dihydrogen to produce the hydride complex **Cat-16c** through reprotonation of the dppm backbone (Scheme 3.13, reaction I). This paper also shows that substitution of the backbone with an electron donating substituent makes the formation of the hydride complex significantly quicker. When a non-substituted dppm back bone is used, **Cat-16c** can only be produced in a 50% yield under 50 bar H_2, over 16 hours. However, the phenyl substituted complex **Cat-17b** can be converted to **Cat-17c** in 89% yields, under atmospheric pressure H_2 in only 5 minutes (Reaction II). The crystal

structure of **Cat-17b** showed a tridentate, facial, κ³-PCP coordination mode. Direct bonding of the carbon of the ligand back bone to the manganese, opposed to an anionic dppm⁻ structure, is confirmed by the short Mn-C bond length of 2.214(3) Å (even shorter than the Mn-P bond lengths (2.2255(9) Å).[35] If these catalysts operate *via* an outer-sphere mechanism, substitution of the dppm backbone could allow for superior catalytic activity. This would allow for quicker uptake of hydrogen and therefore dehydrogenation of the substrate. With this in mind, **Cat-17** was synthesised and tested for *iso*butanol formation.
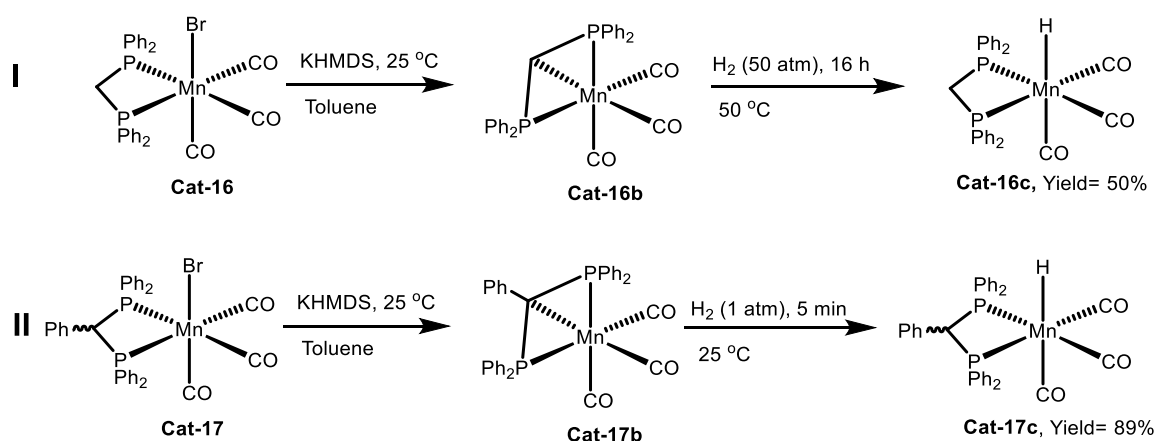
Scheme 3.13: Activation of manganese complexes containing substituted dppm ligands and their reactivity with hydrogen.

Cat-17 was synthesised from a 1:1 solution of the ligand and manganese precursor in THF. After trituration from hexane and further precipitation at -20 °C, the complex with isolated as two isomers depending on the orientation of the phenyl substituent on the ligand backbone (Scheme 3.14). The isomers are isolated in a 5:1 ratio, although it is unclear which isomer is the major one.
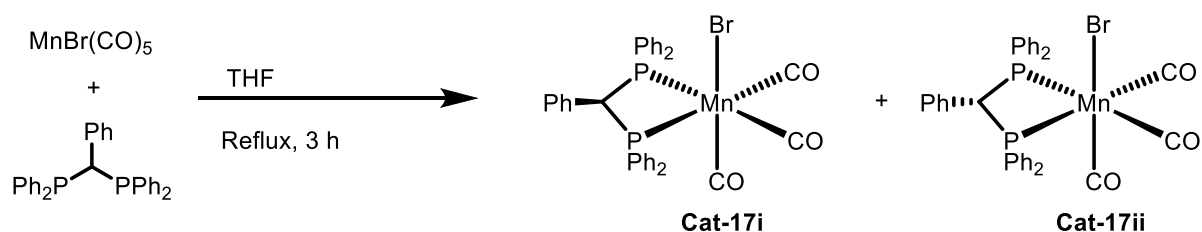
*Scheme 3.14: Formation of both isomers of **Cat-17**.*

In *iso*butanol chemistry, **Cat-17** outperformed the unsubstituted monochelate **Cat-16**, giving yields of 21% compared to 7% (Table 3.7, entry 2). Selectivity was also improved, with relatively less propanol (24% selectivity instead of 31%) being seen. Not only was **Cat-**

17 more active than the unsubstituted monochelate, it also performed better than both **Cat-12** and **Cat-12b** (the previous best catalysts in terms of yield and turn over number respectively), giving TON in excess of 200. The superiority of **Cat-17** relative to all other catalysts supports the proposition that catalysis occurs *via* an outer sphere mechanism.

*Table 3.7: Formation of isobutanol using substituted monochelate **Cat-17**, results from **Cat-16** included again for comparison.*

Entry[a]	Catalyst	EtOH Consumption (%)	iBuOH yield (%)	iBuOH selectivity (%)[b]	TON[c]
1	**16**	25	7	62	67
2	**17**	51	21	71	206

[a] Conditions: 1 mL (17.13 mmol) Ethanol, 10 mL methanol, 0.1 mol% catalyst, 200 mol% NaOMe, 180 °C, 90h. [b] Total selectivity to isobutanol in the liquid fraction determined by gas chromatography, [c] Turnover number (TON) based on mmol of ethanol converted to *iso*butanol per mmol of Mn

Substitution of the dppm backbone with electron donating substituents shows great potential for the production of manganese bidentate catalysts for use in advanced biofuel formation.

3.8 – Summary

The formation of *iso*butanol *via* the heterocoupling of ethanol and methanol using manganese PNP-pincer complexes as catalysts was established. Subsequently, a variety of manganese mono- and bischelated species were synthesised and also tested for the formation of *iso*butanol. Two of the more effective catalysts for this process (**Cat-12b** and **Cat-10**) were then tested for the formation of *n*-butanol *via* the homocoupling of ethanol. With bischelate complexes, the use of harder ligands such as phosphinoamines was found to favour the formation of cationic manganese dicarbonyl complexes. Conversely softer diphosphine ligands preferentially formed neutral manganese carbonyl bromides. While many of these complexes are competent catalysts for Guerbet chemistry, they are significantly slower and thus require much longer run times (90 h) than their ruthenium counterparts. The solid by-products made by these reactions were analysed by ^{1}H and ^{13}C{^{1}H} NMR spectroscopy and found to consist predominantly of sodium formate, with a small amount of sodium acetate also present. The lack of carbonate was of note and

showed the inability of these catalysts to fully dehydrogenate methanol. Preliminary mechanistic studies reveal the instability of complexes **Cat-12** and **Cat-12b** in the presence of base, with **Cat-12b** producing several stable complexes. This showed that a mono- or dihydride species, reported to be the active catalyst generated from [RuCl$_2$(dppm)$_2$],[5] is not likely to be the active catalyst for these manganese complexes. Instead, a dicarbonyl bischelate cation, or some form of monochelate species is more likely.

Finally, substitution of the dppm backbone with an electron donating substituent, such as a phenyl group, was found to vastly increase catalytic performance. **Cat-17** was found to be the most effective of all catalysts tested.

3.9 – Future work

Initially, further work should be done to investigate the nature of the catalyst. Preliminary catalyst-base studies have identified two more complexes of interest, **Cat-12c** and **Cat-12d**. Syntheses of both these complexes, with a variety of different counter ions, have been previously reported.[27] These could be tested for *iso*butanol formation to establish if either shows catalytic competence, giving more evidence about the active catalyst species. If neither show any promise for Guerbet chemistry, then it is likely that another species is being formed under reaction conditions and further mechanistic studies should be undertaken.

The most promising of these complexes for *iso*butanol formation was **Cat-17**. This opens the potential for further substitution of the dppm backbone with electron donating substituents, in order to increase catalytic turnover. Furthermore, different functionality, such as pyridyl, or methoxy groups, could be introduced this way (Figure 3.11). The inclusion of a pyridyl substituent into the backbone may also lead to interesting coordination modes, with nitrogen coordination potentially favoured over phosphorous. This could have a dramatic effect upon reactivity.

Finally, all of the above complexes, with the exception of **Cat-9** and **Cat-10**, have only been tested for Guerbet chemistry.[4] Recent advances in manganese catalysis has shown their use in fields of catalysis such as ester and alkene hydrogenation,[3,4] not to mention a plethora of organic synthetic reactions.[36] As such, there is much potential for these complexes in a variety of other forms of catalysis.
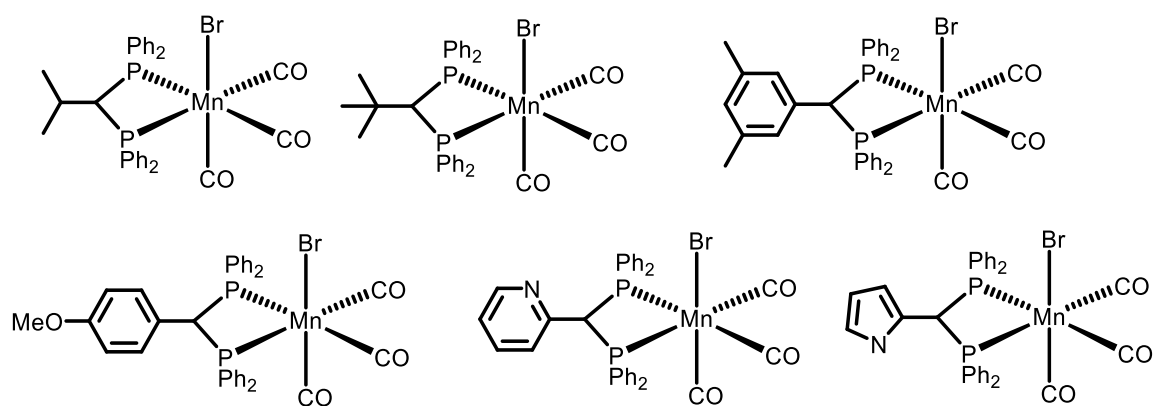
Figure 3.11: A variety of manganese monochelates, bearing electron donating substituents on the backbone.

3.10 – References

1   N. V Kulkarni, W. W. Brennessel and W. D. Jones, *ACS Catal.*, 2018, **8**, 997–1002.

2   S. Fu, Z. Shao, Y. Wang and Q. Liu, *J. Am. Chem. Soc.*, 2017, **139**, 11941–11948.

3   S. Weber, B. Stöger, L. F. Veiros and K. Kirchner, *ACS Catal.*, 2019, **9**, 9715–9720.

4   R. van Putten, E. A. Uslamin, M. Garbe, C. Liu, A. Gonzalez-de-Castro, M. Lutz, K. Junge, E. J. M. Hensen, M. Beller, L. Lefort and E. A. Pidko, *Angew. Chem. Int. Ed.*, 2017, **56**, 7531–7534.

5   G. R. M. Dowson, M. F. Haddow, J. Lee, R. L. Wingad and D. F. Wass, *Angew. Chem. Int. Ed.*, 2013, **52**, 9005–9008.

6   R. L. Wingad, P. J. Gates, S. T. G. Street and D. F. Wass, *ACS Catal.*, 2015, **5**, 5822–5826.

7   R. L. Wingad, E. J. E. Bergström, M. Everett, K. J. Pellow and D. F. Wass, *Chem. Commun.*, 2016, **52**, 5202–5204.

8   K. J. Pellow, R. L. Wingad and D. F. Wass, *Catal. Sci. Technol.*, 2017, **7**, 5128–5134.

9   Y. Liu, Z. Shao, Y. Wang, L. Xu, Z. Yu and Q. Liu, *ChemSusChem*, 2019, **12**, 3069–3072.

10 M. Peña-López, P. Piehl, S. Elangovan, H. Neumann and M. Beller, *Angew. Chem. Int. Ed.*, 2016, **55**, 14967–14971.

11 R. H. Reimann and E. Singleton, *J. Organomet. Chem.*, 1972, **38**, 113–119.

12 W. Strohmeier, *Angew. Chem. Int. Ed.*, 1964, **3**, 730–737.

13 A. M. Bond, R. Colton, A. Van Den Bergen and J. N. Walter, *Organometallics*, 2004, **23**, 3164–3176.

14 W. A. King, B. L. Scott, J. Eckert and G. J. Kubas, *Inorg. Chem.*, 1999, **38**, 1069–1084.

15 P. Atkins, T. Overton, J. Rouke, M. Weller and F. Armstrong, *Inorganic chemistry*, Oxford University Press, Great Clarendon Street, Oxford, 5th edn., 2010.

16   A. L. Rheingold,
      *https://www.ccdc.cam.ac.uk/structures/search?id=doi:10.5517/cc90v7c&sid=Data
      Cite (Accessed: 26/03/2020)*, 2006.

17   S. Elangovan, J. Neumann, J. B. Sortais, K. Junge, C. Darcel and M. Beller, *Nat.
      Commun.*, 2016, **7**, 1–8.

18   N. Deibl and R. Kempe, *Angew. Chem. Int. Ed.*, 2017, **56**, 1663–1666.

19   M. Perez, S. Elangovan, A. Spannenberg, K. Junge and M. Beller, *ChemSusChem*,
      2017, **10**, 83–86.

20   C. Zhu, J. C. A. Oliveira, Z. Shen, H. Huang and L. Ackermann, *ACS Catal.*, 2018, **8**,
      4402–4407.

21   C. Wang, J. Yang, X. Meng, Y. Sun, X. Man, J. Li and F. Sun, *Dalton Trans.*, 2019, **48**,
      4474–4478.

22   J. R. Carney, B. R. Dillon, L. Campbell and S. P. Thomas, *Angew. Chem. Int. Ed.*,
      2018, **57**, 10620–10624.

23   Y. Kita, T. Higuchi and K. Mashima, *Chem. Commun.*, 2014, **50**, 11211–11213.

24   G. X. Wang, J. Yin, J. Li, Z. B. Yin, W. X. Zhang and Z. Xi, *Inorg. Chem. Front.*, 2019, **6**,
      428–433.

25   R. R. Schrock and J. A. Osborn, *J. Chem. Soc. D Chem. Commun.*, 1970, **567**, 567–
      568.

26   J. Ruiz, M. E. G. Mosquera, V. Riera, M. Vivanco and C. Bois, *Organometallics*, 1997,
      16, 3388–3394.

27   G. A. Carriedo, V. Riera and J. Santamaria, *J. Organomet. Chem.*, 1982, **234**, 175–
      183.

28   D. A. Brown, W. K. Glass, K. M. Kreddan, D. Cunningham, P. A. McArdle and T.
      Higgins, *J. Organomet. Chem.*, 1991, **418**, 91–105.

29   S. J. A. Pope and G. Reid, *J. Chem. Soc., Dalton Trans.*, 1999, 1615–1621.

30   G. A. Carried and V. Riera, *J. Organomet. Chem.*, 1981, **205**, 371–379.

31   C. Carlini, M. Di Girolamo, A. Macinai, M. Marchionna, M. Noviello, A. M. Raspolli
      Galletti and G. Sbrana, *J. Mol. Catal. A Chem.*, 2003, **200**, 137–146.

32   R. E. Rodríguez-Lugo, M. Trincado, M. Vogt, F. Tewes, G. Santiso-Quinones and H.
      Grützmacher, *Nat. Chem.*, 2013, **5**, 342–347.

33   M. Nielsen, E. Alberico, W. Baumann, H. J. Drexler, H. Junge, S. Gladiali and M.
      Beller, *Nature*, 2013, **495**, 85–89.

34   M. Andérez-Fernández, L. K. Vogt, S. Fischer, W. Zhou, H. Jiao, M. Garbe, S.
      Elangovan, K. Junge, H. Junge, R. Ludwig and M. Beller, *Angew. Chem. Int. Ed.*,
      2017, **56**, 559–562.

35   N. V. Kireev, O. A. Filippov, E. S. Gulyaeva, E. S. Shubina, L. Vendier, Y. Canac, J. B.

Sortais, N. Lugan and D. A. Valyaev, *Chem. Commun.*, 2020, **56**, 2139–2142.

36   J. R. Carney, B. R. Dillon and S. P. Thomas, *European J. Org. Chem.*, 2016, **2016**, 3912–3929.

Chapter 4- Rhenium based catalysts for the production of advanced biofuels

4.1 – Introduction

Molecular rhenium catalysis has had a resurgence in recent years, largely owing to the successful application of the first-row Group 7 metal manganese.[1] Examples of rhenium complexes for dehydrogenative coupling reactions, and the transfer hydrogenation of ketones and imines outline its potential in homogeneous catalysis (Figure 4.1).[2,3] Many of these examples employ either a Re(V) or Re(II) metal centre.[4, 5] Re(I) has also been studied but ligand development has been largely neglected, with only simple monodentate phosphines being used.[6,7] In many cases no ligands were used at all, and the simple rhenium(I) pentacarbonyl halide or dirhenium decacarbonyl was utilised.[8]

4.1   **4.2**
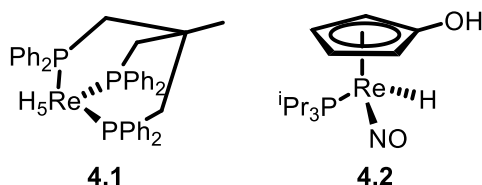
*Figure 4.1: Rhenium catalysts used for dehydrogenative coupling of alcohols (**4.1**), and transfer hydrogenation of ketones and imines (**4.2**).*

One of the first examples of potential catalysis mediated by a Re(I) complex bearing more sophisticated ligands came from the Milstein group in 2013 (Figure 4.2). Here, a Re-PNP pincer complex (**4.3**) was used for the activation of nitriles and CO_2 by metal-ligand cooperation.[9, 10] Catalysis using Re(I) PNP-pincer complexes was realised in 2017, with virtually concurrent papers from the Beller[11] and Sortais[12] groups. Here they reported the synthesis of a Re(I) complex (**Cat-18**) bearing a bis(phosphinoethyl)amine, 'MACHO-style' ligand (Figure 4.2), and demonstrated its use in dehydrogenative coupling and hydrogenation reactions.

Interestingly, when the same ligand is coordinated to iron,[13] ruthenium[14] or manganese[15] it preferentially binds in a meridional coordination, with the two phosphine substituents *trans* to one another. However, on coordination to rhenium a facial geometry with two *cis* phosphine groups is reported. Given the greater ionic radius of Re compared to Mn, Fe and Ru, the phosphine ligands are less hindered and can coordinate in a *cis* arrangement,

without excessive steric clash forcing *trans* geometry. Even though analogous metal precursors are used in the formation of both the manganese and rhenium complexes ([MnBr(CO)$_5$] and [ReBr(CO)$_5$]); the manganese complex preferentially forms the neutral dicarbonyl bromide (see Section 3.1). For rhenium, the cationic tricarbonyl species with a bromide counterion is formed.

4.3   **Cat-18**
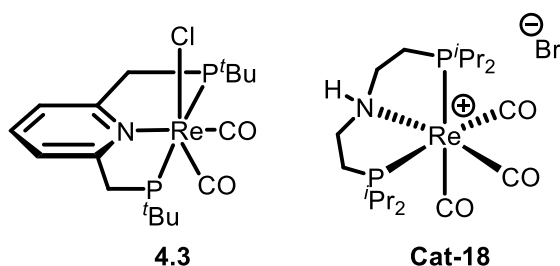
Figure 4.2: Re(I) complexes bearing PNP-pincer ligands.

Since its discovery, **Cat-18** has been used for a variety of reactions, including the N-methylation of anilines and the formation of quinolines *via* acceptorless dehydrogenative coupling,[16,17] while theoretical studies have also been performed on the mechanism of methanol dehydrogenation.[18] Given its established ability to perform borrowed hydrogen type chemistry, and the success of its manganese analogue (see Section 3.2), **Cat-18** was applied to *iso*butanol formation *via* ethanol and methanol heterocoupling.

Unlike Re(I) pincer complexes, rhenium bidentate and bis chelate species have remained virtually unexplored for homogeneous catalysis, with the focus instead being on their interactions with DNA.[19,20] Given the potential shown by manganese bidentate species for the formation of *iso*butanol *via* the Guerbet reaction (Chapter 3), a variety of rhenium mono and bis chelates were synthesised and tested for Guerbet chemistry.

4.2- Re pincer complexes for advance biofuel production

4.2.1 – Advanced biofuel formation catalysed by Cat-18

4.2.1.1 – Formation of *iso*butanol

Cat-18 was tested for the coupling of ethanol and methanol to form *iso*butanol in a 100 mL Parr stainless steel autoclave, and a condition screen conducted with the results shown in Table 4.1. **Cat-18** showed promising activity towards the upgrading of ethanol and methanol to *iso*butanol *via* the Guerbet reaction. Yields of *iso*butanol exceeding 20% were observed over a run time of 66 hours (Table 4.1, Entry 1), with only a minor decrease in

yield observed when the run time was reduced to 18 hours (Entry 2). However, reducing the reaction time further to three hours caused a significant decrease in both yield and selectivity (Entry 6). Varying the temperature had no positive effect on the yield of *iso*butanol (Entries 7 and 8). While increasing the temperature did increase selectivity to *iso*butanol, as propanol yields were significantly reduced, it resulted in no overall improvement in *iso*butanol yield. Reducing the reaction temperature to 160 °C caused a significant decrease in selectivity, with the yields of propanol increasing from 1.5 % (Entry 2) to 4.1 % (Entry 7). Interestingly, these reactions could be performed with reduced catalyst loadings of only 0.07 mol%, as increasing the loading to 0.1 mol% had little effect upon the overall yield (Entry 5). Attempts to decrease base loading also had a detrimental effect upon both ethanol conversion and *iso*butanol yield (Entry 4). Increasing base loadings to 350 mol%, equal to those used by the Lui group for *iso*butanol formation using the analogous manganese catalyst (see Section 3.2),[21] was not beneficial to catalytic activity. Indeed, at this base loading, solid production was so excessive that recovery of enough liquid from the sample to allow for analysis by GC was not possible.

*Table 4.1: Condition screen for formation of isobutanol using **Cat-18**.*
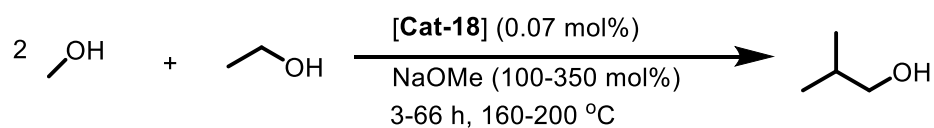
Entry[a]	Temp (°C)	Time (h)	Base loading (mol%)	EtOH Conversion (%)	iBuOH Yield (%)	PrOH Yield (%)	iBuOH Selectivity (%)[b]
1	180	66	200	99	21	0	98.8
2	180	18	200	96	16	2	85
3[c]	180	18	350	-	-	-	-
4	180	18	100	85	10	4	56
5[d]	180	18	200	98	17	1	90
6	180	3	200	73	5	3	40
7	160	18	200	79	7	4	48
8	200	18	200	100	15	0	97

[a] Conditions: 1 mL (17.13 mmol) EtOH, 10 mL MeOH, [b] selectivity calculated from observed products in the liquid fraction [c] large amount of solid produced [d] 0.1 mol% catalyst.

The amount of missing ethanol (the discrepancy between yield of products and ethanol consumed) in these experiments is very large, with ethanol conversion proceeding almost to completion in most cases, yet *iso*butanol yields rarely exceed 20%. Extremely high pressures are observed in the autoclave during these reactions (33 bar after reaction, 9 bar after cooling, Entry 5). This pressure increase is attributed to hydrogen formation, due to the dehydrogenation of methanol and ethanol to formate and acetate, which would explain the discrepancy between ethanol conversion and *iso*butanol yield. This catalyst appears to be far more selective for Tishchenko and Cannizzaro chemistry than for the Guerbet reaction (see Section 3.2.3).

While much less selective for Guerbet chemistry, **Cat-18** is more active than its manganese analogue (12.7 TON h^{-1} compared to 8.5 TON h^{-1}), with comparable *iso*butanol yields seen when using lower catalyst loadings (0.07 mol% compared to 0.1 mol%) (see Section 3.2).

4.2.1.2 – Formation of *n*-butanol

Owing to the success of **Cat-18** for *iso*butanol formation, its application in the homocoupling of ethanol to form *n*-butanol was also investigated (Table 4.2). To allow for easy comparison, the same conditions were used as for *n*-butanol formation using manganese catalysts (see Section 3.4), however, shorter run times were employed.

*Table 4.2: Formation of n-butanol using **Cat-18**.*
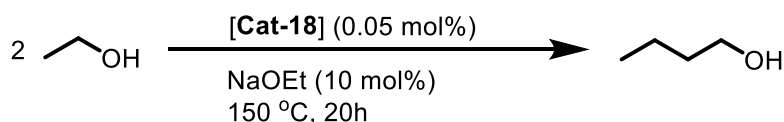
Entry[a]	Ethanol conversion (%)	*n*BuOH Yield (%)	Ethyl acetate yield (%)	*n*BuOH selectivity[b] (%)
1	33	8	1	85

[a] Conditions 10 mL (171.3 mmol) ethanol [b] Total selectivity to *n*-butanol in the liquid fraction determined by gas chromatography.

Cat-18 was significantly more active than both manganese bis chelates tested for this reaction. Activity was almost comparable to that obtained by the Jones group using the manganese analogue, although significantly higher base and catalyst loadings were used in their study (0.2 mol% catalyst, 25 mol% NaOEt, 18% *n*-butanol yield).[22] This indicates that **Cat-18** could be significantly more active for *n*-butanol formation that its manganese analogue. The main by-product observed was ethyl acetate from acceptorless dehydrogenative coupling of ethanol, while small amounts of higher alcohols (0.4% hexanol, and 0.2% octanol) were also seen. This catalyst favoured the formation of linear alcohols over branched alcohols, as no 2-ethylbutanol or 2-ethylhexanol were observed by GC, despite the presence of their linear isomers.

4.2.2 – Effect of varying the phosphine substituent on catalytic activity.

4.2.2.1- Synthesis

Given the initial success of **Cat-18** for advanced biofuel formation, and the large effect that varying the phosphine substituents can have upon the steric and electronic properties of the ligand, several other Re-PNP pincer complexes were targeted for testing.

The synthesis of a variety of Re PNP-pincer complexes has been reported by the Sortais group.[17] Here, the free ligand was reacted with the catalyst precursor under reflux in toluene, giving the desired pincer complexes in high yields (Scheme 4.1).
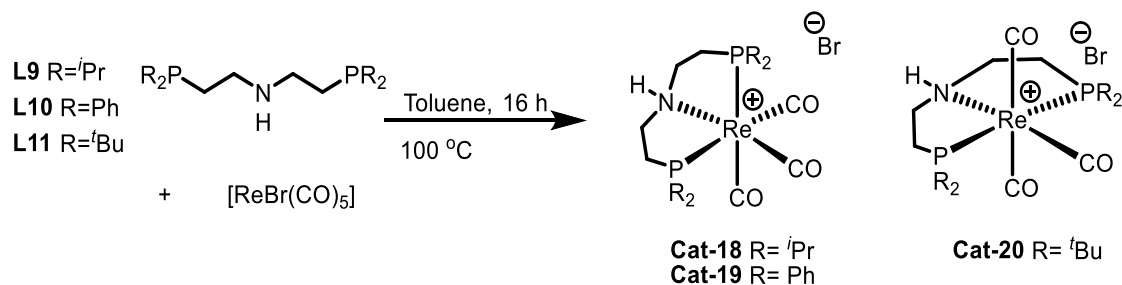
Scheme 4.1: Synthesis of a variety of Re PNP-pincer ligands.

For the N-methylation of anilines, phenyl substituents were found to be most effective, while bulkier *tert*-butyl groups were detrimental to activity. To investigate whether the same effect was seen in Guerbet chemistry, **Cat-19** and **Cat-20** were both synthesised.

Synthesis of **Cat-20** was possible using the above method, albeit in significantly lower yields than those reported (43% compared to 97%). However, production of **Cat-19** was significantly more complicated, with several impurities forming upon reflux. Only a small amount of pure product was isolated, precipitating from the toluene solution upon reflux (15%). **Cat-19** was instead synthesised from a $[Re(CO)_3(H_2O)_3]Br$ precursor (**4.4,** Scheme 4.2). Heating **4.4** with **L10** in a dichloromethane solution for 18 hours, followed by trituration with pentane allowed for isolation of **Cat-19** in much higher yields (46%). The purity of the product was confirmed by $^{31}P\{^1H\}$ NMR spectroscopy, displaying a singlet at 23.1 ppm.
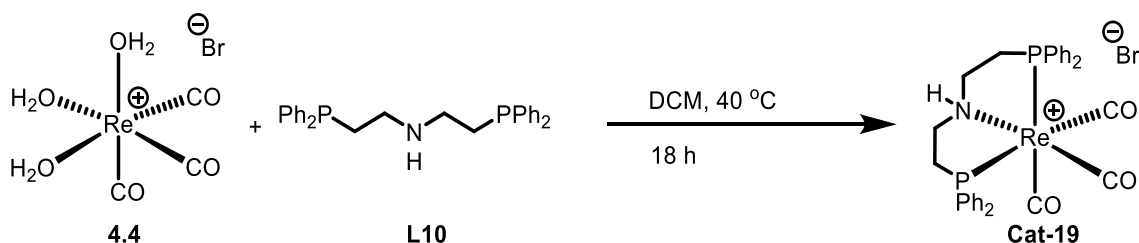
*Scheme 4.2: Formation of **Cat-19** from [Re(CO)$_3$(H$_2$O)]Br precursor.*

4.2.2.2 – Catalysis

Once sufficient amounts of both **Cat-19** and **Cat-20** had been synthesised, both were tested for *iso*butanol formation using the optimum conditions established in Table 4.1, Entry 2 (Table 4.3). **Cat-19** gave a significantly higher yield of *iso*butanol than **Cat-18**, with turnover numbers of 500, it also exhibited much higher selectivity with *n*-propanol yields decreasing to 1%. **Cat-20** on the other hand, was much less active for *iso*butanol formation with yields of only 7%. However, this catalyst is far less selective for alcohol dehydrogenation, with an ethanol conversion of just 30%, compared to 99% for **Cat-19**. As **Cat-20** is slower but more selective for Guerbet chemistry over alcohol dehydrogenation, longer reaction times may enable *iso*butanol yields to reach or exceed those given by **Cat-18** and **Cat-19**. For these catalysts, *iso*butanol formation has almost reached its maximum potential, with ethanol consumption nearing 100%, and little *n*-propanol remaining for further reaction to produce *iso*butanol.

Table 4.3: Formation of isobutanol using Re ^{R}PNP-pincer complexes.

Catalyst[a]	EtOH Conversion (%)	iBuOH Yield (%)	PrOH Yield (%)	iBuOH Selectivity (%)[b]	Turnover Numbers[c]
18	96	16	2	85	229
19	99	35	1	97	500
20	30	7	2	59	100

[a] Conditions: 1 mL (17.13 mmol) EtOH, 10 mL MeOH, 180 °C, 17 h, NaOMe (200 Mol%), 0.07 mol% [Cat] [b] Selectivity calculated from observed products in the liquid fraction, [c] Turnover number (TON) based on mmol of ethanol converted to *iso*butanol per mmol of Re

Cat-19 outperforms all manganese catalysts for *iso*butanol formation in terms of both yield and selectivity, while a significantly lower base loading (200 mol% instead of 350 mol%) is needed.[21] Unlike manganese, where the *iso*propyl and phenyl substituted complexes perform very similarly, on rhenium the phenyl substituted complex significantly outperforms the *iso*propyl.

4.2.2.3 – Synthesis of a fluorinated PNP ligand

A general trend noted between these complexes is that increasing the size and electron donor properties of the phosphine substituents decreases the *iso*butanol yield. It is not clear whether steric or electronic factors play a primary role in dictating catalytic activity, so to investigate this further the fluorinated PNP-ligand **L12** was synthesised. This ligand bears *meta* -CF$_3$ groups on the phenyl substituents of the phosphine groups, decreasing the electron donor ability of the ligand while increasing the π-acceptor quality. Given these substituents are in the *meta* position on the phenyl rings, they should have a limited impact on the steric properties of the ligand.

Ligand **L12** was synthesised in high yields, following a literature procedure (Scheme 4.3).[23] However, when complexation to rhenium was attempted, very little product could be recovered (3-4 mg). Syntheses using both **4.4** and rhenium bromopentacarbonyl precursors were attempted with similar results (Scheme 4.4). The presence of **Cat-21** was identified by mass spectrometry ([M+] *m/z* = 1256.0), and a resonance at 15.05 ppm observed by ^{31}P{^{1}H} NMR spectroscopy. However, enough pure complex to allow for catalytic testing could not be produced, and as such the relative effect of sterics and electronics of the ligand could not be established.
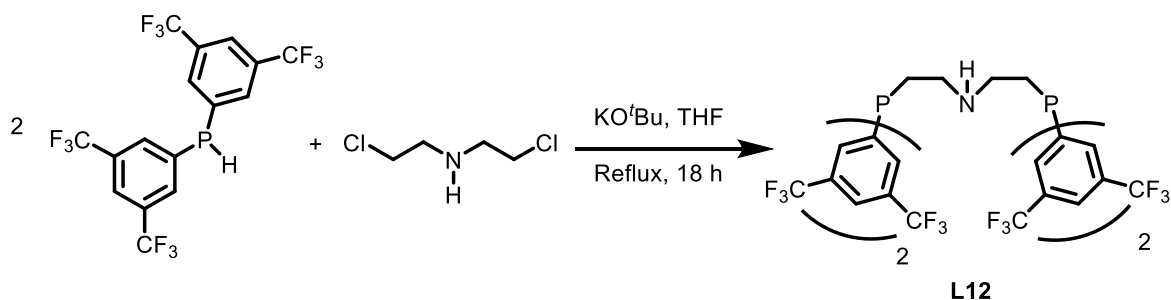
*Scheme 4.3: Synthesis of fluorinated PNP ligand **L12**.*

The electron poor nature of **L12** may be disfavouring complexation to the rhenium centre. Coordination of **L12** to ruthenium is known,[23,24] but no other metal complexes have been reported. As such, how **L12** interacts with less electron rich metals has not been established.
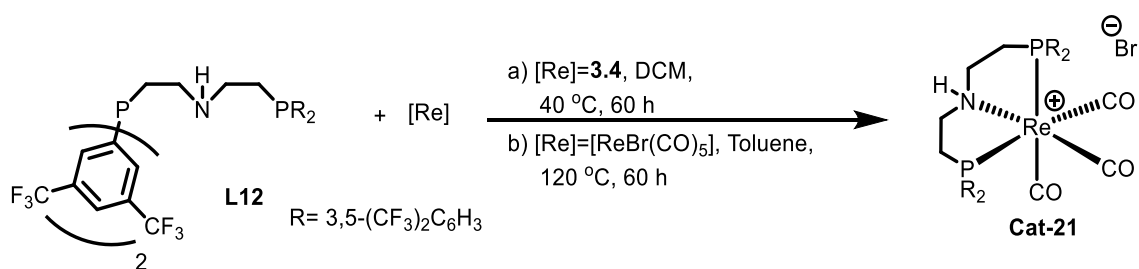
*Scheme 4.4: Attempted synthesis of **Cat-21** from two different Re precursors.*

4.2.3 – Solid analysis

Rhenium pincer complexes produced a large amount of solid by-product, indicating that other catalytic processes besides Guerbet chemistry were occurring. Analysis of the solid by-product allows for identification and quantification of these reactions.

The solid produced during Table 4.1, Entry 1 was analysed. **Cat-18** produced significantly more solid than any of the manganese bis chelates tested (1.0059 g). ^{1}H NMR spectroscopic analysis showed the presence of both sodium formate and sodium acetate, with formate being the major product once again (see Section 3.6.1). However, significantly more acetate was observed in these samples than was observed in the solid produced by manganese catalysts. By ^{1}H NMR spectroscopy, the ratio of formate to acetate was roughly 14:1. The initial molar ratio of methanol to ethanol was 14.4:1, therefore selective dehydrogenation of neither alcohol is especially favoured by **Cat-18**. Much of the missing ethanol in these reactions can be attributed to acetate formation, which then precipitates out of the reaction solution as a sodium salt (Scheme 4.5).
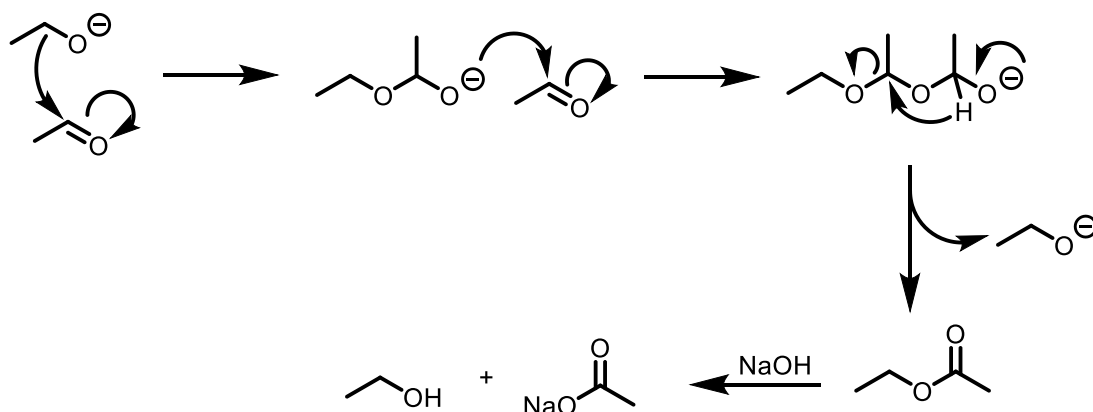
Scheme 4.5: Formation of acetate salts via Tishchenko chemistry.[25]

The production of sodium carbonate was also confirmed by ^{13}C NMR spectroscopy (Figure 4.3) of a catalytic run using base loadings of 350 mol% (Table 4.1, Entry 3). This established

the ability of **Cat-18** to fully dehydrogenate methanol to CO_2 and H_2. Computational studies of methanol dehydrogenation with **Cat-18**, using KOH as a base, found that the rate determining step is likely the hydride transfer from formate to the metal centre.[18] The solid therefore likely contains more formate than carbonate.
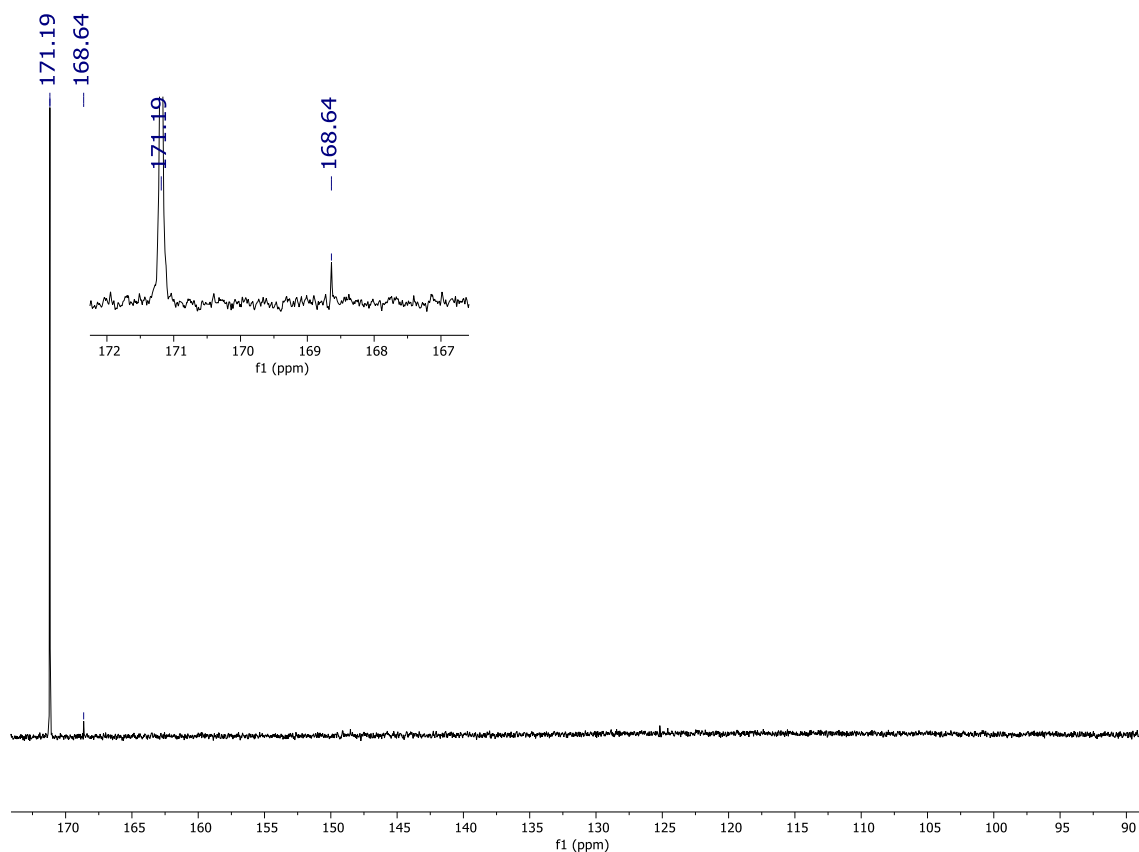
Figure 4.3: ^{13}C (126 MHz, D_2O) spectrum of solid produced during Table 4.1, Entry 3. Inset: expanded section of the formate/ carbonate region.

4.2.4 – Catalytic mechanism

Investigating catalyst activation and the reaction mechanism can help shed light on what may be the rate limiting step for the reaction. It can also help to identify catalytic side reactions and possible catalyst degradation pathways; hence these investigations can aid in the design of more active and selective catalysts.

4.2.4.1- Previous computational work and proposed mechanism

Computational work by the Sortais group investigated the mechanism of catalyst activation in the hydrogenation of carbonyl derivatives.[12] They proposed that several steps are required to move from **Cat-18** to the active species, **Cat-18d** (Scheme 4.6). Initially, **Cat-18** is activated in the presence of base *via* deprotonation of the N-H moiety in the ligand

backbone forming **Cat-18b**. This is followed by isomerisation to the *mer*-[Re(PNP)(CO)$_3$] isomer **Cat-18c**. Finally, a slightly disfavoured dissociation of CO from **Cat-18c** generates the 16 e$^-$ dicarbonyl species **Cat-18d,** which is believed to be the active catalyst. Computational studies were performed using KO^{t}Bu as the base, but a similar mechanism is believed to occur when NaOMe is used instead. Formation of the meridional isomer (**Cat-18c**) is reported to be favoured under basic conditions. Observation of neither **Cat-18c** nor the active catalyst **Cat-18d** has yet been reported by spectroscopic means, and it is worth noting that **Cat-20** was inferior to both **Cat-18** and **Cat-19,** despite being held in a meridional geometry.
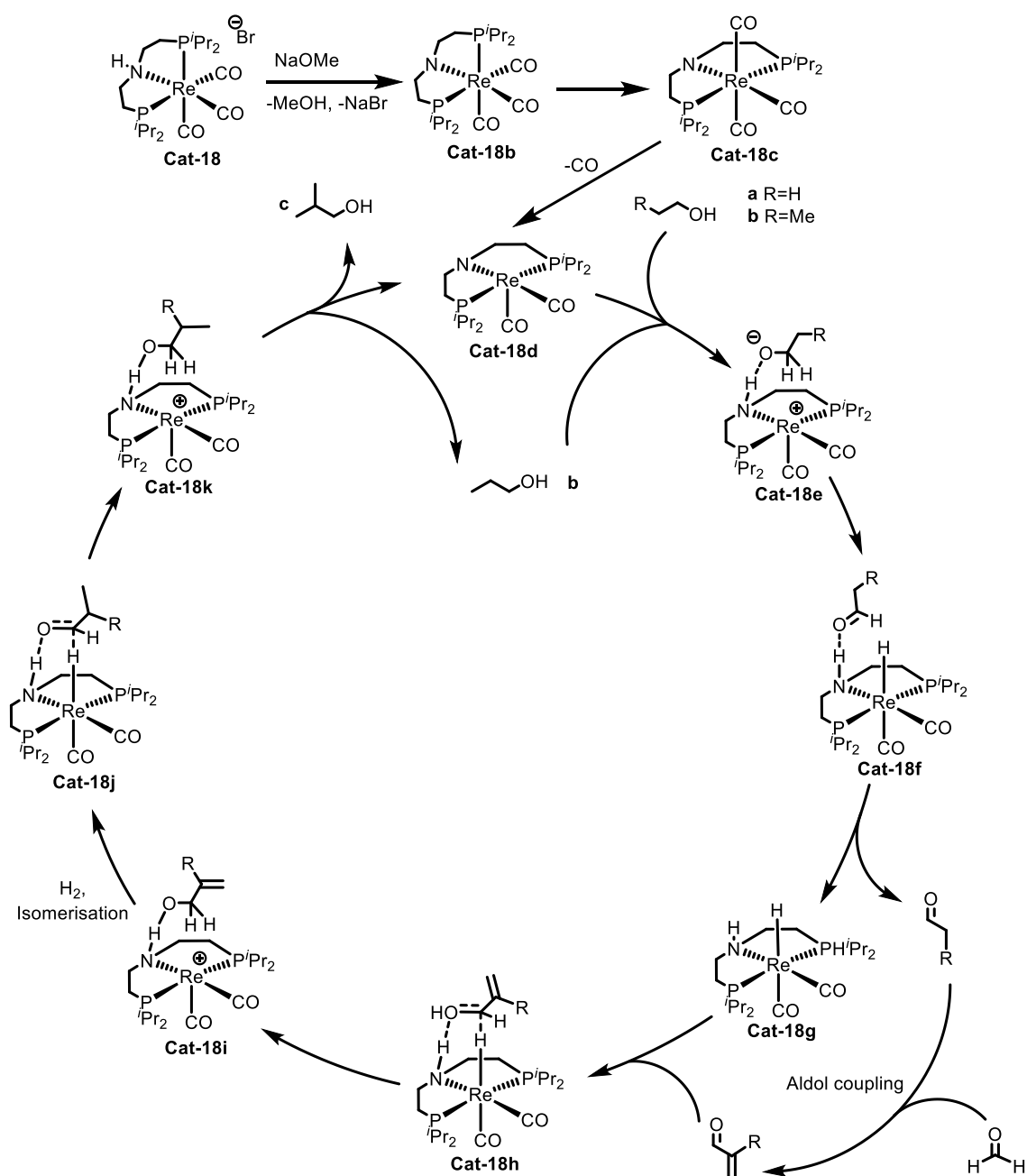
Scheme 4.6: Generation of the active **Cat-18d**, and proposed mechanism for Guerbet chemistry.

By adapting proposed mechanisms for hydrogenation and N-methylation of amines using **Cat-18**, a potential mechanism for the Guerbet reaction can be proposed (Scheme 4.6).[12,17] In this mechanism, ethanol (**a**) interacts with active **Cat-18d** via a hydrogen bond with the deprotonated amine backbone (**Cat-18e**). Dehydrogenation then occurs (**Cat-18f**), forming acetaldehyde and the rhenium hydride complex **Cat-18g**. Once acetaldehyde is formed it reacts with formaldehyde, produced via the same mechanism, in an aldol condensation to give acrylaldehyde. This α,β-unsaturated species reacts with **Cat-18g** via the C=O bond, (**Cat-18h**) and the resulting compound isomerises and reacts via **Cat-18j** and **Cat-18k** to

generate the longer chain alcohol propanol (**b**). Propanol can subsequently re-enter the cycle and generate *iso*butanol (**c**), which does not react further.

4.2.4.2 – Following catalyst activation by $^{31}P\{^1H\}$ NMR spectroscopy

As detailed above, conversion of **Cat-18** to its meridional form **Cat-18c** and subsequently to the active **Cat-18d**, should be a rapid process under basic conditions. This process was followed by $^{31}P\{^1H\}$ NMR spectroscopy to gain insight into the conditions required for catalyst activation.

Initial attempts to form **Cat-18b** and **18c** were made using a methanol solution of **Cat-18** with a 100-fold excess of NaOMe at reflux. After the addition of base, a slight shift in the $^{31}P\{^1H\}$ NMR spectrum from 38.60 ppm to 38.66 ppm was observed. This small change is assigned to the formation of **Cat-18b** (Figure 4.4, B), as formation of this species is favourable with ΔG= -46.6 kcal mol^{-1} when KO^{t}Bu is used as a base.[12] However, further reaction to form **Cat-18c** appears to not be possible at this temperature, as both heating at reflux and heating in a sealed environment using a J. Young's NMR tube saw little to no change in the $^{31}P\{^1H\}$ NMR spectrum. Isomerisation, while still favourable, is significantly less favoured than N-H deprotonation (ΔG= -3.9 kcal mol^{-1}), hence it seems that more forcing conditions are required to initiate this isomerisation.

Complete formation of the active **Cat-18d** could be achieved by heating a basic methanol solution of **Cat-18** in an autoclave at 180 °C (reaction temperature) overnight. The $^{31}P\{^1H\}$ NMR spectrum of the post reaction mixture showed a single resonance at 53.90 ppm (Figure 4.4, C), this is tentatively attributed to **Cat-18d** as sodium formate was also observed in the ^1H NMR spectrum indicating that the active catalyst had been formed. This is produced by the dehydrogenation of methanol and is accompanied by a build-up of pressure in the autoclave (10 bar at the end of reaction) due to dihydrogen production.

While **Cat-18** was largely stable in solution for at least 4 days (confirmed by $^{31}P\{^1H\}$ NMR spectroscopy) (Figure 4.4, A), it was not thermally stable to reaction temperatures for extended periods of time without base present. Heating **Cat-18** in methanol to 180 °C gave three singlets in the $^{31}P\{^1H\}$ NMR spectrum at 46.26, 47.98 and 49.84 ppm. These did not correspond to either **Cat-18** or **Cat-18d** and are therefore likely represent thermal

decomposition products. Due to their absence when base is present it seems that the active catalyst **Cat-18d** is more stable at reaction temperatures that **Cat-18** itself.
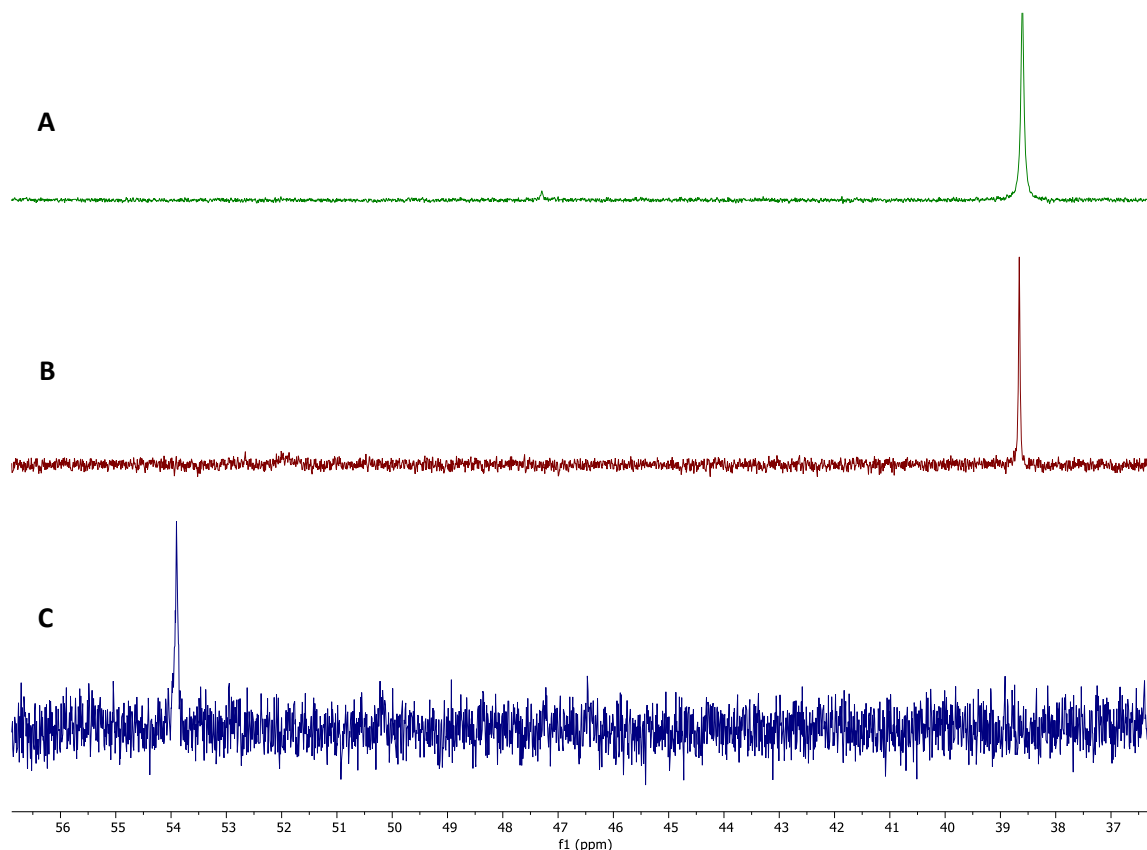
*Figure 4.4: $^{31}P\{^1H\}$ NMR spectrum (202 MHz, MeOH) of (A) **Cat-18** in MeOH for 4 days (peak at 47 ppm, small sign of degradation products) (B) **Cat-18** and NaOMe heated to reflux for 20 hrs (C) **Cat-18** and NaOMe heated to 180 °C for 20 hrs in an autoclave.*

Formation of **Cat-18c** was not possible in refluxing methanol (bp= 64.7 °C). However, on changing the solvent from methanol to ethanol (bp= 78.4 °C) a mixture of **Cat-18** with 100 equivalents of NaOEt refluxed for 18 h allowed the formation of **Cat-18c** to be observed. While a small amount of the *fac* isomer **Cat-18b** was still present, most of the sample was converted to the *mer* geometry. This large change in resonance in the $^{31}P\{^1H\}$ NMR spectrum is due to the phosphine substituents moving from being *cis* to one another to *trans* (Figure 4.5). As acetate was not seen in the ^1H NMR spectrum of the product mixture, it seems unlikely that the active catalyst had formed (see Section 4.2.3). Formation of **Cat-18d** is reported to be slightly disfavoured in methanol (ΔG= 0.8 kcal mol^{-1}),[17] therefore an even higher boiling point solvent may be required to initiate this change. The broadness of the peak at 51.18 ppm suggests some fluxionality in the molecular structure, although it is not currently clear what is causing this broadening.
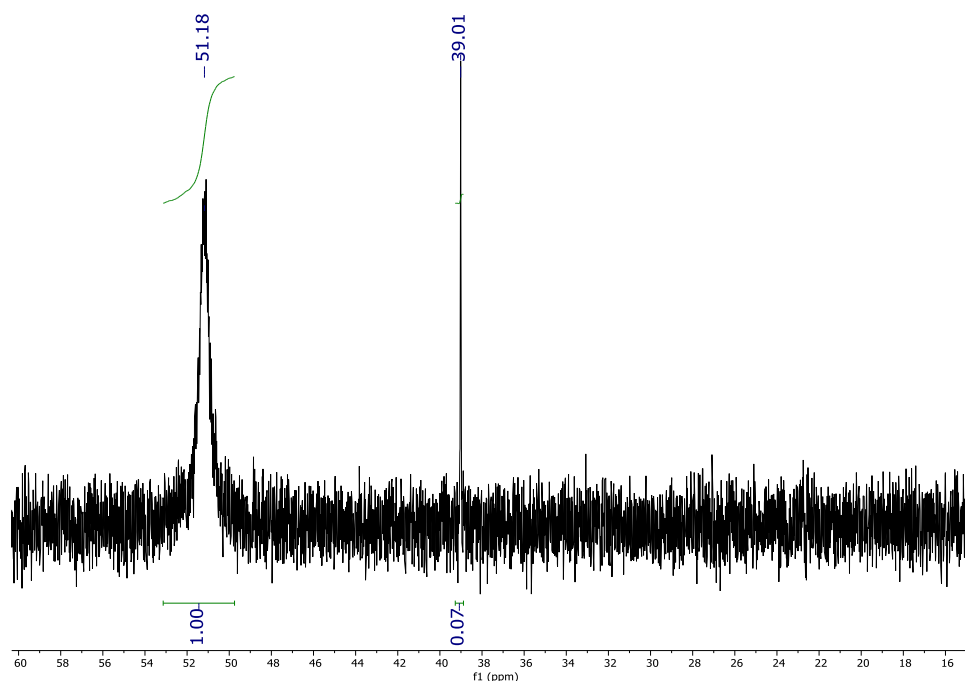
*Figure 4.5: $^{31}P\{^{1}H\}$ (202 MHz, EtOH) NMR spectrum showing the formation of **Cat-18c** by refluxing a basic solution of **Cat-18** in ethanol.*

Tracking the stepwise formation of the active **Cat-18d** from **Cat-18** under a variety of reaction conditions has been possible. This shows the importance of both temperature and base for catalyst activation. While formation of **Cat-18b** appears to be quite facile, subsequent conversion to **Cat-18c** and **Cat-18d** requires more forcing conditions (namely higher temperatures). Meanwhile when high temperatures are used, base is essential for catalyst activation otherwise several other thermal degradation products are observed instead.

4.2.5 – Summary of Rhenium PNP-pincer complexes

Cat-18 – Cat-20 are all competent catalysts for the formation of *iso*butanol from ethanol and methanol. **Cat-18** and **Cat-19** are significantly more active than **Cat-20**, but do show poor selectivity to alcohol formation, instead favouring Tishchenko and Cannizzaro chemistry to produce sodium formate, acetate and carbonate. This preference is shown by the large amount of solid by-product produced during reaction. A general trend is observed where less electron donating phosphine substituents give higher *iso*butanol yields. However, extending this trend further by synthesising **Cat-21** was not possible, as **Cat-21** could not be produced in high enough yields for catalytic testing. It was possible to track

the formation of the active catalyst **Cat-18d** by $^{31}P\{^{1}H\}$ NMR spectroscopy, which showed the importance of both base, and heat in catalyst activation.

4.3 – Rhenium mono and bis chelate complexes for advanced biofuel production

While the ability of rhenium pincer complexes to form *iso*butanol from ethanol and methanol has been established, with rhenium complexes outperforming their manganese analogues, selectivity was still an issue. Manganese mono and bis chelate complexes on the other hand, while slow to facilitate *iso*butanol formation, are much less selective for alcohol dehydrogenation. Formate and acetate are produced in limited quantities, and no carbonate is observed. Combining the increase in turnover number produced by a rhenium centre with the increase in selectivity given by bidentate ligands could help increase the viability of group 7 metal catalysed biofuel production.

4.3.1 – Initial catalyst screen

4.3.1.1 – Catalyst synthesis

For manganese catalysis (see Chapter 3), complexes supported by bis(diphenylphosphino)methane (**L1**) and 2-(diphenylphosphino)ethylamine (**L4**) ligands were found to be the most effective in *iso*butanol formation. As such, rhenium complexes bearing these ligands were synthesised for initial testing.

The rhenium pendent complex **Cat-22** was synthesised according to a literature procedure from a mesitylene solution under reflux.[26] Conversion of this to the cationic *cis* bis chelate **Cat-23** was possible at room temperature using the halide abstractor AgBF$_4$ (Scheme 4.7).[27]
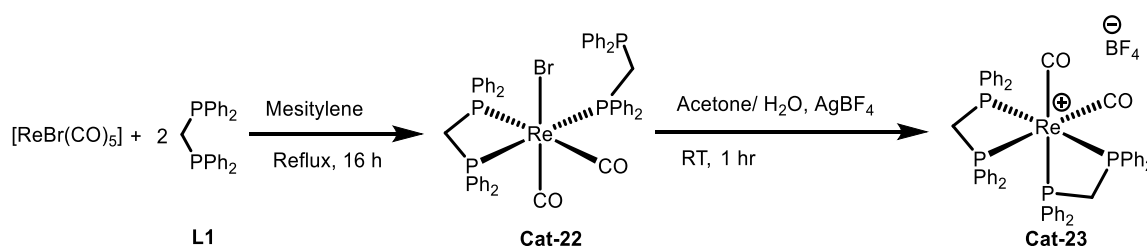
*Scheme 4.7: Synthesis of **Cat-22** and **Cat-23**.*

Literature syntheses of the neutral carbonyl bromide *trans* bis chelate **Cat-24** have been reported.[27] However, they require long reaction times (184 h) and give poor yields (15%). As such, synthesis of **Cat-24** was attempted *via* irradiation, as used in the production of the analogous manganese complex (Scheme 4.8, see Section 3.3.2). After 2 hours of irradiation,

pendent **Cat-22** could be detected by ^{31}P{^{1}H} NMR spectroscopy. However, further reaction to **Cat-24** was slow. After irradiation for 9 days, a complex mixture of free ligand, monochelate complex, pendent complex **Cat-22** and bis chelate **Cat-24** was observed. A small amount of yellow solid precipitated from the reaction mixture and was identified as predominantly **Cat-24**, although some free ligand and **Cat-23** were also present. Unfortunately, a sufficient amount of pure **Cat-24** to allow for catalytic testing could not be produced.
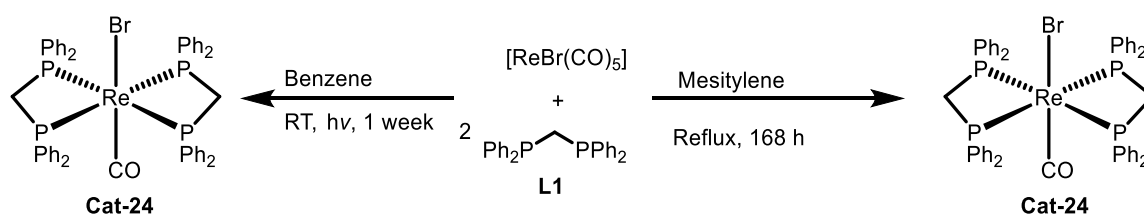
*Scheme 4.8: Various syntheses of **Cat-24**.*

The novel complex **Cat-25** was synthesised from a 2:1 solution of ligand (**L4**, dppea) and rhenium precursor in mesitylene under reflux (Scheme 4.9). Formation of the cationic dicarbonyl complex was confirmed by mass spectrometry ([M$^+$] *m/z* = 701.15), and a *cis* geometry was proposed as 2 peaks at 1920 and 1834 cm^{-1} were observed in the carbonyl region of the IR spectrum. Crystals of X-ray quality were grown by layering a solution of methanol with diethyl ether (Figure 4.6). **Cat-25** displayed a slightly distorted octahedral geometry with the phosphine ligands being *trans* to one another and the carbonyl ligands *cis*, a similar structure to the analogous manganese complex.[28] All bond lengths around the metal centre are significantly longer in complex **Cat-25** than in its manganese analogue (Re-P1 2.3793(5) compared to 2.2898(7) for Mn-P1), this is to be expected given that rhenium has a much greater atomic size. The intra-ligand P-Re-N angles are smaller in **Cat-25**, as is the C1-Re-C2 angle, which is likely a result of the increased bond length reducing steric clash. However, inter-ligand bond angles N1-Re-P2 and P2-Re-P1 are greater than in the analogous manganese complex.[28]
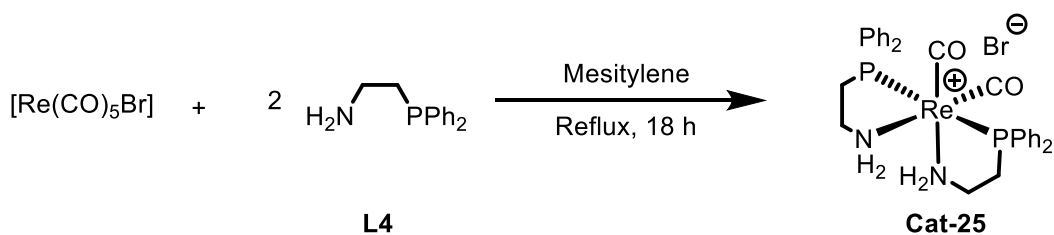
Scheme 4.9: Synthesis of **Cat-25**.
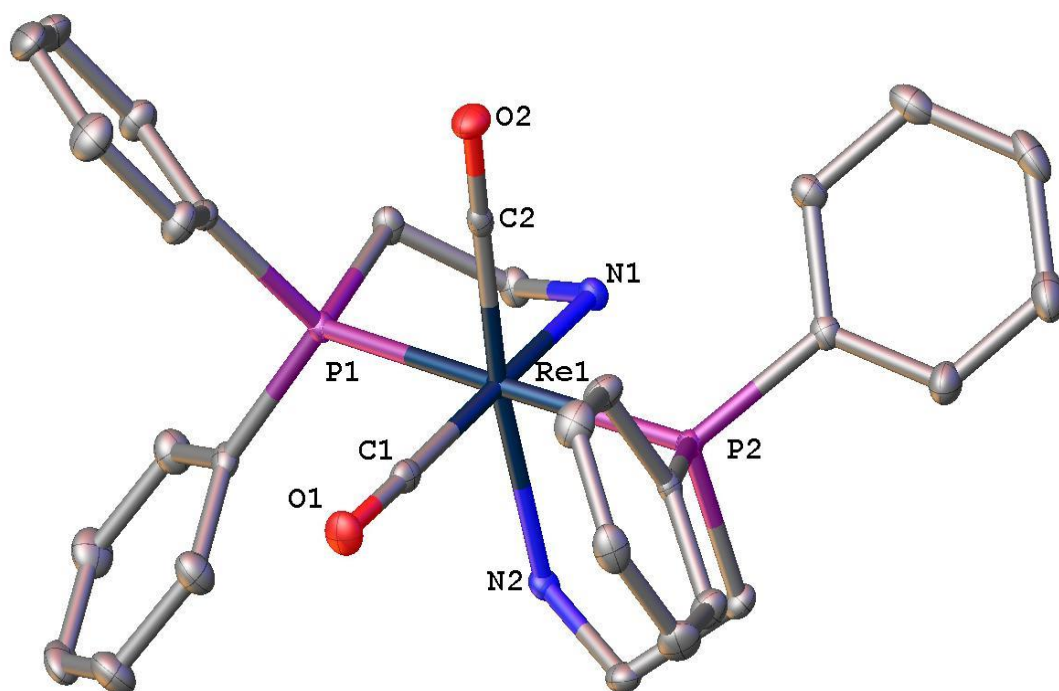
*Figure 4.6: Structure of **Cat-25**. Hydrogen atoms and bromide counter ion omitted for clarity. Selected bond lengths (Å) and angles (°): Re-N1 2.2419(18), Re-N2 2.2576(18), Re-P1 2.3793(5), Re-P2 2.3960(5), Re-C1 1.888(2), Re-C2 1.884(2, P1-Re-P2 173.701(17), P1-Re-N1 80.08(5), P1-Re-N2 97.12(5), C1-Re-C2 89.08(9), P2-Re-N2 79.56(5), P2-Re-N1 94.13(5), N1-Re-N2 82.67(7).*

4.3.1.2 – Catalysis using rhenium bis chelates

For catalysis, focus was directed towards reducing the run times that were required when manganese bis chelate complexes were used (see Section 3.3.4). As such, a run time of 17 hours was chosen to assess catalytic performance. Otherwise, conditions were identical to those used in manganese bis chelate catalysis (See Section 3.3.4).

Table 4.4: Synthesis of isobutanol using rhenium bis chelate catalysts.

Catalyst[a]	EtOH Conversion (%)	iBuOH Yield (%)	PrOH Yield (%)	iBuOH Selectivity (%)[b]	TON[c]
22	-	Trace	0	-	-
23	-	Trace	0	-	-
25	52	12	7	58	124
25[d]	81	28	4	88	283

[a] Conditions: 1 mL (17.13 mmol) EtOH, 10 mL MeOH, 180 °C, 17 h, NaOMe (200 Mol%), 0.1 mol% [Cat] [b] selectivity calculated from observed products in the liquid fraction, [c] Turnover number (TON) based on mmol of ethanol converted to *iso*butanol per mmol of Re, [d] 200 °C

Cat-22 and **Cat-23** showed no signs of catalysis over these run times (Table 4.4, Entries 1 and 2), with negligible ethanol conversions and only trace amounts of *iso*butanol produced. This is much the same as their manganese analogues. **Cat-25** showed much improved performance with 12% *iso*butanol yields over 17h (Entry 3), comparable with the pincer complex **Cat-18**. Ethanol conversion facilitated by **Cat-25** was significantly less than **Cat-18**, and much less solid was present in the post reaction mixture (only 0.34 g over a 17-hour run at 180 °C). This displays the desired increase in selectivity for Guerbet chemistry over Tishchenko or Cannizzaro chemistry. Analysis of this solid also showed no carbonate, indicating that **Cat-25** is less active for methanol dehydrogenation than the pincer complexes. **Cat-25** still suffers from a lack of selectivity in the liquid fraction, with propanol yields of 7% along with 5% 2-methylbutanol (from ethanol-propanol coupling) being produced. Increasing the reaction temperature to 200 °C led to a dramatic increase in both *iso*butanol yield and selectivity, rising by 16% and 30% respectively. These numbers are almost comparable with **Cat-19**, the most active Re pincer complex tested. Increasing the run time could also increase selectivity, but as the focus of this catalysis is on reducing run time, gaining the same effect through an increase in temperature is preferable.

Once the activity of **Cat-25** towards *iso*butanol formation had been established, effort was directed towards investigating the importance of the N-H moiety for reactivity. The secondary amine in the backbone of manganese pincer complexes has been shown to be essential for catalytic activity.[21] Using a dimethylated dppea ligand in conjunction with

ruthenium does not completely inhibit activity for Guerbet chemistry, though it does reduce it by roughly 50%.[29] If this same effect was observed with rhenium catalysts, it would indicate whether these complexes work *via* an inner or outer sphere mechanism. The importance of bis chelation over mono chelation, and the presence of an ethyl backbone, was also investigated (see Section 4.3.5).

4.3.2 – Interaction of diphosphine bis chelates with base

Cat-22 and **Cat-23** were both inactive for Guerbet chemistry, and it was proposed that this may be due to a lack of catalyst activation. To assess this, the reactions of **Cat-22** and **Cat-23** with NaOMe were monitored by $^{31}P\{^1H\}$ NMR spectroscopy. **Cat-22** was completely insoluble in methanol, with no sign of dissolution detected by $^{31}P\{^1H\}$ NMR spectroscopy. **Cat-22** remains insoluble after the addition of 100 eqv. NaOMe and no sign of reaction was observed. While **Cat-23** is readily soluble in MeOH and can be detected by $^{31}P\{^1H\}$ NMR spectroscopy, it also shows little sign of any reaction with NaOMe.
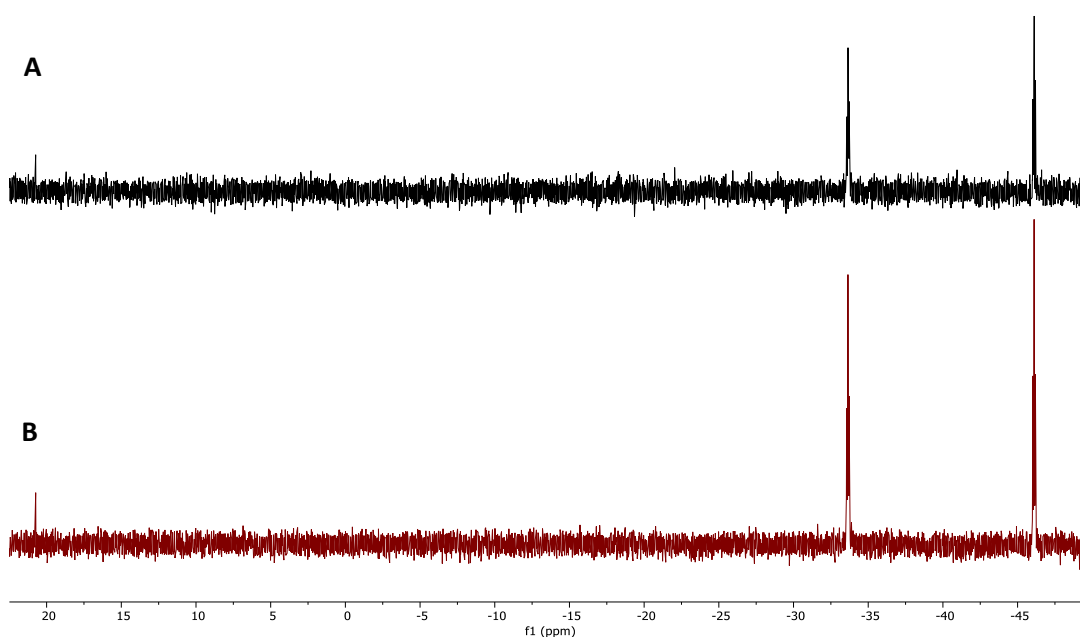
*Figure 4.7: $^{31}P\{^1H\}$ (202 MHz, MeOH) NMR spectrum of (A) **Cat-22** with 100 eqv. NaOMe after heating for 3 days, (B) **Cat-23** with 100 eqv. NaOMe after heating for 3 days.*

Upon heating for 3 days, in a J. Young's NMR tube, **Cat-22** does dissolve in methanol. Analysis by $^{31}P\{^1H\}$ NMR spectroscopy shows that this forms solely the *cis* bis chelate **Cat-23**, with a bromide counterion instead of a tetrafluoroborate (Figure 4.7, A). **Cat-23** shows

no sign of any further reaction, with the *cis* bis chelate being stable under these conditions (Figure 4.7, B). This may help to explain why **Cat-22** and **Cat-23** are catalytically inert. The manganese complex analogous to **Cat-22** reacts quickly with base, giving some of the *cis* and *trans* bis chelate. It also forms a significant amount of free ligand and a monochelate species, displaying the relative instability of the complex (see Section 3.5.2). **Cat-23** on the other hand is very stable under basic conditions and shows no signs of degradation, hence this degradation may be required in order to form the active catalyst. It is possible that **Cat-22** and **Cat-23** may be active over extended run times like their manganese analogues, but given the focus of this work was on reducing reaction time this was not investigated further.

4.3.3 – Catalytic activity of a diphosphine mono chelate complex

Given the poor performance of bis chelate and pendant diphosphine complexes, due to their stability in a *cis* bis chelate conformation under reaction conditions, the diphosphine mono chelate **Cat-26** was investigated instead. Given that this complex is not able to form a bis chelate, and contains a labile bromide ligand, it was proposed that it may give superior catalytic performance (Table 4.5).

Table 4.5: Formation of isobutanol using **Cat-26**.
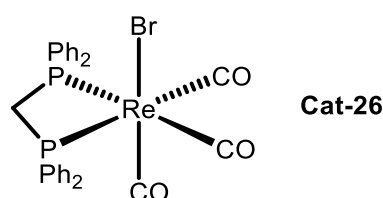
Catalyst[a]	Ethanol Conversion (%)	*Iso*butanol yield (%)	Propanol Yield (%)
26	-	Trace	-

[a] Conditions: 1 mL (17.13 mmol) EtOH, 10 mL MeOH, 180 °C, 17 h, NaOMe (200 Mol%), 0.1 mol% [Cat]

Unfortunately, **Cat-26** also showed little sign of activity over shorter reaction times. While this ligand set is very effective for *iso*butanol formation when complexed to ruthenium,[30] it is significantly less effective when used with rhenium.

The ability of dppm to act as a non-innocent ligand on manganese, and the positive effect that substituting the dppm backbone with electron donating substituents has on catalytic performance has recently been established.[31] If similar reactivity can be shown for rhenium

as well, it is possible that rhenium diphosphine catalysis could be realised with the use of substituted dppm ligands.

4.3.3.1 – Interaction of Cat-26 with KHMDS

Metal-bis(diphenylphosphino)methane (dppm) mono chelate complexes can react with a base such as KHMDS in two separate ways. Firstly, *via* the formation of a dppm⁻ ligand (**Cat-26bi**, Scheme 4.10) which can then react rapidly with electrophiles to form substituted dppm ligands. This type of reactivity is well established and has been noted on a variety of metals.[32,33] Secondly *via* the formation of a κ^3-dppm ligand and the elimination of the bromide ligand (**Cat-26bii**). These complexes can then be re-protonated under forcing conditions to reform the κ^2-dppm and the bromide ligand replaced with another X-type ligand (**Cat-26ciii/civ**). This type of behaviour has thus far only been observed in manganese complexes.[31] Furthermore, in manganese complexes substitution of the dppm backbone with electron donating substituents was found to increase the rate of reaction of the κ^3-dppm complex, thus leading to a more active catalyst (see Section 3.7 for further details). The reactivity of **Cat-26** with KHMDS has not previously been established, and it was proposed that if it reacted in a similar fashion to its manganese analogue then substituting the dppm backbone in these complexes could also lead to a more active catalyst.
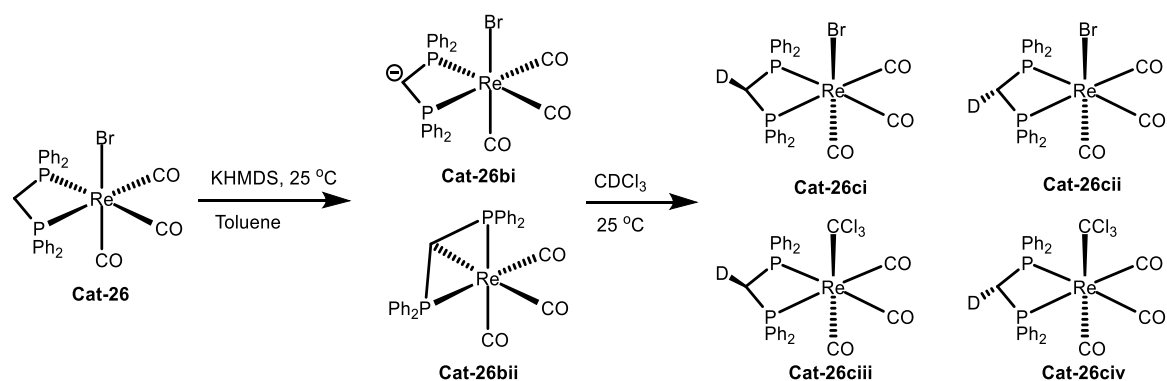
*Scheme 4.10: Reaction of **Cat-26** with KHMDS forming either a bis(diphenylphosphino)methanide complex **Cat-26bi** or a κ^3-diphosphinomethanide complex **Cat-26bii**, and its subsequent reaction with chloroform-d.*

Cat-26 was reacted with KHMDS (1.1 eqv.) in toluene, the toluene was then removed, and the sample was dissolved in CDCl₃. Chloroform-*d* was sufficiently acidic to deuterate the intermediate formed, and thus neither **Cat-26bi** nor **Cat-26bii** were observed in the solution. However, the mode of reactivity of **Cat-26** with KHMDS was established from the

product of the reaction between the intermediate and CDCl₃. The two protons on the dppm backbone in **Cat-26** give different resonances of equal intensity depending on whether they point towards or away from the bromide ligand (multiplets at 5.43 and 4.77 ppm). However, after reacting **Cat-26** with KHMDS and chloroform-*d*, these resonances showed different intensities due to selective formation of one deuterated isomer over the other (Figure 4.8). A similar effect was also seen in the ^{2}D NMR spectrum, with the resonance at 4.79 ppm being the major peak. This effect is not seen when **Cat-26** itself is dissolved in CDCl₃.

The speed of reaction (<10 minutes, room temperature) indicates that **Cat-26** reacts with KHMDS to form a dppm⁻ ligand (**Cat-26bi**). The lack of shift in -(CH₂)- resonances between **Cat-26** and **Cat-26ci/ii** is also evidence of this; substitution of the bromide ligand would likely cause a change in the chemical shift exhibited by the methylene backbone protons. The difference in reactivity between **Cat-26** and the analogous Mn complex indicates that preparing Re complexes supported by substituted dppm ligands would have little effect upon catalytic activity. Therefore, focus was instead directed towards further investigating rhenium complexes supported by phosphinoamine ligands.
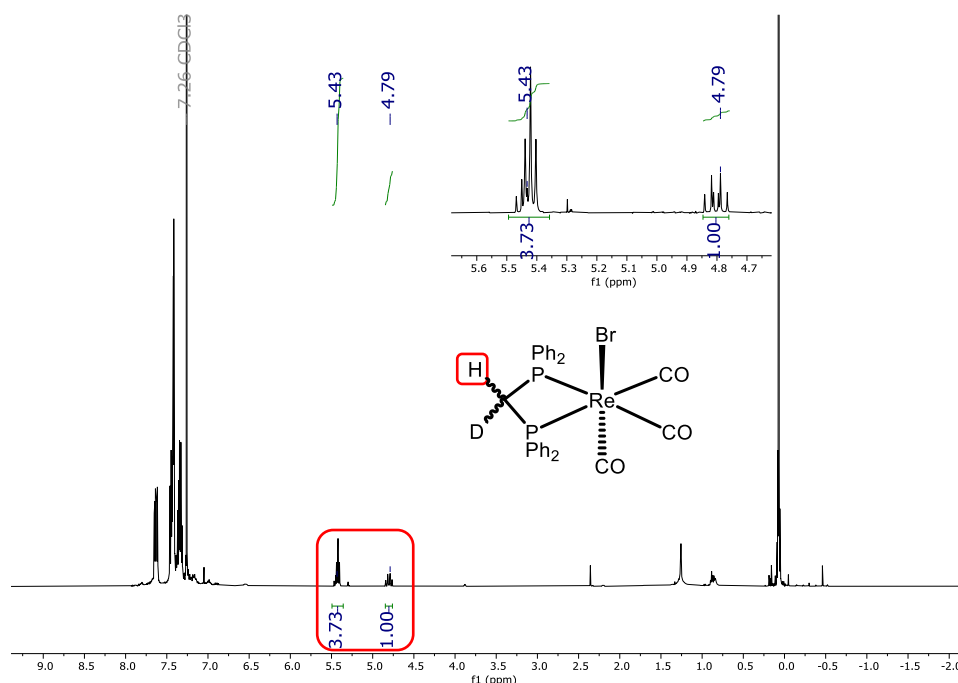
*Figure 4.8: ^{1}H NMR (500 MHz, CDCl₃) spectrum of **Cat-26ci/ii**. Inset showing the methylene backbone region, with inequivalent backbone protons.*

4.3.4 – PN-mono chelate and methylated PN ligands for *iso*butanol formation

4.3.4.1 – Complex synthesis

Ligands **L5** and **L6** were synthesised from diphenylphosphine and the corresponding 2-chloroethylamine. **Cat-27** and **Cat-28** were then synthesised using [ReBr(CO)₅] as a precursor, under reflux in a mesitylene solution (Scheme 4.11). Unlike **Cat-25** which was readily formed in a good yield (62%) after an 18 hour reflux, **Cat-27** required a much longer reflux of 60 hours and was recovered in far lower yields (31%). Formation of the cationic dicarbonyl complex was confirmed by mass spectrometry ([M⁺] *m/z*= 729.180), and a *cis* ligand coordination was indicated by IR spectroscopy. As such, an analogous structure to **Cat-25** was proposed.
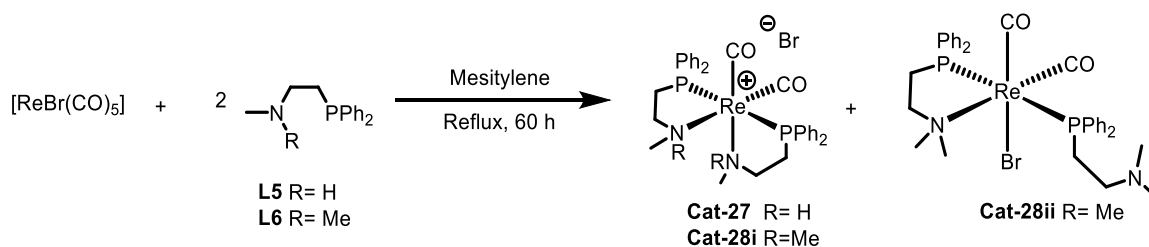
*Scheme 4.11: Synthesis of **Cat-27** and **Cat-28**. Bearing 2° and 3° amine ligands, respectively.*

When the dimethylated phosphinoamine complex was made, very little solid product was isolated. The ³¹P{¹H} NMR spectrum of this product displayed a singlet at 28.9 ppm, and two mutually coupled doublets at 4.4 and 32.3 ppm. These doublets gave a high ²J_{PP} coupling of 209 Hz, indicating coordinated phosphines *trans* to one another. Mass spectrometry shows a parent ion peak at *m/z*= 837.2, which corresponds to a rhenium complex with two carbonyl ligands, two phosphinoamine ligands and a bromide ligand. With this data in mind, the structure **Cat-28ii** is proposed. As two separate species were observed by ³¹P{¹H} NMR spectroscopy, it is believed that in solution **Cat-28** exists in an equilibrium between **Cat-28i** and **Cat-28ii**.

Re-dppea mono chelate **Cat-29** was formed in moderate yields (57%) from a 1:1 mixture of ligand and metal precursor in toluene under reflux (Scheme 4.12). Crystals suitable for analysis by X-ray diffraction were grown from a solution of DCM layered with hexane (Figure 4.9). This complex has a slightly distorted octahedral geometry and shows a similar structure to its manganese analogue, with the ligand coordinated *cis* to the bromide ligand.[28] Both the N1-Re-Br1 and P1-Re-Br1 angles are significantly smaller in the Re

complex though, as is the P1-Re-N1 angle. However, the M-P/N/Br bond lengths are longer for **Cat-29**. Re-C bonds are longer in **Cat-29** compared to **Cat-25**, indicating that **Cat-29** contains a less electron rich metal centre, while intra-ligand P-Re-N angles are very similar between **Cat-29** and **Cat-25**. It therefore seems likely that the size of the P-Re-N angle is due to the small ethyl bridge in the ligand backbone, not steric clash between the two coordinated ligands in **Cat-25**.
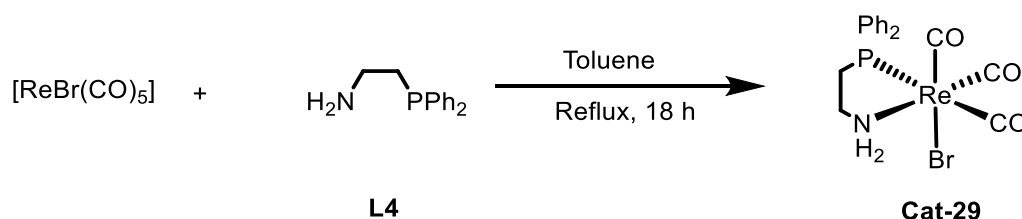
*Scheme 4.12: Synthesis of **Cat-29**.*
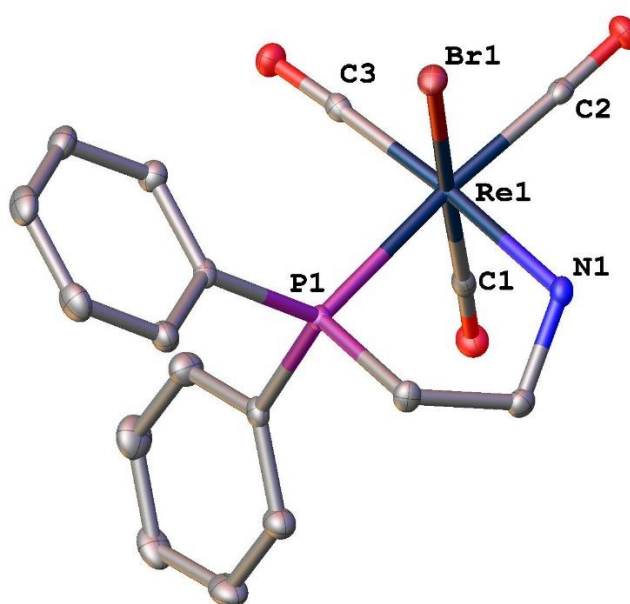
*Figure 4.9: Structure of **Cat-29**. Hydrogen atoms omitted for clarity. Selected bond lengths (Å) and angles (°): Re-P1 2.4313(6), Re-N1 2.236(2), Re-Br 2.6335(3), Re-C1 1.914(2), Re-C2 1.913(2), Re-C3 1.961(2), P1-Re-Br1 86.96, P1-Re-N1 79.94, N1-Re-Br 82.79.*

The rhenium bis chelate bearing two 3-(diphenylphosphino)propylamine (**L13**) ligands (**Cat-30**) was synthesised in a 77% yield *via* an analogous procedure to **Cat-25** (Scheme 4.13). This complex gave a broad singlet at 12.5 ppm in the ^{31}P{^{1}H} NMR spectrum, and two resonances in the IR spectrum at 1913 and 1806 cm^{-1}, as such an analogous structure to **Cat-25** was proposed. Crystals suitable for X-ray analysis were grown by layering a solution of **Cat-30** in DCM with Et$_2$O (Figure 4.10). This confirmed that **Cat-30** showed a similar

structure to the ethyl bridged analogue **Cat-25** with the carbonyl ligands *cis* to one another and the phosphine ligands *trans*. The average Re-C bond length is very similar to that observed in **Cat-25** (1.89 Å compared to 1.886 Å) indicating a very similarly electron rich metal centre. Re-P/N bonds are slightly longer in **Cat-30** compared to **Cat-25**.
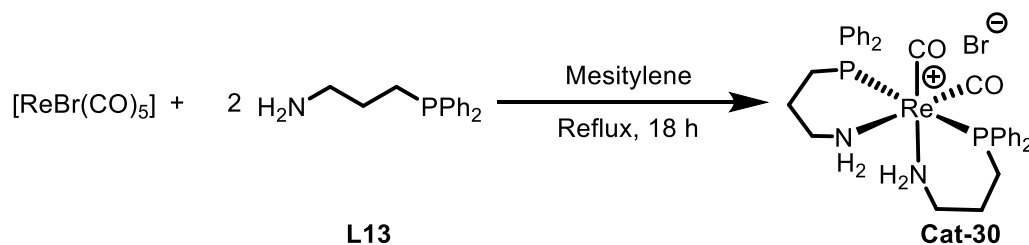
Scheme 4.13: Synthesis of **Cat-30**.
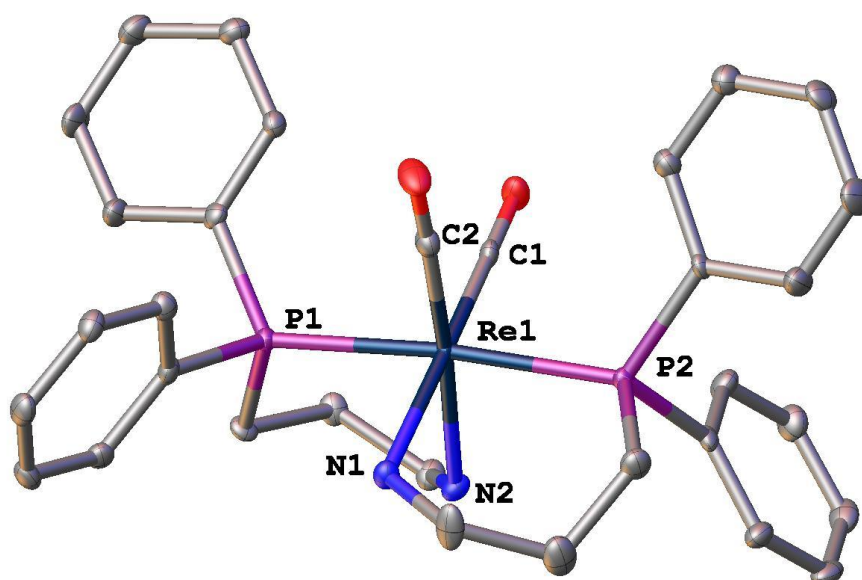
*Figure 4.10: Structure of **Cat-30**. Hydrogen atoms and bromide counter ion omitted for clarity. Selected bond lengths (Å) and angles (°): Re-N1 2.270(3), Re-N2 2.252(3), Re-P1 2.4099(9), Re-P2 2.4057(9), Re-C1 1.878(4), Re-C2 1.902(4), P1-Re-P2 174.60(3), P1-Re-N1 84.87(8), P1-Re-N2 85.26(9), C1-Re-C2 91.26(16), P2-Re-N2 89.90(9), P2-Re-N1 92.14(8), N1-Re-N2 82.62(12).*

4.3.4.2 – Catalysis

The results of using **Cat-27** – **Cat-30** for *iso*butanol formation are shown in Table 4.6. **Cat-29** was active for Guerbet chemistry over 17 hour run times. However, it gave roughly 50% of the yield of **Cat-25**, displaying the importance of a bis chelate type structure for both high yields and selectivity. **Cat-27** was also active, while there was a noticeable drop in yield compared to the non-methylated complex. **Cat-28** on the other hand was completely inactive for *iso*butanol formation displaying the importance of the N-H moiety to catalytic

activity, which indicates that rhenium phosphinoamine catalysts may operate *via* an outer sphere mechanism. It is also possible that the dimethylated analogue produces a more stable chelate, whereas the protonated analogues are less stable and can dissociate, providing a vacant site for catalysis to occur in the inner sphere of the metal. **Cat-30** produced only trace amounts of *iso*butanol showing that the presence of an ethyl backbone, and therefore the formation of a 5-membered ring upon chelation, is also important for high catalytic activity.

Table 4.6: Formation of isobutanol using substituted Re-PN complexes.

Catalyst[a]	EtOH Conversion (%)	iBuOH Yield (%)	PrOH Yield (%)	iBuOH Selectivity (%)[b]	TON[c]
27	40	9	5	70	88
28	1	-	-	-	-
29	26	6	5	45	59
30	-	Trace	-	-	-

[a] Conditions: 1 mL (17.13 mmol) EtOH, 10 mL MeOH, 180 °C, 17 h, NaOMe (200 Mol%), 0.1 mol% [Cat] [b] selectivity calculated from observed products in the liquid fraction, [c] Turnover number (TON) based on mmol of ethanol converted to *iso*butanol per mmol of Re

4.3.5 – Summary of Re mono and bis chelate complexes

Rhenium complexes bearing bidentate ligands were investigated for biofuel formation, with a focus on increasing selectivity for Guerbet chemistry over alcohol dehydrogenation and reducing the run times needed for group 7 bis chelate catalysts.

An initial catalyst screen showed the potential of a Re-dppea bis chelate and the incompetence of Re-diphosphine complexes. Diphosphine complexes interact differently with base than their manganese analogues, forming stable *cis* bis chelates which do not catalyse Guerbet chemistry. Dppm mono chelate **Cat-26** is also ineffective, possibly due to it being unable to form κ^3-PCP ligands, like equivalent manganese complexes. Further work established the importance of both bis chelation and the N-H moiety for Re-dppea catalysts.

While rhenium phosphinoamine bis chelate complexes significantly outperform their manganese analogues, and at 200 °C **Cat-25** gives 28% *iso*butanol in 88% selectivity, these

catalysts still lag significantly behind the state-of-the-art rhenium catalyst, namely, **Cat-19**. As such, further work is required to improve the competence of these catalysts for biofuel production.

4.4 – Future work

Given the relatively little attention that rhenium catalysis has received until now, there are many possible different avenues for future research. Rhenium pincer complexes have shown an incredible affinity for base catalysed alcohol dehydrogenation, even under Guerbet conditions. It is possible that altering the conditions could give almost total selectivity for alcohol dehydrogenation, highlighting the potential of these catalysts for use in hydrogen storage technology (Scheme 4.14).[18] Given these reactions usually take place in an aqueous environment, the stability of Re-pincer complexes to water under basic conditions would first need to be established.

$$CH_3OH \quad + \quad H_2O \quad \xrightarrow{\text{[Re]-pincer}} \quad CO_2 \quad + \quad 3H_2$$
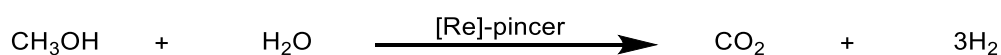
Scheme 4.14: Aqueous dehydrogenation of methanol by a rhenium pincer catalyst.

With these pincer complexes, electron withdrawing phosphine substituents favour overall activity. Electron donating groups decrease the selectivity for alcohol dehydrogenation, but also decrease activity. Expansion of the ligand library to encompass a variety of different phosphine substituents and pincer ligands could help to increase the yield of Guerbet products. Thus far, only 'MACHO-style' ligands have been trialled in conjunction with rhenium for Guerbet chemistry, however, a variety of other pincer complexes have been reported (Figure 4.11, **4.4 – 4.6**).[34,35] Mass testing of many different rhenium complexes could be accomplished using 'high-throughput' screening techniques, this would give a broad scope of ligands and substituents in order to identify an ideal system for Guerbet chemistry. Given the potential rhenium has already shown, it is possible these catalysts could even rival ruthenium systems previously reported.[30,36,37]

4.4   **4.5**   **4.6**
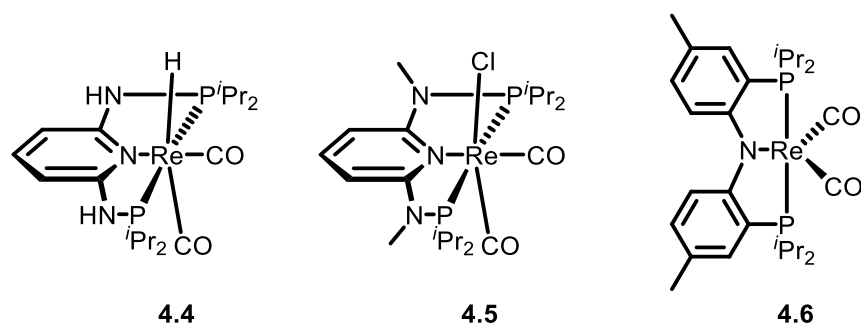
Figure 4.11: Other rhenium pincer complexes to test for Guerbet chemistry.

As there has been no recent published work on rhenium bis chelate catalysis, there are many different directions research could follow. Thus far, rhenium complexes have shown much promise at increasing selectivity for Guerbet chemistry over alcohol dehydrogenation compared to pincer complexes. However, as yields are still substantially lower, increasing productivity needs to be the primary focus. A variety of different phosphinoamine ligands have been used in conjunction with ruthenium for *n*-butanol coupling.[38] Ligands bearing electron withdrawing groups at the nitrogen produce comparable or superior *n*-butanol yields to the unsubstituted dppea ligand. Using these ligands with rhenium for *iso*butanol production could improve catalytic activity and increase product yield (Figure 4.12).

4.7   **4.8**
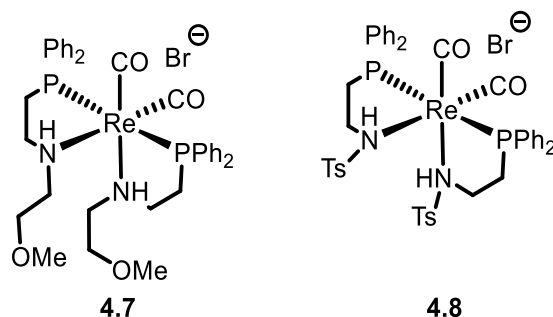
Figure 4.12: Rhenium complexes bearing electron withdrawing nitrogen substituents.

Finally, much like their manganese analogues, there are many other reactions that rhenium bis chelate complexes could be screened for. Manganese bis chelates bearing dppea ligands have been used for the hydrogenation of carbonyl derivatives.[28] Given the superior reactivity **Cat-25** and **Cat-29** show for Guerbet chemistry, it is possible they will outperform their manganese analogues in carbonyl hydrogenation as well. These complexes could also be screened for the same types of borrowed hydrogen reactions to which rhenium pincer complexes have already been applied.[16,17] Only the small bite angle diphosphine ligand **L1** was investigated on rhenium in this study. Increasing the ligand bite angle by using dppe or

dppp (**L2/L3**) could aid catalytic performance (Figure 4.13, **4.9** and **4.10**). On ruthenium, small bite angle ligands are found to be the most effective.[39] However, when iridium is used for Guerbet chemistry, yields of *n*-butanol gradually increase with bite angle.[38] It is therefore possible that a similar trend could be seen with rhenium complexes.
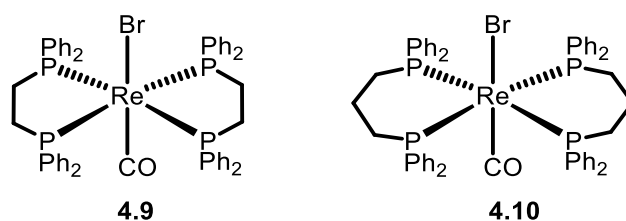
Figure 4.13: Re complexes with increased bite angle diphosphine ligands.

4.5 – References

1 A. Mukherjee and D. Milstein, *ACS Catal.*, 2018, **8**, 11435–11469.

2 H. Jin, J. Xie, C. Pan, Z. Zhu, Y. Cheng and C. Zhu, *ACS Catal.*, 2013, **3**, 2195–2198.

3 A. Landwehr, B. Dudle, T. Fox, O. Blacque and H. Berke, *Chem. Eur. J.*, 2012, **18**, 5701–5714.

4 E. Mejía and A. Togni, *Organometallics*, 2011, **30**, 4765–4770.

5 I. Klopsch, M. Finger, C. Würtele, B. Milde, D. B. Werz and S. Schneider, *J. Am. Chem. Soc.*, 2014, **136**, 6881–6883.

6 Y. Jiang and H. Berke, *Chem. Commun.*, 2007, **34**, 3571–3573.

7 Y. Jiang, J. Hess, T. Fox and H. Berke, *J. Am. Chem. Soc.*, 2010, **132**, 18233–18247.

8 Y. Kuninobu and K. Takai, *Chem. Rev.*, 2011, **111**, 1938–1953.

9 M. Vogt, A. Nerush, M. A. Iron, G. Leitus, Y. Diskin-Posner, L. J. W. Shimon, Y. Ben-David and D. Milstein, *J. Am. Chem. Soc.*, 2013, **135**, 17004–17018.

10 M. Vogt, A. Nerush, Y. Diskin-Posner, Y. Ben-David and D. Milstein, *Chem. Sci.*, 2014, **5**, 2043–2051.

11 P. Piehl, M. Peña-López, A. Frey, H. Neumann and M. Beller, *Chem. Commun.*, 2017, **53**, 3265–3268.

12 D. Wei, T. Roisnel, C. Darcel, E. Clot and J.-B. Sortais, *ChemCatChem*, 2017, **9**, 80–83.

13 E. Alberico, P. Sponholz, C. Cordes, M. Nielsen, H.-J. Drexler, W. Baumann, H. Junge and M. Beller, *Angew. Chem. Int. Ed.*, 2013, **52**, 14162–14166.

14 M. Bertoli, A. Choualeb, A. J. Lough, B. Moore, D. Spasyuk and D. G. Gusev, *Organometallics*, 2011, **30**, 3479–3482.

15 S. Elangovan, C. Topf, S. Fischer, H. Jiao, A. Spannenberg, W. Baumann, R. Ludwig,

K. Junge and M. Beller, *J. Am. Chem. Soc.*, 2016, **138**, 8809–8814.

16   D. Wei, V. Dorcet, C. Darcel and J. B. Sortais, *ChemSusChem*, 2019, **12**, 3078–3082.

17   D. Wei, O. Sadek, V. Dorcet, T. Roisnel, C. Darcel, E. Gras, E. Clot and J.-B. Sortais, *J. Catal.*, 2018, **366**, 300–309.

18   Z. Wei, A. de Aguirre, K. Junge, M. Beller and H. Jiao, *Catal. Sci. Technol.*, 2018, **8**, 3649–3665.

19   I. Maisuls, F. M. Cabrerizo, P. M. David-Gara, B. Epe and G. T. Ruiz, *Chem. Eur. J.*, 2018, **24**, 12902–12911.

20   M. B. Ismail, I. N. Booysen, M. P. Akerman and C. Grimmer, *J. Organomet. Chem.*, 2017, **833**, 18–27.

21   Y. Liu, Z. Shao, Y. Wang, L. Xu, Z. Yu and Q. Liu, *ChemSusChem*, 2019, **12**, 3069–3072.

22   N. V Kulkarni, W. W. Brennessel and W. D. Jones, *ACS Catal.*, 2018, **8**, 997–1002.

23   W. Kuriyama, T. Matsumoto, Y. Ino and O. Ogata, *Novel Ruthenium Carbonyl Complex Having a Tridentate Ligand and Manurfacturing Method and Useage Therefor, WO2011/048727*, 2011.

24   O. Ogata, Y. Nakayama, H. Nara, M. Fujiwhara and Y. Kayaki, *Org. Lett.*, 2016, **18**, 3894–3897.

25   V. Tishchenko, *J. Russ. Phys. Chem. Soc.*, 1906, **38**, 355–418.

26   S. W. Carr, B. L. Shaw and M. Thornton-Pett, *J. Chem. Soc., Dalton. Trans.*, 1987, 1763–1768.

27   A. M. Bond, R. Colton, D. G. Humphrey, P. J. Mahon, G. A. Snook, V. Tedesco and J. N. Walter, *Organometallics*, 1998, **17**, 2977–2985.

28   R. van Putten, E. A. Uslamin, M. Garbe, C. Liu, A. Gonzalez-de-Castro, M. Lutz, K. Junge, E. J. M. Hensen, M. Beller, L. Lefort and E. A. Pidko, *Angew. Chem. Int. Ed.*, 2017, **56**, 7531–7534.

29   R. L. Wingad, P. J. Gates, S. T. G. Street and D. F. Wass, *ACS Catal.*, 2015, **5**, 5822–5826.

30   R. L. Wingad, E. J. E. Bergström, M. Everett, K. J. Pellow and D. F. Wass, *Chem. Commun.*, 2016, **52**, 5202–5204.

31   N. V. Kireev, O. A. Filippov, E. S. Gulyaeva, E. S. Shubina, L. Vendier, Y. Canac, J. B. Sortais, N. Lugan and D. A. Valyaev, *Chem. Commun.*, 2020, **56**, 2139–2142.

32   S. Al-Jibori and B. L. Shaw, *J. Chem. Soc. Chem. Commun.*, 1982, **5**, 286–287.

33   J. Ruiz, M. E. G. Mosquera, V. Riera, M. Vivanco and C. Bois, *Organometallics*, 1997, **16**, 3388–3394.

34   A. J. Kosanovich, W. C. Shih and O. V. Ozerov, *J. Organomet. Chem.*, 2019, **897**, 1–6.

35   M. Mastalir, M. Glatz, E. Pittenauer, G. Allmaier and K. Kirchner, *Org. Lett.*, 2019, **21**, 1116–1120.

36   K. N. T. Tseng, S. Lin, J. W. Kampf and N. K. Szymczak, *Chem. Commun.*, 2016, **52**, 2901–2904.

37   Y. Xie, Y. Ben-David, L. J. W. Shimon and D. Milstein, *J. Am. Chem. Soc.*, 2016, **138**, 9077–9080.

38   H. Aitchison, *A mechanistic study of the catalytic upgrading of ethanol to butanol biofuels, Ph.D. Thesis*, 2018.

39   G. R. M. Dowson, M. F. Haddow, J. Lee, R. L. Wingad and D. F. Wass, *Angew. Chem. Int. Ed.*, 2013, **52**, 9005–9008.

40   K. Keitaro, M. Toyomi, O. Yasushi and Y. Ishii, *Chem. Lett.*, 2009, **38**, 838–839.

Chapter 5 – Guerbet coupling of long chain linear alcohols for potential use as surfactants or lubricants

Disclaimer: Half of this work was conducted at the University of Bristol prior to the Wass group's move to Cardiff university. The latter half was conducted at Cardiff university. This may have led to some discrepancies between results. Work concerning the coupling of propanol, butanol and hexanol was begun by a master's student, Kherina Fenton who worked under the supervision of the author.

5.1 – Introduction

Given the challenges associated with ethanol dehydrogenation all initial research into Guerbet chemistry focussed on longer chain alcohols, primarily *n*-butanol.[1] However, since the first reported coupling of ethanol in 2009 (see Section 1.7.1),[2] it has become the primary focus of modern day Guerbet chemistry, with longer chain alcohols being almost completely neglected. The few reported examples of longer chain aliphatic alcohol coupling in the last decade are found predominantly in the patent literature. One such report in 2014 displayed the use of a variety of precious metals bound to hydrophobic supports for the coupling of a plethora of primary and secondary alcohols.[3] These catalysts gave good yields of coupled product (70% Guerbet alcohol) and by-product formation was low. Furthermore, the use of hydrophobic supports helped prevent loss of catalyst due to leaching by water. However, temperatures in excess of 200 °C were still often required. More recent patents have focussed on system optimisation by the removal of water, which can contribute to catalyst deactivation.[4] The general coupling of a complex mixture of alcohols (*n*-propanol, *n*-butanol, *n*-pentanol and *n*-hexanol) to generate a variety of different Guerbet alcohol products has also been investigated.[4,5]

A recent paper has shown the formation of 2-butyloctanol (**5.3**) *via* the coupling of *n*-hexanol at room temperature using a combination of organic and enzymatic catalysts.[6] This system was able to produce the Guerbet alcohol in high yield and good selectivity as each step had a conversion >92% and a selectivity >97%, giving an overall yield of 62%. While these reactions were conducted at room temperature, owing to their multistep nature completion of all four steps required reaction times up to 73 hours.

Guerbet alcohols (Figure 5.1) are of interest due to their β-branched structure, this helps to lower their melting points relative to those for the linear isomers. This branching also

gives the alcohol a similar structure to a double-tailed surfactant, meaning that after functionalisation they can also be used as emulsifiers.[7] Guerbet alcohol production has already been commercialised and primarily uses Raney-Ni or copper chromite catalysts,[8] although temperatures of at least 220 °C are required.
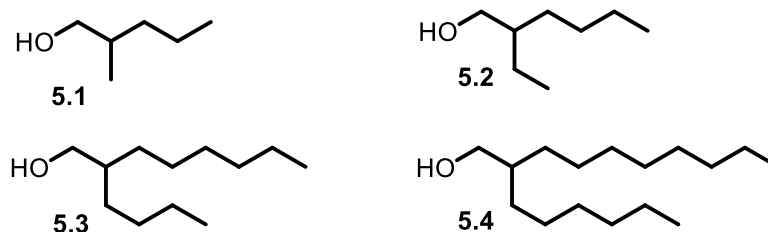
*Figure 5.1: Guerbet alcohols produced from the homocoupling of n-propanol (**5.1**), n-butanol (**5.2**) n-hexanol (**5.3**) and n-octanol (**5.4**).*

While several homogeneous systems for Guerbet alcohol production are known, most either show poor water tolerance or require the use of hazardous solvents such as *p*-xylene (see Section 1.7). Systems developed by the Wass group for ethanol homocoupling show good water tolerance and can work in a neat alcohol system without the need for any further solvent. **Cat-1** and **Cat-4** (Figure 5.2) are currently the most effective Wass group catalysts for ethanol coupling, as such they are ideal candidates to apply to higher alcohol coupling.[9,10] To date, these systems have not been used for the homocoupling of any other alcohols. Although, the presence of a small amount of 2-ethylhexanol (produced by *n*-butanol homocoupling) has been observed in the post reaction mixture of ethanol homocoupling reactions (1.4% over a 24 hr run using **Cat-1**), indicating that they may be active for this conversion.
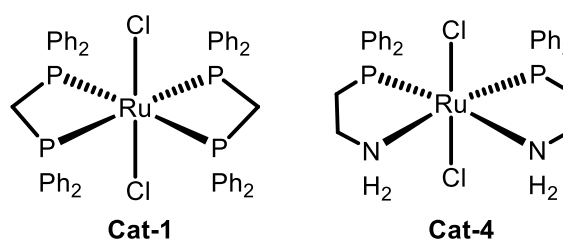
Figure 5.2: The two most effective Wass group catalysts for ethanol homocoupling.[9,10]

5.2 – *n*-Octanol Coupling

n-Octanol was chosen as a model substrate for these reactions, instead of *n*-propanol or *n*-butanol, so that the effect of increased chain length (and the corresponding change in physical properties) would be more apparent (Scheme 5.1).
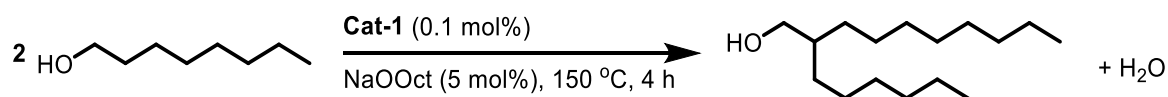
*Scheme 5.1: Homocoupling of n-octanol to form 2-hexyldecan-1-ol by **Cat-1**.*

Conditions for *n*-octanol homocoupling were initially kept identical to those used for ethanol.[9] It was found that the corresponding alkoxide base, sodium ethoxide, gave the highest yields, and consequently for *n*-octanol homocoupling sodium octoxide (NaOOct) was used. While sodium ethoxide is cheap and commercially available, NaOOct must be synthesised before use. This was produced immediately before all catalytic reactions by subjecting *n*-octanol, along with 5 mol% metallic sodium to reflux for 2 hours (Scheme 5.2). This mixture was then directly used for catalysis.
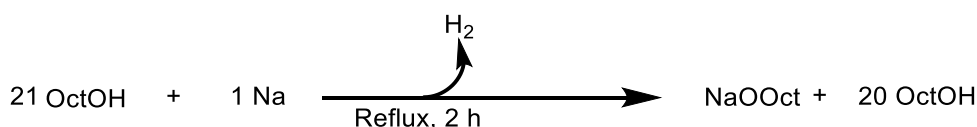
Scheme 5.2: Production of a 5 mol% NaOOct solution in n-octanol for catalysis.

5.2.1 – Analysis of the post reaction mixture

One significant difference between *n*-octanol and ethanol homocoupling is the consistency of the post reaction mixture. For ethanol it is predominantly a homogeneous liquid, with a small amount of solid observed due to the production of sodium acetate. However, *n*-octanol homocoupling produces a waxy solid mixture. As such, analysis of *n*-octanol coupling by the same method used for ethanol was not possible.

For ethanol coupling the reaction mixture is filtered through acidic alumina, before 100 μL is diluted in 1.7 mL diethyl ether and 10 μL of an internal standard is added. As the post reaction mixture from *n*-octanol coupling is a solid, this filtration was not possible. A variety of different methods of analysis were attempted. However, most gave inconsistent results between identical catalytic runs. Consistent, and therefore reliable, analysis was achieved by adding the internal standard (hexadecane) to the reaction vessel before reaction and

then extracting the post reaction mixture in heptane or hexane before filtering through acidic alumina and analysing by GC. This method of analysis was used for all further *n*-octanol coupling reactions.

5.2.2 – Condition screen

To establish if optimal *n*-octanol homocoupling conditions were the same as those used for ethanol, a condition screen was completed in a 100 mL Parr stainless steel autoclave (Table 5.1). Utilising the previously optimised conditions for ethanol homocoupling with *n*-octanol gave 2-hexyldecan-1-ol in a 15% yield, along with 51% conversion (Entry 1). Increasing the reaction temperature to 180 °C gave a slight increase in product yield, although decreasing the temperature to 120 °C almost completely inhibited activity (Entries 2 & 3). Both increasing and decreasing the catalyst loading had a negligible effect upon product yield (Entries 4 & 5). Increasing reaction run time from 4 to 20 hours increased yield and conversion significantly (Entry 6). Furthermore, increasing the base loading had the greatest effect upon the yield. Doubling loadings to 10 mol% resulted in a doubling of the product yield, while having little impact upon *n*-octanol conversion (Entry 7). Halving the base loading had a slight negative effect, although this is not nearly as dramatic as the effect of doubling it (Entry 8). Unsurprisingly, in the absence of base very little product was observed, although significant *n*-octanol conversion was still seen (Entry 9). The best conditions shown in this condition screen for *n*-octanol coupling to produce 2-hexyldecan-1-ol are shown in Entry 7.

Interestingly, in almost all catalytic runs no octyloctanoate was observed. Much like when ethanol is used as a substrate, this catalyst is almost completely selective for the Guerbet product over the Tishchenko in the liquid fraction.[11] Although, the sodium acetate observed in ethanol homocoupling experiments may be generated from ethyl acetate reacting with sodium hydroxide (produced from sodium ethoxide and water), indicating that this system is not completely inactive for Tishchenko chemistry. Indeed, this may explain why a small amount of octyloctanote is observed in Entry 8; only 2.5 mol% base is used, and therefore there is not enough present to convert all the ester produced to octanoate and *n*-octanol.

Table 5.1: Condition screen for n-octanol homocoupling.

Entry[a]	Temperature (°C)	Run time (hr)	Base loading (mol%)	*n*-Octanol conversion (%)	2-Hexyldecan-1-ol Yield (%)
1	150	4	5	51	15
2	180	4	5	53	18
3	120	4	5	20	1
4[b]	150	4	5	43	14
5[c]	150	4	5	47	14
6	150	20	5	61	22
7	150	4	10	51	28
8[d]	150	4	2.5	47	13
9	150	4	0	17	2

[a] Conditions: *n*-Octanol (10 mL), **Cat-1** (0.1 mol%), NaOOct (0 – 10 mol%), 120 – 180 °C, 4 – 20 hr, [b] 0.2 mol% **Cat-1**, [c] 0.05 mol% **Cat-1**, [d] 0.03% octyloctanoate observed.

These results show a large discrepancy between *n*-octanol conversion and 2-hexyldecan-1-ol yield. In some cases, this can be nearly 40% of the total *n*-octanol used (Entry 6). The fate of this missing *n*-octanol is not immediately apparent as no other significant peaks are observed in the GC trace of the post reaction mixture. Given the solid, waxy nature of the post reaction mixture it is possible that the extraction process is suboptimal and some *n*-octanol and 2-hexyldecan-1-ol is trapped in this solid, which may not have dissolved during workup and therefore was not detected by GC.

As both *n*-octanol and 2-hexyldecan-1-ol are liquids at room temperature, yet the post reaction mixture is solid, some higher alcohols must be present. 2-Hexyldecan-1-ol cannot homocouple, given it has a tertiary β-carbon, therefore these higher alcohols can only be produced by 2-hexyldecan-1-ol coupling with *n*-octanol (Scheme 5.3). This may explain why *n*-octanol conversions are high, whereas 2-hexyldecan-1-ol yields remain much lower. These long chain alcohols likely have boiling points significantly higher than 2-hexyldecan-1-ol (195 °C) and as such may not be volatile enough for analysis using gas chromatography. Hence why they are not seen in the GC trace.
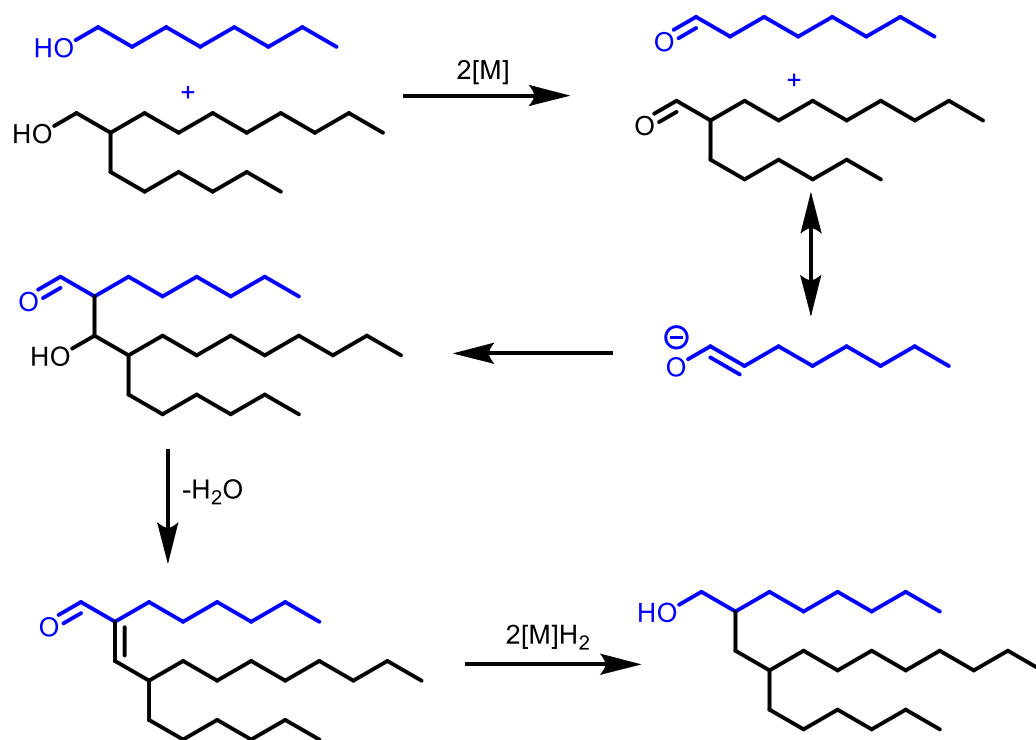
Scheme 5.3: Formation of heavier branched alcohols via coupling with n-octanol.

For their respective homocoupling reactions, *n*-octanol homocoupling occurs more rapidly over 4 hours than ethanol homocoupling (15% 2-hexyldecan-1-ol compared to 10% *n*-butanol). Furthermore, *n*-octanol consumption is significantly higher (51% compared to 11%), although the fate of much of this is not known. However, over 20 hour run times, product yield from ethanol coupling surpasses that of *n*-octanol (33% compared to 22%).[9] While the cause of this is not immediately apparent, it is possible that *n*-octanol loss to the formation of higher alcohols means the amount of *n*-octanol available for the production of 2-hexyldecan-1-ol is lower and therefore lower yields are seen. Another possible explanation is that as higher alcohols form, the reaction gets more viscous and magnetic stirring becomes less efficient, causing reaction rates to slow. Ethanol and *n*-octanol homocoupling show very similar temperature dependences, with little coupling seen at lower temperatures of 120 °C and little benefit observed at temperatures above 150 °C. Increasing the base loading increased the yield of coupled product for both alcohols, although in *n*-octanol this effect was much more pronounced.[12]

5.2.3 – Activity of Cat-4

Once optimal conditions for *n*-octanol homocoupling had been established, the activity of **Cat-4** was tested. Alongside this, **Cat-5** was also investigated (Table 5.2); **Cat-5** is a very

versatile and active catalyst for a variety of different reactions (see Section 2.1.2). However, in ethanol homocoupling it shows poor selectivity to *n*-butanol (12.4%), instead preferentially producing ethyl acetate *via* Tishchenko chemistry.[10,13] Its use for the formation of ethyl acetate from refluxing ethanol in an open system is well documented.[14] As yet, it was unclear if its selectivity would change with alcohol chain length.

*Table 5.2: Catalyst screen for the homocoupling of n-octanol. Run with **Cat-1** included for comparison.*
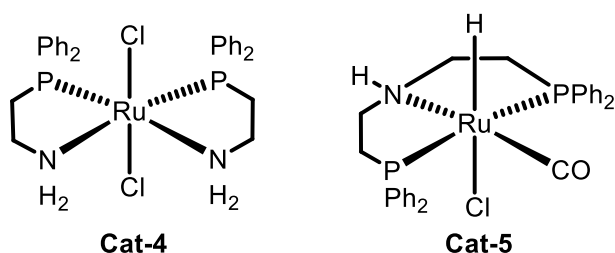
Entry[a]	Catalyst	*n*-Octanol Conversion (%)	2-Hexyldecan-1-ol Yield (%)	Octyl octanoate Yield (%)	Guerbet selectivity (%)[b]
1	1	51	15	0	100
2	4	46	3	1	72
3[c]	5	46	3	20	13

[a] Conditions: *n*-Octanol (10 mL), [Cat] (0.1 mol%), NaOOct (5 mol%), 150 °C, 4 hr, [b] Selectivity for alcohol over ester products, both detected by GC analysis, selectivity determined by products observed in the liquid fraction, [c] 20 hr

While the use of 10 mol% base had given the greatest 2-hexyldecan-1-ol yields, 5 mol% was used for the catalyst screen to allow for ease of comparison to the ethanol system. Over 4 hours, **Cat-4** was significantly inferior to **Cat-1**, producing only 3% 2-hexyldecan-1-ol. Furthermore, **Cat-4** also produced a small amount of octyl octanoate (28% selectivity). None was observed when **Cat-1** was used. This correlates well with what is seen for ethanol homocoupling, where **Cat-4** produced a small amount of ethyl acetate. **Cat-4** produced a significant amount of *n*-butanol over 4 hours (17.1%) whereas very little 2-hexyldecan-1-ol was observed, despite far higher substrate conversions (19% for ethanol, 46% for *n*-octanol).[10] It appears that **Cat-4** favours the production of the highly branched higher alcohols shown in Scheme 5.3 over the simple homocoupling of *n*-octanol. The fact the post reaction mixture is still a waxy solid, despite the lower conversions supports this theory. It has long been believed that catalysts bearing phosphinoamine ligands, such as those used

in **Cat-4**, can operate *via* an outer-sphere mechanism.[15] Whereas for **Cat-1**, there is still much debate as to whether catalysis occurs in the inner- or outer-sphere.[16] If **Cat-4** is using an outer-sphere mechanism, there will be more space around the catalyst to accommodate a long chain, highly branched alcohol. This may be why it appears to favour reacting with further *n*-octanol units to form higher alcohols over terminating at 2-hexyldecan-1-ol. Another possible theory is that **Cat-1** uses smaller, more strained ligands, which results in less space around the catalyst to allow for interaction with a large substrate.

Cat-5 operates very similarly whether ethanol or *n*-octanol are used as the substrate. In both cases selectivity for the Guerbet product is around 13%, despite the different run times used (4 hrs for ethanol coupling).[10] As such, it appears that **Cat-5** always favours the Tishchenko product over the Guerbet, whatever substrate is used. While for *n*-butanol formation **Cat-1** and **Cat-4** show very similar reactivity, for 2-hexyldecan-1-ol **Cat-1** is far superior.

5.3 – Increasing the diphosphine ligand bite angle

To date, **Cat-1** is one of the most effective catalysts for both ethanol and *n*-octanol homocoupling, with other catalysts only being effective for either short or long chain alcohols. For ethanol, extending the carbon backbone of the ligand, and as such increasing the ligand's bite angle, was found to dramatically decrease product yield. Complexes **Cat-2** and **Cat-3** gave only 1.9% *n*-butanol yield compared to 9.6% for **Cat-1**.[9] These complexes were subsequently tested for the coupling of *n*-octanol to see if the same effect was observed (Table 5.3).

*Table 5.3: Investigation into the effect of increasing ligand bite angle upon catalytic activity. Results for **Cat-1** and results for ethanol homocoupling included for comparison.[9]*
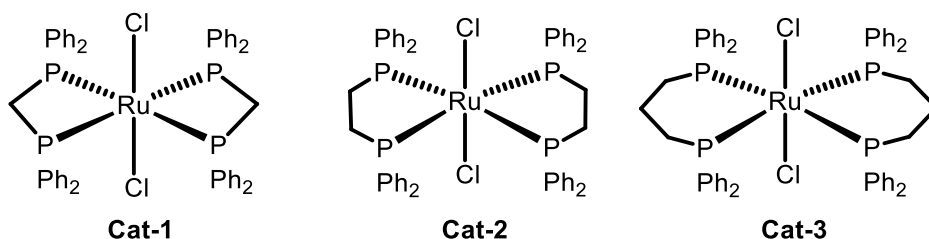
Entry[a]	Catalyst	Alcohol	Substrate conversion (%)	Coupled product yield (%)
1	1	*n*-Octanol	51	15
2	1	Ethanol	10.5	9.6
3	2	*n*-Octanol	25.4	1.2
4[b]	2	Ethanol	2.6	1.9
5	3	*n*-Octanol	23.9	0.9
6[b]	3	Ethanol	2.3	1.9

[a] Conditions: *n*-Octanol (10 mL), [Cat] (0.1 mol%), NaOOct (5 mol%), 150 °C, 4 hr, [b] 20 hr run time

A similar effect was seen for *n*-octanol homocoupling whereby **Cat-1** was the superior catalyst by a large margin. Both **Cat-2** and **Cat-3** performed equally poorly with less than 2% product yield detected in both cases. While similar conversions were observed between **Cat-1** and **Cat-4**, the post reaction mixtures for **Cat-2** and **Cat-3** remained a homogeneous liquid indicating that little higher alcohol formation was occurring. It is unclear as to why the *n*-octanol conversions and 2-hexyldecan-1-ol yields are so different for these complexes. However, it may simply be due to issues with the analytical method. It is worth noting, that a trend of activity decreasing with ring size was not seen. Rather, **Cat-1** showed significantly elevated activity, whereas **Cat-2** and **Cat-3** performed similarly.

There are two different explanations proposed for why this reactivity is observed depending on whether an inner-sphere or outer-sphere mechanism is believed to be operating. For an inner sphere mechanism: coordination of dppm to a metal centre forms a highly strained 4-membered ring. This strain means that one of the phosphines may dissociate to produce a monodenate species and a vacant site on the metal.[17] This vacant site allows for substrate coordination to the metal centre. An example of dppm acting as a monodentate ligand on ruthenium has previously been observed by X-ray crystallography

(Figure 5.3, **5.5**).[9] **Cat-2** and **Cat-3** contain much less strained 5- and 6-membered rings respectively. Therefore, ligand dissociation is much less likely, ergo the complexes are far less active.

5.5
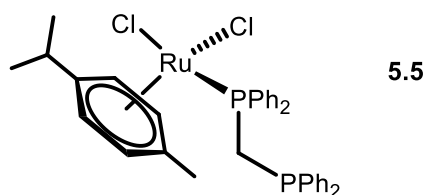
Figure 5.3: Chemical structure shown by X-ray crystallography of dppm acting as a monodentate ligand on ruthenium.

More recent work in the Wass group indicated that **Cat-1** may operate *via* an outer-sphere mechanism. This work suggested that the methylene protons in the carbon backbone of **Cat-1** are sufficiently acidic as to form a hydrogen bond with the alcohol substate and thus incorporate it into the outer sphere of the catalyst for dehydrogenation (Scheme 5.4).[16] However, the protons on the backbone of **Cat-2** and **Cat-3** are not acidic enough for this interaction to be possible. Hence why they show inferior reactivity to **Cat-1**. It is currently unclear whether an inner-sphere or an outer-sphere mechanism is more likely.
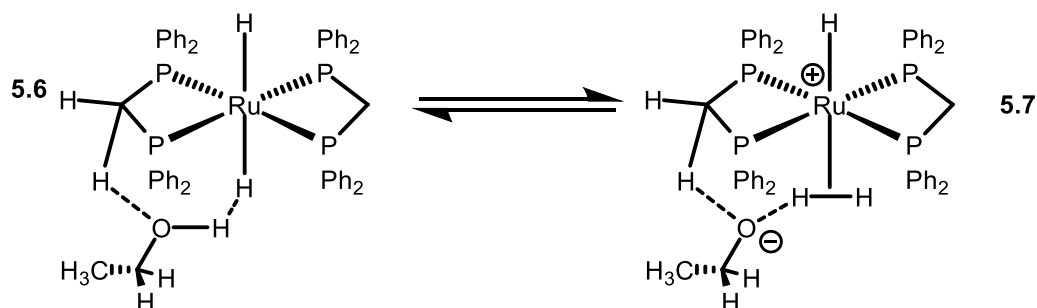
Scheme 5.4: Proposed binding of ethanol into the outer sphere of the catalyst.[16]

5.4 – Solvent Screen

As outlined above, one of the main issues with *n*-octanol coupling is that the post reaction mixture is a waxy solid. All solid would need to be dissolved in heptane before accurate analysis is possible. This leads to doubts as to the validity of analysis, due to possible loss of both substrate and product (see Section 5.2.1). The use of a co-solvent was investigated to see if this could help to prevent the formation of solid, and therefore make analysis easier and more accurate. Moreover, it is also possible that as the reaction mixture

becomes more viscous stirring becomes less efficient; the addition of a co-solvent should also help to prevent this issue.

Several solvents have previously been used alongside **Cat-1** for ethanol homocoupling. While ethyl acetate and DMA completely shut down any catalytic activity, diglyme gave appreciable ethanol conversion, albeit at the loss of selectivity. Toluene on the other hand gave good product turnover over 20 hours and maintained high selectivity to *n*-butanol (>99%).[18] As such, toluene was tested as a solvent for *n*-octanol homocoupling. Xylene was also investigated as it has similar properties to toluene but has a higher boiling point. Finally, diethyl ether was used, as previous studies had shown that ether solvents could be used without completely shutting down activity.[18] Previous solvent studies used a 7:1 solvent:ethanol volumetric ratio. However, for these experiments, as the aim was to prevent solid build up without decreasing activity if possible, a 2:1 volumetric ratio of solvent:substrate was used (Table 5.4).

Table 5.4: Solvent screen for n-octanol coupling.

Entry[a]	Solvent	*n*-Octanol Conversion (%)	2-Hexyldecan-1-ol Yield (%)[b]	Missing *n*-octanol (%)[c]
1	None	51	15	36
2	Toluene	31	11	20
3	Xylene	31	11	20
4	Diethyl ether	35	7	28

[a] Conditions: solvent (20 mL), *n*-octanol (10 mL), [**Cat-1**] (0.1 mol%), NaOOct (5 mol%), 150 °C, 4 hr, [b] products detected by GC analysis, [c] Difference between *n*-octanol conversion and 2-hexyldecan-1-ol yield.

Toluene and xylene performed identically, giving a small decrease in 2-hexyldecan-1-ol yield, accompanied by a more significant decrease in *n*-octanol conversion. Using these solvents the amount of missing *n*-octanol was reduced by 16% compared to the system with no solvent. Furthermore, the post reaction mixture was still mostly liquid, with only a small amount of solid build up observed. This made preparation of samples for analysis far easier. Diethyl ether gave similar *n*-octanol conversion to toluene and xylene, but inferior coupled product yield. It appears that using a more polar solvent either aids in the production of higher alcohols or is not as effective at preventing solid build up. It is not clear if the reduction in missing *n*-octanol is due to the solvent preventing solid build up, or

if it is because using a solvent reduces the concentration of *n*-octanol, thus slowing the reaction and decreasing the rate of higher alcohol formation.

5.5 – Use of an open system

Almost all previous investigations into ethanol homocoupling had used a sealed reaction vessel (autoclave) and high temperatures. A temperature screen had shown that Guerbet reactivity was strongly disfavoured below 150 °C. As the boiling point of ethanol is significantly lower than this (78 °C), the use of an open system was largely ignored. When an open system had been used with a ruthenium-phosphinoamine monochelate catalyst, yields of 12.5% *n*-butanol were achieved, although this did require a run time of 341 hours.[10] It therefore appears that Guerbet chemistry is possible at lower temperatures, albeit at a much slower rate. For open system reactions the Guerbet reactor (Figure 5.4) is used, this allows for molecular sieves to be suspended above the reaction on a sintered glass plug to remove any water produced.

Figure 5.4: The Guerbet reactor used for open system alcohol coupling.

While the use of a closed system allows for higher temperatures, it also prevents the escape of any gasses generated during reaction. A significant amount of pressure is generated during all alcohol coupling reactions, this is mostly due to hydrogen evolution with small amounts of methane also detected. While dihydrogen production is a by-product of ester

formation *via* the Tishchenko reaction (a competing reaction pathway with the Guerbet reaction), it is not clear if the hydrogen produced is recycled back into the system during re-hydrogenation. By using *n*-octanol (bp=195 °C) it is easy to establish if using a closed system is preferable simply because it allows the use of higher temperatures, or if the retention of any gas produced is important for reactivity (Table 5.5).

Table 5.5: Comparison between an open and closed system for n-octanol homocoupling.

Entry[a]	Catalyst	System	*n*-Octanol Conversion (%)	2-Hexyldecan-1-ol Yield (%)
1	1	Closed [b]	51	15
2	1	Open [c]	47	21
3	4	Closed [b]	46	3
4	4	Open [c]	28	5

[a] Conditions: *n*-Octanol (10 mL), [Cat] (0.1 mol%), NaOOct (5 mol%), 150 °C, 4 hr, [b] Closed system: reaction performed in a Parr 100 mL autoclave, [c] Open system: reaction performed in a 50 mL RBF equipped with a reflux condenser and 3 Å molecular sieves.

Both **Cat-1** and **Cat-4** performed superiorly in an open system compared to a closed system. This increase in product yield is attributed to the removal of water by 3 Å molecular sieves, as this prevents any catalyst decomposition and forces the equilibrium towards the coupled product. For both **Cat-1** and **Cat-4** in the open system, *n*-octanol conversion decreases slightly while 2-hexyldecan-1-ol yield increases. It therefore appears that an open system disfavours higher alcohol coupling, however, the cause of this is unclear. This confirms that the benefit of a closed system for short chain alcohol coupling is it allows for higher reaction temperatures to be used. If the boiling point of the alcohol substrate is above the optimum temperature for Guerbet coupling (150 °C), then an open system can be used with no detrimental effect upon reactivity.

5.5.2 – Reaction monitoring study

As comparable *n*-octanol conversions and 2-hexyldecan-1-ol yields were seen between an open and closed system, an open system could be used to monitor the kinetics of reaction. The use of an open system makes taking sequential samples from the reaction mixture far easier, as releasing the pressure build-up before a sample can be taken is not necessary. As such, *n*-octanol coupling with **Cat-1** was followed over a 45-hour period (Figure 5.5).
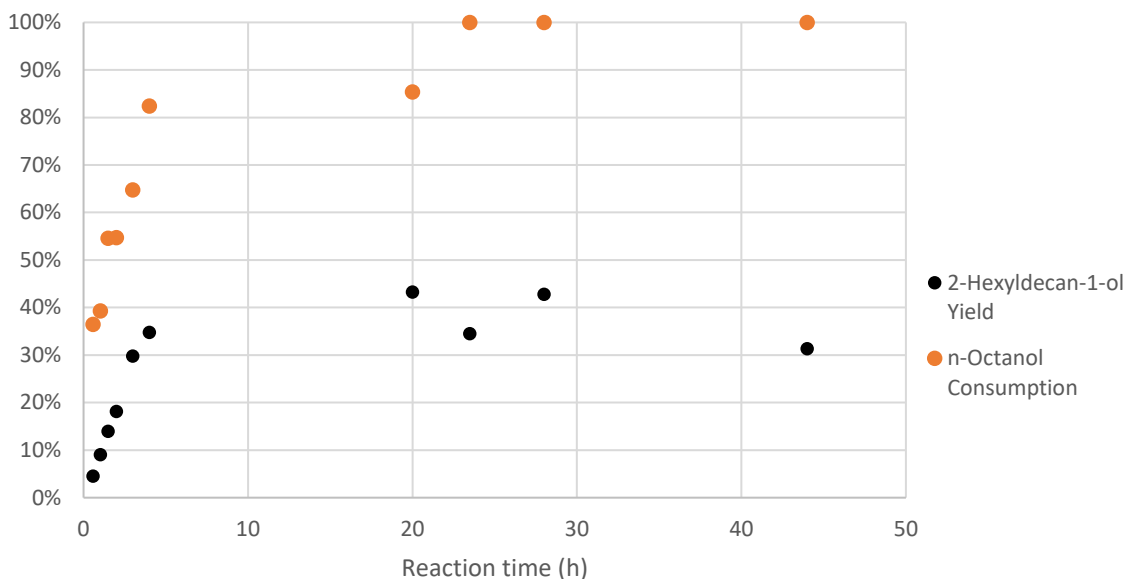
Figure 5.5: n-Octanol conversion and 2-hexyldecan-1-ol yield over time monitored in an open system. To allow for more samples to be taken, 30 mL of alcohol was used instead of the usual 10 mL, catalysts and base loadings were also adjusted accordingly.

Following the kinetics of *n*-octanol coupling once again shows the superiority of the open system. Here, the yield of 2-hexyldecan-1-ol reached 35% in only 4 hours, significantly higher than that observed in previous experiments. It is not clear what has caused this increase in activity, as the proportion of catalyst, base and substrate has been kept constant. *n*-Octanol conversion was also rapid, reaching 82% over the same period. However, as *n*-octanol conversion increased the reaction rate slowed, taking 24 hours for 100% *n*-octanol conversion to be reached. The 2-hexyldecan-1-ol yield reached a maximum of 43% before it slowly started to decrease after 100% *n*-octanol conversion. The cause of this decrease in yield is not immediately apparent, as 2-hexyldecan-1-ol cannot homocouple it is unlikely to be from the production of higher alcohols. It is possible that while **Cat-1** favours Guerbet chemistry over Tishchenko, when all linear alcohol is consumed and thus Guerbet chemistry is not possible the catalyst starts to produce Tishchenko products instead (Scheme 5.5). As such, highly branched esters could be formed. The open system favours the formation of these products as hydrogen can escape, forcing the equilibrium to the right. However, further work is needed to confirm this possibility.
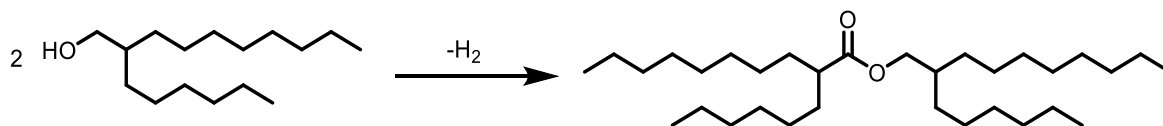
Scheme 5.5: An example of a highly branched ester formed by Tishchenko coupling of 2-hexyldecan-1-ol.

As the reaction becomes more viscous with time, taking samples for analysis also becomes more challenging. While the mixture is a liquid at reaction temperature (150 °C), it quickly solidifies upon cooling making the collection of consistent samples more challenging. This may be the cause of some of the anomalous results seen. Without the use of a solvent (see Section 5.4) this increase in viscosity will always cause issues with reaction sampling.

Interestingly, for the first 4 hours both *n*-octanol consumption and 2-hexyldecan-1-ol yield increase in a linear fashion, with remarkably similar rates. *n*-Octanol consumption is only slightly more rapid than 2-hexyldecan-1-ol formation. It is not clear why *n*-octanol consumption over the first 30 minutes is so much more rapid, then slows to match the rate of the product yield. It is possible that this is an effect of the slow rise to reaction temperature. As shown during the condition screen (Section 5.2.2), running the reaction at 120 °C gives reasonable *n*-octanol conversion (20%) but negligible 2-hexyldecan-1-ol yield (1%). The formation of octanal *via* dehydrogenation of octyl octanoate by Tishchenko chemistry may be possible at a lower temperature than the formation of 2-hexyldecan-1-ol by Guerbet chemistry. This would give the appearance of a high *n*-octanol conversion but low product yield at the beginning of the reaction, although no aldehyde has been observed by GC analysis. As the temperature of the reaction mixture reaches reaction temperature, the rate of higher alcohol formation increases to match that of the *n*-octanol consumption. However, further work is required to establish exactly what happens during the first 30 minutes of reaction.

5.6 – Solid analysis

Ethanol homocoupling reactions produce a significant amount of solid by-product. This is isolatable from the post reaction mixture by filtration, and upon analysis was shown to be predominantly sodium acetate, with a small amount of sodium formate and sodium butanoate also present. To ascertain whether similar solid by-products are produced by *n*-octanol coupling the same analysis was undertaken. Given the post reaction mixture of *n*-

octanol coupling is entirely solid, all salts were isolated *via* aqueous extraction of the heptane solution. After removal of water, 0.49 g of salts were recovered from a standard *n*-octanol coupling run and were analysed by ^{1}H NMR spectroscopy (Figure 5.6).
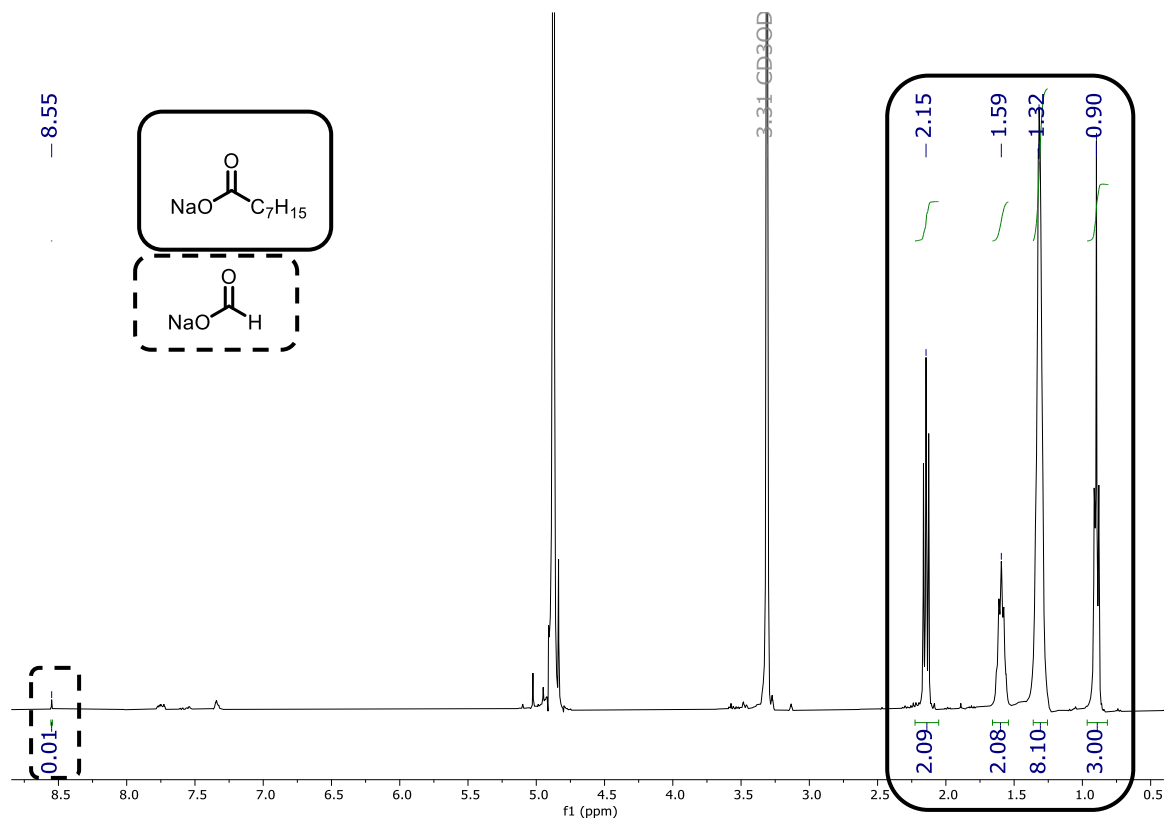
Figure 5. 6: ^{1}H NMR (400 MHz, d$_4$-MeOD) spectrum of the solid isolated from the aqueous layer after extraction of the post reaction mixture from Entry 7, Table 5.1.

This salt by-product is made up almost entirely of sodium octanoate, with a small amount of sodium formate also detected. Sodium octanoate is formed *via* the same process as sodium acetate formation in ethanol homocoupling reactions: Tishchenko chemistry, followed by reaction of the ester produced with sodium hydroxide (Scheme 5.6).[12] This hydroxide is present due to the destruction of the sodium octoxide base by water, which is produced as a side product by the Guerbet reaction. Ruthenium complexes are known to catalyse the production of esters from alcohols.[19] This process does require three *n*-octanol molecules for ester formation and may therefore be less active at higher *n*-octanol conversions.
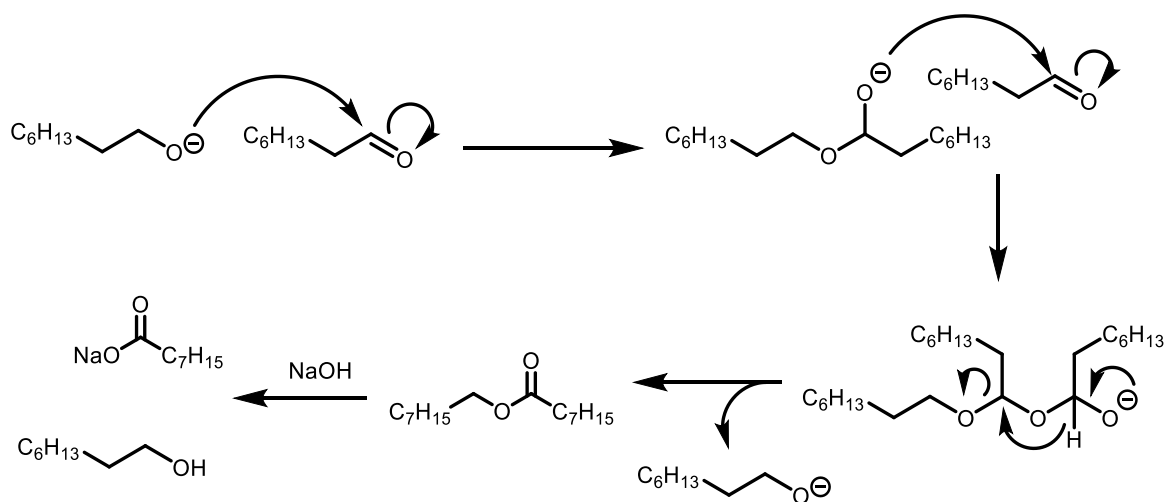
Scheme 5.6: Formation of sodium octanoate via Tishchenko chemistry.

The minor amounts of formate may be produced by decarbonylation of *n*-octanol by **Cat-1** (Scheme 5.7). Ruthenium catalysts active for this process have previously been reported.[20,21] However, as only small amounts of formate are seen, it seems **Cat-1** is a poor decarbonylation catalyst. In ethanol homocoupling, methane is observed as a minor gaseous product, again indicating that decarbonylation does slowly occur during reaction.[9] If the minor formate peak is discounted and the solid is presumed to consist entirely of sodium octanoate, then this accounts for 4.6% of the missing *n*-octanol.

Scheme 5.7: Decarbonylation of n-octanol by a ruthenium catalyst. Ligands omitted for clarity.

5.7 – Preformation of sodium octoxide

To date, all catalytic reactions had been performed with sodium octoxide (NaOOct, **5.8**) produced immediately before reaction (see Section 5.2). However, producing NaOOct *via* this method requires an additional 2 hours prior to catalysis to form the base from *n*-octanol and sodium metal. Given that typical *n*-octanol coupling reactions are only 4 hours long, this significantly increases overall reaction time. As such, the preformation and isolation of NaOOct was investigated. This would make performing catalytic testing significantly easier and remove the need for sodium. The reaction of *n*-octanol and sodium hydride at room temperature in THF (Scheme 5.8), gave NaOOct as a grey/white powder in excellent yields (98%). This could then be used directly for *n*-octanol coupling reactions.
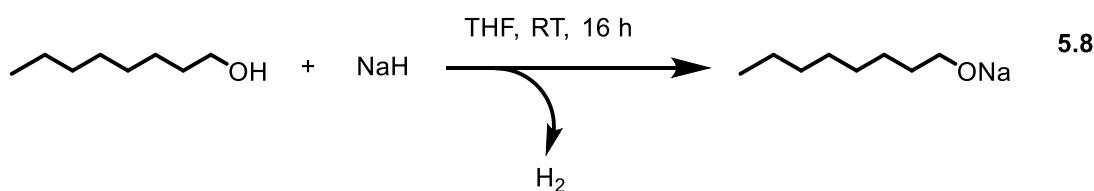
Scheme 5.8: Synthesis of NaOOct.

n-Octanol coupling reactions using preformed sodium octoxide afforded the same waxy solid post reaction as those using the *in situ* NaOOct, and consisted of the same salt mixture (mostly sodium octanoate, with a small amount of formate). While the use of either base gave identical *n*-octanol conversions (51%), the use of preformed base gave significantly higher 2-hexyldecan-1-ol yields (22% compared to 15%). When the preformed base is used it is isolated before use, and thus purity is assured. However, with the *in situ* base no purity tests are conducted prior to reaction and thus complete conversion to NaOOct is never confirmed. This could be the reason for the slightly poorer performance observed with the *in situ* formed base.

Table 5.6: Comparison of the use of preformed and in situ sodium octoxide for n-octanol homocoupling.

Entry[a]	Base	*n*-Octanol Conversion (%)	2-Hexyldecan-1-ol Yield (%)
1	Preformed	51	22
2	*in situ*	51	15

[a] Conditions: *n*-Octanol (10 mL) **Cat-1** (0.1 mol%), NaOOct (5 mol%), 150 °C, 4 hr

5.8 – Medium chain alcohol coupling

With the viability of homocoupling longer alcohol chains established with *n*-octanol, attention was directed towards different chain lengths, namely *n*-propanol, *n*-butanol and *n*-hexanol. The same conditions as those used for *n*-octanol were also employed (0.1 mol% Cat, 5 mol% base, 150 °C, 4 h). Given the superior performance of the preformed base in *n*-octanol coupling, NaOPr, NaOBu and NaOHex were synthesised *via* the procedure shown in Scheme 5.8 prior to catalysis. All substrates were tested with both **Cat-1** and **Cat-4** and the results shown in Table 5.7.

$$[Cat]\ (0.1\ mol\%)$$

HO⌒R → $NaOC_2H_4R$ (5 mol%), 150 °C, 4 h → branched product

R= CH_3, C_2H_5, C_4H_9

5.1 R= CH_3
5.2 R= C_2H_5
5.3 R= C_4H_9
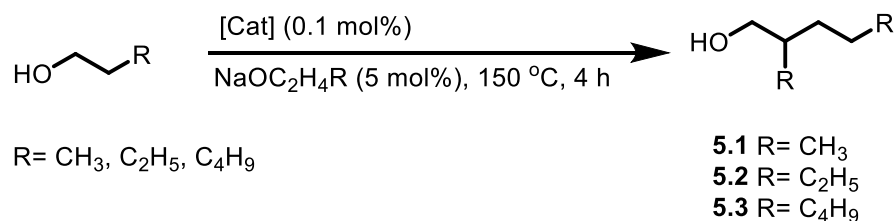
Entry[a]	Catalyst	Substrate	Product	Conversion (%)	Branched Product Yield (%)
1[b]	1	EtOH	**BuOH**	11	10
2[c]	4	EtOH	**BuOH**	19	17
3	1	PrOH	**5.1**	40	15
4	4	PrOH	**5.1**	19	8
5	1	BuOH	**5.2**	36	11
6	4	BuOH	**5.2**	22	3
7	1	HexOH	**5.3**	46	18
8	4	HexOH	**5.3**	40	4
9	1	OctOH	**5.4**	51	22
10	4	OctOH	**5.4**	42	4

[a] Conditions: Alcohol (10 mL), [Cat] (0.1 mol%), $NaOC_2H_5R$ (5 mol%), 150 °C, 4 hr, [b] Taken from ref. 9, [c] Taken from ref. 10.

Cat-1 shows superior performance to **Cat-4** for all higher alcohols. However, this divergence becomes more obvious as the chain length increases. In ethanol coupling, **Cat-4** shows superior performance to **Cat-1** over 4 hour run times.[9,10] For *n*-propanol, **Cat-4** still shows acceptable performance with 8% of the branched alcohol produced (Entry 4), while when *n*-butanol or *n*-hexanol is the substrate only 3% and 4% is produced respectively (Entries 6 and 8). Despite the poor product yields, **Cat-4** still shows moderate substrate conversion, indicating poor catalyst selectivity for the dimeric Guerbet product. As such, much of this missing alcohol is assumed to form either oligomeric Guerbet products (see Scheme 5.3), or esters *via* the Tishchenko reaction. **Cat-4** was shown to form a small amount of octyl octanoate in *n*-octanol coupling, so similar reactivity for medium chain alcohols is expected. In this study however, focus was directed solely towards branched alcohol production. **Cat-1** shows decent activity for branched product production, with

yields of 11 – 18%. However, as seen previously with *n*-octanol coupling there is still a large amount of 'missing alcohol', this is attributed to the formation of higher molecular weight Guerbet oligomers. Currently it is unclear why the performance of **Cat-4** decreases with chain length, whereas **Cat-1** remains much more consistent. Conversions likely increase with chain length as the energy required to dehydrogenate the alcohol and form the aldehyde decreases as the carbon length increases.

Notably, the post reaction mixtures from both *n*-propanol and *n*-butanol coupling remained liquid, and as such were analysed *via* the same process used for ethanol coupling (see Section 5.2.1). However, *n*-hexanol coupling produced a viscous waxy solid similar to that seen with *n*-octanol coupling, and thus the same analysis process was used.

5.9 Summary

The coupling of *n*-octanol to 2-hexyldecan-1-ol was possible with both **Cat-1** and **Cat-4**, although **Cat-1** gave significantly higher yields of the desired Guerbet product. Optimal *n*-octanol homocoupling conditions were predominantly the same as those used for ethanol, except that increasing base loading has a significantly more positive effect upon 2-hexyldecan-1-ol yield. Using diphosphine ligands with longer carbon bridges (**Cat-2** and **Cat-3**) decreased reactivity significantly. The post reaction mixture from *n*-octanol coupling was a waxy solid, and therefore hard to analyse. The addition of a solvent helped to reduce solid formation, although it did also decrease product yield.

Performing *n*-octanol coupling in an open system improved product yields considerably, and as such an open system could be used to monitor reaction kinetics. This found that most of the substrate was consumed in just 4 hours, however, 24 hours was needed to reach full conversion. 2-Hexyldecan-1-ol yield reach a maximum of 43%, although once 100% *n*-octanol conversion was reached this began to decrease, possibly due to the production of ester by-products. Analysis of the sodium salts produced over the course of the reaction shows mostly sodium octanoate, with a small amount of sodium formate; similar to what is seen in ethanol coupling chemistry.

This system could be expanded to the coupling of other medium chain length linear alcohols such as *n*-propanol, *n*-butanol and *n*-hexanol. Over 4 hour run times using **Cat-1**,

yields were acceptable for all alcohols (11-18%). However, for **Cat-4** yields sharply decrease with carbon chain length, while substrate conversion stayed high. As such, **Cat-4** appears to be significantly less selective for Guerbet coupling of higher alcohols than **Cat-1**.

5.10 – Further work

Higher alcohol coupling using ruthenium catalysts has been shown to be possible. However, thus far little insight into the exact mode of reaction and the variety of possible side products has been gained. Further work should start by examining the first 30 minutes of reaction in detail. Kinetic experiments indicate that a significant amount of *n*-octanol is consumed during this time, but little 2-hexyldecan-1-ol is produced (32% compared to 4.5%). Probing this section of the reaction further with some more detailed kinetic analysis may help to reveal what products this *n*-octanol is forming.

Both high molecular weight oligomeric Guerbet products and highly branched esters have been proposed as potential side products for this reaction. However, to date neither of these have been observed in the GC trace of the post reaction mixture. As very heavy compounds it is possible that these species boiling points are too high to allow for detection *via* GC analysis. Thus, other forms of analysis should be employed such as LC-MS and NMR to try to detect and quantify these compounds. This could help to give a more detailed picture of the composition of the post reaction mixture.

Overall, with ethanol coupling reactions using both **Cat-1** and **Cat-4**, conversions are still low (only 10.5% over 4 hrs for **Cat-1**). As such, it is unclear if the high selectivity seen in this process is due to preferential ethanol coupling over higher alcohols, or due to the higher concentration of ethanol compared to other alcohols. As the ability of these catalysts to couple higher alcohols has now been established, competition studies between ethanol and higher alcohol coupling could be performed. This would help to shed further light on the origin of the superior selectivity seen during ethanol coupling.

Thus far, only linear alcohol coupling has been investigated. However, there is no reason to suspect this system would not also work for branched alcohols, so long as the β-carbon contains two C-H bonds. Two commercially available branched alcohols (**5.9** and **5.10**) that could be investigated in Guerbet coupling are shown in Figure 5.7. This work would help to

expand the substrate scope of the reaction and would display how the use of bulkier substates affects reactivity.

5.9   **5.10**
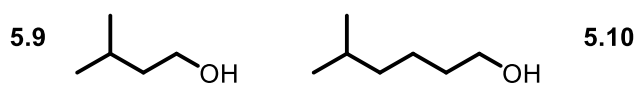
Figure 5.7: Commercially available branched alcohols from Merck for potential use in Guerbet coupling.

5.11 – References

1   P. L. Burk, R. L. Pruett and K. S. Campo, *J. Mol. Catal.*, 1985, **33**, 1–14.

2   K. Koda, T. Matsu-ura, Y. Obora and Y. Ishii, *Chem. Lett.*, 2009, **38**, 838–839.

3   A. Wick and E. U. Mahnke, *Method for Producing Guerbet Alcohols, US 8779216B2*, 2014.

4   J. Dubois, W. Zhao, R. E. A. Roelant, H. Keuken and P. M. Ramos Borges, *Synthesis of Guerbet Alcohols, US10214470B2*, 2019.

5   R. Shong, V. Dwarakanath, S. Thach and G. Winslow, *Mixed Carbon Length Synthesis of Primary Guerbet Alcohols, US9605198B2*, 2017.

6   M. Biermann, H. Gruß, W. Hummel and H. Gröger, *ChemCatChem*, 2016, **8**, 895–899.

7   A. J. O'Lenick, *J. Surfactants Deterg.*, 2001, **4**, 311–315.

8   M. Matsuda and M. Horio, *Process for the preparation of Guerbet alcohols, US4518810*, 1985.

9   G. R. M. Dowson, M. F. Haddow, J. Lee, R. L. Wingad and D. F. Wass, *Angew. Chem. Int. Ed.*, 2013, **52**, 9005–9008.

10   R. L. Wingad, P. J. Gates, S. T. G. Street and D. F. Wass, *ACS Catal.*, 2015, **5**, 5822–5826.

11   S. R. Waldvogel, in *Comprehensive Organic Name Reactions and Reagents*, John Wiley & Sons, Inc., Hoboken, NJ, USA, 2010, pp. 2782–2788.

12   G. R. M. Dowson, *Transformations of Ethanol by Homogeneous Catalysis for Creation of Advanced Biofuels, Ph. D. Thesis, Univeristy of Bristol*, 2012.

13   T. Seki, T. Nakajo and M. Onaka, *Chem. Lett.*, 2006, **35**, 824–829.

14   M. Nielsen, H. Junge, A. Kammer and M. Beller, *Angew. Chem. Int. Ed.*, 2012, **51**, 5711–5713.

15   L. J. Hounjet, M. Bierenstiel, M. J. Ferguson, R. Mcdonald and M. Cowie, *Inorg. Chem*, 2010, **49**, 4288–4300.

16   H. Aitchison, *A mechanistic study of the catalytic upgrading of ethanol to butanol biofuels, Ph.D. Thesis*, 2018.

17   N. V. Kireev, O. A. Filippov, E. S. Gulyaeva, E. S. Shubina, L. Vendier, Y. Canac, J. B. Sortais, N. Lugan and D. A. Valyaev, *Chem. Commun.*, 2020, **56**, 2139–2142.

18   J. Lee, *New Catalysts for the Upgrading of Ethanol to Butanol Biofuels, Ph.D. Thesis, Univeristy of Bristol*, 2015.

19   A. Sølvhøj and R. Madsen, *Organometallics*, 2011, **30**, 6044–6048.

20   P. D. Bolton, M. Grellier, N. Vautravers, L. Vendier and S. Sabo-Etienne, *Organometallics*, 2008, **27**, 5088–5093.

21   L. S. Van Der Sluys, G. J. Kubas and K. G. Caulton, *Organometallics*, 1991, **10**, 1033–1038.

Chapter 6 - Biofuel production using ruthenium complexes containing substituted diphosphine ligands.

6.1 – Introduction

To date, one of the most active catalysts for *n*-butanol production over short reaction times is the mono chelate-cymene system **6.1** (Figure 6.1), giving an *n*-butanol yield of 20.1% with a selectivity of 93.6% in just 4 hours.[1] However, this complex suffers from poor stability under the reaction conditions, quickly forming a catalytically inactive metal residue. This catalyst decomposition means that little further *n*-butanol is produced over longer run times. The equivalent bis chelate complex (**Cat-1**), while slower, is much more stable so produces greater *n*-butanol yields over extended runtimes (35.5% over 24 hours).[1] Complex **6.1** can also be used in *iso*butanol formation (21.8% yield, 88.8 selectivity over 2 hours), although it once again shows the same issues with stability.[2]
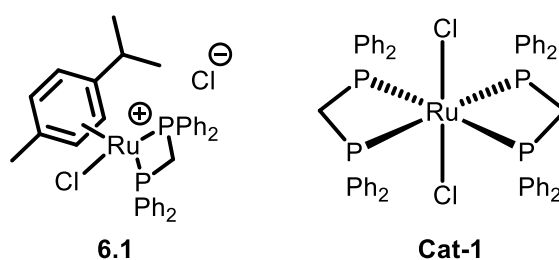
Figure 6.1: Ruthenium complexes used in the production of n-butanol.

Ruthenium complexes are well known for their ability to promote C-H activation and cyclometallation.[3–6] While many of these cyclometallation reactions occur at $C(sp^2)$-H bonds, $C(sp^3)$-H cyclometallation is also known.[7–9] These types of complexes have previously been used as catalysts for a variety of processes.[6,9,10] It was postulated that if a ruthenium half-sandwich complex capable of cyclometallation were used for butanol formation, it could cyclometallate under reaction conditions and produce a more stable catalyst. If this could be achieved, these complexes could marry the high activity of **6.1**, with the longevity of **Cat-1**. To this end, two *ortho*-substituted bis(diphenylphosphino)methane (dppm) ligands were targeted for initial investigation (Figure 6.2), as this ensured the C-H bonds available for potential cyclometallation were held within or close to the metal coordination sphere.

6.2 – Monochelate complex synthesis

6.2.1 – Synthesis of complexes bearing *ortho*-tolyl and *ortho-iso*propyl phosphine ligands

L14   **L15**
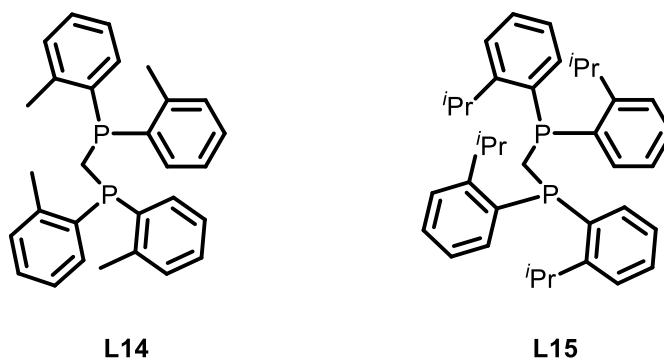
Figure 6.2: Ortho substituted dppm ligands used for complexation.

Ligands **L14** and **L15** (Figure 6.2), containing only simple alkyl substituents in the *ortho* position of the phenyl ring, were coordinated to ruthenium forming half sandwich complexes. Mono chelation was possible in ethanol at room temperature (Scheme 6.1) producing **Cat-31** and **Cat-32** in moderate yields (60% and 58% respectively) as yellow powders. These complexes displayed very different $^{31}P\{^1H\}$ NMR spectroscopic resonances from their unsubstituted analogue.
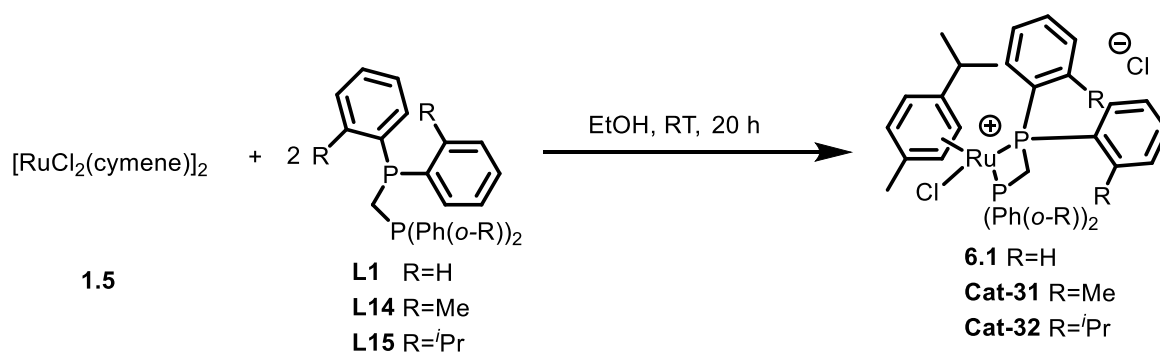
*Scheme 6.1: Synthesis of ruthenium diphosphine monochelate complexes **Cat-31** and **Cat-32**.*

Complex **6.1** gives a singlet at 2.7 ppm in the $^{31}P\{^1H\}$ NMR spectrum,[11] whereas **Cat-31** shows two broad doublets (Table 6.1). It is possible bulkier phosphine substituent in **Cat-31** leads to slower rotation of the cymene group, causing the phosphine groups to appear inequivalent on the $^{31}P\{^1H\}$ NMR timescale. As rotation is slowed, but not completely prevented, the resonances in the NMR spectrum are very broad. Due to this broadening when chloroform-*d* was used as an NMR solvent the calculation of coupling constants was not possible. Sharper resonances were observed using tetrachloroethane (TCE) as a

solvent, therefore this was used to calculate coupling constants. When **Cat-32**, containing an even bulkier diphosphine, was examined two sharp doublets were observed in the $^{31}P\{^1H\}$ NMR spectrum. Here, the phosphine appears to be bulky enough to prevent rotation of the cymene ligand, allowing for complete resolution of the two phosphine environments. This reasoning for the inequivalence would only be possible if the methyl and isopropyl groups on cymene preferentially sit above the phosphine ligands instead of between them. A crystal structure of **6.1** indicated that this may be possible as the isopropyl methyl groups point towards only one phosphine ligand.[12] It is also possible the inequivalence observed may be due to restricted rotation around the P-Ar bond instead, thus leading to phosphine substituents in different conformations and inequivalent phosphine environments. A similar effect has been noted with *ortho*-substituted monodentate phosphines coordinated to platinum and palladium.[13]

Table 6.1: $^{31}P\{^1H\}$ NMR resonances for ruthenium diphosphine monochelate complexes.

Complex	Peak pattern	Shift (ppm)	Coupling (Hz)
6.1[11]	Singlet	2.7	n/a
Cat-31[a]	Broad doublet	1.84, -2.48	n/a
Cat-31[b]	Broad doublet	-0.57, -4.61	85.5-100
Cat-32[a]	Sharp doublet	0.75, -7.95	75.7

[a] Solvent: d-chloroform-d, [b] Solvent: tetrachloroethane, resonances in chloroform too broad for coupling constants to be calculated.

Cat-31 was further examined using variable temperature $^{31}P\{^1H\}$ NMR spectroscopy (Figure 6.3). As the temperature was increased from 25 °C to 85 °C the rotation speed of the cymene group increases, this leads to further broadening and eventual coalescing of the two resonances observed as the two phosphorus environments become equivalent on the NMR timescale. This provides further evidence that the inequivalence seen is due to restricted cymene rotation.
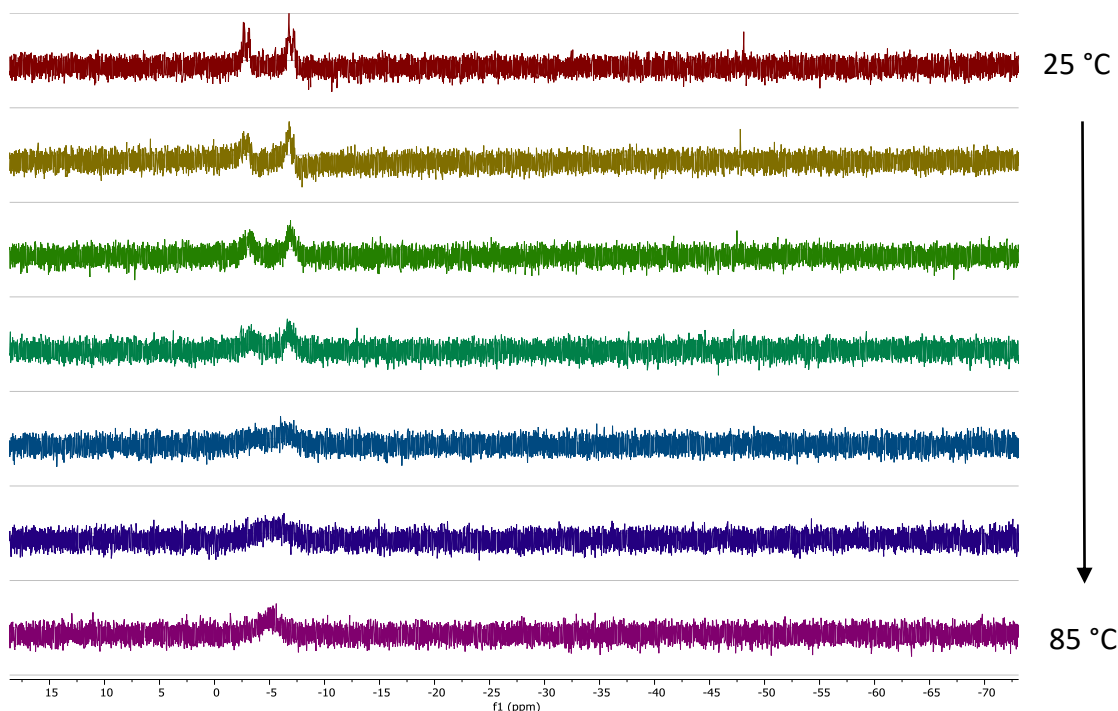
*Figure 6.3: VT $^{31}P\{^1H\}$ NMR (122 MHz, TCE) of **Cat-31** (25 °C – 85 °C).*

6.2.2 – Synthesis of *meta* and *para* tolyl complexes

In order to assess the effect that *ortho* substitution has on restricted cymene rotation, both *meta-* and *para-* bis(ditolylphosphino)methane ligands were synthesised (**L16/L17**). The ligands were produced in 19% and 67% yields respectively by reacting the respective Grignard reagent with bis(dichlorophosphino)methane at -78 °C. Complexation to [RuCl$_2$(cymene)]$_2$, **1.5**, was conducted as shown in Scheme 6.1 producing **Cat-33** and **Cat-34** in a 55% and 54% yield respectively (Figure 6.4).

Cat-33   **Cat-34**
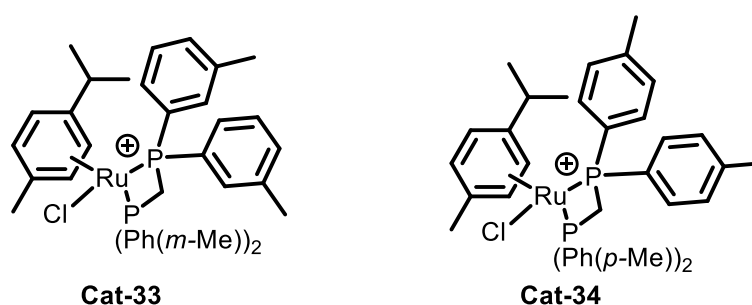
*Figure 6.4: Complexes bearing meta (**Cat-33**) and para (**Cat-34**) tolyl phosphinomethane ligands. Chloride counter ions omitted for clarity.*

Both complexes gave a singlet in the $^{31}P\{^1H\}$ NMR spectrum displaying that restricted rotation is only caused by the *ortho* substituted isomer in the case of tolyl substituted phosphine groups. With the methyl substituents facing away from the metal centre (as in

171

the case of **Cat-33** and **Cat-34**) it is extremely unlikely that cyclometallation would occur, and thus any increase in stability this may cause will be prevented.

6.3 – Bis chelate complex synthesis

Following the successful synthesis of the mono chelate complexes, formation of the bis chelate complexes was also investigated. Production of the bis chelate **Cat-1** from both a Ru(II) and Ru(III) precursor has been reported,[14,15] as such, both precursors were used in the attempted formation of bis chelate complexes using ligands **L14** and **L15**. Unfortunately, when the synthesis of **6.2** was attempted using a Ru(III) precursor (Scheme 6.2, reaction I) only free ligand was observed in the ^{31}P{^{1}H} NMR spectrum of the post reaction mixture, indicating that reduction to the Ru(II) species had not been possible. Mass spectrometry of the post reaction solid showed predominantly free ligand with a small amount of mono-chelate species. Formation of both **6.2** and **6.3** from a Ru(II) precursor (Reaction II) was also unsuccessful. After reaction, predominantly free ligand and free triphenylphosphine were observed by ^{31}P{^{1}H} NMR spectroscopy, with little sign of any chelation. It is proposed that, due to the extra bulk of ligands **L14** and **L15**, bis chelation is not possible. Given the issues with synthesising **6.2** and **6.3** and the ease of synthesis of **Cat-31** and **Cat-32**, further studies on the *ortho*-substituted ligands focussed solely on the mono chelate complexes.
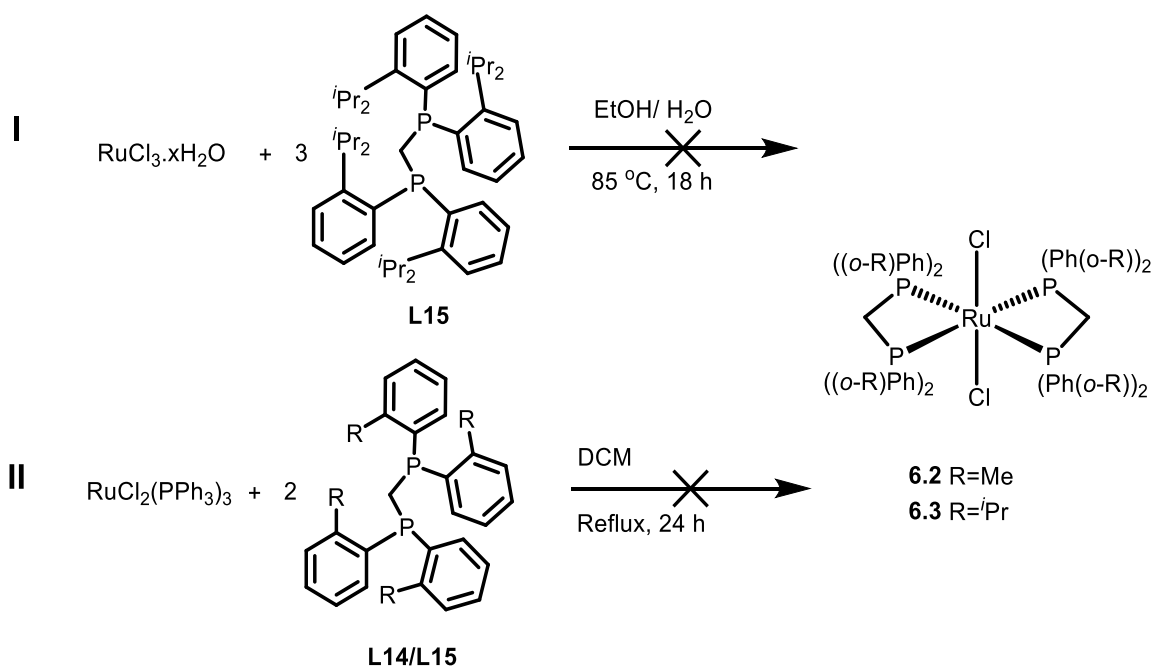
Scheme 6.2: Attempted synthesis of ruthenium bis chelate complexes bearing ortho substituted dppm ligands.

Given less steric interference was exhibited by the *meta* and *para* methyl substituted dppm ligands in **Cat-33** and **Cat-34**, it was proposed that these ligands may be able to form bis chelate complexes analogous to **Cat-1**. Formation was attempted from the [RuCl$_2$(PPh$_3$)$_3$] precursor, as this method required fewer equivalents of ligand (Scheme 6.3). Synthesis of the *meta* (**Cat-35**) and *para* (**Cat-36**) substituted bis chelate complexes was possible in DCM at room temperature in 26% and 41% yields, respectively. The successful formation of these complexes compared to the failure in the formation of the *ortho* substituted bis chelate complexes shows the large effect ligand bulk can have upon the ease of coordination. While **Cat-35** and **Cat-36** may be unable to cyclometallate, they will show what effect increasing the electron donor properties of the ligand has upon the catalytic performance of bis chelate complexes.
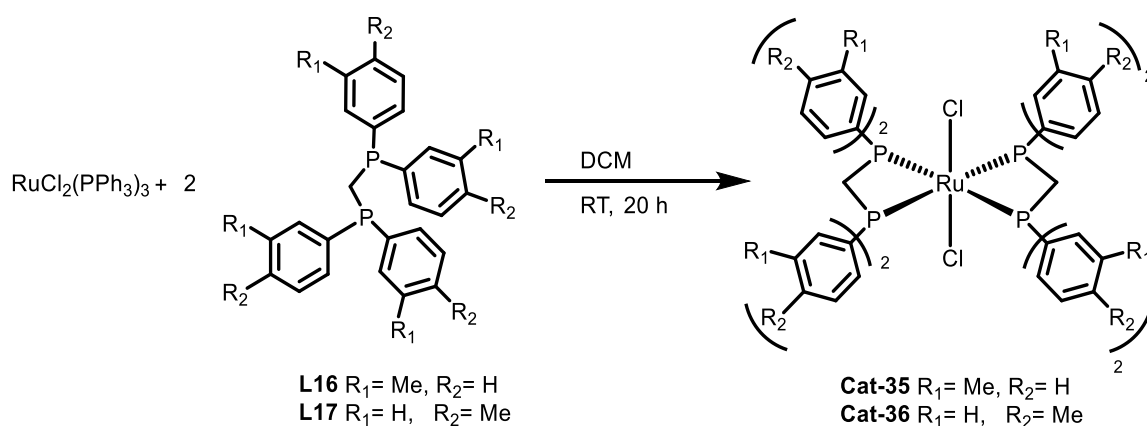
Scheme 6.3: Synthesis of ruthenium bis chelate complexes bearing meta and para substituted dppm ligands.

6.4 – Monochelate stability

The main issue with using monochelate **6.1** for advanced biofuel production is the lack of stability under reaction conditions (150 °C, 5 mol% NaOEt). To ascertain whether **Cat-31** and **Cat-32** show greater stability, both complexes were dissolved in TCE and heated to 145 °C for 18 hours. Over this time both solutions darkened from yellow to brown and a black precipitate began to form. Furthermore, no resonances were observed in the $^{31}P\{^1H\}$ NMR spectrum of either solution. It therefore seemed likely that a heterogeneous ruthenium species had formed, as seen in the post reaction mixture when **6.1** was used for *n*-butanol production.[1] Unfortunately, it appears that **Cat-31** and **Cat-32** do not exhibit any greater thermal stability than **6.1** and thus may provide little benefit when used for biofuel production. **Cat-32** was stable in methanol at 100 °C over 4 hours, with no observed change in the $^{31}P\{^1H\}$ NMR spectrum. Upon the addition of an excess of NaOMe, all resonances relating to the initial complex disappeared and were replaced by a broad singlet at 2.11 ppm, indicating the rapid reaction of **Cat-32** with the strong base. However, it is not clear what species was produced. Heating this mixture to 70 °C for 16 hours caused a significant reduction in peak size, indicating that the species formed was unstable.

Weak bases such as NEt$_3$ and NaOAc are used to promote C(sp^3) cyclometallation in monodentate ruthenium-phosphine complexes.[7,9] To ascertain whether the same effect would be observed with bidentate phosphine ligands, samples of **Cat-32** was reacted separately with both NEt$_3$ and NaOAc in methanol. Upon heating to reflux for 20 hours, a change was observed in the $^{31}P\{^1H\}$ NMR spectrum, showing three peaks at -10.6, -11.8 and -19.7 ppm, indicating that a reaction had occurred. After the reaction of **Cat-32** with NEt$_3$,

subsequent reaction of the complex with NaOMe appeared to be significantly slower, with no change observed by $^{31}P\{^1H\}$ NMR spectroscopy immediately after addition. However, heating to reflux for 48 hours gave the same broad singlet observed when **Cat-32** was reacted with NaOMe directly.

Cat-31 reacted with NEt$_3$ significantly slower than **Cat-32**, however, after heating to reflux in methanol for 24 hours two new singlets at -4.7 and -16.9 ppm were observed in the $^{31}P\{^1H\}$ NMR spectrum, along with a large amount of starting complex. Once again, this showed that **Cat-31** does react with NEt$_3$, although the product that was formed remains uncharacterised. Surprisingly, **Cat-33** also reacted with NEt$_3$, displaying 2 peaks in the $^{31}P\{^1H\}$ NMR spectrum at 7.5 and 7.4 ppm. Given the orientation of the methyl groups in **Cat-33**, cyclometallation would be unlikely. Therefore, it appears that while complexes **Cat-31**, **Cat-32**, and **Cat-33** all react with NEt$_3$, cyclometallation may not be occurring. This would likely be evidenced by two mutually coupled doublets in the $^{31}P\{^1H\}$ NMR due to the phosphorous environments becoming inequivalent.

Initial investigations indicate that weak bases interact differently than strong bases with these ruthenium complexes, and in doing so slow the reaction of the complexes with strong bases like NaOMe. However, it is still unclear if this will aid catalytic performance or not. As a strong base is required for catalyst activation it is possible that the use of the weak base may make this slower.

6.5 – *Iso*butanol production with ruthenium complexes supported by bulky dppm ligands

All isolated complexes were used for the production of *iso*butanol, using optimised conditions previously established in the Wass group in a 100 mL Parr stainless steel autoclave (Table 6.2).[16] Both the mono chelate and bis chelate complexes showed some activity in *iso*butanol production. However, bis chelates were significantly more activity than mono chelate complexes bearing the same ligands, with **Cat-35** (Entry 8) producing 65% *iso*butanol over 2 hours, whereas **Cat-33** gave only 21% (Entry 6). This is similar to what is seen for the unsubstituted dppm ligand, where the bis chelate complex is by far the more effective catalyst.[16] Furthermore, all the mono chelate complexes showed poor stability under reaction conditions, even over 2 hour run times, with the post reaction mixtures being dark brown, due to the production of nanoparticulate ruthenium. For the

bis chelate complexes the post reaction mixtures were still a homogeneous yellow solution. This lack of stability may explain why the mono chelates perform so poorly. The *meta* and *para* ligands performed similarly in both the mono chelate (**Cat-33** and **Cat-34**, Entries 6 & 7) and bis chelate (**Cat-35** and **Cat-36**, Entries 8 & 9) complexes, with the *meta* (**Cat-33** and **Cat-35**) only giving 4% higher product yields in both cases. Given that the extra steric bulk in these ligands is located further from the metal centre, this minor difference in activity is likely down to the effect that *meta* or *para* substitution has upon the electronics of the ligand.

The *ortho*-tolyl mono chelate **Cat-31** performed significantly worse than both the *meta* and *para* substituted complexes, giving only 12% *iso*butanol over 2 hours (Entry 1). However, these yields could be increased to 23% by increasing the run time to 20 hours (Entry 2). While *iso*butanol yields over 20 hours are comparable with the *meta* substituted **Cat-33**, ethanol conversions were significantly higher (77% compared to 29%). This indicates that as the complex starts to degrade, other reaction pathways such as Tishchenko and Cannizzaro chemistry begin to be favoured over Guerbet. Unfortunately, *ortho* substitution on the dppm ligand did not confer any increased stability upon the complex as the post reaction mixture in both cases was dark brown. When the substituent in the *ortho* position was changed to an *iso*propyl group (**Cat-32**, Entry 5), *iso*butanol yields decreased further with only 6% produced over 2 hours. The negative effect that *ortho* substitution has upon product yield can be used as evidence for catalysis occurring *via* an inner sphere mechanism, as restricted access to the metal centre slows *iso*butanol production.

As discussed above, mild Lewis bases such as NEt$_3$ are known to promote cyclometallation in ruthenium complexes bearing monodentate phosphine ligands.[9] Furthermore, the addition of NEt$_3$ to **Cat-31** in methanol displayed some interaction between the two species over 20 hours. However, evidence for cyclometallation remained elusive (see Section 6.3). Whether the addition of NEt$_3$ to the reaction mixture was able to increase the stability of the active catalyst and thus increase product yields was therefore investigated. Given that the reaction of NEt$_3$ with **Cat-31** occurred over a 20-hour period, while the effect of NaOMe was almost instantaneous, **Cat-31** and NEt$_3$ were allowed to react in refluxing methanol for 20 hours before the addition of NaOMe and EtOH. Over a 2-hour run time, **Cat-31** gave identical *iso*butanol yields in the presence or absence of NEt$_3$ (Entry 1 vs Entry 3), while over

20 hours slightly more *iso*butanol was seen when NEt$_3$ was present (Entry 2 vs Entry 4). However, this increase was very low indicating that the addition of NEt$_3$ to the reaction has no effect upon product yields. It is currently unclear if this is due to cyclometallation not occurring in the complex, or if cyclometallation does occur but does not lead to an increase in stability.

Table 6.2: Production of isobutanol using ruthenium complexes bearing bulky dppm ligands.

Entry[a]	Catalyst	Runtime	EtOH conv (%)	*i*BuOH yield (%)	*i*BuOH selectivity (%)[b]	*n*PrOH Yield (%)
1	31	2	33	12	90	2
2	31	20	77	23	93	2
3[c]	31 + NEt$_3$	2	32	12	89	1.5
4[c]	31 + NEt$_3$	20	77	27	95	2
5	32	2	11	6	86	1
6	33	2	29	21	91	2
7	34	2	40	17	91	2
8	35	2	80	65	98	1
9	36	2	81	61	98	1

[a] Conditions: 1 mL (17.13 mmol) EtOH, 10 mL MeOH, 180 °C, NaOMe (1.85 g, 200 mol%), 0.1 mol% [Cat], [b] selectivity calculated from observed products in the liquid fraction, [c] [Cat] (0.1 mol%, 0.01713 mmol) and NEt$_3$ (0.08565 mmol, 5 eqv) heated to reflux in MeOH for 20 hours before being used in catalysis.

6.6 – Attempted formation of cyclometallated complexes

Initial investigations outlined in Section 6.4 indicated that the interaction of **Cat-31** and **Cat-32** with cyclometallation agents did not increase the stability of the catalysts. Given that formation of the cyclometallated complex was attempted *in situ,* it had not been established if such a complex was produced or if another species was preferentially formed leading to no change in the observed stability. As such, formation and isolation of the cyclometallated analogues of **Cat-31** and **Cat-32** was attempted.

For some previously reported palladium complexes simply refluxing the non-cyclometallated species in toluene had been shown to be sufficient for inducing cyclometallation.[17] However, when this method was attempted with **Cat-32** a mixture of different species was observed in the $^{31}P\{^1H\}$ NMR spectrum, with no obvious signs of cyclometallation. A mass spectrum of the product mixture indicated that one of the species formed (m/z= 781.3) corresponded to **Cat-32c** (Scheme 6.4) where toluene had displaced cymene in the complex; no cyclometallated **Cat-32b** was observed.
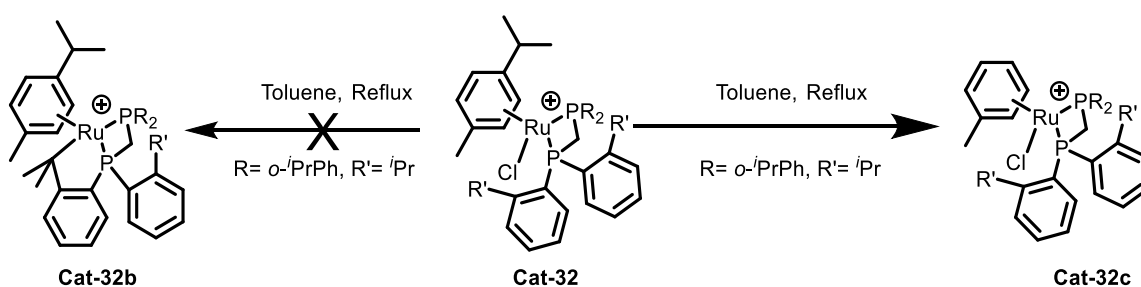
*Scheme 6.4: Attempted cyclometalation of **Cat-32** in toluene. Chloride counterions omitted for clarity.*

As simply refluxing **Cat-32** in toluene proved unsuccessful, another method was attempted. Cyclometallation of sp^3 carbons in ruthenium-cymene complexes bearing monodentate phosphine ligands has been reported using 4 equivalents of sodium acetate in methanol over 4 hours.[7] As the substrates used in this publication were more similar to **Cat-31**, cyclometallation under these conditions was attempted. However, after 4 hours only the non-cyclometallated complex and free ligand was observed, and little further change was seen over 2 days. Even upon heating the mixture to reflux little sign of cyclometallation was detected and **Cat-31** was still the main species present (Scheme 6.5).
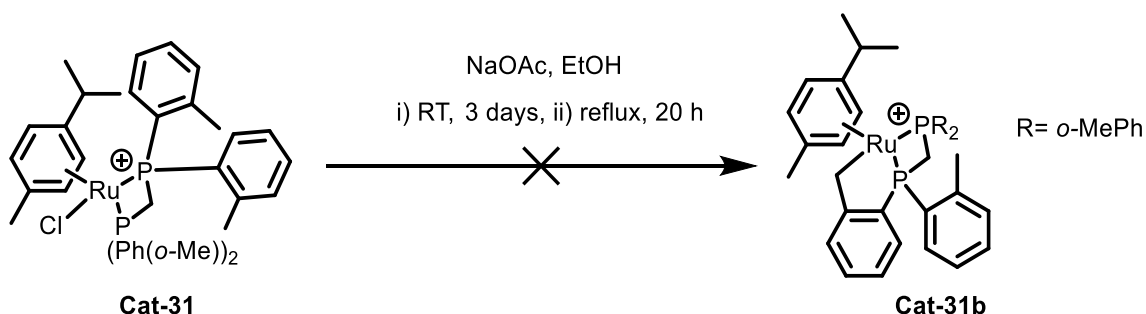
*Scheme 6.5: Attempted formation of cyclometallated complex **Cat-31b** from **Cat-31**. Chloride counterions omitted for clarity.*

Formation of cyclometallated complexes from bidentate ligands appears to be significantly more complicated than from their monodentate analogues. As such, formation of **Cat-31b** and **Cat-32b** *via* established cyclometallation routes appeared to not be possible. The difficulty of cyclometallation could be a contributing factor in why these complexes show no greater stability than their non-substituted analogues.

6.7 – Preparation of *ortho*-phenyl substituted diphosphine ligands

Alkyl substitution at the *ortho* position of the phosphine substituent does not result in any increased catalyst stability. It is postulated that this is due to cymene dissociation from the complex at high temperature, as has been demonstrated in Section 6.6. Cymene dissociation results in the formation of a highly coordinatively unsaturated ruthenium complex which *ortho* substitution cannot compensate for, thus, ruthenium nanoparticle formation is not prevented.

Several recent publications have displayed the displacement of a cymene group from a ruthenium complex by an *ortho* substituted aromatic group attached to a monodentate phosphine.[3,18,19] It is possible that this type of behaviour could be exploited to help stabilise ruthenium-cymene catalysts; decomposition of the complex upon cymene dissociation could be prevented by tethering an aromatic group in the *ortho* position of the phosphine substituent. With this aim in mind, ligand **L18** was targeted and synthesised according to the method below (Scheme 6.6). While a long reaction time was required (3 days reflux) and the yield was low, production of pure **L18** as an air stable white solid was possible. Crystals of **L18** suitable for X-ray analysis were grown by layering a chloroform solution with diethyl ether (Figure 6.5).
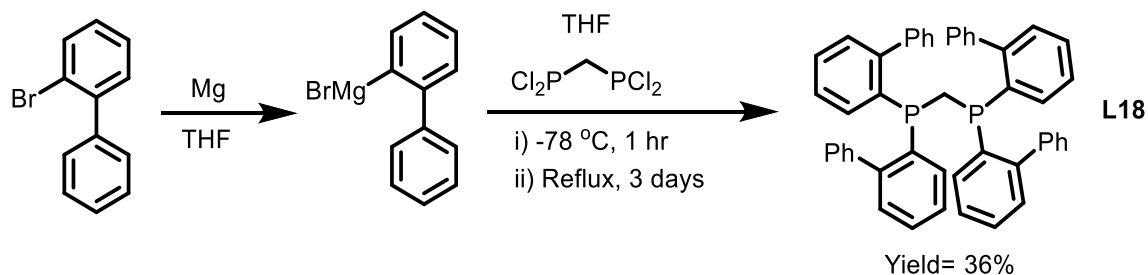
Scheme 6.6: Production of a substituted dppm ligand bearing ortho phenyl groups.

L18 displays a similar structure to unsubstituted dppm (**L1**), however, it contains a significantly larger P1-C1-P2 angle (114.86° compared to 106.39°).[20] This is likely due to

increased steric clash between the bulkier phosphine substituents of **L18**. *Ortho* substitution leads to more congestion around the phosphorous atoms and therefore the greater angle is observed. It seems likely that if *meta* or *para* substituted phenyl rings were used instead that this effect would be lessened. The C2-P1-C14 angle in unsubstituted dppm is only slightly smaller than in **L18** (101.06°compared to 102.58°), indicating that intra-phosphine-substituent steric clash is less than inter-phosphine-substituent. On average both P-C1 and P-C$_{(phenyl)}$ bond lengths are similar in the substituted and unsubstituted ligands (1.857 Å compared to 1.856 Å, and 1.834 Å compared to 1.836 Å respectively).
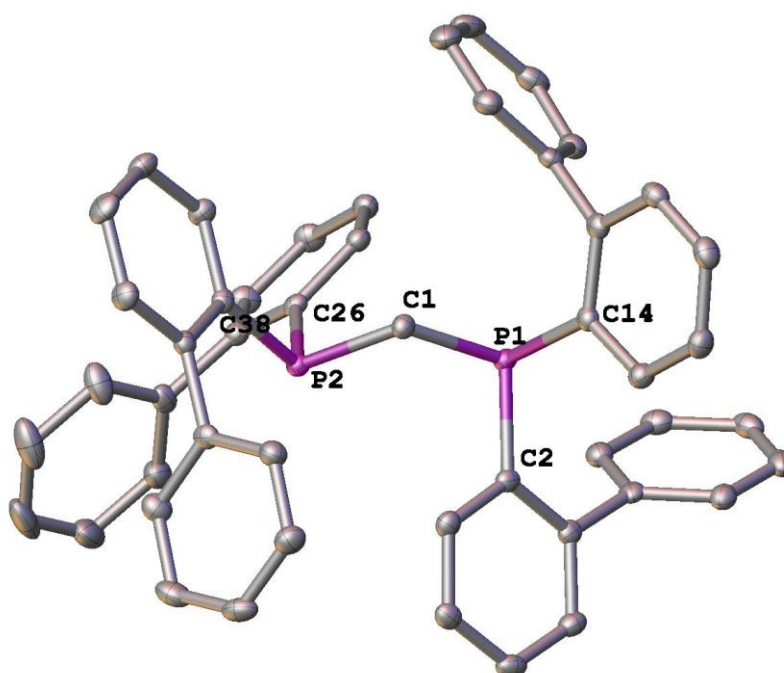
*Figure 6.5: Structure of **L18**. Hydrogen atoms omitted for clarity. Selected bond lengths (Å) and angles (°): C1-P1 1.8568(13), C1-P2 1.8573(13), P1-C2 1.8404(14), P1-C14 1.8489(14), P2-C26 1.8407(13), P2-C38 1.8433(14), P2-C1-P1 114.86(7), C2-P1-C14 102.58(6), C38-P2-C26 103.61(6).*

Unlike the ligands used above, **L18** was completely insoluble in ethanol. As such, DCM was used for the complexation instead and **Cat-37** could be produced in a good yield (76%) as a yellow powder (Scheme 6.7). **Cat-37** displayed two doublets in the ^{31}P{^{1}H} NMR at 5.89 and -4.11 ppm, indicating that the *ortho* phenyl substituents also restrict rotation of the cymene group.
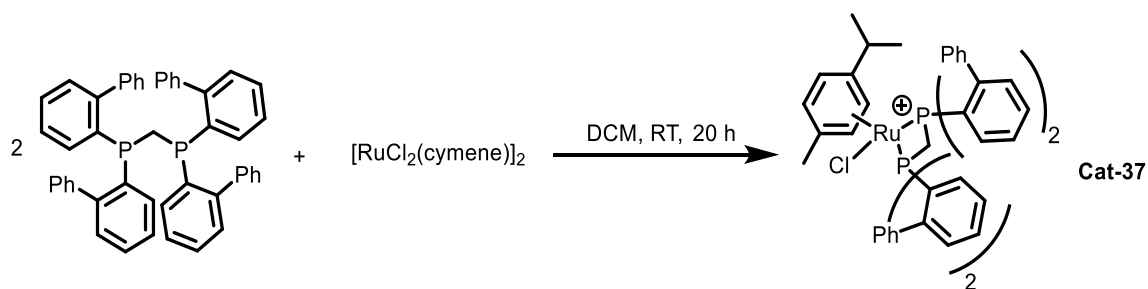
*Scheme 6.7: Synthesis of ruthenium complex **Cat-37**. Chloride counterion omitted for clarity.*

It was hypothesised that the small bite angle of the dppm ligand could lead to the *ortho-*phenyl groups being 'pinned back' and therefore less available to coordinate to the ruthenium if the cymene ligand dissociated. As such, the ethyl-bridged analogue of **L18** was also synthesised using an analogous procedure to that shown in Scheme 6.6 with 1,2-bis(dichlorophosphino)ethane (**L19**). This ligand was then coordinated to ruthenium giving **Cat-38** in a good yield (Scheme 6.8). When dichloromethane was used as the solvent the monodentate species was formed, with the bidentate species **Cat-38** forming after the addition of methanol. While ruthenium bis chelate complexes supported by 1,2-bis(diphenylphosphino)ethane (dppe) ligands have been shown to be largely inactive for both *n*-butanol and *iso*butanol production, the ruthenium half sandwich complexes supported by the same ligand show significantly more activity, albeit at the loss of stability.[1,2,16] Ruthenium complexes supported by dppe ligands are less active than those supported by dppm, although it was predicted that this could be offset by the potential increase in stability over longer reaction times.
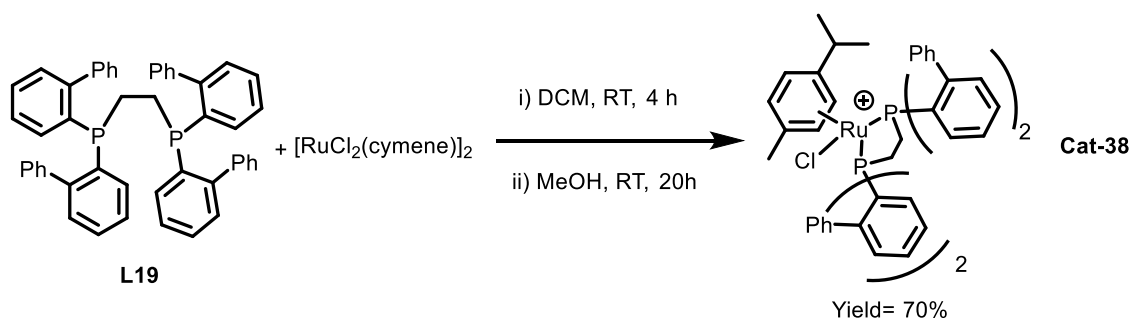
*Scheme 6.8: Synthesis of **Cat-38**. Chloride counterion omitted for clarity.*

The possible issue of the small bite angle of dppm ligands preventing *ortho*-phenyl coordination could also be circumvented by increasing the carbon bridge length between the phenyl group and its *ortho*-substituent. As such, ligand **L20** was also targeted for synthesis. This ligand could potentially increase stability by phenyl coordination, while

maintaining the higher levels of activity achieved with C1 bridging ligands such as dppm. While **L20** was successfully synthesised (Scheme 6.9), only very poor yields were observed (10%). Complexation of **L20** was successful and **Cat-39** was observed by $^{31}P\{^1H\}$ NMR spectroscopy and HR-MS, however, enough pure complex to allow for catalytic testing could not be produced.
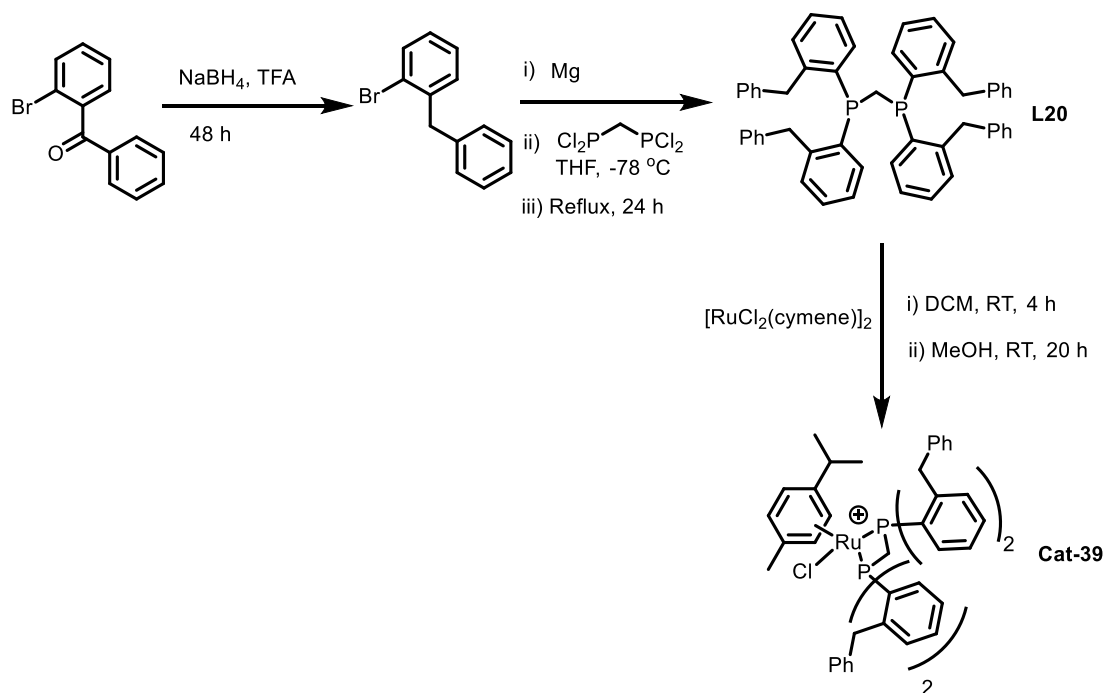
*Scheme 6.9: Synthesis of **L20** and **Cat-39**. Chloride counterion omitted for clarity.*

The effect of heat upon **Cat-37** and **Cat-38** was examined by heating a solution of the complex in toluene in a J. Young's NMR tube, followed by analysis by mass spectrometry (nanospray). After heating for 3 hours, $^{31}P\{^1H\}$ NMR resonances for the complexes **Cat-37** and **Cat-38** are no longer visible, with only a resonance for the free ligand being observed. **Cat-37** displayed a major peak at *m/z*= 825.0 corresponding to the loss of the cymene, with minor peaks for the parent ion and a complex where toluene had replaced the cymene also observed. **Cat-38** displayed a peak at *m/z*= 839.2 corresponding to the loss of cymene, with only a very minor peak for the parent ion, indicating that *ortho*-aromatic coordination may be possible. By contrast, when **Cat-31** (Section 6.2.1) was subjected to the same conditions the major peak observed was for the parent ion, with the peak due to the loss of cymene much smaller. This indicates the potential change in reactivity and stability achieved by *ortho* substitution with an aromatic group. Attempts to cyclometallate **Cat-37** using NEt₃ were unsuccessful, with no sign of reaction observed over 3 days in refluxing methanol.

6.7.1 – Catalytic testing of *ortho*-phenyl substituted diphosphine ligands

Cat-37 and **Cat-38** were used for the production of *iso*butanol under the same conditions as all other previously synthesised complexes (Table 6.3). However, over a 2-hour run time **Cat-37** still decomposed to give a dark brown post reaction mixture indicating that stability had not been improved (Entry 1); attempts to form the active catalyst *in situ* also gave inferior results (Entry 3). Extending run times to 20 hours gave greater *iso*butanol yields (Entry 2), but to no greater extent than that seen using **Cat-31**, indicating that *ortho* phenyl substitution does not improve catalyst stability. **Cat-38** performed similarly to **Cat-37** over 2-hour runtimes (Entry 4), and it was noted that the post reaction mixture was still yellow and largely homogeneous. Over a 20-hour run time *iso*butanol yields of 34% were observed, outperforming all ruthenium half-sandwich complexes supported by substituted dppm based ligands tested over the same run time. However, further work is still required to establish whether this effect is due to the *ortho* aromatic substitution or the extended ligand backbone.

Table 6.3: Production of isobutanol using ruthenium complexes bearing ortho phenyl substituted diphosphine ligands.

Entry[a]	Catalyst	Runtime	EtOH conv (%)	iBuOH yield (%)	iBuOH selectivity (%)[b]	Propanol Yield (%)
1	37	2	35	8	83	1.5
2	37	20	75	18	87	3
3	[RuCl$_2$(cymene)]$_2$ + L18	2	28	4	79	1
4	38	2	29	8	87	1
5	38	20	91	34	96	2

[a] Conditions: 1 mL (17.13 mmol) EtOH, 10 mL MeOH, 180 °C, NaOMe (200 Mol%), 0.1 mol% [Cat], [b] selectivity calculated from observed products in the liquid fraction.

6.8 – Summary

A variety of substituted dppm ligands were synthesised and coordinated to [RuCl$_2$(cymene)]$_2$ producing the corresponding ruthenium-cymene mono chelate complexes. Attempts to form bis chelate complexes with the *ortho* substituted ligands were

unsuccessful due to the increased bulk making coordination challenging. Although, formation of bis chelates from the *meta* and *para* substituted ligands was possible.

The interaction between the cyclometallation agent NEt$_3$ and the mono chelate complexes was studied, while a reaction between the two species does occur, it is not clear what product is formed. It seems unlikely that cyclometallation has occurred given a similar effect is noted with the *meta* substituted complex which is unable to cyclometallate due to the methyl group being too far from the metal centre. All complexes were tested for *iso*butanol production. Here it was noted that the bis chelate complexes vastly outperformed their mono chelate counterparts. *Ortho* substitution also led to a less effective catalyst and the addition of NEt$_3$ to the reaction mixture made little difference to overall yields. Cyclometallation of the precatalyst under catalysis like reaction conditions does not appear to be possible, with the monochelate complexes being too unstable. Substitution of the dppm ligand in the *meta* and *para* positions also makes little difference to catalytic performance. Attempts to pre-form the cyclometallated complexes to confirm the effect this has on catalytic performance were unfortunately unsuccessful.

Synthesis and complexation of an *ortho*-phenyl substituted dppm ligand was possible. However, this displayed no superior reactivity or stability when compared to the *ortho*-tolyl complex **Cat-31**. Extension of the ligand backbone, along with *ortho* phenyl substitution did give a more stable catalyst, with higher *iso*butanol yields observed over 20 hours. However, it is currently unclear if this is due to the phenyl substitution or just the backbone extension.

6.9 – Future work

Ortho substituted dppm ligands do not outperform their unsubstituted analogues or show any increased stability under reaction conditions, even when attempts to induce cyclometallation are made. It seems likely that this is due to a lack of formation of the cyclometallated complexes under reaction conditions. Further work is required to find a method to successfully cyclometallate sp^3 carbons on bidentate ligands in ruthenium cymene complexes. Then the cyclometallated complexes **Cat-31b** and **Cat-32b** can be pre-formed and tested for catalysis. This would then establish whether cyclometallation has a positive effect upon catalyst stability.

Given the greater *iso*butanol yields **Cat-38** produced over a 20-hour run, *ortho* aromatic substituted diphosphine ligands merit further investigation. Successfully synthesising sufficient amounts of **Cat-39** for catalytic testing would aid in establishing whether it is the *ortho* substitution or the elongated ligand backbone that is responsible for the increased stability of **Cat-38**. Testing the unsubstituted dppe ligand over longer run times would also aid in this investigation.

Ortho substitution has shown little promise in increasing either complex stability or activity, with bulky substituents being detrimental to catalytic performance. Thus far the focus has been on altering the steric bulk of the ligand, with little attention paid to tuning the electronics. Increasing or decreasing the electron donor properties of the ligand could aid in increasing ligand-metal bonding strength, thus leading to a more stable complex. Below (Figure 6.6), two ligands with electron donating (**6.4**) and electron withdrawing (**6.5**) phenyl substituents have been suggested. Synthesising these ligands and coordinating them to [RuCl$_2$(cymene)]$_2$ would help to establish whether electronics can also play a role in increasing complex stability.
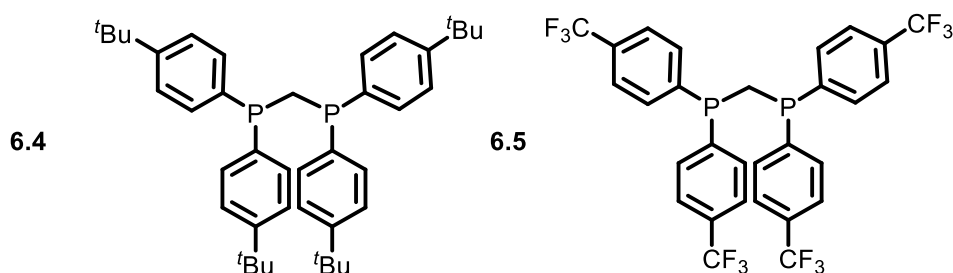
*Figure 6.6: Diphosphine ligands electron donating (**6.4**) and electron withdrawing (**6.5**) para substituents.*

While the *meta* and *para* substituted complexes outperformed their *ortho* analogues, these complexes showed no greater activity than complexes containing unsubstituted dppm ligands. These ligands were also time consuming and expensive to synthesise, whereas unsubstituted dppm is commercially available. As such, these ligands and complexes are of little interest for future biofuels work and thus require little further research. Although, it is possible that while these ligands do not outperform dppm on ruthenium, they may be more effective when used with other metals such as manganese.

6.11 – Full thesis summary

This thesis has established the use of **Cat-5** in the functionalisation of triglycerides towards β-methylated alcohols and shown that this system can be used for the functionalisation of complex mixtures of fatty acid chains. Glycerol by-products can be removed from these reactions in the solid by-product. However, the requirement for high base loadings is still an issue.

Manganese catalysts supported by bidentate ligands have been shown to act as catalysts for the Guerbet reaction, albeit over significantly longer runtimes than their tridentate and ruthenium analogues.

Rhenium catalysts supported by tridentate ligands are also effective for *iso*butanol production from methanol and ethanol. However, these complexes suffer from poor overall selectivity, instead favouring alcohol dehydrogenation. Using rhenium bischelate complexes supported by phosphinoamine ligands helps to alleviate this issue, although these catalysts are not as active. Overall rhenium complexes significantly outperform their manganese analogues.

Cat-1 is active for the coupling of higher alcohols as well as ethanol. However, as the alkyl chain length increased the post reaction mixture becomes a solid mass, making work-up and analysis challenging. **Cat-4** is active for this conversion as well, but its selectivity drops rapidly with alkyl chain length.

Ortho substituted ruthenium-cymene dppm complexes show no increase in stability over their unsubstituted analogues. It appears that cyclometallation of these complexes is far more challenging than their monodentate analogues as well. *Ortho*-aryl substitution has shown some potential, however, more work is required to establish the cause of this.
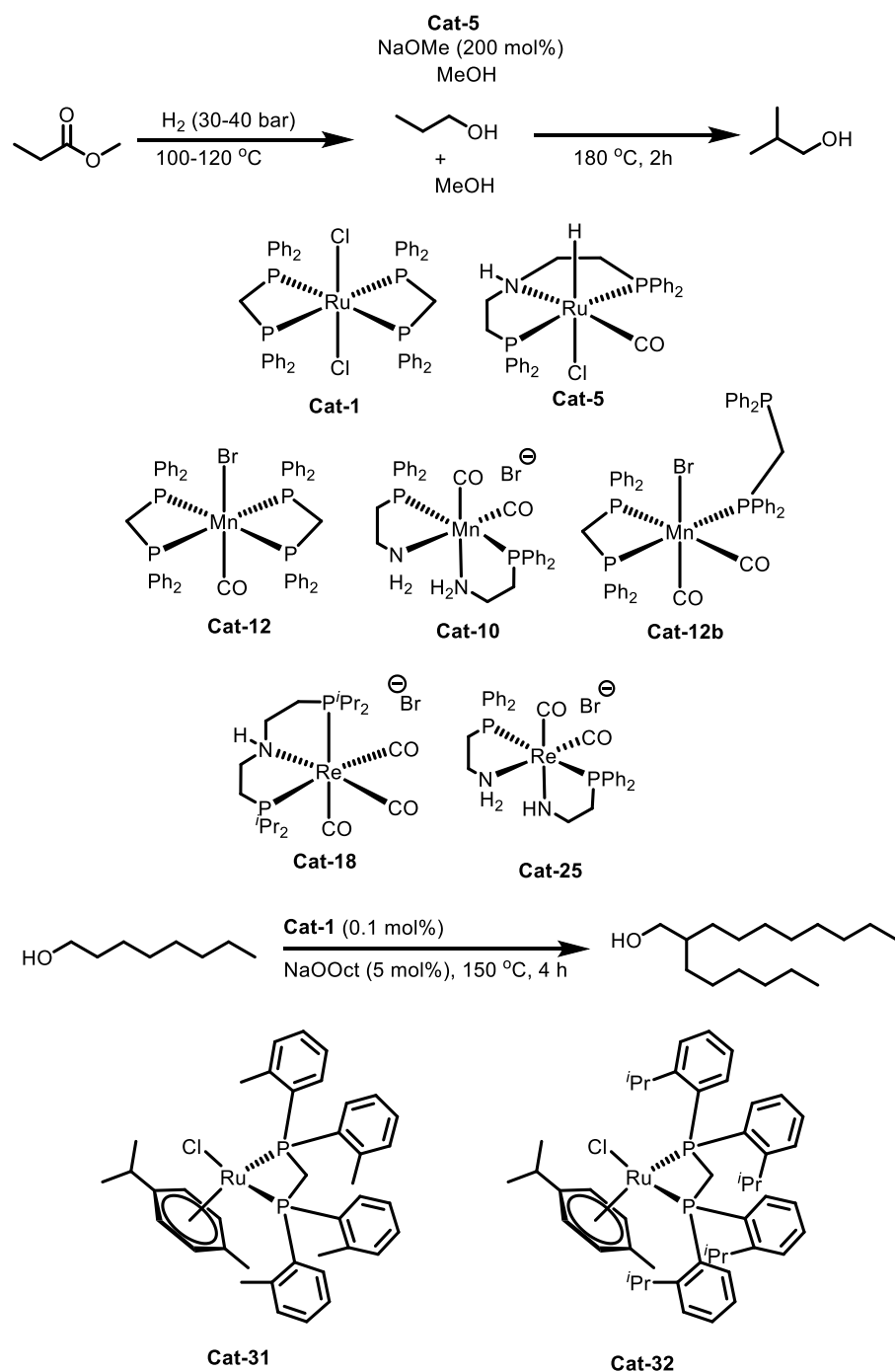
Figure 6.7: Relevant catalysts and reactions to this thesis.

6.10 – References

1   G. R. M. Dowson, M. F. Haddow, J. Lee, R. L. Wingad and D. F. Wass, *Angew. Chem. Int. Ed.*, 2013, **52**, 9005–9008.

2   *K. Pellow, Unpublished results, University of Bristol*, 2015.

3   T. J. Geldbach, P. S. Pregosin and A. Albinati, *Organometallics*, 2003, **22**, 1443–1451.

4   G. Venkatachalam, R. Ramesh and S. M. Mobin, *J. Organomet. Chem.*, 2005, **690**,

3937–3945.

5   P. Diversi, G. Ingrosso, A. Lucherini, F. Marchetti, V. Adovasio and M. Nardelli, *J. Chem. Soc., Dalton Trans.*, 1991, 203–213.

6   N. U. Din Reshi, D. Senthurpandi and A. G. Samuelson, *J. Organomet. Chem.*, 2018, **866**, 189–199.

7   R. Sun, X. Chu, S. Zhang, T. Li, Z. Wang and B. Zhu, *Eur. J. Inorg. Chem.*, 2017, **2017**, 3174–3183.

8   W. Baratta, P. Da Ros, A. Del Zotto, A. Sechi, E. Zangrando and P. Rigo, *Angew. Chem. Int. Ed.*, 2004, **43**, 3584–3588.

9   S. Giboulot, S. Baldino, M. Ballico, H. G. Nedden, D. Zuccaccia and W. Baratta, *Organometallics*, 2018, **37**, 2136–2146.

10   P. Piehl, R. Amuso, E. Alberico, H. Junge, B. Gabriele, H. Neumann and M. Beller, *Chem. Eur. J.*, 2020, **26**, 6050–6055.

11   S. B. Jensen, S. J. Rodger and M. D. Spicer, *J. Organomet. Chem.*, 1998, **556**, 151–158.

12   C. Daguenet, R. Scopelliti and P. J. Dyson, *Organometallics*, 2004, **23**, 4849–4857.

13   R. A. Baber, A. G. Orpen, P. G. Pringle, M. J. Wilkinson and R. L. Wingad, *Dalton Trans.*, 2005, 659–667.

14   M. Al-Noaimi, I. Warad, O. S. Abdel-Rahman, F. F. Awwadi, S. F. Haddad and T. B. Hadda, *Polyhedron*, 2013, **62**, 110–119.

15   J. Chatt and R. G. Hayter, *J. Chem. Soc.*, 1961, 896–904.

16   R. L. Wingad, E. J. E. Bergström, M. Everett, K. J. Pellow and D. F. Wass, *Chem. Commun.*, 2016, **52**, 5202–5204.

17   F. Cocco, A. Zucca, S. Stoccoro, M. Serratrice, A. Guerri and M. A. Cinellu, *Organometallics*, 2014, **33**, 3414–3424.

18   L. Rafols, S. Torrente, D. Aguilà, V. Soto-Cerrato, R. Pérez-Tomás, P. Gamez and A. Grabulosa, *Organometallics*, 2020, **39**, 2959–2971.

19   J. W. Faller and D. G. D'Alliessi, *Organometallics*, 2003, **22**, 2749–2757.

20   F. Varga, C. Rajnák, J. Titiš, J. Moncoľ and R. Boča, *Dalton Trans.*, 2017, **46**, 4148–4151.

Chapter 7: Experimental

7.1 – General Considerations

Unless otherwise stated all procedures were conducted under an inert (N_2) atmosphere using standard Schlenk line techniques, or in an inert glovebox under an Ar atmosphere. All glassware was dried in a 200 °C oven for at least an hour before use. Common solvents (MeCN, Et_2O, toluene, DCM, THF and hexane) were obtained from a Grubbs type purification system and degassed by sparging with N_2 before use. Methanol and ethanol were purchased from Acros Organics and were kept over 3 Å molecular sieves in an inert atmosphere and degassed by sparging before use. When required, other solvents (eg. benzene) were dried over CaH_2, purified by vacuum transfer, and degassed by sparging before use. Deuterated solvents were purchased from Sigma Aldrich and were kept over 3 Å molecular sieves in an inert atmosphere and degassed by freeze-pump-thaw techniques before use. Unless otherwise stated all chemicals were purchased from Sigma Aldrich, Alfa Aesar or Fisher and used without further purification. Supplier information about chemicals used in specific chapters is given in their experimental section. H_2 research grade reagent gas was purchased from BOC and used without further purification. Unless otherwise stated all catalytic experiments were conducted in a 100 mL Parr stainless steel autoclave. Separate PTFE inserts were used for catalytic runs using different metals to avoid cross contamination. These were then immersed in sodium hypochlorite for at least 1 hour, before being washed thoroughly with distilled water and acetone and then dried in a 70 °C oven after use.

All NMR spectra were recorded on Jeol ECS300, Jeol ECS400, Jeol ECZ400, Bruker Avance 500 MHz, Bruker DPZ 400 MHz or Varian 500a spectrometers. All ^1H and ^{13}C NMR chemical shifts were reported in ppm relative to the deuterated solvent. ^{31}P NMR are referenced relative to 85% H_3PO_4 external standard. HR-MS analysis (nanospray) was conducted on a Waters Synapt G2S spectrometer. Solid state infrared (IR) spectroscopic data was recorded on a Perkin-Elmer FT-IR instrument as solid samples in air. X-ray diffraction experiments were carried out at 100(2) K on a Bruker APEX II diffractometer using Mo-K$_\alpha$ radiation (λ= 0.71073 Å). Catalytic results were analysed using GC-FID on an Agilent 7820A GC equipped with a carbowax capillary column 30 m x 0.32 mm, I.D. 0.25 μm. Method: Starting oven

temp 60 °C, hold at 70 °C for 5 min, heat to 220 °C at 40 °C/min, hold at 220 °C for 5 min, total run time ~ 14 min.

Ligands **L1, L2, L3** and **L9** (10 wt% solution in THF) along with **Cat-5** and **Cat-6** were purchased from Sigma Aldrich and used without further purification.

7.2 – Chapter 2 Experimental

Octanol, trilaurin, 1-hexene, 2-hexene, Ru/C (5 wt%) and copper chromite were purchased from Sigma Aldrich and used without further purification. Methyl propanoate, propanol, tripropionin, ethyl acetate and glyceryl trioctanoate were purchased from Sigma Aldrich and stored over 4 Å molecular sieves under a nitrogen atmosphere.

Cat-11 was kindly supplied by Dr Alex Riley and had been prepared according to a literature procedure.[1] **Cat-4**[2] and **Cat-1**[3] were prepared according to literature procedures.

7.2.1 – General procedure for methyl propanoate hydrogenation

Cat-5 (6.3 mg, 0.01038 mmol, 0.1 mol%) and sodium methoxide (1.12 g, 20.77 mmol, 200 mol%) were added to a clean, oven-dried, fitted PTFE insert equipped with a stirrer bar. The autoclave was sealed and put under an inert (N_2) atmosphere. Methanol (10 mL) was injected into the autoclave through an inlet, against a flow of nitrogen, followed by methyl propanoate (1 mL, 10.38 mmol). The autoclave was resealed and charged with H_2 (40 bar) and then placed into a pre-heated (100 °C) aluminium heating mantle for 16 h. After the reaction run time, the autoclave was cooled in an ice-water bath. The autoclave was vented slowly to remove excess H_2. A liquid sample was removed, filtered through a short plug of acidic alumina, and analysed by GC (100 μL of sample, 25 μL of hexadecane standard, 1 mL Et_2O).

7.2.2 – General procedure for the conversion of propanol to *iso*butanol

Cat-5 (8.12 mg, 0.01338 mmol 0.1 mol%) and sodium methoxide (1.45 g, 26.76 mmol, 200 mol%) were added to a clean, oven-dried, fitted PTFE insert equipped with a stirrer bar. The autoclave was sealed and put under an inert (N_2) atmosphere. Methanol (10 mL) was injected into the autoclave through an inlet, against a flow of nitrogen, followed by propanol (1 mL, 13.38 mmol). The autoclave was resealed and placed into a pre-heated (180 °C) aluminium heating mantle for 2 h. After the reaction run time, the autoclave was cooled to in an ice-water bath. The autoclave was vented to remove any gas generated

during the reaction. A liquid sample was removed, filtered through a short plug of acidic alumina, and analysed by GC (100 μL of sample, 25 μL of hexadecane standard, 1 mL Et$_2$O).

7.2.3 – General procedure for the formation of *iso*butanol from methyl propanoate

Method A: Cat-5 (6.3 mg, 0.01038 mmol, 0.1 mol%) and sodium methoxide (1.12 g, 20.77 mmol, 200 mol%) were added to a clean, oven-dried, fitted PTFE insert equipped with a stirrer bar. The autoclave was sealed and put under an inert (N$_2$) atmosphere. Methanol (10 mL) was injected into the autoclave through an inlet, against a flow of nitrogen, followed by methyl propanoate (1 mL, 10.38 mmol). The autoclave was resealed, charged with H$_2$ (30 bar) and placed into a pre-heated (180 °C) aluminium heating mantle for 16 h. After the reaction run time, the autoclave was cooled in an ice-water bath. The autoclave was slowly vented to remove excess H$_2$. A liquid sample was removed, filtered through a short plug of acidic alumina, and analysed by GC (100 μL of sample, 25 μL of hexadecane standard, 1 mL Et$_2$O).

Method B: Cat-5 (6.3 mg, 0.01038 mmol, 0.1 mol%) and sodium methoxide (1.12 g, 20.77 mmol, 200 mol%) were added to a clean, oven-dried, fitted PTFE insert equipped with a stirrer bar. The autoclave was sealed and put under an inert (N$_2$) atmosphere. Methanol (10 mL) was injected into the autoclave through an inlet against a flow of nitrogen followed by methyl propanoate (1 mL, 10.38 mmol). The autoclave was resealed, charged with H$_2$ (40 bar) and placed into a pre-heated (100 °C) aluminium heating mantle for 16 h. After the reaction run time, the autoclave was cooled in an ice-water bath, reattached to a Schlenk line and slowly vented to remove excess H$_2$, and a small liquid sample removed for analysis before resealing. The autoclave was then placed in a preheated (180 °C) aluminium heating mantle for 2 h. After the reaction run time, the autoclave was cooled in an ice-water bath. A liquid sample was removed, filtered through a short plug of acidic alumina, and analysed by GC (100 μL of sample, 25 μL of hexadecane standard, 1 mL Et$_2$O).

7.2.4 – General procedure for the conversion of tripropionin to *iso*butanol

Method A: Cat-5 (7.56 mg, 0.0125 mmol, 0.3 mol%) and sodium methoxide (1.35 g, 24.9 mmol, 600 mol%) were added to a clean oven-dried fitted PTFE insert equipped with a stirrer bar. The autoclave was sealed and put under an inert (N$_2$) atmosphere. Methanol (10 mL) was injected into the autoclave through an inlet, against a flow of nitrogen, followed by tripropionin (1 mL, 4.15 mmol). The autoclave was resealed and stirred at room

temperature for 10 minutes. It was then charged with H_2 (30 bar) and placed into a pre-heated (180 °C) aluminium heating mantle for 17 h. After the reaction run time, the autoclave was cooled in an ice-water bath. The autoclave was slowly vented to remove excess H_2. A liquid sample was removed, filtered through a short plug of acidic alumina, and analysed by GC (100 μL of sample, 10 μL of hexadecane standard, 1.7 mL Et_2O).

Method B: Cat-5 (7.56 mg, 0.0125 mmol, 0.3 mol%) and sodium methoxide (1.35 g, 24.9 mmol, 600 mol%) were added to a clean oven-dried fitted PTFE insert equipped with a stirrer bar. The autoclave was sealed and put under an inert (N_2) atmosphere. Methanol (10 mL) was injected into the autoclave through an inlet, against a flow of nitrogen, followed by tripropionin (1 mL, 4.15 mmol). The autoclave was resealed and stirred at room temperature for 45 minutes. It was then charged with H_2 (40 bar) and placed into a pre-heated (100 °C) aluminium heating mantle for 16 h. After the reaction run time, the autoclave was cooled in an ice-water bath, reattached to a Schlenk line, slowly vented to remove excess H_2, then sealed again. The autoclave was then placed in a preheated (180 °C) aluminium heating mantle for 2 h. After the reaction run time, the autoclave was cooled in an ice-water bath. A liquid sample was removed, filtered through a short plug of acidic alumina, and analysed by GC (100 μL of sample, 10 μL of hexadecane standard, 1.7 mL Et_2O).

7.2.5 – Attempted hydrogenation of tripropionin with Cat-1

Cat-1 (11.7 mg, 0.0125 mmol, 0.3 mol%) and sodium methoxide (1.35 g, 24.9 mmol, 600 mol%) were added to a clean oven-dried fitted PTFE insert equipped with a stirrer bar. The autoclave was sealed and put under an inert (N_2) atmosphere. Methanol (10 mL) was injected into the autoclave through an inlet, against a flow of nitrogen, followed by tripropionin (1 mL, 4.15 mmol). The autoclave was resealed and stirred at room temperature for 1 hour, to allow for transesterification. It was then charged with H_2 (40 bar) and placed into a pre-heated (100 °C) aluminium heating mantle for 17 h. After the reaction run time, the autoclave was cooled in an ice-water bath, and all remaining H_2 slowly vented. A liquid sample was removed, filtered through a short plug of acidic alumina, and analysed by GC (100 μL of sample, 10 μL of hexadecane standard, 1.7 mL Et_2O).

7.2.6 – General procedure using a dual catalysts system

As for '7.2.4 – General procedure for the conversion of tripropionin to *iso*butanol', method B above, except **Cat-1** (11.7 mg, 0.0125 mmol, 0.3 mol%) was added to the autoclave at the beginning of the reaction, alongside **Cat-5** and NaOMe.

7.2.7 – *Iso*butanol formation from ethyl acetate

As for 7.2.3 – method B above, except ethyl acetate (1 mL, 10.2 mmol) was added to the autoclave instead of tripropionin. **Cat-5** (6.2 mg, 0.0102 mmol, 0.1 mol%), **Cat-1** (9.6 mg, 0.0192 mmol, 0.1 mol%) and NaOMe (1.106 g, 200 mol%) were used.

7.2.8 – General procedure of methanol-octanol heterocoupling

Ruthenium complex (0.0063 mmol, 0.1 mol%) and sodium methoxide (0.68 g, 12.65 mmol, 200 mol%) were added to a clean, oven-dried, fitted PTFE insert equipped with a stirrer bar. The autoclave was sealed and put under an inert (N_2) atmosphere. Methanol (10 mL) was injected into the autoclave through an inlet against, a flow of nitrogen, followed by octanol (1 mL, 6.37 mmol). The autoclave was resealed and placed into a pre-heated (180 °C) aluminium heating mantle for 2 h. After the reaction run time, the autoclave was cooled in an ice-water bath. The autoclave was vented to remove any gas generated during the reaction. A liquid sample was removed, filtered through a short plug of acidic alumina, and analysed by GC (100 μL of sample, 10 μL of hexadecane standard, 1.7 mL Et_2O).

7.2.9 – General procedure for the conversion of glyceryl trioctanoate to β-methylated alcohol

As for '7.2.4 – General procedure for the conversion of tripropionin to *iso*butanol' method B. Low concentration: Glyceryl trioctanoate (1 mL, 2.03 mmol), **Cat-5** (3.7 mg, 0.0061 mmol, 0.3 mol%), NaOMe (0.658 g, 12.19 mmol, 600 mol%) used. High concentration: Glyceryl trioctanoate (2.81 mL, 5.71 mmol), **Cat-5** (10.4 mg, 0.0171 mmol, 0.3 mol%), NaOMe (1.85 g, 34.25 mmol, 600 mol%) used. Post reaction mixture was neutralised with 1 M HCl, extracted with toluene and analysed by GC-MS.

7.2.10 – General procedure for the conversion of trilaurin to β-methylated alcohol

As for '7.2.4 – General procedure for the conversion of tripropionin to *iso*butanol' method B, except trilaurin was added into the autoclave at the same time as catalyst and base. Low concentration: Trilaurin (2.65 g, 4.14 mmol), **Cat-5** (7.6 mg, 0.0125 mmol, 0.3 mol%),

NaOMe (1.345 g, 24.89 mmol, 600 mol%) used. High concentration: Trilaurin (3.65 g, 5.71 mmol), **Cat-5** (10.4 mg, 0.0171 mmol, 0.3 mol%), NaOMe (1.85 g, 34.25 mmol, 600 mol%) used. Post reaction mixture was neutralised with 1 M HCl, extracted with toluene and analysed by GC-MS.

7.2.11 – General procedure for the hydrogenation of alkenes

Cat-5 (9.71 mg, 0.016 mmol, 0.1 mol%) and sodium methoxide (1.73 g, 31.99 mmol, 200 mol%) were added to a clean, oven-dried, fitted PTFE insert equipped with a stirrer bar. The autoclave was sealed and put under an inert (N_2) atmosphere. Methanol (10 mL) was injected into the autoclave through an inlet, against a flow of nitrogen, followed by 1-hexene (2 mL, 16 mmol). The autoclave was resealed and charged with H_2 (40 bar) and then placed into a pre-heated (100 °C) aluminium heating mantle for 18 h. After the reaction run time, the autoclave was cooled in an ice-water bath. The autoclave was vented slowly to remove excess H_2. A liquid sample was removed and filtered before being diluted with d^4-methanol and analysed by ^1H NMR spectroscopy. Hydrogenation of 2-hexene attempted with 0.2 mol% **Cat-5** and 400 mol% base.

7.2.12 – General procedure for formation of β-methylated alcohols from methyl oleate

As for '7.2.3 – General procedure for the formation of *iso*butanol from methyl propanoate, method B' except methyl oleate (2 mL, 5.9 mmol), **Cat-5** (3.6 mg, 0.0059 mmol) and NaOMe (0.64 g, 11.79 mmol) was used. Post reaction mixture was neutralised with 1 M HCl, extracted with toluene and analysed by GC-MS.

7.2.13 – General procedure for formation of β-methylated alcohols from coconut oil

As for '7.2.4 – General procedure for the conversion of tripropionin to *iso*butanol, method B' except coconut oil (2.65 g, 4.15 mmol), **Cat-5** (0.0075 mg, 0.01245 mmol) and NaOMe (1.35 g, 24.89 mmol) was added to the autoclave at the same time as the catalyst and base. Post reaction mixture was neutralised with 1 M HCl, extracted with toluene and analysed by GC-MS.

7.2.14 – General procedure for *iso*butanol production using a heterogeneous catalyst

As for '7.2.4 – General procedure for the conversion of tripropionin to *iso*butanol' method B.

7.2.15 – General procedure for the neat hydrogenation of triglycerides

Cat-5 (37 mg, 0.061 mmol, 0.3 mol%) and sodium methoxide (0.1646 g, 3 mmol, 15mol%) were added to a clean, oven-dried, fitted PTFE insert equipped with a stirrer bar. The autoclave was sealed and put under an inert (N_2) atmosphere. Glyceryl trioctanoate (10 mL, 20.3 mmol) was injected into the autoclave through an inlet, against a flow of nitrogen. The autoclave was resealed, charged with H_2 (40 bar) and then placed into a pre-heated (100 °C) aluminium heating mantle for 18 h. After the reaction run time, the autoclave was cooled in an ice-water bath and vented slowly to remove excess H_2. A liquid sample was removed, filtered through a short plug of acidic alumina, and analysed by GC (100 µL of sample, 10 µL of hexadecane standard, 1.7 mL Et_2O).

7.2.16 – Interaction of Cat-5 with base and tripropionin

A solution of NaOMe (0.3382 g, 6.26 mmol) in methanol (3 mL) was added to a stirred suspension of **1** (0.038 g, 0.063 mmol) in methanol (7 mL). This was stirred at room temperature for 1 hour before being analysed by $^{31}P\{^1H\}$ NMR spectroscopy. Tripropionin (1 mL) was added and the mixture stirred at room temperature for a further hour before being analysed again by $^{31}P\{^1H\}$ and ^1H NMR spectroscopy.

7.2.17 – Solid analysis – pre reaction

Sodium methoxide (0.675 g, 12.5 mmol), was dissolved in methanol (5 mL) with stirring. To this solution, tripropionin (0.5 mL) was added. The mixture was allowed to stir at room temperature for 1 hr. The white solid produced was isolated by filtration, dried *in vacuo,* and analysed by ^1H NMR spectroscopy.

7.2.18 – Solid analysis – post reaction

The post reaction mixture (Table 2.4, Entry 5), was isolated by Büchner filtration and washed with toluene (50 mL). the white solid was dried *in vacuo* for 1 hour before being weighed (0.72 g). ^1H and $^{13}C\{^1H\}$ NMR analysis was undertaken in D_2O.

7.2.19 – Production of sodium glyceroxide

Glycerol (6.14 mL, 7.7 g, 83.3 mmol) and 90% dry NaH (2 g, 83 mmol) were both weighed into separate Schlenk flasks, THF (50 mL) was added to each flask. The suspension of NaH in THF was added slowly to the glycerol solution, with stirring. Care was taken to avoid excess bubbling, as the reaction was highly exothermic. The Schlenk flask containing the

NaH was washed through with more THF (25 mL). The reaction mixture was allowed to stir at room temperature for 18 hours before the THF was removed *in vacuo* leaving a grey/white solid (Yield= 7.79 g, 68.3 mmol, 82.3%).

7.3 – Chapter 3 Experimental

Mn(CO)$_5$Br was purchased from Sigma Aldrich and used without further purification. Bis(diphenylphosphino)amine,[4] 2-(diphenylphosphino)ethylamine,[5] **Cat-7**,[6] **12**,[7] **12b**,[8] **13**,[7] **9**,[9] **10**,[9] **16**,[10] and **17**[11] were synthesised according to literature procedures.

7.3.1 – Catalyst synthesis

7.3.1.1 – Synthesis of Cat-10b (*trans*-[Mn(CO)$_2$(dppea)$_2$]Br)

Diphenylphosphinoethylamine (0.2 g, 0.872 mmol) and Mn(CO)$_5$Br (0.1 g, 0.364 mmol) were both separately dissolved in benzene (3.5 mL). The ligand solution was added dropwise to the manganese precursor solution at room temperature, and then washed through with 1 mL benzene. Reaction mixture was covered with foil and irradiated with long wave UV light for 2 days, after which a deep red solution had formed. The sample was recrystalised from benzene (2.5 ml) and ethanol (35 mL). This gave dark red crystals that were isolated by filtration and dried *in vacuo* (Yield= 0.0393 g, 0.061 mmol, 17.4%). Single crystals for use in X-ray diffraction were grown using the above method.

^{31}P{^{1}H} NMR (122 MHz, CD$_2$Cl$_2$): (δ, ppm) 89.2

^{1}H NMR (400 MHz, CD$_2$Cl$_2$): (δ, ppm) 7.28-7.15 (br, s, 5H) 7.14-6.99 (br, s, 5H) 2.62-2.32 (br, s, 4H, (CH$_2$)$_2$) 1.40-1.25 (br, s, 2H, NH$_2$)

HR MS (Nanospray): m/z calc for [M]$^+$ C$_{30}$H$_{32}$MnN$_2$O$_2$P$_2$ 569.1320 Found 569.1322 (0.4 ppm)

IR (ν, cm-1) 1869

7.3.1.2 – Synthesis of Cat-14 (MnBr(CO)$_3$(dppa))

Bis(diphenylphosphino)amine (0.147 g, 0.382 mmol) and Mn(CO)$_5$Br (0.1 g, 0.364 mmol) were dissolved separately in toluene (6.5 mL). The ligand solution was then added dropwise to the Mn precursor solution and washed through with 3 mL toluene; this was left stirring at room temperature for 10 minutes. The solution was then heated to 120 °C overnight.

The solution was then filtered and solvent removed *in vacuo*. The resulting powder was washed with hexane (3 x 6 mL) giving a yellow power (Yield= 0.1410 g, 0.23 mmol, 67.22%).

$^{31}P\{^1H\}$ NMR (122 MHz, CDCl$_3$): (δ, ppm) 82.53

^1H NMR (300 MHz, CDCl$_3$): (δ, ppm) 7.65-7.26 (br, m, 20H), 4.91 (v br, s, 1H, NH)

HR MS (Nanospray): m/z calc for [M-Br]$^+$ C$_{27}$H$_{21}$MnNO$_3$P$_2$ 524.0377 Found 524.0387 (1.9 ppm)

IR (ν, cm-1) 2021, 1951, 1905

7.3.1.3 – Synthesis of Cat-15 ([*trans*-Mn(CO)$_2$(dppa)$_2$]Br)

Bis(diphenylphosphino)amine (0.62 g, 1.61 mmol) and Mn(CO)$_5$Br (0.2 g, 0.728 mmol) were dissolved separately in toluene (7 mL). The ligand was then added dropwise to the Mn precursor and washed through with 3 mL toluene; this was left stirring at room temperature for 10 minutes. The solution was then heated to 120 °C for 5 hrs. The solution was then filtered and left for 7 days at room temperature, over this time orange crystals began to form. **Cat-15** was isolated by filtration and dried *in vacuo* giving orange solid (Yield= 0.0460 g, 0.048 mmol, 6.6%). Single crystals for use in X-ray diffraction were grown by layering a DCM solution with pentane.

$^{31}P\{^1H\}$ NMR (122 MHz, CDCl$_3$): (δ, ppm) 104.93

^1H NMR (300 MHz, CDCl$_3$): (δ, ppm) 7.31-7.26 (br, m, 10H), 7.22-7.14 (br, m, 30H) , 5.14 (br, s, 2H, NH)

HR MS (Nanospray): m/z calc for [M-Br]$^+$ C$_{50}$H$_{42}$MnN$_2$O$_2$P$_4$ 881.1577 Found 881.1579 (0.2 ppm)

IR (ν, cm-1) 1839

7.3.2 – Catalysis

Catalytic reactions were carried out in a 100 mL Parr stainless steel autoclave with aluminium heating mantle and using magnetic stirring.

7.3.2.1 – General catalytic procedure- *iso*butanol formation

A manganese complex (0.017 mmol, 0.1 mol%) and sodium methoxide (1.85 g, 34.26 mmol, 200 mol%) were added to a clean oven-dried fitted PTFE insert equipped with a stirrer bar in a glove box. The autoclave was sealed in a glove box and then put under a nitrogen atmosphere on a Schlenk line. Methanol (10 mL) was injected into the autoclave through an inlet against a flow of nitrogen followed by ethanol (1 mL, 17.13 mmol). The autoclave was sealed and placed into the pre-heated (180 °C) aluminium heating mantle for 90 h. After the reaction run time, the autoclave was cooled to room temperature in an ice-water bath. The autoclave was vented to remove any gas generated during the reaction. A liquid sample was removed, filtered through a short plug of acidic alumina and analysed by GC (100 μL of sample, 10 μL of hexadecane standard, 1.7 mL Et_2O).

7.3.2.2 – General catalytic procedure- *n*-butanol formation

A manganese complex and sodium ethoxide (1.17 g, 17.19 mmol, 10 mol%) were added to a clean oven-dried fitted PTFE insert equipped with a stirrer bar in a glove box. The autoclave was sealed in a glove box and then put under a nitrogen atmosphere on a Schlenk line. Ethanol (10 mL) was injected into the autoclave through an inlet against a flow of nitrogen. The autoclave was sealed and placed into the pre-heated (150 °C) aluminium heating mantle for 90 h. After the reaction run time, the autoclave was cooled to room temperature in an ice-water bath. The autoclave was vented to remove any gas generated during the reaction. A liquid sample was removed, filtered through a short plug of alumina (acidic) and analysed by GC (100 μL of sample, 10 μL of hexadecane standard, 1.7 mL Et_2O).

7.3.2.3 – Catalyst and base NMR studies- Cat-12

Cat-12 (0.005 g, 0.005 mmol) was added to an NMR tube in a glovebox, this was then suspended in MeOH (1 mL), an excess of NaOMe was then added, and the subsequent suspension analysed by $^{31}P\{^1H\}$ NMR spectroscopy. This solution was then re-examined after 3 days.

7.3.2.4 – Catalyst and base NMR studies- Cat-12b

Cat-12b (0.019 g, 0.02 mmol) was added to an NMR tube in a glovebox, this was then suspended in MeOH (1 mL), an excess of NaOMe was then added, upon which all the solid

dissolved, this solution was analysed by $^{31}P\{^1H\}$ NMR spectroscopy. This solution was then re-examined after 3 days.

7.3.3 – Solid product analysis

Post reaction mixture was filtered by Büchner filtration to isolate the solid product. This was washed with toluene (3 x 5 mL), giving a fine brown solid which was then dried under vacuum for 1 hour. The sample was weighed, and a small amount was dissolved in D_2O before analysis by ^1H and $^{13}C\{^1H\}$ NMR spectroscopy.

7.4 – Chapter 4 Experimental

$Re(CO)_5Br$, bis[2-(ditertbutylphosphino)ethyl]amine solution (10 wt% in THF) (**L10**), bis[(2-diphenylphosphino)ethyl]ammonium chloride (**L11**.HCl), bis(3,5-di(trifluoromethyl)phenyl)phosphine, bis(2-chloroethyl)amine hydrochloride and 3-(diphenylphosphino)propylamine (**L13**) were purchased from Sigma Aldrich and used without further purification.

2-(diphenylphosphino)ethylamine,[5] **Cat-18**,[12] **Cat-20**,[13] **3.4**,[14] **L12**,[15] **Cat-22**,[16] **Cat-23**[17] and **Cat-26**[18] were produced *via* literature procedures. 2-(diphenylphosphino)-N-methylethylamine (**L5**) was kindly supplied by Dr H. Aitchison and was prepared by a modified literature proccdure.[5] 2-(diphenylphosphino)-N,N-dimethylethylamine (**L6**) was prepared *via* a modified literature procedure.[5]

7.4.1 – Catalyst synthesis
7.4.1.1 – Synthesis of Cat-19 ([(Re(CO)$_3$(PNP^{Ph})]Br)

Bis[(2-diphenylphosphino)ethyl]ammonium chloride (0.1 g) was suspended in toluene (4 mL) in a round bottom flask. NaOH (10 wt% in water) was added sequentially while stirring until all starting material has dissolved. The aqueous layer was then removed, and the organic layer washed with distilled water (3 x 2 mL) and dried over sodium sulphate. Toluene was removed *in vacuo* giving bis[(2-diphenylphosphino)ethyl]amine as a clear oil.

[Re(CO)$_3$(H$_2$O)$_3$]Br (0.081 g, 0.2 mmol) was measured out in a Schlenk flask and suspended in dichloromethane (2 mL). The ligand was dissolved in DCM (4 mL) and added dropwise to the complex while stirring, the Schlenk was then washed through with DCM (2 mL). The suspension was heated to 40 °C for 18 hours, giving a clear oil and a fine grey suspension.

The solution was filtered and reduced in volume by approx. 50% and triturated with pentane giving a file white powder. This was isolated by filtration and dried *in vacuo* (Yield= 0.072 g, 0.091 mmol, 45.5%). The NMR data was consistent with the literature.[13]

$^{31}P\{^1H\}$ NMR (122 MHz, CDCl$_3$): (δ, ppm) 23.09 ppm

7.4.1.2 – Synthesis of Cat-21 ([Re(CO)$_3$(L12)]Br)

A solution of **L12** (0.075 g, 0.0742 mmol) in DCM (3.8 mL) was slowly added to a stirred suspension of [Re(CO)$_3$(H$_2$O)$_3$]Br (30 mg, 0.0742 mmol) in DCM (1.5 mL). The suspension was heated to 40 °C for 2 days, giving a golden-brown solution and white powder. The solution was filtered, reduced to ~1 mL and triturated with hexane (10 mL) giving a brown solid. This was washed with hexane (5 mL) and dried *in vacuo* (Yield= 0.0085 g, 0.0064 mmol, 8.6 %).

MS (Nanospray): m/z [M]$^+$ 1256.

Insufficient product recovered for further analysis.

7.4.1.3 – Synthesis of Cat-25 ([Re(CO)$_2$(dppea)$_2$]Br)

A solution of 2-(diphenylphosphino)ethylamine (0.225 g, 0.9848 mmol) in mesitylene (8 mL) was added slowly to a stirred suspension of Re(CO)$_5$Br (0.2 g, 0.4924 mmol) in mesitylene (8 mL). This was stirred at room temperature for 5 minutes before heating to reflux for 18 hours. Upon heating the suspension dissolved to give a clear, colourless solution. After reflux, a pale-yellow solution and an off-white solid were observed, the solution was cooled in an ice-water bath causing further precipitation. The solid was isolated by filtration, washed with hexane (3 x 8 mL), and dried *in vacuo* giving an off-white powder (Yield= 0.3045 g, 0.305 mmol, 62%). Single crystals for use in X-ray diffraction were grown by layering a solution of methanol with Et$_2$O.

$^{31}P\{^1H\}$ NMR (122 MHz, CDCl$_3$): (δ, ppm) 41.28

^1H NMR (300 MHz, CDCl$_3$): (δ, ppm) 7.83 (br, m, 4H), 7.64 (br, m, 4H), 7.50 (br, m, 12H), 5.69 (br, t, 2H), 3.73 (br, q, 2H), 2.90 (br, t, 2 H), 2.69 (br, s, 2H), 2.43 (br, s, 2H), 2.19 (br, s, 2H).

HR MS (Nanospray): m/z calc for [M]$^+$ C$_{30}$H$_{32}$ReN$_2$O$_2$P$_2$ 701.1497 Found 701.1491 (0.9 ppm)

IR (ν, cm-1) 1920, 1834 cm^{-1}

7.4.1.4 – Synthesis of Cat-27 ([Re(CO)$_2$(Me-dppea)$_2$]Br)

A solution of 2-(diphenylphosphino)-N-methylethylamine (0.1198 g, 0.4924 mmol) in mesitylene (4 mL) was added slowly to a stirred suspension of Re(CO)$_5$Br (0.1 g, 0.2462 mmol) in mesitylene (4 mL). This was stirred at room temperature for 10 minutes before heating to reflux for 60 hours. Upon heating the suspension dissolved to give a clear, colourless solution. After reflux, an off-white suspension was observed. The solid was isolated by filtration, washed with hexane (3 x 8 mL), and dried *in vacuo* giving an off-white powder (Yield= 0.0616 g, 0.0762 mmol, 31%).

^{31}P{^{1}H} NMR (122 MHz, CDCl$_3$): (δ, ppm) 38.03 ppm

^{1}H NMR (300 MHz, CDCl$_3$): (δ, ppm) 7.88 (br, m, 4H), 7.65 (br, m, 4H), 7.50 (br, m, 6H), 7.36 (br, m, 6H), 5.72 (br, s, 2H), 3.36 (br, m, 4H), 2.72 (br, m, 2H), 2.56 (br, m, 2H), 1.93 (s, 3H), 1.85 (s, 3H).

HR MS (Nanospray): m/z calc for [M]$^+$ C$_{32}$H$_{36}$ReN$_2$O$_2$P$_2$ 729.1810 Found 729.1805 (0.7 ppm)

IR (ν, cm-1) 1921, 1835 cm^{-1}

7.4.1.5 – Synthesis of Cat-28 ([Re(CO)$_2$(Me$_2$-dppea)$_2$]Br)

A solution of 2-(diphenylphosphino)-N,N-dimethylethylamine (0.1267 g, 0.4924 mmol) in mesitylene (4 mL) was added slowly to a stirred suspension of Re(CO)$_5$Br (0.1 g, 0.2462 mmol) in mesitylene (4 mL). This was stirred at room temperature for 10 minutes before heating to reflux for 90 hours. Upon heating the suspension dissolved to give a clear, colourless solution. The solution was allowed to cool to room temperature, filtered and triturated with hexane (30 mL). The precipitate was isolated *via* filtration and dried *in vacuo* (Yield= 0.0221 g, 0.0264 mmol, 5.4%).

^{31}P{^{1}H} NMR (122 MHz, CDCl$_3$): (δ, ppm) 32.24 (d, ^{2}J$_{PP}$= 209 Hz), 28.76 (s), 4.17 (d, ^{2}J$_{PP}$= 209 Hz)

^{1}H NMR (300 MHz, CDCl$_3$): (δ, ppm) 7.69 (br, m, 10H), 7.43 (br, m, 15H), 3.18 (s, 3H), 3.04 (s, 3H), 2.38 (s, 2H), 2.19 (br, s, 4H), 2.12 (s, 2H) (other methylene protons not visible).

HR MS (Nanospray): m/z calc for [M]$^+$ C$_{34}$H$_{41}$ReN$_2$O$_2$P$_2$Br 837.1384 Found 837.1360 (-2.9 ppm)

IR (ν, cm-1) 2020, 1916, 1882, 1827 cm^{-1}

7.4.1.6 – Synthesis of Cat-29 (Re(CO)$_3$(dppea)Br)

A solution of 2-(diphenylphosphino)ethylamine (0.113 g, 0.4924 mmol) in toluene (7 mL) was added slowly to a stirred suspension of Re(CO)$_5$Br (0.2 g, 0.4924 mmol) in toluene (7 mL). The suspension was heated to reflux for 18 hours. Upon heating the suspension dissolved to give a clear, colourless solution. The solution was allowed to cool and toluene was removed *in vacuo*. The crude solid was dissolved in THF (12 mL) and filtered, giving a golden solution. The solution was reduced to 1.5 mL and triturated with hexane (20 mL). The off-white solid produced was isolated by filtration and dried *in vacuo* (Yield= 0.1474 g, 0.279 mmol, 56.7%). Single crystals for use in X-ray diffraction were grown by layering a DCM solution with hexane.

^{31}P{^{1}H} NMR (122 MHz, CDCl$_3$): (δ, ppm) 28.42

^{1}H NMR (300 MHz, CDCl$_3$): (δ, ppm) 7.72 (br, m, 2H), 7.58 (br, m, 2H), 7.42 (br, m, 6H), 3.91 (br, s, 1H), 3.17 (br, s, 1H), 2.75 (br, m, 2H), 2.35 (br, s, 1H).

IR (ν, cm-1) 2018, 1907, 1876 cm^{-1}

HR MS (Nanospray): *m/z* calc for [M-Br]$^+$ C$_{17}$H$_{16}$NO$_3$PRe 500.0425 Found 500.0410 (-3.0 ppm)

7.4.1.7 – Synthesis of Cat-30 ([Re(CO)$_2$(dpppa)$_2$]Br)

A solution of 3-(diphenylphosphino)propylamine (0.1797 g, 0.739 mmol) in mesitylene (6 mL) was added slowly to a stirred suspension of ReBr(CO)$_5$ (0.15 g, 0.369 mmol) in mesitylene (6 mL), the ligand was washed with mesitylene (1 mL). This was stirred at room temperature for 5 minutes before heating to reflux for 18 hours. Upon heating the suspension dissolved to give a clear, colourless solution. After reflux, a colourless solution and a white solid were observed, the solution was cooled in an ice-water bath causing further precipitation. The solid was isolated by filtration, washed with hexane (3 x 7 mL),

and dried *in vacuo* giving a white powder (Yield= 0.2059 g, 0.255 mmol, 69%). Single crystals for use in X-ray diffraction were grown by layering a DCM solution with Et_2O.

$^{31}P\{^1H\}$ NMR (122 MHz, $CDCl_3$): (δ, ppm) 12.47 (br s)

^1H NMR (300 MHz, $CDCl_3$): (δ, ppm) 7.79 (br m, 4H), 7.50 (br m, 16H), 5.22 (br t, 2H, $^2J_{PH}$ = 11.4 Hz), 3.14 (br m, 4H), 2.22 (br m, 8H), 1.90 (br m, 2H).

HR MS (Nanospray): m/z calc for $[M]^+$ $C_{32}H_{36}N_2O_2P_2Re$ 729.1810 Found 729.1818 (1.1 ppm)

IR (ν, cm-1) 1913, 1806 cm^{-1}

7.4.2 – Catalysis

7.4.2.1 – General catalytic procedure- *iso*butanol formation

A rhenium complex (0.0119 mmol, 0.07 mol%) and sodium methoxide (1.85 g, 34.26 mmol, 200 mol%) were added to a clean oven-dried fitted PTFE insert equipped with a stirrer bar in a glove box. The autoclave was sealed in a glove box and then put under a nitrogen atmosphere on a Schlenk line. Methanol (10 mL) was injected into the autoclave through an inlet against a flow of nitrogen followed by ethanol (1 mL, 17.13 mmol). The autoclave was sealed and placed into the pre-heated (180 °C) aluminium heating mantle for 17 h. After the reaction run time, the autoclave was cooled to room temperature in an ice-water bath. The autoclave was vented to remove any gas generated during the reaction. A liquid sample was removed, filtered through a short plug of acidic alumina and analysed by GC (100 μL of sample, 10 μL of hexadecane standard, 1.7 mL Et_2O).

7.4.2.2 – General catalytic procedure- *n*-butanol formation

Cat-18 (0.056 g, 0.0856 mmol, 0.05 mol%) and sodium ethoxide (1.17 g, 17.19 mmol, 10 mol%) were added to a clean oven-dried fitted PTFE insert equipped with a stirrer bar in a glove box. The autoclave was sealed in a glove box and then put under a nitrogen atmosphere on a Schlenk line. Ethanol (10 mL) was injected into the autoclave through an inlet against a flow of nitrogen. The autoclave was sealed and placed into the pre-heated (150 °C) aluminium heating mantle for 20 h. After the reaction run time, the autoclave was cooled to room temperature in an ice-water bath. The autoclave was vented to remove any gas generated during the reaction. A liquid sample was removed, filtered through a short

plug of alumina (acidic) and analysed by GC (100 μL of sample, 10 μL of hexadecane standard, 1.7 mL Et$_2$O).

7.4.3 – Cat-18 base interaction experiments

7.4.3.1 – Open system base reactions

Cat-18 (0.003 g, 0.0046 mmol), was dissolved in dry, degassed methanol (2 mL) and NaOMe (0.247 g, 4.6 mmol, 1000 fold excess) was added to the solution. This was put under reflux for 20 hours, and the product analysed by ^{31}P{^{1}H} NMR spectroscopy.

^{31}P{^{1}H} NMR (202 MHz, MeOH): (δ, ppm) 38.66 (s)

7.4.3.2 – Closed system base experiments

Cat-18 (0.007 g, 0.0107 mmol) and NaOMe (0.58 g, 10.7 mmol, 1000 fold excess) were loaded in an oven dried fitted PTFE insert in a 300 mL Parr stainless steel autoclave. The autoclave was then put under a nitrogen atmosphere, sealed and heated to 180 °C for 18 hours. The autoclave was cooled to room temperature using an ice-water bath, and then reattached to a Schlenk line. A sample of liquid was extracted under a backflow of nitrogen and analysed by ^{31}P{^{1}H} NMR spectroscopy. Any solid produced was analysed by ^{1}H NMR spectroscopy as detailed below.

^{31}P{^{1}H} NMR (202 MHz, MeOH): (δ, ppm) 53.90 (s)

7.4.3.3 – High temperature experiments without base

Performed as above, except no NaOMe was added into the autoclave. Analysed by ^{31}P{^{1}H} NMR spectroscopy.

^{31}P{^{1}H} NMR (202 MHz, MeOH): (δ, ppm) 46.26 (s), 47.98 (s), 49.84 (s).

7.4.3.4 – Open system base reactions- Ethanol solvent

Cat-18 (0.028 g, 0.043 mmol), was dissolved in dry, degassed ethanol (5 mL) and NaOEt (0.29 g, 4.3 mmol, 100 fold excess) was added to the solution. This was put under reflux for 20 hours, resulting in a golden solution. The product was analysed by ^{31}P{^{1}H} spectroscopy.

^{31}P{^{1}H} NMR (202 MHz, EtOH): (δ, ppm) 51.18 (br, s), 39.01 (s)

7.4.3.5 – Open system base tests- Cat-22 and 23

Performed as above, with 0.0038 mmol complex and 0.381 mmol (100-fold excess) NaOMe. Samples were heated at reflux for 3 days. Analysis by $^{31}P\{^1H\}$ NMR spectroscopy.

Cat-22: $^{31}P\{^1H\}$ NMR (202 MHz, MeOH): (δ, ppm) -33.65 (t, $^2J_{pp}$= 17.1 Hz), -46.11 (t, $^2J_{pp}$= 17.0 Hz)

Cat-23: $^{31}P\{^1H\}$ NMR (202 MHz, MeOH): (δ, ppm) -33.64 (t, $^2J_{pp}$= 17.0 Hz), -46.10 (t, $^2J_{pp}$= 17.0 Hz)

7.4.4 – Ligand activation of Cat-26

Cat-26 (0.05 g, 0.068 mmol) was suspended in toluene (2.7 mL) and stirred for 5 minutes at room temperature. KHMDS (0.5 M in toluene) (0.15 mL, 0.0748 mmol) was slowly added while stirring, forming a cloudy yellow suspension. This was stirred at room temperature for 18 hours. Toluene was removed *in vacuo* and the sample dissolved in $CDCl_3$, before being filtered through celite and analysed by $^{31}P\{^1H\}$ and ^1H NMR spectroscopy.

$^{31}P\{^1H\}$ NMR (202 MHz, $CDCl_3$): (δ, ppm) -37.67 (s), -37.88 (s), -37.99 (s), -38.19 (s).

^1H NMR (500 MHz, $CDCl_3$): (δ, ppm) 7.63 (br, m, 4H), 7.43 (br, m, 10H), 7.34 (br, m, 6H), 5.43(m, 0.86H), 4.80 (m, 0.23H).

7.4.5 – Solid analysis- post reaction

The post reaction mixture (Table 4.1, Entry 1) was isolated by Büchner filtration and washed with toluene (100 mL). The white solid was dried under vacuum for 1 hour before being weighed (1.006 g). ^1H and $^{13}C\{^1H\}$ NMR analysis was undertaken in D_2O.

7.5 – Chapter 5 Experimental

Sodium (stored under kerosene), xylene, and sodium hydride (dry, 90%) were purchased from Sigma Aldrich and used without further purification. Octanol, propanol, butanol and hexanol were purchased from Sigma Aldrich, degassed before use and stored over 4 Å molecular sieves under a nitrogen atmosphere.

Cat-1,[3] **Cat-4**,[2] **Cat-2**[19] and **Cat-3**[20] were prepared according to literature procedures.

7.5.1 – General procedure of octanol homocoupling (closed system)

Sodium metal (72.2 mg, 3.14 mmol, 5 mol%) was weighed in paraffin oil, washed with heptane and suspended in octanol (10.51 mL, 67 mmol, 105 mol%) with stirring. This suspension was then put under reflux at 200 °C for 2 hours. The solution was allowed to cool before being filtered to remove any unreacted sodium.

Cat-1 (0.0595 g, 0.0633 mmol, 0.1 mol%), was added to a clean, oven-dried, fitted PTFE insert equipped with a stirrer bar in an autoclave. The autoclave was then sealed and put under an inert atmosphere. The octanol/ NaOOct solution was then added to the autoclave, followed by hexadecane (1 mL) under a backflow of nitrogen. The autoclave was resealed and heated to 150 °C for 4 hours. After the reaction time the autoclave was cooled in an ice-water bath. Excess gas was vented and the post reaction mixture was dissolved in heptane (100 mL) with rapid stirring, when necessary a spatula was used to break up the solid. A sample was filtered through a short plug of acidic alumina and analysed by GC.

7.5.2 – General procedure for octanol homocoupling- solvent screen

As for '7.5.1 – General procedure of octanol homocoupling (closed system)' above except a solvent (toluene, xylene, diethyl ether, 20 mL) was added into the autoclave before sealing and heating. The post reaction mixture was dissolved in 80 mL heptane.

7.5.3 – General procedure for octanol homocoupling (open system)

Sodium metal (72.2 mg, 3.14 mmol, 5 mol%) was weighed in paraffin oil, washed with heptane and suspended in octanol (10.51 mL, 67 mmol, 105 mol%) with stirring in a 2-necked Schlenk flask equipped with a reflux condenser. This suspension was then put under reflux at 200 °C for 2 hours. After reflux, the solution was allowed to cool, then **Cat-1** (0.0595 g, 0.0633 mmol, 0.1 mol%) was added to the solution, along with hexadecane (1 mL). 3 Å molecular sieves were loaded onto a sintered glass plug at the base of the reflux condenser. The reaction mixture was heated to 150 °C for 4 hours. After the reaction time the flask was cooled in an ice-water bath, and the post reaction mixture was dissolved in heptane (100 mL) with rapid stirring, when necessary a spatula was used to break up the solid. A sample was filtered through a short plug of acidic alumina and analysed by GC.

7.5.4 – Kinetic reaction studies

Samples prepared as for '7.5.3 – General procedure of octanol homocoupling (open system)' except 0. 5 mL aliquots of reaction mixture were taken out at specified time periods (30 min, 1 h, 1.5 h, 2 h, 3 h, 4 h, 20 h, 24 h, 28 h, 44 h). These aliquots were dissolved in heptane (5 mL) and filtered through a short plug of acidic alumina before analysis by GC.

7.5.5 – Solid analysis

The post reaction mixture from Table 5.1, Entry 7 was dissolved in heptane and stirred vigorously for 30 minutes. Distilled water (50 mL) was added to the solution and the mixture stirred for another 20 minutes. The aqueous layer was then removed and evaporated to dryness under reduced pressure leaving a white solid residue. This residue was dissolved in d^4-MeOH and analysed by ^{1}H NMR spectroscopy.

Solid analysis of a standard octanol coupling catalytic run (150 °C, 4 h, 5 mol% base loading 0.1 mol% **Cat-1**) produced 4.9 g solid residue.

7.5.6 – Preformation of alkoxide base- general procedure

Alcohol and 90% dry NaH were both weighed into separate Schlenk flasks, THF (50 mL) was added to each flask. The suspension of NaH in THF was added slowly to the alcohol solution, with stirring. Care was taken to avoid excess bubbling, as the reaction was highly exothermic. The Schlenk flask containing the NaH was washed through with more THF (25 mL). The reaction mixture was allowed to stir at room temperature for 18 hours before the THF was removed *in vacuo* leaving a grey/white solid.

Alcohol = Octanol (6.9 mL, 43.7 mmol), NaH (1.165 g, 43.7 mmol) used. (Yield=6.5 g, 98%) ^{1}H NMR (400 MHz, d^4-MeOD): (δ, ppm) 3.54 (t, J= 6.66 Hz, 2H), 1.51 (m, 2H), 1.33 (br m, 10H), 0.90 (t, J= 6.9 Hz, 3H)

Alcohol= Propanol (7.48 mL, 100 mmol), NaH (2.4 g, 100 mmol) used. (Yield= 7.1 g, 86%) ^{1}H NMR (500 MHz, d^4-MeOD): (δ, ppm) 3.50 (t, J= 6.71 Hz, 2H), 1.53 (sextet, J= 7.36 Hz, 2H), 0.92 (t, J= 7.46 Hz, 3H),

Alcohol= Butanol (9.15 mL, 100 mmol), NaH (2.4 g, 100 mmol) used. (Yield= 7.4 g, 77%) ^{1}H NMR (400 MHz, d^4-MeOD): (δ, ppm) 3.54 (t, J= 6.60 Hz, 2H), 1.50 (br m, 2H), 1.38 (br m, 2H), 0.94 (t, J= 7.35 Hz, 3H)

Alcohol= Hexanol (12.55 mL, 100 mmol), NaH (2.4 g, 100 mmol) used. (Yield= 8.35 g, 67%) ^{1}H NMR (400 MHz, d^4-MeOD): (δ, ppm) 3.54 (t, J= 6.71 Hz, 2H), 1.52 (br m, 2H), 1.34 (br m, 6H), 0.91 (t, J= 7.10 Hz, 3H)

7.5.7 – Octanol Coupling- Preformed base

1 (0.0595 g, 0.0633 mmol, 0.1 mol%) and sodium octoxide (0.485 g, 3.2 mmol, 5 mol%) were added to a clean, oven-dried, fitted PTFE insert equipped with a stirrer bar in an autoclave. The autoclave was sealed and put under an inert (N$_2$) atmosphere. Octanol (10 mL) and hexadecane (1 mL) were injected into the autoclave against a backflow of nitrogen. The autoclave was resealed and heated to 150 °C for 4 hours. After the reaction time the autoclave was cooled in an ice-water bath. Excess gas was vented, and the post reaction mixture was dissolved in hexanes (100 mL) with rapid stirring, when necessary a spatula was used to break up the solid. A sample was filtered through a short plug of acidic alumina and analysed by GC.

7.5.8 – General procedure for midchain alcohol coupling

Cat-1 (0.1 mol%) and the corresponding alkoxide base (5 mol%) were added to a clean, oven-dried, fitted PTFE insert equipped with a stirrer bar in an autoclave. The autoclave was sealed and put under an inert (N$_2$) atmosphere. Alcohol (10 mL) and hexadecane (1 mL, for hexanol coupling) were injected into the autoclave against a backflow of nitrogen. The autoclave was resealed and heated to 150 °C for 4 hours. After the reaction time the autoclave was cooled in an ice-water bath and excess gas was vented.

For propanol and butanol coupling analysis was conducted as follows: A small amount of the post reaction mixture was filtered through a short plug of acidic alumina. A sample was prepared for GC analysis (100 µL of sample, 10 µL of hexadecane standard, 1.7 mL Et$_2$O).

For hexanol coupling analysis was conducted as follows: The post reaction mixture was dissolved in hexanes (100 mL) with rapid stirring, when necessary a spatula was used to break up the solid. A sample was filtered through a short plug of acidic alumina and analysed by GC.

7.6 – Chapter 6 Experimental

[Ru(cymene)Cl$_2$]$_2$ (**1.5**), RuCl$_3$.xH$_2$O and tetrachloroethane were purchased from Sigma Aldrich and used without further purification.

Ligands d*o*tpm (**L14**) and d*o^{iPr}*ppm (**L15**) were kindly supplied by Dr. Richard Wingad and were prepared *via* a literature method.[21] RuCl$_2$(PPh$_3$)$_3$[22] and 1-benzyl-2-bromobenzene[23] were prepared according to a literature procedure.

7.6.1 – Ligand synthesis

7.6.1.1 – Preparation of L14 (d*o*tpm)

Magnesium turnings (0.9724 g, 40 mmol) were suspended in THF (25 mL), along with a single crystal of iodine. To the suspension, 2-bromotoluene (6.157 g, 4.33 mL, 36 mmol) in THF (35 mL) was added dropwise. The mixture was then heated to reflux for 3 hours, before being allowed to cool to room temperature and filtered into a dropping funnel. This was then added dropwise over 20 minutes to a solution of bis(dichlorophosphino)methane (1.481 g, 0.985 mL, 6.8 mmol) in THF (18 mL) at -78 °C. The dropping funnel was washed through with a further 5 mL of THF and stirred at -78 °C for 1 hr before being allowed to gradually warm to room temperature. This was then stirred at room temperature overnight. The THF was then removed *in vacuo* leaving a green solid which was dissolved in DCM (100 mL). Degassed deionised water (60 mL) was added to the DCM solution and stirred for 10 minutes, two heaped spatulas of ammonium chloride were added, and the mixture allowed to separate. The organic layer was then taken, dried over magnesium sulphate, filtered, and all solvent removed *in vacuo* leaving a white solid. This was then triturated with methanol (40 mL) to give a fluffy white powder that was dried under reduced pressure (Yield= 1.71 g, 3.88 mmol, 57.1%).

^{31}P{^{1}H} and ^{1}H NMR spectrum compare well with literature.[24]

^{31}P{^{1}H} NMR (122 MHz, CDCl$_3$): (δ, ppm) -43.67

^{1}H NMR (300 MHz, CDCl$_3$): (δ, ppm) 7.09-7.33 (br m, 16H, Ar-H), 2.60 (t, $^2J_{PH}$= 2.7 Hz, 2H, -(CH$_2$)-), 2.29 (s, 12H, Ar-CH$_3$)

7.6.1.2 – Preparation of L16 (d*m*tpm)

Magnesium turnings (0.4862 g, 20 mmol) were suspended in THF (12 mL), along with a single crystal of iodine. To the suspension, 3-bromotoluene (3.079 g, 2.18 mL, 18 mmol) in THF (17 mL) was added dropwise. The mixture was then heated to reflux for 3 hours, before being allowed to cool to room temperature and filtered into a dropping funning. This was

then added dropwise over 20 minutes to a solution of bis(dichlorophosphino)methane (0.74 g, 0.463 mL, 3.4 mmol) in THF (10 mL) at -78 °C. The dropping funnel was washed through with a further 3 mL of THF and stirred at -78 °C for 1 hr before being allowed to gradually warm to room temperature. This was then stirred at room temperature overnight. The THF was then removed *in vacuo* leaving a green solid which was dissolved and DCM (50 mL). Degassed deionised water (30 mL) was added to the DCM solution and stirred for 10 minutes, two heaped spatulas of ammonium chloride were added, and the mixture allowed to separate. The organic layer was then taken, dried over magnesium sulphate, filtered, and all solvent removed *in vacuo* leaving a white viscous liquid (Yield= 0.2884 g, 0.65 mmol, 19.3%).

$^{31}P\{^1H\}$ NMR (162 MHz, CDCl$_3$): (δ, ppm) -21.34

^1H NMR (400 MHz, CDCl$_3$): (δ, ppm) 6.98-7.24 (br m, 16H, Ar-H), 2.77 (br t, 2H, -(CH$_2$)-), 2.28 (s, 12H, Ar-CH$_3$)

^{13}C NMR (100 MHz, CDCl$_3$): (δ, ppm) 138.95 (t, J=3.3 Hz, Ar-C), 138.93 (t, J=3.7 Hz, Ar-C), 133.72 (t, J=11.0 Hz, Ar-C), 129.95 (t, J=9.5 Hz, Ar-C), 129.58 (s, Ar-C), 128.31 (t, J=3.5 Hz, Ar-C), 77.36 (s, PCP), 21.58 (Ar-CH$_3$)

HR MS (Nanospray): m/z calc for [M]$^+$ C$_{29}$H$_{31}$P$_2$ 441.1901 Found 441.1903 (0.5 ppm)

7.6.1.3 – Preparation of L17 (d*p*tpm)

Magnesium turnings (0.4862 g, 20 mmol) were suspended in THF (12 mL), along with a single crystal of iodine. To the suspension, 4-bromotoluene (3.079 g, 2.21 mL, 18 mmol) in THF (17 mL) was added dropwise. The mixture was then heated to reflux for 2.5 hours, before being allowed to cool to room temperature and filtered into a dropping funning. This was then added dropwise over 20 minutes to a solution of bis(dichlorophosphino)methane (0.74 g, 0.463 mL, 3.4 mmol) in THF (10 mL) at -78 °C. The dropping funnel was washed through with a further 3 mL of THF and stirred at -78 °C for 1 hr before being allowed to gradually warm to room temperature. This was then stirred at room temperature overnight. The THF was then removed *in vacuo* leaving a green solid which was dissolved and DCM (50 mL). Deionised water (30 mL) was added to the DCM solution and stirred for 10 minutes, two heaped spatulas of ammonium chloride were

added, and the mixture allowed to separate. The organic layer was then taken, dried over magnesium sulphate, filtered, and all solvent removed *in vacuo* leaving a white viscous oil. This was triturated with *n*-hexane giving a white powder which was dried under reduced pressure (Yield= 1.009 g, 2.29 mmol, 67.4 %).

^{31}P{^{1}H} and ^{1}H NMR spectrum compare well with literature.[25]

^{31}P{^{1}H} NMR (162 MHz, CDCl$_3$): (δ, ppm) -24.52

^{1}H NMR (400 MHz, CDCl$_3$): (δ, ppm) 7.26-7.35 (br m, 8H, Ar-H), 7.10 (br d, J= 7.7 Hz, 8H, Ar-H) 2.73 (t, $^2J_{PH}$= 1.6 Hz, 2H, -(CH$_2$)-), 2.32 (s, 12H, Ar-CH$_3$)

7.6.1.4 – Preparation of L18 (dopppm)

Magnesium turnings (0.4862 g, 20 mmol) were suspended in THF (8 mL), along with a single crystal of iodine. To the suspension, 2-bromobiphenyl (2.72 g, 2.01 mL, 11.7 mmol) in THF (14 mL) was added dropwise. The mixture was then heated to reflux for 3 hours, before being allowed to cool to room temperature and filtered into a dropping funning. The magnesium turnings were washed with a further 20 mL of THF. This was then added dropwise over 30 minutes to a solution of bis(dichlorophosphino)methane (0.4803 g, 0.3 mL, 2.2 mmol) in THF (7 mL) at -78 °C. The dropping funnel was washed through with a further 30 mL of THF and stirred at -78 °C for 1 hr before being allowed to gradually warm to room temperature and roughly a third of the THF removed under reduced pressure. This was then heated to reflux (70 °C) for 4 days. The THF was then removed *in vacuo* leaving a brown solid which was dissolved in DCM (50 mL). Deionised water (35 mL) was added to the DCM solution and stirred for 10 minutes, four heaped spatulas of ammonium chloride were added, and the mixture allowed to separate before the organic layer was taken and the aqueous layer washed with a further 10 mL DCM. The combined organic layers were then dried over magnesium sulphate and filtered, the MgSO$_4$ was washed with DCM (3 x 10 mL) and all solvent removed *in vacuo* leaving an off-white solid. This was dissolved in DCM (10 mL) and triturated with methanol (50 mL) giving an off-white powder. This was washed with methanol (3 x 10 mL) and dried *in vacuo* (Yield= 0.545 g, 0.7912 mmol, 36 %). Single crystals for use in X-ray diffraction were grown by layering a CDCl$_3$ solution with Et$_2$O.

^{31}P{^{1}H} NMR (162 MHz, CDCl$_3$): (δ, ppm) -37.21

^{1}H NMR (400 MHz, CDCl$_3$): (δ, ppm) 7.22 (m, 16H, Ar-H), 7.04 (br m, 8H, Ar-H), 6.82 (m, 12H, Ar-H), 1.95 (t, $^2J_{PH}$= 6 Hz, 2H, P-(CH$_2$)-P)

^{13}C NMR (100 MHz, CDCl$_3$): (δ, ppm) 147.1 (t, J$_{CP}$= 13.65 Hz), 141.80 (t, J$_{CP}$= 2.70 Hz), 138.31 (t, J$_{CP}$= 8.5 Hz), 132.16, 130.21, 129.96, 127.93, 127.53, 127.45, 126.80, 77.28

HR MS (Nanospray): m/z calc for [M+Na]$^+$ C$_{49}$H$_{38}$P$_2$Na 711.2346 Found 711.2329 (-2.4 ppm)

7.6.1.5 – Preparation of L19 (d*o*pppe)

Magnesium turnings (0.4862 g, 20 mmol) were suspended in THF (8 mL), along with a single crystal of iodine. To this 2-bromobiphenyl (2.84 g, 2.10 mL, 12.2 mmol) in THF (13 mL) was added dropwise. The mixture was then heated to reflux for 3 hours, before being allowed to cool to room temperature and filtered into a dropping funning. The magnesium turnings were washed with a further 35 mL of THF. This was then added dropwise over 30 minutes to a solution of 1,2-bis(dichlorophosphino)ethane (0.533 g, 0.35 mL, 2.3 mmol) in THF (9 mL) at -78 °C. The dropping funnel was washed through with a further 15 mL of THF and the solution stirred at -78 °C for 1 hr before being allowed to gradually warm to room temperature. This was then heated to reflux (70 °C) overnight. The THF was then removed *in vacuo* leaving a brown solid which was dissolved in DCM (60 mL). Deionised water (40 mL) was added to the DCM solution and stirred for 10 minutes and the mixture allowed to separate before the organic layer was taken and the aqueous layer extracted with a further 20 mL DCM. The combined organic layers were then dried over magnesium sulphate and filtered, the MgSO$_4$ was washed with DCM (3 x 10 mL) and all solvent removed *in vacuo* leaving a golden solid. This was dissolved in DCM (10 mL) and triturated with methanol (50 mL) giving a fine white powder, this was washed with methanol (2 x 15 mL) and dried *in vacuo* (Yield= 0.474 g, 0.6749 mmol, 29 %).

^{31}P{^{1}H} NMR (162 MHz, CDCl$_3$): (δ, ppm) -28.64

^{1}H NMR (400 MHz, CDCl$_3$): (δ, ppm) 7.32 (td, 4H, Ar-H), 7.20 (m, 16H, Ar-H), 7.12 (dq, 4H, Ar-H), 6.99 (dq, 4H, Ar-H), 6.80 (d, 8H, Ar-H), 1.46 (t, $^2J_{PH}$= 4.2 Hz, 4H, P-(CH$_2$)$_2$-P)

^{13}C NMR (100 MHz, CDCl$_3$): (δ, ppm) 147.6, 141.90 (t, J$_{CP}$= 2.70 Hz), 137.2 (t, J$_{CP}$= 9 Hz), 132.1, 130.04, 130.0 (shoulder) 128.2, 127.6, 127.3, 126.8, 77.3

HR MS (Nanospray): m/z calc for [M+] C$_{50}$H$_{41}$P$_2$ 703.2683 Found 703.2682 (-0.1 ppm)

7.6.1.6 – Preparation of L20 (do*bzppm*)

Magnesium turnings (0.2 g, 8.2 mmol) were suspended in THF (5 mL), along with a single crystal of iodine. To this 1-benzyl-2-bromobenzene (0.6840 g, 2.8 mmol) in THF (7 mL) was added dropwise. The mixture was then heated to reflux for 3 hours, before being allowed to cool to room temperature and filtered into a dropping funning. The magnesium turnings were washed with a further 6 mL of THF. This was then added dropwise over 15 minutes to a solution of bis(dichlorophosphino)methane (0.114 g, 0.071 mL, 0.52 mmol) in THF (5 mL) at -78 °C. The dropping funnel was washed through with a further 5 mL of THF and the solution stirred at -78 °C for 1 hr before being allowed to gradually warm to room temperature. This was then heated to reflux (70 °C) overnight. The THF was then removed *in vacuo* leaving a brown solid which was dissolved in DCM (30 mL). Deionised water (20 mL) was added to the DCM solution and stirred for 10 minutes and the mixture allowed to separate before the organic layer was taken and the aqueous layer extracted with a further 10 mL DCM. The combined organic layers were then dried over magnesium sulphate, filtered, and all solvent removed *in vacuo* leaving a yellow oil. This was dissolved in DCM (4 mL) and triturated with methanol (40 mL) giving a white liquid which was dried *in vacuo* (Yield= 0.0925 g, 0.1242 mmol, 24 %).

$^{31}P\{^{1}H\}$ NMR (162 MHz, CDCl$_3$): (δ, ppm) -44.56

^{1}H NMR (400 MHz, CDCl$_3$): (δ, ppm) 7.08 (br m, 36H, Ar-H), 4.02 (s, 8H, Ar-CH$_2$-Ar) 2.54 (t, $^{2}J_{PH}$= 3.3 Hz, 2H, P-(CH$_2$)-P)

^{13}C NMR (100 MHz, CDCl$_3$): (δ, ppm) 140.75, 132.08, 130.04, 129.81, 129.36, 129.02, 128.85, 128.54, 128.18, 126.54, 126.14, 125.40, 77.30, 40.59

HR MS (Nanospray): m/z calc for [M+] C$_{53}$H$_{47}$P$_2$ 745.3153 Found 745.3159 (0.8 ppm)

7.6.2 – Complex synthesis

7.6.2.1 – Preparation of Cat-31 ([RuCl(cymene)(do*tpm*)]Cl)

Do*tpm* (**L16**) (40 mg, 0.091 mmol) and [RuCl$_2$(cymene)]$_2$ (25.2 mg, 0.041 mmol) were dissolved in ethanol (14 mL and 3 mL respectively). **L16** was added dropwise to the ruthenium precursor and washed through with ethanol (2 mL), the brown solution was then allowed to stir at room temperature for 20 hours, during which time it became orange.

The solution was reduced to 50% its original volume, filtered and then the remaining solvent was removed *in vacuo* giving an orange oil. The oil was triturated with diethyl ether (10 mL) giving an orange solid, which was isolated by filtration, washed with further diethyl ether (2 x 5 mL) and dried *in vacuo* giving **Cat-31** as an orange powder (37 mg, 0.0496 mmol, 60%).

$^{31}P\{^1H\}$ NMR (122 MHz, CDCl$_3$): (δ, ppm) 1.84 (br d), -2.48 (br d).

$^{31}P\{^1H\}$ NMR (122 MHz, TCE): (δ, ppm) -0.57 (br d, $^2J_{PP}$= 93 Hz), -4.61 (br d, $^2J_{PP}$= 93 Hz).

^1H NMR (300 MHz, CDCl$_3$): (δ, ppm) 7.38 (br m, Ar-H), 7.12 (br m, Ar-H), 6.87 (br m, 2H, Ar-H), 6.03 (m, 2H, Ar-H), 4.77 (q, 1H, ^2J= 12.5 Hz, P-C(H)-P), 4.46 (br s, 1H, P-C(H)-P), 2.68 (m, 1H, Ar-C(H)), 2.33 (s, 1H, Ar-C(H)), 2.23 (br s, 1H, Ar-C(H)), 1.95 (br s, 8H, Ar-C(H)), 1.72 (br s, 3H, Ar-CH$_3$), 0.85 (br m, 3H). Other resonances are hidden beneath solvent peak/ diethyl ether impurity).

HR MS (Nanospray): m/z calc for [M]$^+$ C$_{30}$H$_{44}$P$_2$ClRu 711.1650 Found 711.1641 (-1.3 ppm)

7.6.2.2 – Preparation of Cat-32 ([RuCl(cymene)(do^{iPr}ppm)]Cl)

Do^{iPr}ppm (**L17**) (54 mg, 0.0977 mmol) and [RuCl$_2$(cymene)]$_2$ (30 mg, 0.04899 mmol) were dissolved in ethanol (15 mL and 5 mL respectively). **L17** was added dropwise to the ruthenium precursor forming an orange solution and washed through with ethanol (2 mL). This solution was then allowed to stir at room temperature for 20 hours, during which time it became light orange/ yellow. The solution was reduced to 50% its original volume, filtered and then the remaining solvent was removed *in vacuo* giving an orange oil. The oil was triturated with diethyl ether (20 mL) giving an orange solid, which was isolated by filtration, washed with further diethyl ether (2 x 7 mL) and dried *in vacuo* giving **Cat-32** as a yellow powder (48.4 mg, 0.05635 mmol, 57.5%).

$^{31}P\{^1H\}$ NMR (122 MHz, CDCl$_3$): (δ, ppm) 0.75 (d, $^2J_{PP}$= 75.7 Hz), -7.95 (d, $^2J_{PP}$= 75.7 Hz).

^1H NMR (300 MHz, CDCl$_3$): (δ, ppm) 8.03 (m, 2H, Ar-H), 7.61 (br m, 5H, Ar-H), 7.40 (br m, 5H, Ar-H), (several aromatic resonances hidden beneath solvent peak), 6.56 (m, 1H, Ar-H)), 6.32 (m, 1H, Ar-H), 6.26 (m, 1H, Ar-H), 6.07 (m, 1H, Ar-H), 5.80 (m, 1H, Ar-H), 4.74 (q, 1H, P-C(H)-P, J= 12.9 Hz), 4.49 (m, 1H, P-C(H)-P), 3.38 (br m, 1H, Ar-C(H)Me$_2$ (cymene)), 3.04 (m, 1H, Ar-C(H)Me$_2$), 2.87 (m, 1H, Ar-C(H)Me$_2$), 2.79 (m, 1H, Ar-C(H)Me$_2$), 2.50 (m, 1H, Ar-

C(H)Me$_2$), 1.68 (s, 3H, Ar-CH$_3$), 1.46 (d, 3H, CH$_3$ (^{i}Pr), ^{2}J$_{HH}$= 6.7 Hz), 1.42 (d, 3H, CH$_3$ (^{i}Pr), ^{2}J$_{HH}$= 6.7), 1.34 (d, 3H, CH$_3$ (^{i}Pr), ^{2}J$_{HH}$= 7.1Hz), 1.27 (d, 3H, CH$_3$ (^{i}Pr), ^{2}J$_{HH}$= 6.6 Hz), 1.13 (d, 3H, CH$_3$ (^{i}Pr), ^{2}J$_{HH}$= 7.3 Hz), 0.97 (d, 3H, CH$_3$ (^{i}Pr), ^{2}J$_{HH}$= 6.7 Hz), 0.44 (d, 3H, CH$_3$ (^{i}Pr), ^{2}J$_{HH}$= 6.4 Hz), 0.39 (d, 3H, CH$_3$ (^{i}Pr), ^{2}J$_{HH}$= 6.4 Hz), 0.31 (d, 3H, CH$_3$ (^{i}Pr), ^{2}J$_{HH}$= 6.5 Hz), 0.15 (d, 3H, CH$_3$ (^{i}Pr), ^{2}J$_{HH}$= 6.2 Hz).

HR MS (Nanospray): m/z calc for [M]$^+$ C$_{47}$H$_{60}$P$_2$ClRu 823.2902 Found 823.2908 (0.7 ppm)

7.6.2.3 – Preparation of Cat-33 ([RuCl(cymene)(d*m*tpm)]Cl)

D*m*tpm (100 mg, 0.227 mmol) and [RuCl$_2$(cymene)]$_2$ (63 mg, 0.102 mmol) were dissolved in ethanol (25 mL and 7 mL respectively). D*m*tpm was added dropwise to the ruthenium precursor and washed through with ethanol (2.5 mL), the brown solution was then allowed to stir at room temperature for 48 hours, during which time it turned orange. The solution was reduced to 50% its original volume, filtered and then the remaining solvent was removed *in vacuo* giving an orange oil. The oil was triturated with diethyl ether (25 mL) giving an orange solid, which was isolated by filtration, washed with further diethyl ether (2 x 7 mL) and dried *in vacuo* giving **Cat-33** as an orange powder (83.7 mg, 0.112 mmol, 55%).

^{31}P{^{1}H} NMR (122 MHz, CDCl$_3$): (δ, ppm) 1.97 (s)

^{1}H NMR (300 MHz, CDCl$_3$): (δ, ppm) 7.47-7.01 (br m, 16H, Ar-H), 6.30 (dd, 4H, Ar-H), 4.85 (br m, 1H, PC(H)P), 4.50 (br m, 1H, PC(H)P), 2.54 (br m, 1H, Ar-C(H)Me$_2$), 2.36 (s, 6H, Ar-CH$_3$), 2.27 (s, 6H, Ar-CH$_3$), 1.51 (s, 3H, Ar(cymene)-CH$_3$), 1.11 (d, 6H, Ar-C(CH$_3$)$_2$, ^{2}J$_{HH}$= 6.9 Hz).

HR MS (Nanospray): m/z calc for [M]$^+$ C$_{39}$H$_{44}$P$_2$ClRu 711.1650 Found 711.1677 (3.8 ppm)

7.6.2.4 – Preparation of Cat-34 ([RuCl(cymene)(d*p*tpm)]Cl)

D*p*tpm (120 mg, 0.272 mmol) and [RuCl$_2$(cymene)]$_2$ (83 mg, 0.136 mmol) were dissolved in ethanol (30 mL and 9 mL respectively). D*m*tpm was added dropwise to the ruthenium precursor and washed through with ethanol (3 mL), the brown solution was then allowed to stir at room temperature for 3 days, during which time it became orange. This solution was then heated to 80 °C for 3 hrs, before being reduced to 50% its original volume, filtered and the remaining solvent removed *in vacuo* giving an orange oil. The oil was triturated

with diethyl ether (30 mL) giving an orange solid, which was isolated by filtration, washed with further diethyl ether (3 x 7 mL) and dried *in vacuo* giving **Cat-34** as an orange powder (101 mg, 0.134 mmol, 54%).

$^{31}P\{^1H\}$ NMR (122 MHz, CDCl$_3$): (δ, ppm) 1.58 (s)

^1H NMR (300 MHz, CDCl$_3$): (δ, ppm) 7.46 (br m, 4H, Ar-H), 7.36 (br m, 4H, Ar-H), 7.28 (br m, 4H, Ar-H), 7.22 (br m, 4H, Ar-H), 6.29 (s, 4H, Ar-H), 4.70 (m, 1H, PC(H)P), 4.46 (m, 1H, PC(H)P), 2.37 (s, 6H, Ar-CH$_3$), 3.35 (s, 6H, Ar-CH$_3$), 1.57 (s, 3H, Ar(cymene)-CH$_3$), 1.10 (d, 6H, Ar-C(CH$_3$)$_2$, $^2J_{HH}$= 6.9 Hz).

HR MS (Nanospray): m/z calc for [M]$^+$ C$_{39}$H$_{44}$P$_2$ClRu 711.1650 Found 711.1651 (0.1 ppm)

7.6.2.5 – Preparation of Cat-35 (RuCl$_2$(d*m*tpm)$_2$)

D*m*tpm (0.1 g, 0.227 mmol) in DCM (4 mL) was added dropwise to a solution of RuCl$_2$(PPh$_3$)$_3$ (0.109 g, 0.114 mmol) in DCM (4 mL) over 5 minutes and washed through with 2 mL DCM. This solution was allowed to stir at room temperature for 18 hours, during which time it faded from dark brown to orange. The solution was the reduced to roughly half its original volume and filtered to remove insoluble impurities. The remainder of the solvent was removed *in vacuo* and the solid produced was triturated with hexane (30 mL) giving a pale-yellow powder. This was washed with diethyl ether (3 x 5 mL) before drying *in vacuo* (Yield= 0.0313 g, 0.0297 mmol, 26%).

$^{31}P\{^1H\}$ NMR (122 MHz, CDCl$_3$): (δ, ppm) -7.22 (s)

^1H NMR (300 MHz, CDCl$_3$): (δ, ppm) 7.12 (br m, 9H, Ar-H), 7.06 (br m, 15H, Ar-H), 4.98 (t, 4H, $^2J_{HP}$ = 4.3 Hz, PC(H)$_2$P), 2.05 (s, 24H, Ar-CH$_3$), other aromatic resonances hidden by solvent peak.

HR MS (Nanospray): m/z calc for [M]$^+$ C$_{58}$H$_{60}$P$_4$Cl$_2$Ru 1052.2066 Found 1052.2063 (-0.3 ppm)

7.6.2.6 – Preparation of Cat-36 (RuCl$_2$(d*p*tpm)$_2$)

D*p*tpm (0.2 g, 0.454 mmol) in DCM (5 mL) was added dropwise to a solution of RuCl$_2$(PPh$_3$)$_3$ (0.218 g, 0.218 mmol) in DCM (5 mL) over 5 minutes and washed through with 2 mL DCM. This solution was allowed to stir at room temperature for 18 hours, during which time it

faded from dark brown to orange. The solution was the reduced to roughly half its original volume and filtered to remove insoluble impurities. The remaining solution was triturated with hexane (35 mL) giving a pale-yellow powder. This was washed with diethyl ether (3 x 5 mL) before drying *in vacuo* (Yield= 0.0954 g, 0.0906 mmol, 41%).

$^{31}P\{^1H\}$ NMR (122 MHz, CDCl$_3$): (δ, ppm) -8.14 (s)

^1H NMR (300 MHz, CDCl$_3$): (δ, ppm) 6.94 (br m, 16H, Ar-H), 4.93 (t, 4H, $^2J_{HP}$ = 4.11 Hz, PC(H)$_2$P), 2.29 (s, 24H, Ar-CH$_3$), other aromatic resonances hidden by solvent peak.

HR MS (Nanospray): m/z calc for [M]$^+$ C$_{58}$H$_{60}$P$_4$Cl$_2$Ru 1052.2066 Found 1052.2063 (-0.3 ppm)

7.6.2.7 – Preparation of Cat-37 ([RuCl(cymene)(dopppm)]Cl)

D*opppm* (0.205 g, 0.298 mmol) in DCM (5 mL) was added dropwise to a solution of [RuCl$_2$(cymene)]$_2$ (0.083 g, 0.1355 mmol) in DCM (5 mL) and washed through with DCM (2 mL). This solution was allowed to stir at room temperature for 20 hours. DCM was then removed under reduced pressure leaving a red solid. This solid was dissolved in methanol (12 mL) and then filtered to remove any excess ligand. The solid left was washed with methanol (5 mL). Methanol was removed under reduced pressure and the solid produced was triturated with Et$_2$O (10 mL), washed with Et$_2$O (2 x 5 mL), purified by filtration and dried *in vacuo* producing **Cat-37** as a yellow powder (Yield= 0.2044 g, 0.2054 mmol, 75.8%)

$^{31}P\{^1H\}$ NMR (122 MHz, CDCl$_3$): (δ, ppm) 5.89 (d, $^2J_{PP}$= 65.7 Hz), -4.11 (d, $^2J_{PP}$= 67.4 Hz)

^1H NMR (300 MHz, CDCl$_3$): (δ, ppm) 7.20 (m, 34H, Ar-H), 6.22 (br m, 4H, Ar-H), 5.51 (br s, 1H), 5.26 (br s, 1H), 4.76 (br s, 1H), 3.92 (m, 1H), 2.39 (sept, 1H, $^2J_{HH=}$ 7 Hz), 1.68 (s, 3H), 1.03 (d, 6H, $^2J_{HH=}$ 66.7 Hz).

HR MS (Nanospray): m/z calc for [M]$^+$ C$_{59}$H$_{52}$P$_2$ClRu 959.2276 Found 959.2281 (0.5 ppm)

7.6.2.8 – Preparation of Cat-38 ([RuCl(cymene)(dopppe)]Cl)

D*opppe* (0.2095 g, 0.298 mmol) in DCM (5 mL) was added dropwise to a solution of [RuCl$_2$(cymene)]$_2$ (0.083 g, 0.1355 mmol) in DCM (5 mL) and washed through with DCM (2 mL). This was allowed to stir at room temperature for 4 hours forming a deep red solution. Methanol (20 mL) was then added, and the solution quickly changed colour to orange and

a small amount of precipitate formed, this mixture was stirred overnight. The solution was reduced to half volume under reduced pressure and filtered before being reduced to dryness, leaving an orange solid. The solid was triturated with Et_2O (12 mL), washed with Et_2O (2 x 5 mL), purified by filtration and dried *in vacuo* producing **Cat-38** as an orange powder (Yield= 0.1940 g, 0.1923 mmol, 70.9%).

$^{31}P\{^1H\}$ NMR (122 MHz, $CDCl_3$): (δ, ppm) 72.81 (br s)

^1H NMR (300 MHz, $CDCl_3$): (δ, ppm) 7.56 (br m, 4H, Ar-H), 7.30 (br m, 12H, Ar-H), 7.10 (br m, 10H, Ar-H), 6.91 (br m, 7H), 6.47 (br m, 7H), 5.93 (br s, 2H, PCH), 5.39 (br s, 2H, PCH) 2.34 (sept, 1H, $^2J_{HH=}$ 7 Hz), 1.64 (s, 3H), 0.88 (d, 6H, $^2J_{HH=}$ 7 Hz).

HR MS (Nanospray): m/z calc for $[M]^+$ $C_{60}H_{54}P_2ClRu$ 973.973.2433 Found 973.2465 (3.3 ppm)

7.6.2.9 – Preparation of Cat-39 ([RuCl(cymene)(d*o*bzppm)]Cl)

D*o*bzppm (0.0392 g, 0.053 mmol) in DCM (2 mL) was added dropwise to a solution of $[RuCl_2(cymene)]_2$ (0.011 g, 0.0175 mmol) in DCM (2 mL) and washed through with DCM (2 mL). This was allowed to stir at room temperature for 4 hours forming a deep red solution. Methanol (10 mL) was then added, and the solution was stirred overnight, during which time it changed colour from red to orange. The solution was reduced to half volume under reduced pressure and filtered before being reduced to dryness leaving a brown solid. The solid was triturated with Et_2O (15 mL), washed with Et_2O (5 mL), purified by filtration and dried *in vacuo* producing **Cat-39** as a dark orange powder (enough for one NMR, exact yield not calculated).

$^{31}P\{^1H\}$ NMR (122 MHz, $CDCl_3$): (δ, ppm) 1.70 (d, $^2J_{PP=}$ 82.7 Hz), -4.18 (d, $^2J_{PP=}$ 82.9 Hz)

HR MS (Nanospray): m/z calc for $[M]^+$ $C_{63}H_{60}P_2ClRu$ 1015.2902 Found 1015.2889 (-1.3 ppm)

7.6.3 – Base NMR reactions
7.6.3.1 – Interaction of Cat-32 with weak bases

Cat-32 (0.1 g, 0.0116 mmol) was measured out into a J. Youngs' NMR tube, this was dissolved in methanol (1 mL) and either NEt_3 (5.89 mg, 0.058 mmol, 8 µL, 5 eqv.) or NaOAc (3.8 mg, 0.0464 mmol, 4 eqv.) were added. The sample was then heated to reflux for 16

hours, before being examined by $^{31}P\{^1H\}$ NMR spectroscopy. The sample was then heated to 100 °C for 3 hours, before re-examining.

7.6.3.2 – Interaction of Cat-32 with NaOMe

Cat-32 (0.1 g, 0.0116 mmol) was measured out into a J. Youngs' NMR tube, this was dissolved in methanol (1 mL) and an excess of NaOMe was added. This solution was examined by $^{31}P\{^1H\}$ NMR spectroscopy before heating to reflux for 16 hours and re-examining by $^{31}P\{^1H\}$ NMR spectroscopy.

7.6.3.3 – Interaction of Cat-31 and 33 with NEt₃

As above, except ruthenium complex (0.01 g, 0.014 mmol) and NEt$_3$ (7.11 mg, 0.07 mmol, 9.8 µL) were used.

7.6.4 – Catalysis
7.6.4.1 – General procedure for *iso*butanol formation

A ruthenium complex (0.017 mmol, 0.1 mol%) and sodium methoxide (1.85 g, 34.26 mmol, 200 mol%) were added to a clean oven-dried fitted PTFE insert equipped with a stirrer bar under air. The autoclave was then put under a nitrogen atmosphere on a Schlenk line. Methanol (10 mL) was injected into the autoclave through an inlet against a flow of nitrogen followed by ethanol (1 mL, 17.13 mmol). The autoclave was sealed and placed into the pre-heated (180 °C) aluminium heating mantle for 2-20 h. After the reaction run time, the autoclave was cooled to room temperature in an ice-water bath. The autoclave was vented to remove any gas generated during the reaction. A liquid sample was removed, filtered through a short plug of acidic alumina and analysed by GC (100 µL of sample, 10 µL of hexadecane standard, 1.7 mL Et$_2$O).

7.6.4.2 – Catalysis with preactivation with NEt₃

As above except before reaction the ruthenium complex (0.017 mmol) was heated to reflux in methanol with 5 eqv. NEt$_3$ (0.086 mmol) for 16 hrs before being injected into an autoclave containing NaOMe (1.85 g) alongside ethanol (1 mL).

7.7 – Crystallographic structure and refinement data

*Table 7.1: Crystal data and structure refinement for **Cat-13**.*

Identification code	Cat-13
Empirical formula	$C_{57}H_{52}Br_{0.69}Cl_{12.32}MnOP_4$
Formula weight	1423.11
Temperature/K	100(2)
Crystal system	triclinic
Space group	*P*-1
***a*/Å**	12.3291(2)
***b*/Å**	14.1908(3)
***c*/Å**	19.9098(4)
α/°	101.2140(10)
β/°	102.7600(10)
γ/°	111.0480(10)
Volume/Å³	3023.86(10)
Z	2
ρ_{calc}g/cm³	1.563
μ/mm⁻¹	1.361
F(000)	1441.0
Crystal size/mm³	0.481 × 0.356 × 0.234
Radiation	MoKα (λ = 0.71073)
2θ range for data collection/°	3.224 to 55.788
Index ranges	-16 ≤ h ≤ 16, -18 ≤ k ≤ 18, -26 ≤ l ≤ 26
Reflections collected	55926
Independent reflections	14406 [R_{int} = 0.0524, R_{sigma} = 0.0500]
Data/restraints/parameters	14406/88/725
Goodness-of-fit on F^2	1.093
Final R indexes [I>=2σ (I)]	R_1 = 0.0454, wR_2 = 0.0804
Final R indexes [all data]	R_1 = 0.0640, wR_2 = 0.0856
Largest diff. peak/hole / e Å⁻³	0.82/-0.63

*Table 7.2: Crystal data and structure refinement for **Cat-10b**.*

Identification code	Cat-10b
Empirical formula	$C_{35}H_{41}BrMnN_2O_3P_2$
Formula weight	734.49
Temperature/K	100(2)
Crystal system	triclinic
Space group	*P*-1
a/Å	9.8537(3)
b/Å	13.7201(3)
c/Å	13.7612(3)
α/°	89.968(2)
β/°	71.183(2)
γ/°	82.227(2)
Volume/Å^3	1742.97(8)
Z	2
ρ_{calc}g/cm^3	1.399
μ/mm^{-1}	1.653
F(000)	758.0
Crystal size/mm^3	0.459 × 0.224 × 0.115
Radiation	MoKα (λ = 0.71073)
2θ range for data collection/°	3 to 52.044
Index ranges	-12 ≤ h ≤ 12, -16 ≤ k ≤ 16, -16 ≤ l ≤ 16
Reflections collected	27912
Independent reflections	6854 [R_{int} = 0.0725, R_{sigma} = 0.0735]
Data/restraints/parameters	6854/0/413
Goodness-of-fit on F^2	0.890
Final R indexes [I>=2σ (I)]	R_1 = 0.0340, wR_2 = 0.0592
Final R indexes [all data]	R_1 = 0.0567, wR_2 = 0.0641
Largest diff. peak/hole / e Å^{-3}	0.52/-0.29

Table 7.3: Crystal data and structure refinement for **Cat-15**.

Identification code	Cat-15
Empirical formula	$C_{52}H_{46}BrCl_4MnN_2O_2P_4$
Formula weight	1131.44
Temperature/K	100(2)
Crystal system	monoclinic
Space group	$P2_1/n$
a/Å	12.537(2)
b/Å	23.722(5)
c/Å	17.588(3)
α/°	90
β/°	94.992(11)
γ/°	90
Volume/Å^3	5211.2(17)
Z	4
ρ_{calc}g/cm^3	1.442
μ/mm^{-1}	1.390
F(000)	2304.0
Crystal size/mm^3	0.346 × 0.216 × 0.099
Radiation	MoKα (λ = 0.71073)
2Θ range for data collection/°	2.89 to 55.994
Index ranges	-15 ≤ h ≤ 16, -29 ≤ k ≤ 31, -23 ≤ l ≤ 17
Reflections collected	47473
Independent reflections	12453 [R_{int} = 0.0742, R_{sigma} = 0.0719]
Data/restraints/parameters	12453/1/603
Goodness-of-fit on F^2	1.015
Final R indexes [I>=2σ (I)]	R_1 = 0.0435, wR_2 = 0.0903
Final R indexes [all data]	R_1 = 0.0829, wR_2 = 0.1037
Largest diff. peak/hole / e Å^{-3}	0.70/-0.43

Table 7.4: Crystal data and structure refinement for **Cat-25**.

Identification code	Cat-25
Empirical formula	$C_{34}H_{42}BrN_2O_3P_2Re$
Formula weight	854.74
Temperature/K	99.98
Crystal system	monoclinic
Space group	$P2_1/c$
a/Å	9.7634(2)
b/Å	21.8195(4)
c/Å	15.8673(3)
α/°	90
β/°	97.3290(10)
γ/°	90
Volume/Å^3	3352.63(11)
Z	4
ρ_{calc}g/cm^3	1.693
μ/mm^{-1}	4.948
F(000)	1696.0
Crystal size/mm^3	0.538 × 0.16 × 0.04
Radiation	MoKα (λ = 0.71073)
2Θ range for data collection/°	3.734 to 60.338
Index ranges	-13 ≤ h ≤ 13, -30 ≤ k ≤ 30, -22 ≤ l ≤ 22
Reflections collected	56044
Independent reflections	9928 [R_{int} = 0.0341, R_{sigma} = 0.0243]
Data/restraints/parameters	9928/0/406
Goodness-of-fit on F^2	1.058
Final R indexes [I>=2σ (I)]	R_1 = 0.0217, wR_2 = 0.0439
Final R indexes [all data]	R_1 = 0.0271, wR_2 = 0.0453
Largest diff. peak/hole / e Å^{-3}	0.90/-1.33

*Table 7.5: Crystal data and structure refinement for **Cat-29**.*

Identification code	Cat-29
Empirical formula	$C_{18}H_{18}BrCl_2NO_3PRe$
Formula weight	664.31
Temperature/K	99.99
Crystal system	monoclinic
Space group	$P2_1/c$
a/Å	11.3995(4)
b/Å	11.7397(4)
c/Å	15.4962(6)
α/°	90
β/°	92.6836(19)
γ/°	90
Volume/Å^3	2071.53(13)
Z	4
ρ_{calc}g/cm^3	2.130
μ/mm^{-1}	8.149
F(000)	1264.0
Crystal size/mm^3	0.339 × 0.248 × 0.176
Radiation	MoKα (λ = 0.71073)
2Θ range for data collection/°	4.354 to 56.558
Index ranges	-15 ≤ h ≤ 15, -15 ≤ k ≤ 15, -20 ≤ l ≤ 20
Reflections collected	30202
Independent reflections	5145 [R_{int} = 0.0335, R_{sigma} = 0.0226]
Data/restraints/parameters	5145/0/252
Goodness-of-fit on F^2	1.045
Final R indexes [I>=2σ (I)]	R_1 = 0.0170, wR_2 = 0.0390
Final R indexes [all data]	R_1 = 0.0190, wR_2 = 0.0396
Largest diff. peak/hole / e Å^{-3}	1.67/-0.67

*Table 7.6: Crystal data and structure refinement for **Cat-30**.*

Identification code	Cat-30
Empirical formula	$C_{32}H_{38}BrN_2O_3P_2Re$
Formula weight	826.69
Temperature/K	100.11
Crystal system	triclinic
Space group	P-1
a/Å	11.4430(2)
b/Å	17.3552(4)
c/Å	18.1242(4)
α/°	66.2390(10)
β/°	73.4960(10)
γ/°	74.8580(10)
Volume/Å³	3114.08(12)
Z	4
ρ_{calc}g/cm³	1.763
μ/mm⁻¹	5.324
F(000)	1632.0
Crystal size/mm³	0.43 × 0.2 × 0.08
Radiation	MoKα (λ = 0.71073)
2Θ range for data collection/°	2.6 to 60.144
Index ranges	-16 ≤ h ≤ 13, -24 ≤ k ≤ 24, -25 ≤ l ≤ 25
Reflections collected	68081
Independent reflections	18222 [R_{int} = 0.0562, R_{sigma} = 0.0574]
Data/restraints/parameters	18222/94/822
Goodness-of-fit on F²	1.003
Final R indexes [I>=2σ (I)]	R_1 = 0.0330, wR_2 = 0.0658
Final R indexes [all data]	R_1 = 0.0628, wR_2 = 0.0754
Largest diff. peak/hole / e Å⁻³	1.53/-1.85

*Table 7.7: Crystal data and structure refinement for **L20**.*

Identification code	L20
Empirical formula	$C_{49}H_{38}P_2$
Formula weight	688.73
Temperature/K	99.95
Crystal system	triclinic
Space group	P-1
a/Å	10.6429(3)
b/Å	12.7956(4)
c/Å	13.8327(4)
α/°	92.934(2)
β/°	90.054(2)
γ/°	105.930(2)
Volume/Å³	1808.83(9)
Z	2
ρ_{calc}g/cm³	1.265
μ/mm⁻¹	0.156
F(000)	724.0
Crystal size/mm³	0.485 × 0.275 × 0.18
Radiation	MoKα (λ = 0.71073)
2Θ range for data collection/°	2.948 to 55.9
Index ranges	-14 ≤ h ≤ 14, -16 ≤ k ≤ 16, -18 ≤ l ≤ 18
Reflections collected	33254
Independent reflections	8657 [R_{int} = 0.0350, R_{sigma} = 0.0343]
Data/restraints/parameters	8657/0/460
Goodness-of-fit on F²	1.031
Final R indexes [I>=2σ (I)]	R_1 = 0.0368, wR_2 = 0.0856
Final R indexes [all data]	R_1 = 0.0490, wR_2 = 0.0917
Largest diff. peak/hole / e Å⁻³	0.42/-0.29

7.8 – References

1   E. Iengo, E. Zangrando, E. Baiutti, F. Munini and E. Alessio, *Eur. J. Inorg. Chem.*, 2005, **2005**, 1019–1031.

2   Y. Kita, T. Higuchi and K. Mashima, *Chem. Commun.*, 2014, **50**, 11211–11213.

3   J. Chatt and R. G. Hayter, *J. Chem. Soc.*, 1961, 896–904.

4   B. J. Johnson, S. V Lindeman and N. P. Mankad, *Inorg. Chem.*, 2014, **53**, 10611–10619.

5   A. Habtemariam, B. Watchman, B. S. Potter, R. Palmer, S. Parsons, A. Parkin and P. J. Sadler, *J. Chem. Soc. Dalt. Trans.*, 2001, 1306–1318.

6   S. Elangovan, C. Topf, S. Fischer, H. Jiao, A. Spannenberg, W. Baumann, R. Ludwig, K. Junge and M. Beller, *J. Am. Chem. Soc.*, 2016, **138**, 8809–8814.

7   R. H. Reimann and E. Singleton, *J. Organomet. Chem.*, 1972, **38**, 113–119.

8   G. A. Carriedo, V. Riera and J. Santamaria, *J. Organomet. Chem.*, 1982, **234**, 175–183.

9   R. van Putten, E. A. Uslamin, M. Garbe, C. Liu, A. Gonzalez-de-Castro, M. Lutz, K. Junge, E. J. M. Hensen, M. Beller, L. Lefort and E. A. Pidko, *Angew. Chem. Int. Ed.*, 2017, **56**, 7531–7534.

10   G. A. Carried and V. Riera, *J. Organomet. Chem.*, 1981, **205**, 371–379.

11   N. V. Kireev, O. A. Filippov, E. S. Gulyaeva, E. S. Shubina, L. Vendier, Y. Canac, J. B. Sortais, N. Lugan and D. A. Valyaev, *Chem. Commun.*, 2020, **56**, 2139–2142.

12   P. Piehl, M. Peña-López, A. Frey, H. Neumann and M. Beller, *Chem. Commun.*, 2017, **53**, 3265–3268.

13   D. Wei, O. Sadek, V. Dorcet, T. Roisnel, C. Darcel, E. Gras, E. Clot and J.-B. Sortais, *J. Catal.*, 2018, **366**, 300–309.

14   N. Lazarova, S. James, J. Babich and J. Zubieta, *Inorg. Chem. Commun.*, 2004, **7**, 1023–1026.

15   W. KURIYAMA, T. MATSUMOTO, Y. INO and O. OGATA, *Novel Ruthenium Carbonyl Complex Having a Tridentate Ligand and Manurfacturing Method and Useage Therefor, WO2011/048727*, 2011.

16   S. W. Carr, B. L. Shaw and M. Thornton-Pett, *J. Chem. Soc. Dalt. Trans.*, 1987, 1763–1768.

17   A. M. Bond, R. Colton, D. G. Humphrey, P. J. Mahon, G. A. Snook, V. Tedesco and J. N. Walter, *Organometallics*, 1998, **17**, 2977–2985.

18   G. A. Carriedo, M. L. Rodríguez, S. García-Granda and A. Aguirre, *Inorganica Chim. Acta*, 1990, **178**, 101–106.

19   M. A. Fox, J. E. Harris, S. Heider, V. Pérez-Gregorio, M. E. Zakrzewska, J. D. Farmer, D. S. Yufit, J. A. K. Howard and P. J. Low, *J. Organomet. Chem.*, 2009, **694**, 2350–2358.

20   I. Warad, Z. Al-Othman, S. Al-Resayes, S. S. Al-Deyab and E. R. Kenawy, *Molecules*, 2010, **15**, 1028–1040.

21   S. J. Dossett, A. Gillon, A. G. Orpen, J. S. Fleming, P. G. Pringle, D. F. Wass and M. D. Jones, *Chem. Commun.*, 2001, 699–700.

22   S. F. Colson and S. D. Robinson, *Inorganica Chim. Acta*, 1988, **149**, 13–14.

23   Y. Cheng, W. Dong, L. Wang, K. Parthasarathy and C. Bolm, *Org. Lett.*, 2014, **16**, 2000–2002.

24   P. W. Clark and B. J. Mulraney, *J. Organomet. Chem.*, 1981, **217**, 51–59.

25   V. W. W. Yam, K. K. W. Lo, C. R. Wang and K. K. Cheung, *J. Phys. Chem. A*, 1997, **101**, 4666–4672.